Novel Gas Sensor Solutions for Air Quality Monitoring

by

Kyle Mallires

A Dissertation Presented in Partial Fulfillment
of the Requirements for the Degree
Doctor of Philosophy

Approved November 2020 by the
Graduate Supervisory Committee:

Erica Forzani, Chair
Nongjian Tao, Chair (deceased)
Terry Alford
Di Wang
Peter Wiktor
Xiaojun Xian

ARIZONA STATE UNIVERSITY

December 2020

ABSTRACT

Global industrialization and urbanization have led to increased levels of air pollution. The costs to society have come in the form of environmental damage, healthcare expenses, lost productivity, and premature mortality. Measuring pollutants is an important task for identifying its sources, warning individuals about dangerous exposure levels, and providing epidemiologists with data to link pollutants with diseases. Current methods for monitoring air pollution are inadequate though. They rely on expensive, complex instrumentation at limited fixed monitoring sites that do not capture the true spatial and temporal variation. Furthermore, the fixed outdoor monitoring sites cannot warn individuals about indoor air quality or exposure to chemicals at worksites. Recent advances in manufacturing and computing technology have allowed new classes of low-cost miniature gas sensor to emerge as possible alternatives. For these to be successful however, there must be innovations in the sensors themselves that improve reliability, operation, and their stability and selectivity in real environments.

Three novel gas sensor solutions are presented. The first is the development of a wearable personal exposure monitor using all commercially available components, including two metal oxide semiconductor gas sensors. The device monitors known asthma triggers: ozone, total volatile organic compounds, temperature, humidity, and activity level. Primary focus is placed on the ozone sensor, which requires special circuits, heating algorithm, and calibration to remove temperature and humidity interferences. Eight devices are tested in multiple field tests. The second is the creation of a new compact optoelectronic gas sensing platform using colorimetric microdroplets printed on the surface of a complementary-metal-oxide-semiconductor (CMOS) imager. The nonvolatile liquid

microdroplets provide a homogeneous, uniform environment that is ideal for colorimetric reactions and lensless optical measurements. To demonstrate one type of possible indicating system gaseous ammonia is detected by complexation with Cu(II). The third project continues work on the CMOS imager optoelectronic platform and develops a more robust sensing system utilizing hydrophobic aerogel particles. Ammonia is detected colorimetrically by its reaction with a molecular dye, with additives and surface treatments enhancing uniformity of the printed films. Future work presented at the end describes a new biological particle sensing system using the CMOS imager.

DEDICATION

In loving memory of my advisor Dr. Nongjian Tao. Without your mentorship this work

would not have been possible.

I also want to thank my family for their endless love and support.

ACKNOWLEDGMENTS

TABLE OF CONTENTS

LIST OF TABLES

LIST OF FIGURES

xiii

1   INTRODUCTION: THE IMPORTANCE OF AIR QUALITY AND OPPORTUNITIES FOR GAS SENSORS

Deteriorating air quality worldwide, driven by unprecedented rates of industrialization and urbanization, has led to incontrovertible evidence that air pollution is as an international health, environmental, and economic issue [1-3]. The World Health Organization (WHO) estimates 7 million deaths were attributable to air pollution in 2016, with 9 out of 10 people breathing air containing high levels of pollutants [4, 5]. The Global Burden of Disease study came to a similar conclusion with air pollution ranking as one of the leading causes of mortality and morbidity, causing 6.5 million deaths and 167.3 million disability adjusted life years in 2015 [6]. The global welfare costs associated with premature deaths from ambient air pollution are estimated at $3 trillion (USD) in 2015 and projected to rise to $18-25 trillion in 2060 [7]. Without a doubt, these figures are concerning, and many government agencies around the world are responding by cooperating to set more stringent limits on pollutants and improve monitoring programs [8-15].

The link between illness and high levels of anthropogenic air pollutants has been known for nearly a century. Incidents of unusually high mortality rates coinciding with extreme urban pollution events were well documented, such as the Meuse Valley Fog of 1930 and the Great Smog of London in 1952, setting off initial epidemiological research [16, 17]. Soon after, the United States and United Kingdom each passed their first pieces of federal legislation pertaining to air pollution, the 1955 Air Pollution Control Act and the Clean Air Act of 1956 [18, 19]. This led to many subsequent forms of legislation and amendments in the U.S. and Europe that set aside money to fund research, develop

networks of fixed monitoring sites, and enforce limits on emissions, the most notable being the Clean Air Act of 1970 (U.S.) just preceded by the formation of the Environmental Protection Agency (EPA) [2, 20, 21]. These programs were successful and did a great deal to improve air quality in developed countries that had already gone through their industrial revolutions.

Despite improvements over the past few decades in the U.S. and Europe, excess morbidity and mortality continue to be detected at current ambient air pollution levels [22-24]. Newer scientific studies have shown that some pollutants can harm public health even at very low levels. There may not be a "safe" level for certain pollutants [24]. What's more, developing countries going through rapid industrialization and urbanization are confronting severe levels of air pollution due to augmented transport, energy, and construction sectors with few restrictions [25]. To draw a comparison, 49% of cities with more than 100,000 inhabitants in high-income countries exceed WHO air quality guidelines, while that number increases to 97% for low- and middle-income countries [8]. India and China, with their large emerging economies and populations, are no exception. Air quality ranks within the top five risk factors for mortality in these two countries [6]. They are also particularly vulnerable to environmental effects like ozone layer depletion, soil and water contamination, and eutrophication, which ultimately damages crops, livestock, and fisheries that has further implications on health and quality of life [1].

Elucidating the direct health effects from breathing air pollutants continues to be an active area of research. The mechanism for each pollutant is unique, but in general inhaling air pollutants initiates pulmonary oxidative stress and inflammation [26]. Studies have consistently shown this in humans [27, 28], animals [29-32], and in vitro [33]. Short-

term exposure, in the simplest case, causes temporary discomfort, such as headaches, nausea, dizziness, and irritation of the mucous membranes. As the level of exposure increases one may experience wheezing, coughing, chest tightness, and breathing difficulties that restrict activities [1]. Pollutants will exacerbate existing respiratory conditions too. Short-term exposure has been correlated with increased hospital admissions and mortality for asthma, pneumonia, bronchitis, and chronic obstructive pulmonary disorder (COPD) in both rural and urban areas [1, 25, 34-40]. While respiratory effects are intuitively linked with air pollution, more recent evidence has emerged linking air pollution with cardiovascular mortality and morbidity (eg. stroke, heart attack, arrhythmias) even at present ambient concentrations [2, 41]. Long-term exposure can further aggravate these problems and harm all organ systems of the body with various long-term effects manifesting in the form of chronic diseases. This includes the onset of asthma, COPD, and a variety of cancers including lung cancer [1, 2, 25, 34, 42]. Children, the elderly, diabetics, and those with pre-existing pulmonary or cardiovascular conditions are most susceptible to these negative effects [2, 25]. Sensitive individuals are even impacted on low pollution days [1, 24].

The Clean Air Act required the EPA to set National Ambient Air Quality Standards (NAAQS) for six ambient air pollutants considered harmful to public health and the environment. These six criteria pollutants are ozone, nitrogen dioxide, sulfur dioxide, carbon monoxide, lead, and particulate matter [43]. All are primarily formed in combustion processes except for ozone which is a secondary pollutant [44]. The EPA also monitors emissions of 187 additional hazardous air pollutants (HAPs) known to harm the environment and/or cause cancer or other serious health effects, many of which are volatile

organic compounds (VOCs) [45]. This only covers outdoor emissions though, The Clean Air Act does not regulate indoor air quality (IAQ) [46].

The chemical and particulate pollutants found indoors can be very different than those found outdoors. Depending on the sources and whether or not there is adequate ventilation it is possible for indoor pollution to reach much more hazardous levels [46]. Building materials, upholstery, paint, human activities (eg. smoking, cooking, fragrances), and biologics (eg. mold, pests, pets) can release thousands of types of VOCs inside a home [47-49]. Less is known about the health effects of VOCs, especially mixtures, compared with ambient air pollutants. This makes classifying them as a hazard challenging. With respect to comfort VOCs are associated with the perception of odor [50]. Interestingly, the EPA and WHO track VOCs differently. The primary focus of the EPA is on how VOCs will contribute to photochemical smog, while the WHO puts special attention on a few VOCs they deem to be the biggest threat regarding IAQ (ie. benzene, formaldehyde, naphthalene, trichloroethylene, tetrachloroethylene) [51, 52].

Workers, especially those on industrial sites, are at a unique risk to breathing many types of harmful chemicals and materials. The Occupational Safety and Health Act of 1970 (U.S.) created the National Institute for Occupational Safety and Health (NIOSH) and the Occupational Safety and Health Administration (OSHA) to recommend safe guidelines and enforce laws protecting worker safety [53]. NIOSH and OSHA recommend and enforce limits on hundreds of hazardous chemicals and materials that workers may come into contact with in a wide variety of industries [54-56]. They have developed and published official methods for sampling, measurement, and validation for chemical analysis

including personal sampling, IAQ investigations, and instrumental analysis [57-59]. The European Union has similar programs to protect workers (EU-OSHA) [60, 61].

Tracking air quality and emissions is an enormous and costly task, but necessary to assess the potential environmental and health effects pollution can have on a particular region. Currently the WHO compiles data sent in from more than 4,300 cities in 108 countries [62]. The exact guidelines vary from country to country, but in the U.S., with regards to ambient pollution, federal, state, and local governments have implemented fixed monitoring site networks to track the six criteria pollutants and in some instances the HAPs. The problem is the continuous spatial and temporal variation in pollutants, especially in urban environments, is at a finer scale than the monitoring sites can resolve [2, 3, 41, 49, 63-67]. This makes estimating the health effects pollutants have on individuals as they move throughout the day from one microenvironment to another subject to varying degrees of error. New tools like geographic information systems (GIS), land use regression models (LUR), dispersion models, and hybrid models may provide more refined estimates with improved spatiotemporal resolution, but they do not replace the quality of data from measuring devices [2, 3, 14, 64-66].

Increasing the number of fixed monitoring sites to significantly improve resolution is not a viable option. The requirement for the physical plots of land, expensive instrumentation, and man-hours to operate the sites is too costly and just not scalable. Furthermore, using ambient air quality data to assess the effect of pollutants on health is inherently limited because people spend such a large amount of time indoors. As mentioned before, the pollutants encountered indoors can be dramatically different than those found outdoors. IAQ requires its own investigation and monitoring equipment. At industrial sites

workers may be exposed to hazardous chemicals and materials unique to their work environment that cannot be easily anticipated and measured by installing fixed monitoring devices. The analytical methods published by NIOSH and OSHA are cumbersome and require special equipment (eg. sorption tubes, pumps, spectrometers) [57, 58]. Some of the personal monitors (eg. handheld readers, color indicating badges) they suggest to supplement personal protective equipment (PPE) are unreliable (ie. poor accuracy/precision, cross-sensitivities) and do not provide continuous real-time monitoring [54, 68]. Properly assessing air quality, personal exposure, and protecting worker safety will require new technological innovations.

Low-cost gas sensors represent a rapidly growing class of measurement tools being developed for the fields of ambient air quality, IAQ, and worker safety [65, 66, 69-74]. Sensor devices are currently available to monitor a range of air pollutants and new devices are continually being introduced. These types of sensors are not only orders of magnitude cheaper than their instrumental counterparts, they are also much smaller, sometimes surface-mountable as a single chip, and require less power. Improvements in computing capabilities, wireless communication, and power management/storage have enabled researchers to begin to design practical wireless networked and wearable exposure monitors previously not possible. This has even attracted the attention of the EPA as a way to fill in the gaps of their existing fixed monitoring site networks and improve epidemiological studies [75-77]. The rise in evidence for the high spatiotemporal variability of pollutants combined with an increase in asthma and other health conditions sensitive to air pollution continues to motivate finer-grained and more personalized air monitoring data collection. Opportunities abound to augment existing air monitoring

efforts and perhaps provide avenues to new air monitoring applications. Regardless of the positive attention these types of sensors are receiving though, there are still many challenges to overcome in transforming them into reliable measuring devices that can provide meaningful datasets.

This report will be organized as follows: Chapter 2 will discuss chemical measurement technology relevant for gas-phase pollutants and hazardous chemicals. It will familiarize the reader with gold standard instrumental techniques and the state of the art in terms of commercially available low-cost gas sensors. Chapter 3 will introduce Project 1, the development of a wearable personal exposure monitor using only commercial off-the-shelf (COTS) sensors and components. The challenges of calibrating these sensors and correcting for environmental interferences is examined in detail. Chapter 4 will introduce Project 2, the creation of a new single-chip gas sensing platform using colorimetric microdroplets printed on a complementary metal-oxide-semiconductor (CMOS) imager. This novel platform attempts to solve some of the technical problems found with many COTS gas sensors, like the difficult calibration discussed in Project 1. Chapter 5 will introduce Project 3, generating printed gas sensors on a CMOS imager that are environmentally robust by utilization of hydrophobic aerogel particles. The resulting porous, hydrophobic matrix of the microsensors is beneficial for improving the sensor response and resistance to environmental interferents. Chapter 6 concludes the discussion with final remarks and thoughts for future work including a description with preliminary data for a biological particle sensor using the CMOS imager.

References

[1]   I. Manisalidis, E. Stavropoulou, A. Stavropoulos, and E. Bezirtzoglou, "Environmental and Health Impacts of Air Pollution: A Review," *Public Health Front.*, vol. 8, no. 14, pp. 1-13, 2020, 10.3389/fpubh.2020.00014.

[2]   R. D. Brook, B. Franklin, W. Cascio, Y. Hong, G. Howard *et al.*, "Air Pollution and Cardiovascular Disease," AHA Scientific Statement, pp. 2655-2671, 2004, 10.1161/01.CIR.0000128587.30041.C8.

[3]   HEI Panel on the Health Effects of Traffic-Related Air Pollution, "Traffic-Related Air Pollution: A Critical Review of the Literature on Emissions, Exposure, and Health Effects," Health Effects Institute Special Report 17, 2010, Health Effects Institute, Boston, MA, USA.

[4]   WHO, "Burden of Disease from the Joint Effects of Household and Ambient Air Pollution for 2016," Public Health, Social and Environmental Determinants of Health Department, World Health Organization, Geneva, Switzerland. 2018.

[5]   WHO, "Air Pollution", 2020. [Online] Available: http://www.who.int/airpollution/en/, Accessed on: June 4, 2020.

[6]   C. J. L. Murray *et al.*, "Global, Regional, and National Comparative Risk Assessment of 79 Behavioural, Environmental and Occupational, and Metabolic Risks or Clusters of Risks, 1990-2015: a Systematic Analysis for the Global Burden of Disease Study 2015," *Lancet*, vol. 388, pp. 1659-1724, 2016.

[7]   OECD, "The economic consequences of outdoor air pollution," The Organisation for Economic Co-operation and Development, Paris, France. 2016.

[8]   WHO, "WHO Global Ambient Air Quality Database," 2018. [Online] Available: https://www.who.int/airpollution/data/cities/en/, Accessed on: June 2, 2020.

[9]   UNFCC, "What is the Kyoto Protocol?," 1997. [Online] Available: https://unfccc.int/kyoto_protocol, Accessed on: October 6, 2019.

[10]   UNFCC, "Copenhagen Climate Change Conference," 2009. [Online] Available: https://unfccc.int/process-and-meetings/conferences/past-conferences/copenhagen-climate-change-conference-december-2009/copenhagenclimate-change-conference-december-2009, Accessed on: October 6, 2019.

[11]   UNFCC, "Durban Climate Change Conference," 2011. [Online] Available: https://unfccc.int/process-and-meetings/conferences/past-conferences/copenhagen-climate-change-conference-december-2009/copenhagenclimate-change-conference-december-2009, Accessed on: October 6, 2019.

[12] UNFCC, "The Paris Agreement," 2016. [Online] Available: https://unfccc.int/process-and-meetings/the-paris-agreement/the-paris-agreement, Accessed on: June 4, 2020.

[13] CAAC, "State Council Air Pollution Prevention and Control Action Plan," Clean Air Alliance of China, Beijing, China. 2013.

[14] A. Miranda, C. Silveira, J. Ferreira, A. Monteiro, D. Lopes, H. Relvas *et al.*, "Current Air Quality Plans in Europe Designed to Support Air Quality Management Policies," *Atmos. Pollut. Res.*, vol. 6, pp. 434-443, 2015, 10.5094/APR.2015.048.

[15] EPA, "Overview of the Clean Air Act and Air Pollution," 2020. [Online] Available: https://www.epa.gov/clean-air-act-overview, Accessed On: June 4, 2020.

[16] B. Nemery, P. H. M. Hoet, A. Nemmar, "The Meuse Valley Fog of 1930: an Air Pollution Disaster," *Lancet*, vol. 357, pp. 704-708, 2001.

[17] W. P. D. Logan, "Mortality in the London Fog Incident, 1952," *Lancet*, Feb. 14, 1953, pp. 336-338.

[18] USA, "Air Pollution Control Act 1955," Public Law 159, Chapter 360, July 14, 1955, pp. 322-323.

[19] UK, "Clean Air Act 1956," Chapter 52, July 5, 1956.

[20] USA, "Clean Air Act 1970," Public Law 91-604, Dec. 31, 1970, pp. 1676-1713.

[21] EPA, "Evolution of the Clean Air Act," 2017. [Online] Available: https://www.epa.gov/clean-air-act-overview/evolution-clean-air-act, Accessed On: June 4, 2020.

[22] C. A. Pope III, "Epidemiology of Fine Particulate Air Pollution and Human Health: Biologic Mechanisms and Who's at Risk?," *Environ. Health Perspect.*, vol. 108, no. 4, pp. 713-723, 2000.

[23] R. D. Brook, J. R. Brook, and S. Rajagopalan, "Air Pollution: The 'Heart' of the Problem," *Curr. Hypertens. Rep.*, vol. 5, pp. 32-39, 2003.

[24] EPA, "Air Pollution: Current and Future Challenges," 2019. [Online] Available: https://www.epa.gov/clean-air-act-overview/air-pollution-current-and-future-challenges, Accessed On: June 3, 2020.

[25] X. Q. Jiang, X. D. Mei, and D. Feng, "Air Pollution and Chronic Airway Diseases: What Should People Know and Do?," *J. Thorac. Dis.*, vol. 8, no. 1, pp. E31-E40, 2016, 10.3978/j.issn.2072-1439.2015.11.50.

[26] F. J. Kelly, "Oxidative Stress: Its Role in Air Pollution and Adverse Health Effects," *Occup. Environ. Med.*, vol. 60, pp. 612-616, 2003, 10.1136/oem.60.8.612.

[27] A. J. Ghio, C. Kim, and R. B. Devlin, "Concentrated Ambient Air Particles Induce Mild Pulmonary Inflammation in Healthy Human Volunteers," *Am. J. Respir. Crit. Care Med.*, vol. 162, pp. 981-988, 2000.

[28] R. M. Aris, D. Christian, P. Q. Hearne *et al.*, "Ozone-Induced Airway Inflammation in Human Subjects as Determined by Airway Lavage and Biopsy," *Am. Rev. Respir. Dis.*, vol. 148, pp. 1363-1372, 1993, 10.1164/ajrccm/148.5.1363.

[29] J. J. Godleski, R. W. Clarke, B. A. Coull *et al.*, "Composition of Inhaled Urban Air Particles Determines Acute Pulmonary Responses," *Ann. Occup. Hyg.*, vol. 46, no. 1, pp. 419-424, 2002, 10.1093/annhyg/mef706.

[30] D. L. Costa and K. L. Dreher, "Bioavailable Transition Metals in Particulate Matter Mediate Cardiopulmonary Injury in Healthy and Compromised Animal Models," *Environ. Health Perspect.*, vol. 105, no. 5, pp. 1053-1060, 1997.

[31] J. D. Brain, N. C. Long, S. F. Wolfthal *et al.*, "Pulmonary Toxicity in Hamsters of Smoke Particles from Kuwaiti Oil Fires," *Environ. Health Perspect.*, vol. 106, pp. 141-146, 1998.

[32] X. Y. Li, P. S. Gilmour, K. Donaldson *et al.*, "Free Radical Activity and Pro-Inflammatory Effects of Particulate Air Pollution (PM10) in vivo and in vitro," *Thorax*, vol. 51, pp. 1216-1222, 1996, 10.1136/thx.51.12.1216.

[33] T. Kennedy, A. J. Ghio, W. Reed *et al.*, "Copper-Dependent Inflammation and Nuclear Factor-KappaB Activation by Particulate Air Pollution," *Am. J. Respir. Cell Mol. Biol.*, vol. 19, pp. 366-378, 1998.

[34] N. Kunzli, R. Kaiser, S. Medina, M. Studnicka, O. Chanel, P. Filliger *et al.*, "Public-Health Impact of Outdoor and Traffic-Related Air Pollution: a European Assessment," *Lancet*, vol. 356, pp. 795-801, 2000.

[35] K. R. Pride, J. L. Peel, B. F. Robinson, A. Busacker, J. Grandpre *et al.*, "Association of Short-Term Exposure to Ground-Level Ozone and Respiratory Outpatient Clinic Visits in a Rural Location – Sublette County, Wyoming, 2008-2011," *Environ. Res.*, vol. 137, pp. 1-7, 2015, 10.1016/j.envres.2014.10.033.

[36] M. Ji, D. S. Cohan, and M. L. Bell, "Meta-Analysis of the Association Between Short-Term Exposure to Ambient Ozone and Respiratory Hospital Admissions," *Environ. Res. Lett.*, vol. 6, pp. 1-11, 2011, 10.1088/1748-9326/6/2/024006.

[37] M. Medina-Ramon, A. Zanobetti, and J. Schwartz, "The Effect of Ozone and PM10 on Hospital Admissions for Pneumonia and Chronic Obstructive Pulmonary

Disease: A National Multicity Study," *Am. J. Epidemiol.*, vol. 163, no. 6, pp. 579-588, 2006, 10.1093/aje/kwj078.

[38]   C. Paulu and A. E. Smith, "Tracking Associations Between Ambient Ozone and Asthma-Related Emergency Department Visits Using Case-Crossover Analysis," *J. Public Health Manag. Pract.*, vol. 14, no. 6, pp. 581-591, 2008.

[39]   S. Yamazaki, M. Shima, M. Ando, and H. Nitta, "Modifying Effect of Age on the Association between Ambient Ozone and Nighttime Primary Care Visits Due to Asthma Attack," *J. Epidemiol.*, vol. 19, no. 3, pp. 143-151, 2009, 10.2188/jea.JE20081025.

[40]   Q. Yang, Y. Chen, Y. Shi, R. T. Burnett, K. M. McGrail *et al.*, "Association Between Ozone and Respiratory Admissions Among Children and the Elderly in Vancouver, Canada," *Inhal. Toxicol.*, vol. 15, pp. 1297-1308, 2003, 10.1080/08958370390241768.

[41]   K. K. Lee, M. R. Miller, and A. S. V. Shah, "Air Pollution and Stroke," *J. Stroke*, vol. 20, no. 1, pp. 2-11, 2018, 10.5853/jos.2017.02894.

[42]   C. A. Pope III, R. T. Burnett, M. J. Thun, E. E. Calle, D. Krewski *et al.*, "Lung Cancer, Cardiopulmonary Mortality, and Long-Term Exposure to Fine Particulate Air Pollution," *JAMA*, vol. 287, no. 9, pp. 1132-1141, 2002.

[43]   EPA, "Criteria Air Pollutants," 2018. [Online] Available: https://www.epa.gov/criteria-air-pollutants, Accessed On: June 3, 2020.

[44]   J. H. Seinfeld and S. N. Pandis, *Atmospheric Chemistry and Physics: From Air Pollution to Climate Change*. New York, NY, USA: John Wiley & Sons, 1998, pp. 1-1326.

[45]   EPA, "Initial List of Hazardous Air Pollutants with Modifications," 2020. [Online] Available: https://www.epa.gov/haps/initial-list-hazardous-air-pollutants-modifications, Accessed On: June 4, 2020.

[46]   EPA, "Introduction to Indoor Air Quality," 2020. [Online] Available: https://www.epa.gov/indoor-air-quality-iaq/introduction-indoor-air-quality, Accessed On: June 3, 2020.

[47]   A. P. Jones, "Indoor Air Quality and Health," *Atmos. Environ.*, vol. 33, pp. 4535-4564, 1999.

[48]   T. Tanaka-Kagawa, S. Uchiyama, E. Matsushima, A. Sasaki, H. Kobayashi *et al.*, "Survey of Volatile Organic Compounds Found in Indoor and Outdoor Air Samples from Japan," *Bull. Natl. Inst. Health Sci.*, vol. 123, pp. 27-31, 2005.

[49]   EPA, *America's Children and the Environment, Third Edition*. Research Triangle Park, NC, USA: U.S. EPA, 2013, pp. 1-390.

[50]   European Collaborative Action, "Urban Air, Indoor Environment, and Human Exposure, Environment and Quality of Life, Report No. 22, Risk Assessment In Relation to Indoor Air Quality," European Commission, Joint Research Centre, Brussels, Belgium, EUR 19529 EN, 2000.

[51]   EPA, "Technical Overview of Volatile Organic Compounds," 2017. [Online] Available: https://www.epa.gov/indoor-air-quality-iaq/technical-overview-volatile-organic-compounds, Accessed On: June 4, 2020.

[52]   WHO, *WHO Guidelines for Indoor Air Quality, Selected Pollutants*. Copenhagen, Denmark: WHO Regional Office for Europe, 2010, pp. 1-454.

[53]   USA, "OSH Act of 1970," Public Law 91-596, Dec. 29, 1970.

[54]   Construction Safety Council, *Health Hazards in Construction*. Hillside, IL, USA: Construction Safety Council, 2012, pp. 1-247.

[55]   OSHA, "Chemical Hazards and Toxic Substances," 2020. [Online] Available: https://www.osha.gov/SLTC/hazardoustoxicsubstances/, Accessed On: June 4, 2020.

[56]   CDC, "Chemicals: Managing Chemical Safety in the Workplace," 2017. [Online] Available: https://www.cdc.gov/niosh/chemicals/default.html, Accessed On: June 4, 2020.

[57]   R. Andrews and P. F. O'Connor, *NIOSH Manual of Analytical Methods (NMAM), Fifth Edition*. Washington D.C., USA: CDC, NIOSH, 2020.

[58]   OSHA, "Sampling and Analysis," 2020. [Online] Available: https://www.osha.gov/SLTC/samplinganalysis/index.html, Accessed On: June 4, 2020.

[59]   OSHA, "OSHA Technical Manual," 2020. [Online] Available: https://www.osha.gov/dts/osta/otm/, Accessed On: June 4, 2020.

[60]   EU, "The Protection of the Health and Safety of Workers from the Risks Related to Chemical Agents at Work," Council Directive 98/24/EC, April 7, 1998, pp. 1-22.

[61]   EU, "Establishing Indicative Limit Values by Implementing Council Directive 80/1107/EEC on the Protection of Workers From the Risks Related to Exposure to Chemical, Physical and Biological Agents at Work," Commission Directive 91/322/EEC, May 29, 1991, pp. 1-3.

[62]   WHO, "WHO Global Ambient Air Quality Database," 2018. [Online] Available: https://www.who.int/airpollution/data/cities/en/, Accessed On: June 2, 2020.

[63]   M. Eeftens, R. Beelen, K. de Hoogh, T. Bellander, G. Cesaroni *et al.*, "Development of Land Use Regression Models for PM2.5, PM2.5 Absorbance, PM10, and PMCoarse in 20 European Study Areas; Results of the ESCAPE Project," *Environ. Sci. Technol.*, vol. 46, pp. 11195-11205, 2012, 10.1021/es301948k.

[64]   J. D. Marshall, E. Nethery, and M. Brauer, "Within-Urban Variability in Ambient Air Pollution: Comparison of Estimation Methods," *Atmos. Environ.*, vol. 42, pp. 1359-1369, 2008, 10.1016/j.atmosenv.2007.08.012.

[65]   M. Gao, J. Cao, and E. Seto, "A Distributed Network of Low-Cost Continuous Reading Sensors to Measure Spatiotemporal Variations of PM2.5 in Xi'an, China," *Environ. Pollut.*, vol. 199, pp. 56-65, 2015, 10.1016/j.envpol.2015.01.013.

[66]   M. Masiol, S. Squizzato, D. Chalupa, D. Q. Rich, and P. K. Hopke, "Spatial-Temporal Variations of Summertime Ozone Concentrations Across a Metropolitan Area Using a Network of Low-Cost Monitors to Develop 24 Hourly Land-Use Regression Models," *Sci. Total Environ.*, vol. 654, pp. 1167-1178, 2019, 10.1016/j.scitotenv.2018.11.111.

[67]   R. N. Colvile, E. J. Hutchinson, J. S. Mindell, and R. F. Warren, "The Transport Sector as a Source of Air Pollution," *Atmos. Environ.*, vol. 35, pp. 1537-1565, 2001.

[68]   M. Gerboles, D. Buzica, L. Amantini, and F. Lagler, "Laboratory and Field Comparison of Measurements Obtained Using the Available Diffusive Samplers for Ozone and Nitrogen Dioxide in Ambient Air," *J. Environ. Monit.*, vol. 8, pp. 112-119, 2006, 10.1039/B511271K.

[69]   W. F. Cheung, T. H. Lin, and Y. C. Lin, "A Real-Time Construction Safety Monitoring System for Hazardous Gas Integrating Wireless Sensor Network and Building Information Modeling Technologies," *Sensors (Basel)*, vol. 18, pp. 1-24, 2018, 10.3390/s18020436.

[70]   M. Loh, D. Sarigiannis, A. Gotti, S. Karakitsios, A. Pronk *et al.*, "How Sensors Might Help Define the External Exposome," *Int. J. Environ. Res. Public Health*, vol. 14, pp. 1-14, 2017, 10.3390/ijerph14040434.

[71]   W. Y. Yi, K. M. Lo, T. Mak, K. S. Leung, Y. Leung, and M. L. Meng, "A Survey of Wireless Sensor Network Based Air Pollution Monitoring Systems," *Sensors (Basel)*, vol. 15, pp. 31392-31427, 2015, 10.3390/s151229859.

[72]   L. Morawska, P. K. Thai, X. Liu, A. Asumadu-Sakyi, G. Ayoko *et al.*, "Applications of Low-Cost Sensing Technologies for Air Quality Monitoring and

Exposure Assessment: How Far Have They Gone?," *Environ. Int.*, vol. 116, pp. 286-299, 2018, 10.1016/j.envint.2018.04.018.

[73] S. Steinle, S. Reis, and C. E. Sabel, "Quantifying Human Exposure to Air Pollution – Moving from Static Monitoring to Spatio-Temporally Resolved Personal Exposure Assessment," *Sci. Total Environ.*, vol. 443, pp. 184-193, 2013, 10.1016/j.scitotenv.2012.10.098.

[74] R. Baron and J. Saffell, "Amperometric Gas Sensors as a Low Cost Emerging Technology Platform for Air Quality Monitoring Applications: A Review," *ACS Sens.*, vol. 2, pp. 1553-1566, 2017, 10.1021/acssensors.7b00620.

[75] EPA, "Sensor Evaluation Report," U.S. EPA, Office of Research and Development, National Exposure Research Laboratory, EPA/600/R-14/143, 2014.

[76] EPA, "Research and Development Highlights: Mobile Sensors and Applications for Air Pollutants," U.S. EPA, EPA/600/R-14/051, 2013.

[77] EPA, "Air Sensor Guidebook," U.S. EPA, Office of Research and Development, National Exposure Research Laboratory, EPA/600/R-14/159, 2014.

2 AIR QUALITY MONITORING: GOLD STANDARDS AND STATE OF THE ART

2.1 Introduction

Air quality measurements have a rich history going back almost 200 years. For example, regular ozone measurements date back as early as the 1850s. Christian Friedrich Schönbein (1799-1868) was the first to isolate ozone and develop a simple, semi-quantitative test for its measurement [78-81]. He coated filter paper with a paste made from potassium iodide and starch. Iodide oxidizes to iodine in the presence of ozone, which in turn forms a blue complex with starch. A standardized numbering system (0-10) was used to rate the degree of color change. This colorimetric method employing "Schönbein paper", as it was called, spread throughout Europe, Australia, and North America. By the end of the 19th century commercially available Schönbein paper was being used at over 300 monitoring sites worldwide [79, 81].

Despite the success of this technique for its time, there were notable problems. For one, the test was only semi-quantitative and relied on a user's visual acuity to judge color change. It was also noted that airflow and humidity affected sensitivity [79, 80]. Another drawback was exposing Schönbein paper to ambient air typically lasted several hours and it correlated with the exposure maximum instead of the average concentration [78, 79]. Many scientists recognized these problems and over time the first quantitative test for ozone was developed and improved to the point that starting in 1876 regular measurements were taken at the Montsouris Observatory in Paris, France [79, 81]. This new method bubbled air samples through a solution containing arsenite. Ozone stoichiometrically oxidizes arsenite to arsenate, and the amount converted was calculated by colorimetric

titration. Improvements were continually made over the years to eliminate and correct for interferents. Still though, the process was labor intensive and could not provide real-time, continuous monitoring. Eventually, solid-state electronics and computers made it possible to develop instrumental analyzers that replaced these tedious wet chemical methods. By the 1970s chemists were measuring ozone with chemiluminescent analyzers that required much simpler operation and were capable of real-time, continuous monitoring. At the end of that decade most chemiluminescent analyzers had already been superseded by an even simpler method, ultraviolet (UV) absorption, which is still being used today [82].

This evolution of tedious wet chemistry techniques to more practical instrumental analyzers is true of many pollutants, as evidenced by the chronology of approved methods published by the EPA [82-84]. Today there are thousands of gas-phase sampling methods and approved instruments published by agencies around the world to best standardize measurements for ambient air quality, IAQ, emissions, and worker safety [55-59, 85-89]. Many instrumental techniques considered the gold standard for quantifying their respective analyte can sample air directly without pre-treatment, like in the case of UV-absorbance photometry for ozone [90, 91]. Others still require manual capture and chemical treatments before laboratory analysis is possible [81, 92]. In some cases, where there is great need, the entire manual operation has been automated [93]. The purpose of these gold standard methods is to provide the most accurate and reliable measurements possible; otherwise the quality of the data could be questioned and its meaning would be left up to interpretation (as was the case with Schönbein paper). Of course, the drawback is many of these techniques come at a high cost, require personnel with extensive training, and necessitate sophisticated instruments that are large and power hungry. This precludes their use in many

practical applications for health, safety, and the environment. Low-cost gas sensors have the ability to succeed in these areas, but it is important to understand how they contrast with their gold standard counterparts. The next section will introduce a few of the most common classes of gold standard techniques with specific examples. The techniques to be briefly covered are gas chromatography (GC), photometry, the handheld photoionization detector (PID), and sorption methods. All of these techniques can be found in official methods published by regulatory agencies, like the EPA for example. The section afterwards will discuss state-of-the-art, COTS, low-cost gas sensors for monitoring pollutants and harmful chemicals. The most common classes, metal oxide semiconductor (MOS), pellistor/catalytic bead sensor (CBS), amperometric electrochemical sensor (ECS), and portable colorimetric tube (PCT) will be presented. This will provide an overview of the current state of affairs in gas-phase pollution sensing and highlight the motivation and steps that must be taken to close the gap between these two distinct groups.

2.2 Gold Standard Gas-Phase Measurement Techniques

2.2.1 Gas Chromatography

Chromatography is unrivaled in the analysis of complex multicomponent mixtures and is used in all scientific fields. In principle, it can separate any combination of molecules in a sample including even isomers and enantiomers [94]. A sample is dissolved in a mobile phase and forced through an immiscible stationary phase which is fixed in place in a column or on a solid surface. As the analyte moves through the column it partitions between the mobile and stationary phases. Each chemical component partitions to a different degree and as a consequence the sample components separate into discrete bands that can be

individually identified and quantified by a detector at the end of the column [95]. In GC

the mobile phase is an inert carrier gas, such as H_2, He, or N_2. The sample, a gas or volatile

liquid, is injected at a port that introduces it into the column for separation. Programmed

temperature ramps at the injection port and column enhances separation and detection.

Compounds can be identified by their retention time as they leave the column [96]. A huge

variety of refined and more advanced methods have been developed that utilize sorbent

materials, cryogenic temperatures, and multiple columns in tandem (multi-dimensional

GC) to further lower detection limits and separate difficult mixtures [94, 97, 98]. A wide

array of detectors are available depending on the analyte of interest. Some of the most

common in air analysis are the flame ionization detector (FID, hydrocarbons and other

organics), thermal conductivity detector (TCD, anything with different thermal

conductivity than the carrier gas), photoionization detector (PID, typically organics with

ionizable functional groups), flame photometric detector (FPD, sulfur and phosphorus

compounds), electron capture detector (ECD, halogenated hydrocarbons), and mass

spectrometry (MS, anything above mass/charge ratio cutoff) [99-101]. An added advantage

to MS is it can speciate difficult to identify analytes by their unique fragmentation spectra

[98, 102, 103]. Figure 2.1 shows a simplified schematic of a gas chromatograph.
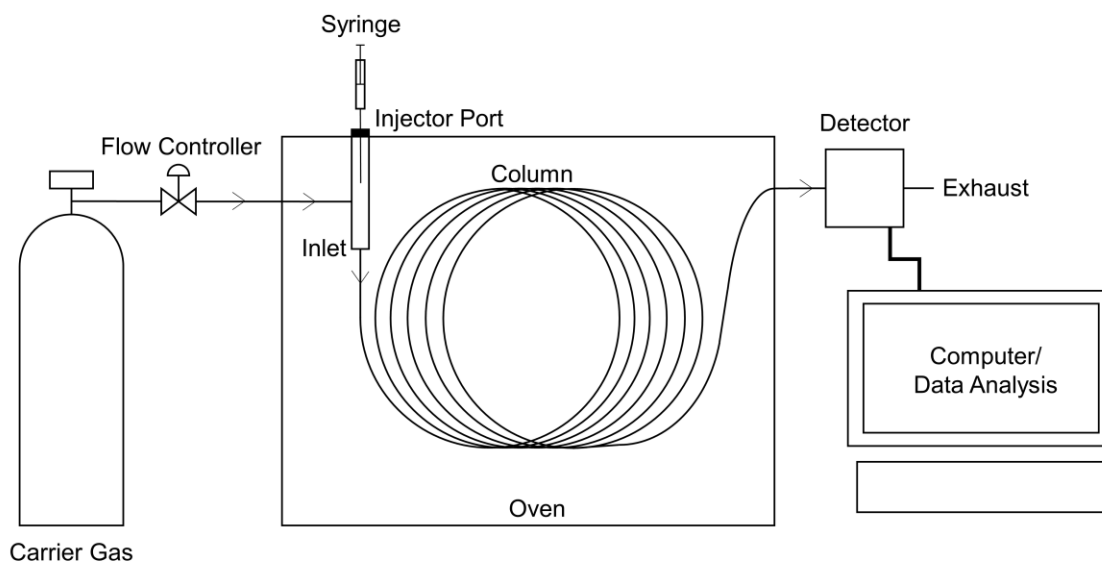
Figure 2.1 Simplified schematic of gas chromatograph with labeled components.

One notoriously difficult challenge in air quality was identifying and individually quantifying the hundreds to thousands of VOCs present in air samples [81, 91]. This seemingly monumental task though is now routinely accomplished by GC coupled with either FID or MS detectors (these are most typical). Highly reliable columns give reproducible elution times and has allowed creation of vast libraries to support users in identifying compounds (and also mass spectra libraries when using MS) [94]. GC with the appropriate detector has such excellent detection limits, separation capability, and reproducibility that it is favored by many regulatory agencies when developing standardized measurement methods for difficult mixtures [100, 102]. The drawbacks though are very high cost (>$100k USD), high complexity (requires highly trained personnel and continual attention/adjustments/calibration), large size, and power inefficiency [91, 100]. Another disadvantage is many techniques require sampling and pre-

concentration which makes it an indirect analytical method rather than direct, and makes it more labor intensive compared with instruments that sample from air directly [94]. This ultimately limits its use from many applications where GC separation capabilities would be ideal. Work is being done to develop micro-GC systems that are portable, lower cost, and power efficient but it is still an area of active research and not yet reliable or commercially available [99, 104].

2.2.2 Photometry

In the most general sense, photometry is the measurement of light. Photometric instruments for quantifying trace gases make use of fluorescence, chemiluminescence, and absorption. For example, four of the six criteria pollutants may be monitored using photometric instrumentation [82]. Sulfur dioxide can be detected by UV-fluorescence, carbon monoxide by gas-correlation filter non-dispersive infrared (GCF-NDIR), nitrogen dioxide (and simultaneously nitric oxide) by chemiluminescence, and ozone most commonly by UV-absorption [81, 82, 91, 100]. These instruments are simpler and less expensive than GC, provide continuous real-time monitoring, and sample ambient air directly without pre-treatment. Demand for instruments that are robust against varying environmental conditions, humidity, and common interfering gases has driven innovation in their design so that now these commonly used methods are all highly accurate, precise, and selective. Although these techniques are refined they still have limitations. Cost, size, and power consumption still limit utility outside of fixed air quality monitoring sites and source emissions testing [100].

Figure 2.2 A commercially available Model 202 UV-absorbance ozone monitor by 2B Technologies Inc.

UV-absorbance is the most widely accepted method for monitoring ozone (and is used in chapter 3 as a reference method) [105, 106]. Figure 2.2 shows a commercially available UV-absorbance ozone analyzer. The technique passes 254 nm UV light from a low-pressure mercury lamp through ambient air being pumped through an optical detection cell. Ozone conveniently absorbs at 254 nm. As the UV light exits the detection cell it passes through an optical filter centered at 254 nm and its intensity is measured by a photodiode [105-107]. Not many other gases absorb at this wavelength, but there is potential positive interference from environments with lots of aromatic VOCs or trace mercury vapor [106, 108]. Humidity can scatter UV light and result in negative interference [109]. To calculate absorbance and remove potential interferents a reference measurement is needed with ozone removed and all other gases present. To achieve this an ozone scrubber is employed that uses Hopcalite or MnO_2 to selectively remove ozone [106, 108].

21

A valve switches between sampling ambient air into the detection cell and sampling ambient air that has passed through the scrubber. Both streams pass through a section of Nafion tubing before entering the detection cell to guarantee the humidity in the sampled air and scrubbed air are equivalent [107, 109]. Figure 2.3 shows a schematic for a UV-absorbance ozone analyzer. Using the Beer-Lambert Law, equation 2.1, the absorbance and concentration of ozone can be calculated from the ratio of sampled air intensity and scrubbed reference air intensity [110].

$$A = -\text{Log}_{10}\left(\frac{I}{I_0}\right) = \varepsilon cl \tag{2.1}$$

Here A is absorbance, I is the intensity of the air sampled directly, I_0 is the intensity of the scrubbed reference measurement, ε is the molar absorptivity of ozone, c is the concentration of ozone, and l is the path length of the optical detection cell. Pressure and temperature in the detection cell is used with the ideal gas law to convert the concentration of ozone to a mixing ratio, usually parts per billion by volume (ppbv or simply ppb) [111]. An advantage to this method is that it is absolute, meaning it measures the concentration of ozone directly by relying on the molar absorptivity value ε [108]. Theoretically no calibration is necessary, but non-linearity in the photodiode response and electronics can result in small measurement error. Therefore, a calibration is performed against a NIST-traceable standard ozone spectrophotometer to determine small offset and slope correction factors [107].
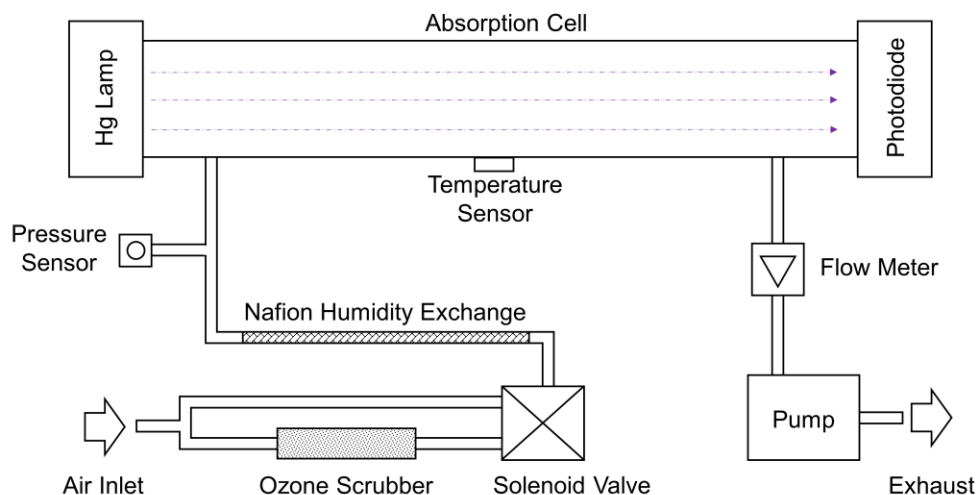
Figure 2.3 Simplified schematic of UV-absorbance ozone monitor with labeled components.

There is no question that UV-absorbance for ozone has evolved spectacularly into a powerfully robust technique for ambient air monitoring compared with its colorimetric predecessors (ie. Schönbein paper and arsenite/arsenate titration). Even it has disadvantages though. Cost, size, and power consumption prevent adoption in personal monitoring and high-density urban monitoring networks. Progress has been made in developing handheld UV-absorbance ozone monitors, but the requisite path length for the detection cell and power necessary for the UV-source (typically mercury lamp) limit the extent of miniaturization and mobility, not to mention cost [90].

2.2.3 Handheld Photoionization Detector

A need to detect VOCs drove the development of the ionization detector. First came the FID, which requires a hydrogen flame. Ions formed in the flame could be measured as

a current between two biased electrodes [112]. There was a desire for a portable device that could be used in the field though, and this approach was not practical since it requires a source of hydrogen gas (ie. compressed cylinder). It is also a fire and explosive hazard in certain atmospheres. The breakthrough came with the first commercially available portable PID in 1974 [113]. Figure 2.4 shows a commercially available handheld PID. Instead of a hydrogen flame, this detector uses UV light to ionize a target gas. The freed electron and generated radical cation accelerate towards biased electrodes and the resulting photocurrent is proportional to the concentration of gas present [113, 114]. Figure 2.5 is a diagram of the internal components and working principle of a PID. This detector is considered non-selective, or broadband, because it will detect any gas with an ionization energy below the photon energy of the UV source. A typical lamp is low-pressure krypton with 10.6 eV photon energy. Other common sources are 9.6 eV and 11.7 eV. The lamp choice will determine the selectivity and sensitivity of the PID, with greater energy photons ionizing more types of gases and therefore being less selective [115]. None of the lamps are energetic enough to ionize major atmospheric components like N_2, O_2, CO_2, or Ar so they can operate in ambient air. This technique is considered non-destructive because the majority of ionized molecules are reduced back to their neutral state at the cathode [116].

Figure 2.4 A commercially available handheld MiniRae Lite PID monitor by RAE Systems Inc.
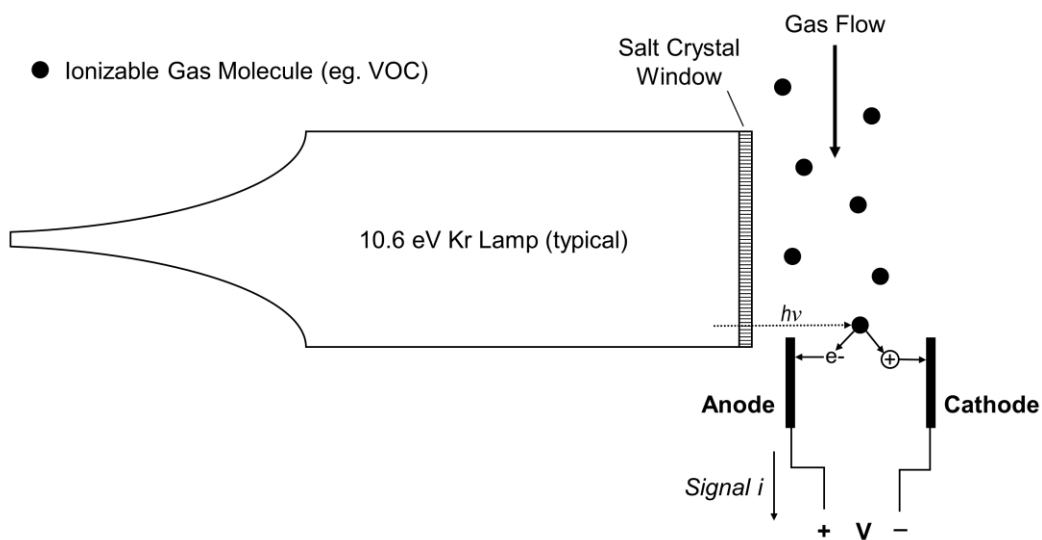
Figure 2.5 Simplified diagram of the PID working mechanism and critical internal components.

In chapter 3 a PID is used as a portable reference method to estimate total VOCs (TVOC) during field testing. The PID can be used this way because it is sensitive to most types of VOCs and its response will be a summation of all ionizable gases present (mostly, if not exclusively, VOCs in the environments tested). There are many instances in the literature of PIDs being used to estimate TVOC. Examples of the wide variety of settings include retail stores, daycare centers, photocopy centers, and dense urban areas to list just a few [117-120]. Response times of only a few seconds and high rates of data acquisition together with mobility make mapping out spatiotemporal variations in an environment possible. Leak and spill detection, industrial hygiene, environmental remediation, and hazardous waste monitoring all benefit from PIDs [113]. The EPA even calls for use of a PID in monitoring fugitive emissions in pipelines and chemical processing equipment [83]. The limitation with this type of instrument is the same as the photometric and portable photometric instruments mentioned in the previous section. The hardware (eg. UV lamp) inherently limits miniaturization, cost reduction, and power efficiency. The handheld devices are too bulky and heavy to use as a wearable personal exposure monitor, for instance. At a few thousand dollars (USD) they will always be limited to industrial and research activities. In addition to these issues a PID is only useful when non-selectivity is not a problem either.

2.2.4 Sorbent Methods

The criteria pollutants all have well refined instrumental methods that conveniently sample ambient air directly, but many other organic and inorganic pollutants that make up the HAPs, common indoor air pollutants, or volatile chemicals and solvents found in

26

industrial settings may require more laborious procedures [57-59, 83, 86, 88]. In many

cases sorbent materials are used to pre-concentrate the analyte of interest by either active

(ie. requires flow, pumping) or passive (ie. diffusion) sampling [81, 91, 99, 100]. Sorbents

are materials with very high active surface areas like silica gel, activated carbon, alumina,

zeolites, and molecular sieves. They are typically packed in tubes or filter cartridges and

the sorbent may be coated with a chemical to enhance specificity towards the analyte like

sodium fluoride, sulfuric acid, phosphoric acid, oxalic acid, or sodium carbonate [92, 121].

A related system that functions quite similarly is the denuder sampling tube, which is a

glass tube coated with chemical layer(s) to enhance adsorption and capture analytes in

sequential zones [93]. For any of these trapping systems a sampling period can last for

minutes up to months long. After sampling the analyte must be desorbed. This is usually

done by aqueous or organic washing, but sometimes thermal desorption is used [93, 122].

Now the gaseous analyte is concentrated and trapped in a liquid medium where it can be

chemically modified to facilitate detection (except in the case of thermal desorption where

its concentrated vapors are drawn directly into an instrument). Common detection

techniques are GC, high-pressure liquid chromatography (HPLC), ion chromatography,

UV-Vis-NIR spectrophotometry, and wet chemical titrations [91, 92]. These techniques

are designed to be very sensitive (low detection limit) and most importantly very selective,

so the data is high quality when done right. The disadvantages are they require tedious

manual labor with many opportunities for error, highly trained personnel, harmful

chemicals, and often expensive instrumentation. They also do not provide the fine temporal

resolution of the photometric analyzers that sample air continuously. There are many

opportunities for developing new sensing technologies where the only reference methods

available are these slow procedures. Figure 2.6 shows examples of commercially available sorbent tubes.
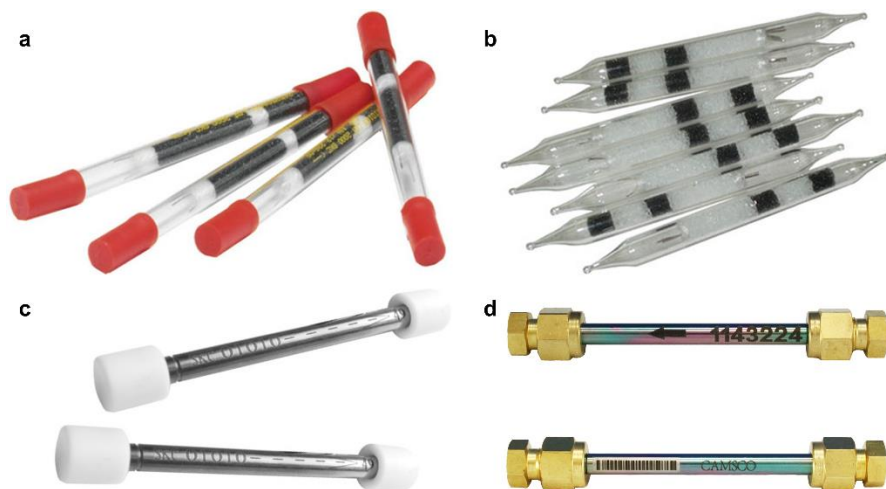
Figure 2.6 Various commercially available sorbent packed gas sampling tubes: (a) Casella charcoal in glass, (b) Casella silica gel in glass, (c) SKC Tenax in stainless steel, and (d) Camsco Carbopack in stainless steel.

Ammonia is an example of a well-known chemical that does not have a refined instrumental method available for its measurement. Ammonia plays an important role in the chemical and fertilizer industries, and is also used as a refrigerant. Outdoors it gets into the atmosphere primarily through agriculture, livestock, and biogenic sources. It also plays an important role in secondary particle formation [123]. For these reasons it is important to be able to take accurate measurements of ammonia from the air we breathe. Published methods for detection of gaseous ammonia all use sorbent tubes treated with an acid to trap the ammonia (NH_3) as ammonium (NH_4^+). Then subsequent washing and identification can be performed at a laboratory by a technician. NIOSH methods 6015 and 6016 prescribe the use of visible absorption spectroscopy and ion chromatography for detection,

28

respectively [124, 125]. Both of these methods require generation of standard solutions for washing and chemically modifying ammonia, and calibration standards for the instruments. The process is slow and would benefit from a new sensing methodology. Chapters 4 and 5 describe two novel approaches for developing a new mobile optoelectronic chemical detection platform with gaseous ammonia used as an example.

2.3 State-of-the-Art Commercially Available Gas Sensors

2.3.1 Metal Oxide Semiconductor

MOS are the best studied group of gas sensors. High sensitivity, rapid response, and reversibility have made them popular as a potential emerging technology for many sectors [126]. Furthermore, their ability to be manufactured in large batches using micro-electromechanical systems (MEMS) fabrication technology makes mass production easy, keeps costs low, and lends them to being small in size [126, 127]. The sensor exploits the catalytic properties of certain metal oxides towards oxidizing and reducing gases as variations in electrical conductivity [128]. N-type MOS are the most common, like SnO_2, In_2O_3, and ZnO. In manufacturing, thin films can be prepared by a variety of techniques, including chemical vapor deposition (CVD) and physical vapor deposition (PVD) methods [129]. The MOS sensing layer has a high active surface area, sometimes even nanocrystalline and porous, which imparts its excellent sensitivity to trace gases [130]. Films are deposited over interdigitated electrodes on an electrically insulating layer to make resistance measurements possible. The other side of the insulator has a heating element to form a microhotplate. The entire assembly can be part of a larger substrate for mechanical support depending on the MEMS fabrication process [131]. Figure 2.7 shows

29

the basic working components of a MOS gas sensor and two examples of commercially available products that are used in chapter 3 for measuring ozone and VOCs.
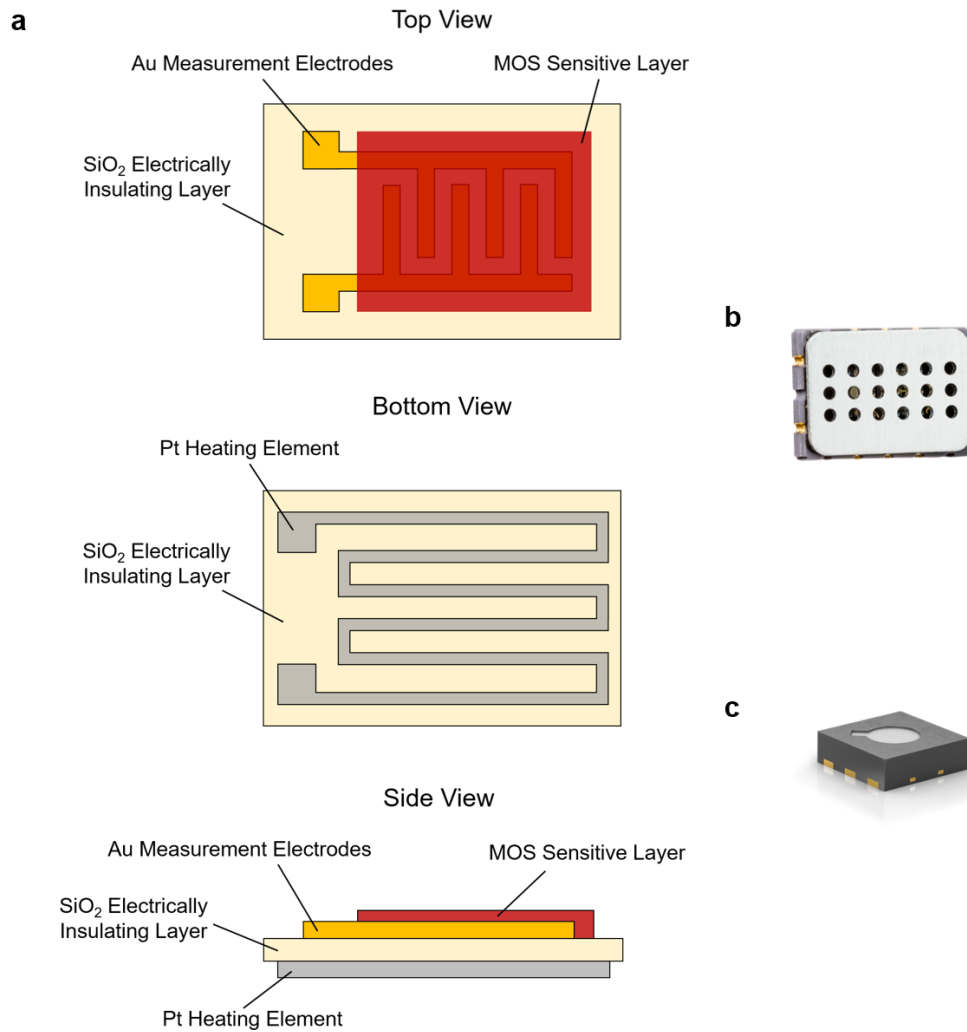
Figure 2.7 (a) Components of a MOS gas sensor. (b) SGX Sensortech MiCS-2614 Ozone Sensor. (c) Sensirion SGPC3 TVOC sensor.

The mechanism for the change in resistance of the MOS in response to different gases is dependent on the adsorption and desorption of charged surface states. At a typical operating temperature of 200-400°C atmospheric oxygen chemisorbs onto the MOS surface, dissociates into atomic oxygen, and traps electrons from the conduction band at

the surface [132]. A buildup of net negative charge on the surface creates a depletion layer, or space charge region, extending inward toward the bulk [128, 129]. In an n-type semiconductor this layer which is deficient in mobile electron charge carriers has a higher resistance than the bulk (the opposite is true for p-type MOS). The distance the electric field penetrates into the bulk and forms a depletion layer can be characterized by the Debye length. Across this distance the energy of the conduction band bends upward by qV_s [131]. This is the additional potential energy necessary for an electron in the bulk to travel to the negatively charged surface and ultimately into a neighboring crystallite. At every crystallite-crystallite junction (ie. grain boundaries) there is a Schottky-like potential barrier the electron has to overcome to travel through the MOS film. The overall effect is MOS resistance is greater at the elevated working temperature with chemisorbed oxygen ions. Other gases besides oxygen can influence surface states too [127, 130]. A molecule with its lowest unoccupied molecular orbital below the Fermi level is an electron acceptor, or oxidizing gas (eg. ozone, NO_2), and withdraws more electrons from the conduction band. This increases the width of the depletion layer which increases MOS resistance. A molecule with its highest occupied molecular orbital above the Fermi level is an electron donor, or reducing gas (eg. VOCs, CO, H_2), and donates electrons back to the conduction band by reacting with and removing surface bound oxygen. This decreases the width of the depletion layer which decreases MOS resistance [132]. For these reasons the conductometric response of a MOS gas sensor is highly dependent on the structure and morphology of the film. Figure 2.8 shows energy diagrams for an electron traversing through multiple crystallites and the band bending effect extending from the surface into the bulk.

31
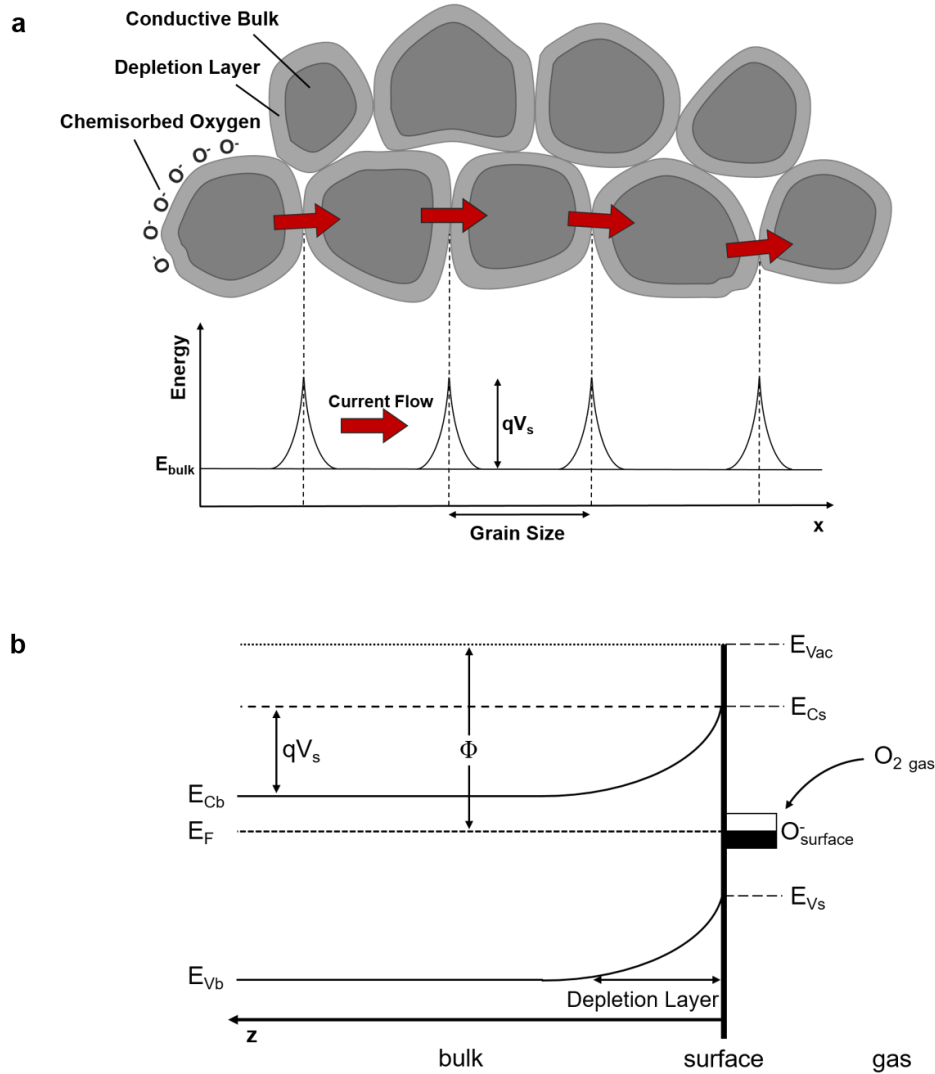
Figure 2.8 (a) Energy diagram for an electron following the path of the arrows through potential energy barriers, qV_s, at each grain boundary due to band bending. (b) Energy diagram along z-axis extending from the surface into the bulk of a MOS crystallite. Oxygen ionosorbs and traps an electron at the Fermi level, E_F, on the surface. This generates a depletion layer with net positive charge to balance the negative surface charge. The conduction and valence bands in the bulk, E_{Cb} and E_{Vb}, are each band bending upward by qV_s. Their respective surface values are E_{Cs} and E_{Vs}. Φ is the work function.

The catalytic mechanism for interacting with oxidizing and reducing gases makes MOS a nonselective, broadband type sensor. Fine tuning the type of metal oxide, dopants, structure/morphology, operating temperature, and measurement mode (eg. DC resistance,

32

AC impedance) can improve selectivity and other sensing characteristics, but to date there is no perfectly selective MOS [130]. Even ambient humidity leads to adsorbed water interfering with surface states and conductivity [131]. In some cases filters (eg. charcoal, zeolite) are placed over the MOS to improve selectivity [129]. The large number of potential interferents is just one of the many pitfalls of MOS gas sensors. Another is their intrinsic nonlinear response, which can be approximated (in the simplest cases) with a root power law [130]. Sensors with a linear response are always most practical for having the simplest calibration and best confidence intervals/estimation capabilities compared with more complex models. Finally, the elevated temperature of MOS sensors creates many problems. Mainly they are power consumption, difficulty maintaining a stable operating temperature, and the thermally driven degradation of all MOS components that manifests as drift [133-135]. One promising area of innovation is shifting MOS fabrication from MEMS processes to CMOS processes. This allows MOS to be even smaller, more thermally efficient, and therefore more power efficient. The "CMOS" gas sensor is also capable of onboard computing and digital output [134, 136]. Regardless of their drawbacks though, MOS are still an excellent choice of COTS gas sensor when small size is key. Chapter 3 goes into detail on the construction and calibration of a wearable device using MOS sensors for ozone and TVOC measurements.

2.3.2 Pellistor/Catalytic Bead Sensor

The CBS, also known as a pellistor, has been used to detect combustible gases for several decades. It was initially implemented for monitoring gas in coal mines and actually replaced the canaries they had been using for a long time [137]. A resistive platinum

heating element is embedded in a small catalytic metal or metal oxide pellet (eg. Pt, Pd, Th compounds). The pellet is kept at a stable operating temperature, usually 400-600°C, by passing current through the embedded resistor. When a combustible gas contacts the catalytic surface it oxidizes in an exothermic reaction and increase the temperature of the pellet [138, 139]. Platinum has a positive coefficient of temperature resistance (C_t) so its electrical resistance increases with increasing temperature [137]. A reference pellet kept at the same operating temperature without any catalyst (so it is inert) is combined in series with the sensing pellet as part of a Wheatstone bridge. In clean air the bridge is balanced, but in a combustible gas the bridge becomes imbalanced and an output voltage can be measured [140]. Since the platinum electrical resistance-temperature relationship is linear across 500-1000°C (constant C_t) the change in measured potential at the bridge is linearly proportional to the concentration of combustible gas [137]. Figure 2.9 shows two commercially available CBS and a diagram of the sensing pellets in series.

CBS are cheap, sensitive, and have a linear response, all of which make them easy to use. Their applications are limited though since they are nonselective to all combustible gases (eg. CO, H_2, CH_4, VOCs) and their detection limits are not very good. This has typically restricted them to alarm systems and lower explosive limit (LEL) monitors for safety measures at industrial sites, petrochemical facilities, and mines [137, 141]. They are also influenced by ambient temperature fluctuations, which can be a problem for portable devices [138]. Catalytic materials can also be subject to inhibition and poisoning by chemicals found at industrial sites, like sulfur-, silicon-, and halogenated-compounds [137]. They operate at a higher temperature than their MOS cousins, are less energy efficient, and bulkier as there has been less pressure to adopt MEMS and CMOS processing

strategies. MOS are also sensitive to a greater variety of gases, while CBS only responds to combustible (ie. reducing) gases. Their one advantage though is a linear response, and some labs have begun to develop more intelligent and energy efficient systems utilizing CMOS fabrication [141].
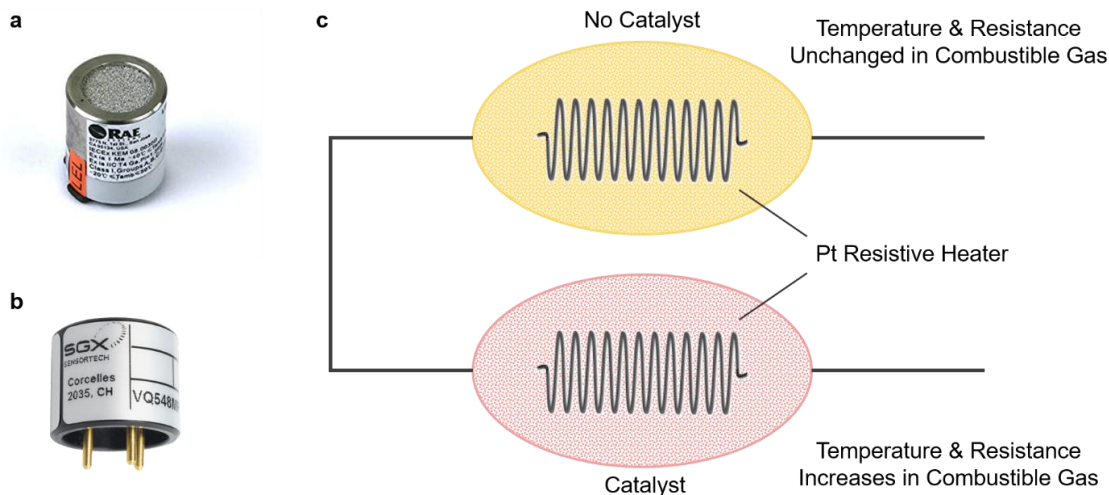
Figure 2.9 Catalytic bead sensors for detecting combustible gases by (a) RAE Systems Inc. and (b) SGX Sensortech. (c) Diagram of the sensing pellet (with catalyst) and reference pellet (without catalyst) in series, which form half of the Wheatstone bridge used to make measurements.

2.3.3 Amperometric Electrochemical Sensor

ECS have been used in many industries as toxic gas sensors since the 1970s and are related to the fuel cell. Gases that can be monitored this way are CO, H_2S, NO, NO_2, O_3, O_2, SO_2, NH_3, HCN, Cl_2, HCl, HBr, HF, CS_2, H_2O_2, H_2, and some VOCs [142, 143]. Besides alarm systems they have had success in commercialized devices like the blood alcohol content (BAC) breathalyzer, domestic carbon monoxide monitor, and handheld devices for industrial work in the field (similar uses as handheld PID). The success of this class of sensor stems from its superior selectivity compared with MOS and CBS, its linear

response, negligible power requirements, and well understood mechanism of detection (amperometry) [143]. An ECS is usually composed of three electrodes, a mineral acid electrolyte (eg. $H_2SO_{4(aq)}$), and a gas permeable membrane. The target gas diffuses through a gas permeable membrane to reach the working electrode (WE). The WE is coated with a high surface area catalyst like a noble metal (eg. Pt) to facilitate an electrochemical reaction. The target gas makes contact with the WE and electrolyte at a 3-phase boundary. There the target gas is either oxidized or reduced depending on the type of ECS. At a counter electrode (CE) the opposite redox reaction takes place to balance the flow of current. A reference electrode (RE) is used to anchor the WE at a desired fixed potential to maintain sensitivity and selectivity. The external circuit is called a potentiostat and uses feedback to supply current through the CE while keeping the WE potential fixed with respect to the RE [144, 145]. Since the kinetics of the electrochemical reaction at the WE are fast compared with diffusion of the gas the overall process is diffusion limited. This means the current being measured between the WE and CE is linearly proportional to the target gas concentration [142]. Figure 2.10 shows two commercially available ECS and a diagram of the major working components.
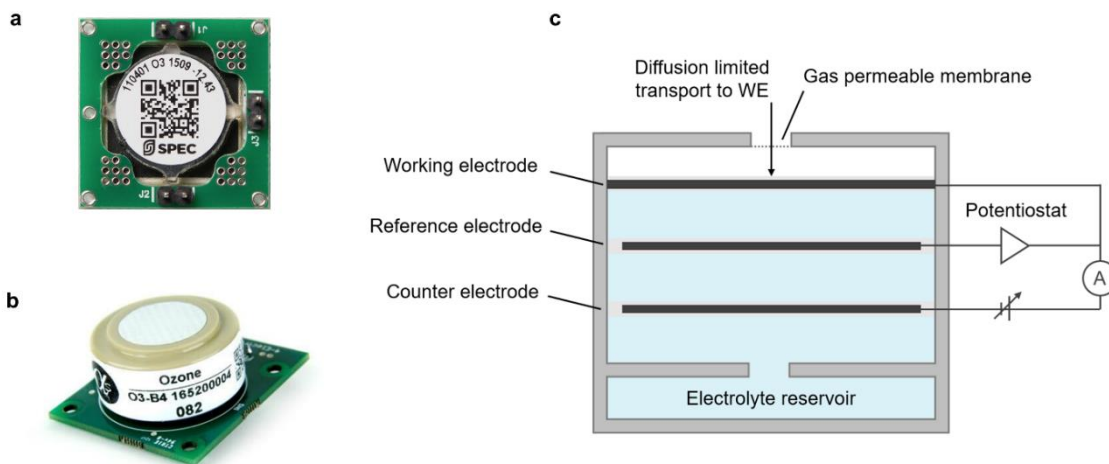
Figure 2.10 Commercially available amperometric electrochemical sensors by (a) SPEC Sensors and (b) Alphasense. (c) Diagram of ECS with important working components labeled.

Although the ECS has higher selectivity compared with MOS and CBS it still suffers from cross-sensitivities in the presence of particularly reactive gases (eg. O_3 with NO_2) and environmental interferences. Moisture can pass in and out of the cell through the gas permeable membrane depending on the relative humidity (RH). This changes the volume of electrolyte, and in both extremes results in sensor failure [146]. Temperature fluctuations change the sensor output and must be corrected for if deploying these sensors in an outdoor environment [147]. Besides modeling this behavior some manufacturers have devised an ECS with a fourth electrode that allows for temperature correction [148]. Other challenges are catalytic poisoning, a limited shelf life (some manufacturers say 6-12 months), and temporal drift [149]. Nevertheless many studies have shown promise in using them in high-density air monitoring networks to assist existing fixed monitoring sites [150,

151]. Unfortunately there are limitations in miniaturization to fit them into wearable devices or existing mobile technology (eg. cellphones, tablets). The geometry of the cell combined with the electrolyte reservoir means ECS cannot be as small as MOS and CBS, especially the newer CMOS fabricated varieties available on the horizon. ECS also requires a more complicated measurement circuit, the potentiostat, which has a larger footprint than the much simpler measurement circuits for MOS and CBS (ie. voltage divider and Wheatstone bridge).

2.3.4 Portable Colorimetric Tube

The first colorimetric detector tube patent in the United States was granted in 1919. A mixture of iodine pentoxide and sulfuric acid impregnated in pumice qualitatively identified carbon monoxide as it was oxidized to carbon dioxide, and the reagent left a color stain [152]. Early tubes were mostly used in confined spaces like the mining industry where CO and H_2S are the main toxic gases. The creation of OSHA regulations in the 1970s prompted development of many more types of colorimetric tubes [153]. Now several companies mass produce PCT for quantifying hundreds of different chemical gases, vapors, and aerosols. Colorimetry is a proven and accepted method that imparts a degree of selectivity, compared to other sensing mechanisms, because it relies on a specific chemical reaction [154]. They are commonly used for emergency response to spills and leaks, hazmat incidents, determining occupational exposure, fire investigations, and many other circumstances that require portable, simple, inexpensive, and most importantly reliable detection methods [152, 153]. PCT are glass tubes filled with a granular carrier solid impregnated with indicating reagents. The tube is hermetically sealed at both ends to

38

protect the reactive indicators inside. Each end must be broken off and the tube is immediately used just one time, then discarded. A predetermined volume of air is passed through the tube by either a hand pump or battery powered pump. Other varieties passively sample by diffusion and can even be worn to estimate average exposure over several hours. A colored stain forms along the length of the tube in proportion to the concentration of the target analyte. Gradations on the tube indicate the concentration of the chemical detected [152, 155]. Figure 2.11 shows an example of four commercially available PCT.

Figure 2.11 Portable colorimetric tubes by RAE Systems Inc. and Draeger for detection on carbon monoxide and benzene.

Although PCT are a proven method they have some limitations and disadvantages. Sampling only covers a small area for a short time. Gases and vapors are dynamic so this is not always ideal. Improper sampling with the pump and user interpretation of the color

stain line can result in erroneous concentration readings. There can also be cross-sensitivities with other gases, especially those with the same chemical functionality (eg. alcohols, aromatics, etc.) [152, 153, 155]. Pre-layers and pre-tubes that scrub interfering compounds and excess moisture work in some instances, but are not always effective. PCT are really best suited to provide semi-quantitative estimates. Errors typically are 10-15% with 25% being considered an industry standard quality limit [154, 156]. This level of error though may be acceptable when detecting for the presence of harmful gases that can occur over several orders of magnitude (eg. spill site, hazmat) to determine the potential for danger.

There are two obvious differences in the operation of PCT versus the other types of gas sensors presented here. The first is the one-time use nature of the tubes. This could be seen as an inconvenience compared with the reversibility of the other sensors. In actuality it is part of what has made these detectors so successful. The one-time use PCT are essentially "factory calibrated" in that the sensing formulation inside the tube is highly controlled during manufacturing and preserved until the glass seal is broken. This dramatically reduces the burden on the user by eliminating the need for calibrations. The second is the requirement of the user's own judgement for determining chemical concentration by gradations along the length of the tube. This keeps cost low and operation simple for intense field work when time is of the essence (eg. emergency response), but it can also introduce error. Chapters 4 and 5 attempt to build on the strengths of the colorimetric approach and improve its weaknesses with the development of a new optoelectronic gas sensing platform. In each of these chapters a consistent, selective formulation for ammonia detection is characterized that allows for multiple sensors to be

produced with the same calibration. The optics read color change of the sensing material directly so there is no user error in taking measurements. The sensors also show the ability to provide continuous real-time measurement by tracking the rate of color change and have reversibility.

2.4 Final Remarks

The differences between gold standard "reference methods" and state-of-the-art commercially available gas sensors is quite obvious. Reference methods were developed with accuracy and precision being foremost in importance. Cost and complexity came second, with prices ranging from approximately $3000 to greater than $100,000 (USD) and highly specialized technicians required for operation and maintenance. This prevents their use beyond a limited number of niche fields. Gas sensors, on the other hand, were designed to have simple operation and be inexpensive, usually less than $10 each. Simple operation does not mean simple information though. The data from these sensors is subject to much scrutiny, because of their susceptibility to interfering gases, changes in the environment, and drift, all while being expected to function with minimal technical intervention. Selecting the best gas sensor for a particular application and calibrating it for an anticipated environment has turned out to be a great challenge for many researchers. Points of contention are the plausibility of data without regular calibration, and in cases where regular calibration may be possible, that its costs will quickly become larger than money saved by using low-cost gas sensors in the first place [157]. Fortunately, knowledge and experience with these types of tools continues to grow and there is starting to be a paradigm shift in acceptance that these sensors will begin to supplement and maybe even

eventually supplant the reference methods. Part of the evidence for this is the amount of attention being given to these sensors by regulatory agencies and councils as realistic next generation technology [72, 75-77, 154, 158, 159]. One exciting area is the development of wearable personal exposure monitors, spurred on by new awareness of the high spatiotemporal variance in pollutants and an increase in asthma and other related health conditions [158]. The next chapter introduces Project 1, which covers the design and testing of a wearable personal exposure monitor using COTS parts, including two MOS gas sensors for detecting ozone and VOCs. The challenges of stabilizing operating temperature, extending battery life, and calibrating for a wide range of environmental conditions all while trying to keep the user experience as simple as possible are discussed in detail.

References

[55]   OSHA, "Chemical Hazards and Toxic Substances," 2020. [Online] Available: https://www.osha.gov/SLTC/hazardoustoxicsubstances/, Accessed On: June 4, 2020.

[56]   CDC, "Chemicals: Managing Chemical Safety in the Workplace," 2017. [Online] Available: https://www.cdc.gov/niosh/chemicals/default.html, Accessed On: June 4, 2020.

[57]   R. Andrews and P. F. O'Connor, *NIOSH Manual of Analytical Methods (NMAM), Fifth Edition*. Washington D.C., USA: CDC, NIOSH, 2020.

[58]   OSHA, "Sampling and Analysis," 2020. [Online] Available: https://www.osha.gov/SLTC/samplinganalysis/index.html, Accessed On: June 4, 2020.

[59]   OSHA, "OSHA Technical Manual," 2020. [Online] Available: https://www.osha.gov/dts/osta/otm/, Accessed On: June 4, 2020.

[72]   L. Morawska, P. K. Thai, X. Liu, A. Asumadu-Sakyi, G. Ayoko et al., "Applications of Low-Cost Sensing Technologies for Air Quality Monitoring and Exposure Assessment: How Far Have They Gone?," Environ. Int., vol. 116, pp. 286-299, 2018, 10.1016/j.envint.2018.04.018.

[75]   EPA, "Sensor Evaluation Report," U.S. EPA, Office of Research and Development, National Exposure Research Laboratory, EPA/600/R-14/143, 2014.

[76]   EPA, "Research and Development Highlights: Mobile Sensors and Applications for Air Pollutants," U.S. EPA, EPA/600/R-14/051, 2013.

[77]   EPA, "Air Sensor Guidebook," U.S. EPA, Office of Research and Development, National Exposure Research Laboratory, EPA/600/R-14/159, 2014.

[78]   J. A. Anel, "Atmospheric Ozone: Historical Background and State-of-the-Art," *Contemp. Phys.*, vol. 57, no. 3, pp. 417-420, 2016, 10.1080/00107514.2016.1156748.

[79]   R. D. Bojkov, "Surface Ozone During the Second Half of the Nineteenth Century," *J. Appl. Meteorol. Climatol.*, vol. 25, no. 3, pp. 343-352, 1986.

[80]   T. Weidinger, G. Baranka, R. Balazs, and K. Toth, "Comparison of 19th Century and Present Concentrations and Depositions of Ozone in Central Europe," *Acta. Silv. Lign. Hung.*, vol. 7, pp. 23-38, 2011.

[81]   K. C. Clemitshaw, "A Review of Instrumentation and Measurement Techniques for Ground-Based and Airborne Field Studies of Gas-Phase Tropospheric Chemistry," *Crit. Rev. Environ. Sci. Technol.*, vol. 34, pp. 1-108, 2004, 10.1080/10643380490265117.

[82]   EPA, "Sampling Methods for Criteria Pollutants," 2020. [Online] Available: https://aqs.epa.gov/aqsweb/documents/codetables/methods_criteria.html, Accessed On: September 1, 2020.

[83]   EPA, "Air Emission Measurement Center: EMC Promulgated Test Methods," 2020. [Online] Available: https://www.epa.gov/emc/emc-promulgated-test-methods, Accessed On: September 2, 2020.

[84]   EPA, "EPA Scientists Develop and Evaluate Federal Reference & Equivalent Methods for Measuring Key Air Pollutants," 2019. [Online] Available: https://www.epa.gov/air-research/epa-scientists-develop-and-evaluate-federal-reference-equivalent-methods-measuring-key, Accessed On: September 3, 2020.

[85]   DEFRA, "Air Quality Monitoring Methods," 2020. [Online] Available: https://uk-air.defra.gov.uk/networks/monitoring-methods, Accessed On: August 30, 2020.

[86]   ISO, "International Organization for Standardization Homepage," 2020. [Online] Available: https://www.iso.org/home.html, Accessed On: August 30, 2020.

[87]   EC, "Implementation of Ambient Air Quality Legislation," 2020. [Online] Available: https://ec.europa.eu/environment/air/quality/assessment.htm, Accessed On: August 30, 2020.

[88]   ASTM, "ASTM Homepage," 2020. [Online] Available: https://www.astm.org/, Accessed On: August 30, 2020.

[89]   Australia NSW, "How We Monitor Air Pollution," 2020. [Online] Available: https://www.environment.nsw.gov.au/topics/air/air-quality-basics/sampling-air-pollution, Accessed On: August 30, 2020.

[90]   P. C. Andersen, C. J. Williford, and J. W. Birks, "Miniature Personal Ozone Monitor Based on UV Absorbance," *Anal. Chem.*, vol. 82, no. 19, pp. 7924-7928, 2010, 10.1021/ac1013578.

[91]   D. D. Parrish and F. C. Fehsenfeld, "Methods for Gas-Phase Measurements of Ozone, Ozone Precursors and Aerosol Precursors," *Atmos. Environ.*, vol. 34, pp. 1921-1957, 2000.

[92]   E. J. Williams, S. T. Sandholm, J. D. Bradshaw, J. S. Schendel, A. O. Langford *et al.*, "An Intercomparison of Five Ammonia Measurement Techniques," *J. Geophys. Res.*, vol. 97, no. D11, pp. 11,591-11,611, 1992.

[93]   M. G. Mennen, B. G. Van Elzakker, E. M. Van Putten, J. W. Uiterwijk, T. A. Regts *et al.*, "Evaluation of Automatic Ammonia Monitors for Application in an Air Quality Monitoring Network," *Atmos. Environ.*, vol. 30, no. 19, pp. 3239-3256, 1996.

[94]   Y. I. Yashin and A. Y. Yashin, "Analytical Chromatography. Methods, Instrumentation and Applications," *Russ. Chem. Rev.*, vol. 75, no. 4, pp. 329-340, 2006, 10.1070/RC2006v075n04ABEH003607.

[95]   D. A. Skoog and J. J. Leary, *Principles of Instrumental Analysis, Fourth Edition*. Philadelphia, PA, USA: Saunders College Publishing, 1992, pp. 579-601.

[96]   D. A. Skoog and J. J. Leary, *Principles of Instrumental Analysis, Fourth Edition*. Philadelphia, PA, USA: Saunders College Publishing, 1992, pp. 605-625.

[97]   F. L. Dorman, E. B. Overton, J. J. Whiting, J. W. Cochran, and J. Gardea-Torresdey, "Gas Chromatography," *Anal. Chem.*, vol. 80, no. 12, pp. 4487-4497, 2008, 10.1021/ac800714x.

[98]   L. N. Williamson and M. G. Bartlett, "Quantitative Gas Chromatography/Time-of-Flight Mass Spectrometry: A Review," *Biomed. Chromatogr.*, vol. 21, pp. 664-669, 2007, 10.1002/bmc.847.

[99]   M. Marc, M. Tobiszewski, B. Zabiegala, M. de la Guardia, and J. Namiesnik, "Current Air Quality Analytics and Monitoring: A Review," *Anal. Chim. Acta*, vol. 853, pp. 116-126, 2015, 10.1016/j.aca.2014.10.018.

[100] M. Marc, B. Zabiegala, and J. Namiesnik, "Mobile Systems (Portable, Handheld, Transportable) for Monitoring Air Pollution," *Crit. Rev. Anal. Chem.*, vol. 42, pp. 2-15, 2012, 10.1080/10408347.2011.607079.

[101] J. Dewulf, H. Van Langenhove, and G. Wittmann, "Analysis of Volatile Organic Compounds Using Gas Chromatography," *Trends Anal. Chem.*, vol. 21, pp. 637-646, 2002.

[102] I. Spanik and A. Machynakova, "Recent Applications of Gas Chromatography with High-Resolution Mass Spectrometry," *J. Sep. Sci.*, vol. 41, no. 1, pp. 163-179, 2018, 10.1002/jssc.201701016.

[103] M. R. Jacobs, E. F. Hilder, and R. A. Shellie, "Applications of Resistive Heating in Gas Chromatography: A Review," *Anal. Chim. Acta*, vol. 803, pp. 2-14, 2013, 10.1016/j.aca.2013.04.063.

[104] J. C. Soo, E. G. Lee, R. F. LeBouf, M. L. Kashon, and W. Chisholm, "Evaluation of a Portable Gas Chromatograph with Photoionization Detector Under Variations of VOC Concentration, Temperature, and Relative Humidity," *J. Occup. Environ. Hyg.*, vol. 15, no. 4, pp. 351-360, 2018, 10.1080/15459624.2018.1426860.

[105] H. Tanimoto, H. Mukai, S. Hashimoto, and J. E. Norris, "Intercomparison of Ultraviolet Photometry and Gas-Phase Titration Techniques for Ozone Reference Standards at Ambient Levels," *J. Geophys. Res.*, vol. 111, D16313, pp. 1-11, 2006, 10.1029/2005JD006983.

[106] E. J. Williams, F. C. Fehsenfeld, B. T. Jobson, W. C. Kuster, P. D. Goldan *et al.*, "Comparison of Ultraviolet Absorbance, Chemiluminescence, and DOAS Instruments for Ambient Ozone Monitoring," *Environ. Sci. Technol.*, vol. 40, no. 18, pp. 5755-5762, 2006, 10.1021/es0523542.

[107] 2B Technologies Inc., "Ozone Monitor: Operation Manual, Model 202, Rev. H," Boulder, CO, USA, 2B Technologies Inc., pp. 1-45, 2015.

[108] 2B Technologies Inc., "UV-Absorbing Interferences in Ozone Monitors," Boulder, CO, USA, 2B Technologies Inc., Technical Note No. 40, pp. 1-6, 2015.

[109] K. L. Wilson and J. W. Birks, "Mechanism and Elimination of a Water Vapor Interference in the Measurement of Ozone by UV Absorbance," *Environ. Sci. Technol.*, vol. 40, no. 20, pp. 6361-6367, 2006, 10.1021/es052590c.

[110] D. A. Skoog and J. J. Leary, *Principles of Instrumental Analysis, Fourth Edition*. Philadelphia, PA, USA: Saunders College Publishing, 1992, pp. 123-147.

[111] 2B Technologies Inc., "Explanation of Temperature and Pressure Corrections in Ozone Measurements of Mixing Ratios," Boulder, CO, USA, 2B Technologies Inc., Technical Note No. 010, pp. 1-3, 2007.

[112] RAE Systems Inc., "Comparison of Photoionization Detectors (PIDs) and Flame Ionization Detectors (FIDs)," San Jose, CA, USA, RAE Systems Inc., Application Note AP-226, 01/04/WH, pp. 1-2.

[113] RAE Systems Inc. The PID Handbook, Theory and Applications of Direct-Reading Photoionization Detectors (PIDs). San Jose, CA, USA. RAE Systems Inc. pp. 1-166, 2013.

[114] S. Mergemeier, I. Ebner, and F. Scholz, "Basic Experimental Studies on the Operation of Photoionization Detectors," *Fresenius J. Anal. Chem.*, vol. 361, pp. 29-33, 1998.

[115] Ion Science, "Technical Overview, PID Explained," Stafford, TX, USA, Ion Science, Advanced Gas Sensing Technologies, Application Article 105, pp. 1-2.

[116] TSI Inc., "Photo-Ionization Detection (PID) Technology," Shoreview, MN, USA, TSI Inc., Application Note TSI-147, Rev. B, pp. 1-3, 2013.

[117] C. Jia, K. Cao, R. Valaulikar, X. Fu, and A. B. Sorin, "Variability of Total Volatile Organic Compounds (TVOC) in the Indoor Air of Retail Stores," *Int. J. Environ. Res. Public Health*, vol. 16, pp. 4622-4630, 2019, 10.3390/ijerph16234622.

[118] M. Noguchi, A. Mizukoshi, Y. Yanagisawa, and A. Yamasaki, "Measurements of Volatile Organic Compounds in a Newly Built Daycare Center," *Int. J. Environ. Res. Public Health*, vol. 13, pp. 736-749, 2016, 10.3390/ijerph13070736.

[119] D. Singh, A. Kumar, B. P. Singh, K. Anandam, M. Singh *et al.*, "Spatial and Temporal Variability of VOCs and its Source Estimation During Rush/Non-Rush Hours in Ambient Air of Delhi, India," *Air Qual. Atmos. Health*, vol. 9, pp. 483-493, 2016, 10.1007/s11869-015-0354-3.

[120] A. B. Stefaniak, P. N. Breysse, M. P. M. Murray, B. C. Rooney, and J. Schaefer, "An Evaluation of Employee Exposure to Volatile Organic Compounds in Three Photocopy Centers," *Environ. Res. Sec. A*, vol. 83, pp. 162-173, 2000, 10.1006/enrs.2000.4061.

[121] C. Perrino, D. Ramirez, and I Allegrini, "Monitoring Acidic Air Pollutants Near Rome by Means of Diffusion Lines: Development of a Specific Quality Control Procedure," *Atmos. Environ.*, vol. 35, pp. 331-341, 2001.

[122] M. A. S. Garcia, R. J. Timmis, N. Van Dijk, J. D. Whyatt, I. D. Leith *et al.*, "Directional Passive Ambient Air Monitoring of Ammonia for Fugitive Source Attribution; A Field Trial with Wind Tunnel Characteristics," *Atmos. Environ.*, vol. 167, pp. 576-585, 2017, 10.1016/j.atmosenv.2017.07.043.

[123] S. N. Behera, M. Sharma, V. P. Aneja, and R. Balasubramanian, "Ammonia in the Atmosphere: A Review on Emission Sources, Atmospheric Chemistry and

Deposition on Terrestrial Bodies," *Environ. Sci. Pollut. Res.*, vol. 20, pp. 8092-8131, 2013, 10.1007/s11356-013-2051-9.

[124] NIOSH, *NIOSH Manual of Analytical Methods (NMAM), Fourth Edition*. Washington D.C., USA. Ammonia, Method 6015. 1994.

[125] NIOSH, *NIOSH Manual of Analytical Methods (NMAM), Fourth Edition*. Washington D.C., USA. Ammonia, Method 6016. 1996.

[126] A. Dey, "Semiconductor Metal Oxide Gas Sensors: A Review," *Mat. Sci. Eng. B.*, vol. 229, pp. 206-217, 2018, 10.1016/j.mseb.2017.12.036.

[127] G. Korotcenkov, V. Brinzari, and B. K. Cho, "In2O3- and SnO2-Based Thin Film Ozone Sensors: Fundamentals," *J. Sensors*, vol. 2016, pp. 1-31, 2016, 10.1155/2016/3816094.

[128] Figaro, "Operating Principle: MOS Type," 2018. [Online] Available: https://www.figarosensor.com/technicalinfo/principle/mos-type.html, Accessed On: September 2, 2020.

[129] N. Barsan, M. Schweizer-Berberich, and W. Gopel, "Fundamental and Practical Aspects in the Design of Nanoscaled SnO2 Gas Sensors: A Status Report," *Fresnius J. Anal. Chem.*, vol. 365, pp. 287-304, 1999.

[130] N. Barsan and U. Weimar, "Conduction Model of Metal Oxide Gas Sensors," *J. Electroceramics*, vol. 7, pp. 143-167, 2001.

[131] N. Barsan and U. Weimar, "Understanding the Fundamental Principles of Metal Oxide Based Gas Sensors; The Example of CO Sensing with SnO2 Sensors in the Presence of Humidity," *J. Phys. Condens. Matter*, vol. 15, pp. RR813-RR839, 2003.

[132] M. Batzill and U. Diebold, "The Surface and Materials Science of Tin Oxide," *Prog. Surf. Sci.*, vol. 79, pp. 47-154, 2005.

[133] G. Korotcenkov and B. K. Cho, "Instability of Metal Oxide-Based Conductometric Gas Sensors and Approaches to Stability Improvement (Short Survey)," *Sens. Actuators B. Chem.*, vol. 156, pp. 527-538, 2011, 10.1016/j.snb.2011.02.024.

[134] E. Lackner, J. Krainer, R. Wimmer-Teubenbacher, F. Sosada, C. Gspan *et al.*, "CMOS Integrated Nanocrystalline SnO2 Gas Sensors for CO Detection," *Procedia Eng.*, vol. 168, pp. 297-300, 2016, 10.1016/j.proeng.2016.11.200.

[135] I. Elmi, S. Zampolli, E. Cozzani, F. Mancarella, and G. C. Cardinali, "Development of Ultra-Low-Power Consumption MOX Sensors with ppb-Level VOC Detection Capabilities for Emerging Applications," *Sens. Actuators B. Chem.*, vol. 135, pp. 342-351, 2008, 10.1016/j.snb.2008.09.002.

[136] H. Liu, L. Zhang, K. H. H. Li, and O. K. Tan, "Microhotplates for Metal Oxide Semiconductor Gas Sensor Applications – Towards the CMOS-MEMS Monolithic Approach," *Micromachines*, vol. 9, pp. 557-580, 2018, 10.3390/mi9110557.

[137] J. Chou. Hazardous Gas Monitors: A Practical Guide to Selection, Operation and Applications. New York, NY, USA. McGraw-Hill. 1999. pp. 27-45.

[138] L. Boon-Brett, J. Bousek, and P. Moretto, "Reliability of Commercially Available Hydrogen Sensors for Detection of Hydrogen at Critical Concentrations: Part II – Selected Sensor Test Results," *Int. J. Hydrog. Energy*, vol. 34, pp. 562-571, 2009, 10.1016/j.ijhydene.2008.10.033.

[139] J. Riegel and K. H. Hardtl, "Analysis of Combustible Gases in Air with Calorimetric Gas Sensors Based on Semiconducting BaTiO3 Ceramics," *Sens. Actuators B. Chem.*, vol. B1, pp. 54-57, 1990.

[140] Figaro, "Operating Principle: Catalytic Type," 2018. [Online] Available: https://www.figarosensor.com/technicalinfo/principle/catalytic-type.html, Accessed On: September 2, 2020.

[141] Y. Nemirovsky, S. Stolyarova, T. Blank, S. Bar-Lev, A. Svetlitza *et al.*, "A New Pellistor-Like Gas Sensor Based on Micromachined CMOS Transistor," *IEEE Trans. Electron Devices*, vol. 65, no. 12, pp. 5494-5498, 2018, 10.1109/TED.2018.2878015.

[142] Figaro, "Operating Principle: Electrochemical Type," 2018. [Online] Available: https://www.figarosensor.com/technicalinfo/principle/electrochemical-type.html, Accessed On: September 2, 2020.

[143] R. Baron and J. Saffell, "Amperometric Gas Sensors as a Low Cost Emerging Technology Platform for Air Quality Monitoring Applications: A Review," *ACS Sens.*, vol. 2, pp. 1553-1566, 2017, 10.1021/acssensors.7b00620.

[144] Alphasense, "How Electrochemical Gas Sensors Work," Essex, UK, Alphasense Ltd., Alphasense Application Note AAN 104, Issue 12, pp. 1-4.

[145] M. L. Hitchman, N. J. Cade, T. K. Gibbs, and N. J. M. Hedley, "Study of the Factors Affecting Mass Transport in Electrochemical Gas Sensors," *Analyst*, vol. 122, pp. 1411-1417, 1997.

[146] Alphasense, "Humidity Extremes: Drying Out and Water Absorption," Essex, UK, Alphasense Ltd., Alphasense Application Note AAN 106, Issue 12, pp. 1-7.

[147] Alphasense, "Environmental Changes: Temperature, Pressure, Humidity," Essex, UK, Alphasense Ltd., Alphasense Application Note AAN 110, Issue 12, pp. 1-6.

[148] O. A. M. Popoola, G. B. Stewart, M. I. Mead, and R. L. Jones, "Development of a Baseline-Temperature Correction Methodology for Electrochemical Sensors and its Implications for Long-Term Stability," *Atmos. Environ.*, vol. 147, pp. 330-343, 2016, 10.1016/j.atmosenv.2016.10.024.

[149] M. Raninec, "Overcoming the Technical Challenges of Electrochemical Gas Sensing," Norwood, MA, USA, Analog Devices, Technical Article, pp. 1-5, 2019.

[150] N. Masson, R. Piedrahita, and M. Hannigan, "Quantification Method for Electrolytic Sensors in Long-Term Monitoring of Ambient Air Quality," *Sensors*, vol. 15, pp. 27283-27302, 2015, 10.3390/s151027283.

[151] M. I. Mead, O. A. M. Popoola, G. B. Stewart, P. Landshoff, and M. Calleja, "The Use of Electrochemical Sensors for Monitoring Urban Air Quality in Low-Cost, High-Density Networks," *Atmos. Environ.*, vol. 70, pp. 186-203, 2013, 10.1016/j.atmosenv.2012.11.060.

[152] Drager. Drager-Tubes & CMS-Handbook: Soil, Water, and Air Investigations as well as Technical Gas Analysis, 18th Edition. Lubeck, Germany. Drager Safety AG & Co KGaA. 2015. pp. 1-456.

[153] RAE Systems Inc. *Gas Detection Tubes and Sampling Handbook, Second Edition*. San Jose, CA, USA. RAE Systems Inc. 2013. pp. 1-133.

[154] DHS, "Portable Colorimetric Tubes for Chemical Vapor Detection Market Survey Report," Las Vegas, NV, USA, National Security Technologies, LLC. System Assessment and Validation for Emergency Responders (SAVER), pp. 1-14, 2014.

[155] Honeywell International. *Gas Detection Tubes and Sampling Handbook*. San Jose, CA, USA. Honeywell International. 2014. pp. 1-120.

[156] RAE Systems Inc., "Accuracy Comparisons of RAE Systems Gas Detection Tubes," San Jose, CA, USA, RAE Systems Inc., Technical Note TN-143, 01/05/WH, pp. 1-2.

[157] D. E. Williams, "Low Cost Sensor Networks: How Do We Know the Data Are Reliable?," *ACS Sens.*, vol. 4, pp. 2558-2565, 2019, 10.1021/acssensors.9b01455.

[158] E. G. Snyder, T. H. Watkins, P. A. Solomon, E. D. Thoma, R. W. Williams *et al.*, "The Changing Paradigm of Air Pollution Monitoring," *Environ. Sci. Technol.*, vol. 47, pp. 11369-11377, 2013, 10.1021/es4022602.

[159] S. Reis, E. Seto, A. Northcross, N. W. T. Quinn, M. Convertino *et al.*, "Integrating Modelling and Smart Sensors for Environmental and Human Health," *Environ. Model Softw.*, vol. 74, pp. 238-246, 2015, 10.1016/j.envsoft.2015.06.003.

3   A LOW-COST WEARABLE PERSONAL EXPOSURE MONITOR FOR

STUDYING RESPIRATORY DISEASES USING METAL OXIDE SENSORS

3.1 Introduction

Mass industrialization around the world has led to an increase in air pollution, causing various environmental health problems [160-164]. For example, breathing pollutants into ones lungs causes oxidative damage and inflammation [165]. Short-term exposure can be irritating, whereas long-term exposure can lead to the development of chronic illnesses like asthma and chronic obstructive pulmonary disorder [166, 167]. People suffering from these respiratory diseases are at an increased risk from air pollution, even when concentrations are below proposed safe limits [168, 169]. This makes studying the effect air quality has on at-risk individuals of vital importance.

A major challenge in studying how pollutants trigger respiratory symptoms is accurately tracking a person's exposure. Most studies rely on fixed air quality monitoring sites, but the sparse fixed sites provide only limited pollution information [170, 171]. Furthermore, most people spend the majority of their time indoors where air quality is usually worse [172-174]. For these reasons, developing a wearable device that tracks a person's microenvironment is essential for researchers to link respiratory symptoms with their causes. There is currently no commercially available wearable tracking device that measures pollutants in the air. Other researchers have built personal environmental monitor prototypes in both portable and wearable formats to study exposure for respiratory health [175-179]. Here I present a wrist-worn device that monitors ozone, TVOC, temperature, humidity, and activity level dubbed the "Asthma Research Tool", or ART. ART combines these sensors in a compact, light-weight form factor for under $150, and the ozone sensor

is calibrated to correct for both ambient temperature and humidity interference. This study reports the development, calibration, and testing of eight ART devices for environmental health applications.
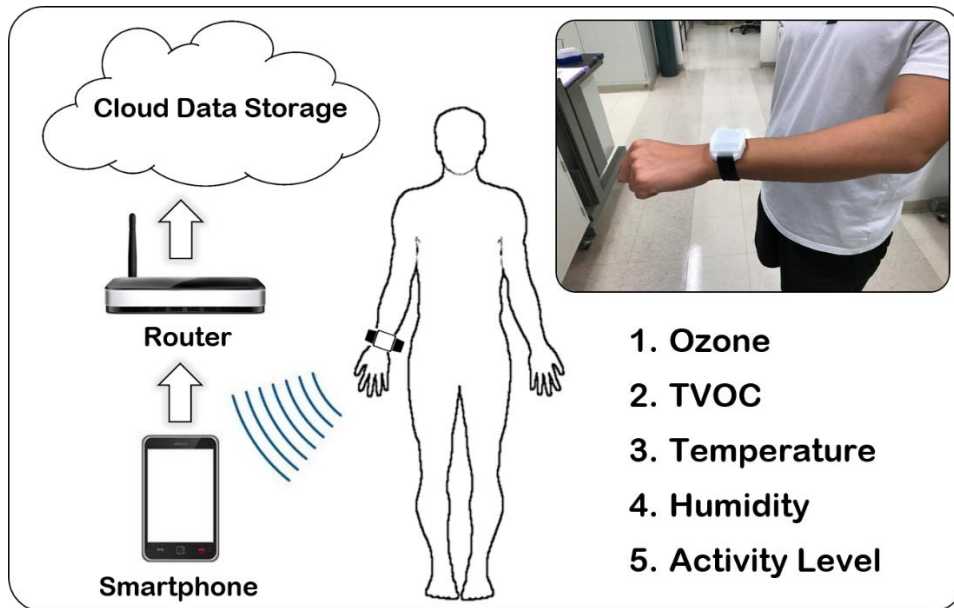
Figure 3.1 An overview of the Asthma Research Tool (ART) system. ART is worn on the wrist to monitor personal exposure linked to asthma symptoms. Data stored on flash memory can be transferred wirelessly through Bluetooth to an enabled receiving device. An app manages data, and as it aggregates it can be moved to a secure cloud database.

3.2 Device Overview

ART was designed with the user experience in mind to make implementation in a clinical study practical (Figure 3.1). It weighs only 64 grams and is intended to be worn on the wrist for user comfort, continuous personal monitoring, and convenient air sampling with minimal obstruction. Data can be recorded from its five sensors autonomously at one-minute intervals to flash memory for up to a year. With 48 hours of battery life the device only needs to be plugged-in nightly by the user. Three colored LEDs give basic feedback

on charging and device operation. Retrieving data is accomplished by wireless transmission via Bluetooth Low Energy (BLE) to a tablet or smartphone. Data transfer can be initiated on-demand or set up to perform automatically (when in wireless range, ~30 ft.). It is also possible to stream data in real-time at one second intervals. An app manages transferred data and can upload the data to a secure cloud database for easy access.

ART tracks five parameters linked to asthma, including ozone, TVOC, temperature, humidity and activity. Ozone is a powerful irritant and component of smog correlated with asthma symptoms [165-169, 180, 181]. The EPA has compiled and summarized clinical data regarding the effects of ozone on the respiratory system to guide them in setting safety limits and has found that 60 ppb is the lowest concentration that causes a decrement in lung function and airway inflammation in healthy individuals. Those with asthma or other respiratory diseases may have adverse effects at lower concentrations, but the exact concentration is unknown and will probably vary on a case-by-case basis depending on the severity of the disease, prevalence of medication use, physical exertion, and the presence of other pollutants [182, 183]. Ozone has been shown to be able to be tracked using a MOS gas sensor by several other research groups [127, 175-179, 184-187]. I selected the SGX Sensortech MiCS-2614 ozone sensor because at the time of purchase it was the only commercially available, surface mountable ozone sensor on the market [188]. It has a 10 ppb limit of detection (LOD) which should allow it to be useful in detecting potentially harmful concentrations of ozone. VOCs are leading indoor air pollutants and tend to build up indoors [189-191]. It is still unknown whether VOCs are responsible for developing the onset of asthma and exacerbating symptoms, and more research in this area is necessary [192, 193]. The problem is that present toxicological knowledge is limited when it comes

52

to understanding the combined effect of many pollutants at low concentrations [194]. Moreover, VOCs are associated with the perception of odors that can be interpreted as harmful and elicit asthma symptoms [195]. Studying these compounds individually is complicated by them being found in mixtures, with the chemicals present over a wide range of concentrations, and needing multiple detection techniques to quantify them all, usually by expensive equipment (eg. GC-MS) [194]. TVOC is the concept of calculating a single concentration that represents all the VOCs in an air sample. Researchers have already demonstrated MOS sensors are capable of measuring VOCs for air quality determination and odor identification [196, 197]. ART measures TVOC using the Sensirion SGPC3 MOS sensor. It was chosen for its small size, low power consumption, and it comes from the factory pre-calibrated with digital ppb output. Sensirion calibrates these from 0.3 to 30 ppm and they measure at ppb range resolution. It also performs humidity correction and dynamic baseline adjustment [198, 199]. Temperature and humidity are important environmental parameters that must also be tracked. It is well known that extreme environments and weather changes can trigger asthma symptoms [200-202]. Lastly, exercise is one of the most common triggers of asthma [203]. This is tracked with a triaxial accelerometer, as this has been shown in many previous works to be a useful approach for measuring activity level and physical exertion [204, 205]. Since each individual with asthma has a unique lifestyle and manages their disease differently it is hard to predict how each of these potential triggers may affect them. The purpose of ART is to provide a research tool for epidemiologists to study how asthma triggers and their combinations exacerbate respiratory symptoms. An eventual goal would be to provide a device that can

give real-time feedback and warnings to a user, but at this point the knowledge is too limited.

3.3 Principle of MOS Gas Sensors

MOS gas sensors are popular for their small size and high sensitivity. They employ an n-doped metal oxide (eg. SnO_2, In_2O_3, ZnO, WO_3) usually containing a doping agent (e.g. Pd, Pt, Au) in thermal contact with a heating element to maintain the sensor at an elevated working temperature (typically 200-400°C) [206]. Oxygen from the surrounding atmosphere reacts on the heated metal oxide surface, drawing electrons from the conduction band and increasing its resistance [130, 132]. In its heated, activated state the metal oxide is highly sensitive to oxidizing (e.g. ozone) and reducing (e.g. VOCs) gases [127, 207]. For this reason MOS sensors may be subject to chemical interference [206, 132] and humidity effects [131] determined by their chemical composition and operating parameters. Fluctuations in ambient temperature can also affect the working temperature of the MOS which can shift its response [127, 207]. Since a wearable device will be in many different environments these effects had to be compensated for. The Sensirion TVOC and Sensortech ozone sensing layer compositions are proprietary and not made known by the manufacturers. The TVOC sensor is provided pre-calibrated, but the ozone sensor requires additional circuitry and calibration. The development of correction algorithms and validation of the ozone sensor will be a primary focus in subsequent sections.

3.4 Materials & Methods

3.4.1 Hardware

All components are COTS and fit on a single printed circuit board (PCB). An InnoComm BM15_AN microcontroller (MCU) provides coordination of peripherals with SPI and I2C communication, 12-bit analog to digital converter (ADC), and BLE communication with a built-in trace antenna. The ozone sensor (model MiCS-2614) is manufactured by SGX Sensortech. To protect it from dust contamination and reduce convective cooling it is covered with a borosilicate and polytetrafluoroethylene (PTFE) fiber mesh filter (Pallflex Emfab Filters). The ozone sensor requires its own measurement circuit, heating circuit, and calibration, all of which will be described in subsequent sections. The low-power TVOC sensor (model SGPC3) is manufactured by Sensirion, which is pre-calibrated with a built-in temperature regulating hot plate, dynamic baseline correction, and humidity correction [199]. Digital temperature and humidity sensors are combined into the Sensirion SHT30-DIS-B. A NXP MMA8652FC, 3-axis, ±8 g-force, 12-bit, digital accelerometer provides information on activity level. Additional supporting components include an embedded real-time clock from NXP (PCF85263A) and 128 Mbit Windbond flash memory (W25Q128JVSIM-ND). An 820 mAh lithium-polymer battery powers the device.

3.4.2 Device Casing

The case enclosing the PCB and battery is machined by a CNC (Roland MDX-540) from a block of Teflon PTFE (McMaster-Carr) chosen for its inertness. The top of the case has a pattern of air holes to allow passive airflow to the sensors within. A 20 mm wide

black silicone rubber watch band (Barton Watch Bands) is attached to the case by push pins.
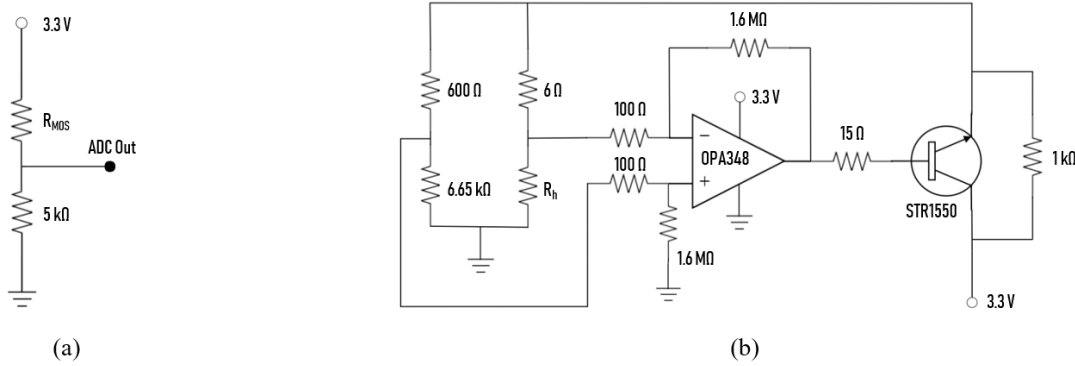
Figure 3.2 (a) MiCS-2614 Measurement Circuit, where R_{MOS} is the resistance of the metal oxide sensing layer. (b) MiCS-2614 Heating Circuit, where R_h is the resistance of the resistive heating element.

3.4.3 Ozone Sensor Measurement & Heating Circuits

The MiCS-2614 ozone sensor requires additional circuitry for its operation. To measure the resistance of the metal oxide a voltage divider is created by placing a 5 kohm, 0.1% precision resistor in series with the metal oxide (Figure 3.2a). The ADC averages a burst of 15 consecutive measurements at 1 kHz across the 5 kohm series resistor to calculate the metal oxide resistance.

The heating circuit drives the resistive heating element built into the MiCS-2614 ozone sensor. To help maintain a stable operating temperature a feedback mechanism was introduced that puts the heating element in a Wheatstone bridge (Figure 3.2b), similar to the one by Benammar and Maskell [208]. The bridge is balanced when the heating element

is maintained at 66.5 ohms (determined to be the ideal resistance from measurements made with manufacturer provided evaluation boards).

The ozone sensor draws 32 mA of current to keep the metal oxide heated. To extend the battery life of the device the heating element was cycled at 60 second periods. The sensor is left off for 40 seconds, then turned on for 20 seconds. The resistance of the metal oxide is measured immediately before the heater switches off. Cycling the heater increased battery life from 18 hours to 48 hours.

There is a pre-heating period every time a device is powered on to prepare the metal oxide surface. The heating circuit applies continuous power for 15 minutes after which the periodic cycling resumes. No measurements are taken during the pre-heating period.

A "burn-in" procedure was necessary to prepare all new ozone sensors, where they operated in a manufacturer supplied evaluation board for two weeks before being soldered to a device and calibrated. This helped give the ozone sensors a more stable output.

3.4.4 Ozone Sensor Calibration

Ozone sensor calibration was performed in a 1.25 L glass chamber placed in an environmentally controlled glove box (MTI). Temperature and humidity inside the glove box were maintained at predetermined levels throughout the procedure. Zero air (Matheson, Air Ultra Zero) was delivered through PTFE tubing to a UV ozone generator (UVP SOG-2). The ozonated air then flowed through Nafion tubing within the glove box, allowing it to become humidified, before reaching the ozone sensor in the device. Reference ozone measurements were made by drawing air from the glass chamber through PTFE tubing to an EPA FEM UV absorbance ozone monitor (2B Technologies 202)

recording 1 minute averages. The FEM ozone monitor was calibrated (NIST traceable) at the manufacturer prior to ART calibration and testing.

The calibration procedure was designed to capture the MiCS-2614 ozone sensor response to changes in ambient temperature, humidity, and ozone concentration. Temperature was adjusted to 15, 30, and 45°C. Ozone concentrations were set to 0, 55, 110, and 165 μg/m^3 (0, 30, 60, 90 ppb at 45°C). Absolute humidity was maintained at 2.6, 7.8, 15.0, and 21.2 g/m^3 at both 30°C and 45°C. At 15°C the saturation pressure of water limited humidity to 2.6, 5.1, 7.8, and 10.3 g/m^3. The range of each parameter was chosen to represent realistic ambient conditions that the device may encounter. All combinations of these settings yielded 48 MOS resistance responses in total. A table with the exact parameters for the 48 calibration points can be found in Appendix S1. Each time a parameter was changed in the calibration chamber the sensors being calibrated were given at least one hour to fully stabilize before a measurement was taken. One hour was determined to be a conservative wait time from empirical observations that it usually took the sensors 20 to 30 minutes to reach equilibrium in their environment. The resistance of the MOS ozone sensors was very stable at the end of each wait period and the final measurement taken before changing parameters was used to characterize the sensor response.

3.4.5 Device Testing

After calibration the eight ART devices were tested in four different environments. Indoor stationary monitoring was performed inside a laboratory for 11 days. Outdoor stationary monitoring was performed behind a researcher's home in Tempe, AZ for 10

days. An alternating indoor-outdoor test was performed where the devices were moved from the space behind a researcher's home to inside their living room at two-hour intervals. Finally, a researcher brought the devices with them for 24 hours, keeping an activity log and performing scripted activities. Ozone reference measurements were recorded using a FEM ozone monitor (2B Technologies 202). TVOC measurements were compared with a handheld PID (RAE MiniRAE Lite, calibrated 0-100 ppm isobutylene per manufacturer's guidelines).

3.5 Results

3.5.1 Ozone Sensor Heating Circuit

The calibration data are used to determine if the feedback mechanism in the heating circuit is compensating for ambient temperature (Figure 3.3). This governs whether temperature must be included in the calibration equation or not. Measurements from the heating circuit output show the feedback mechanism is responding to changes in temperature appropriately and effectively maintaining the heating element resistance at 66.5 ohms. Unfortunately it is not able to stabilize the resistance of the metal oxide. It is likely that the heating element itself is being maintained at a steady temperature, but the thermally inefficient insulator separating the heating element and metal oxide is preventing the two from existing in thermal equilibrium. The metal oxide, with one side exposed to ambient air, is at a lower temperature than the heating element and is influenced more strongly by changes in the ambient environment. This type of simple feedback circuit was chosen because it is described well in the literature [208] and capable of being incorporated with a COTS sensor. Other groups have found more elaborate methods to control the

operating temperature of MOS sensors [209-211], although their solutions cannot be retrofitted onto a COTS design. For the ART devices, ozone sensor calibration will require an explicit regression equation that includes ambient temperature to fully compensate for its effect.

3.5.2 Ozone Sensor Calibration

An explicit regression equation for predicting ozone was preferred over nonparametric and machine learning models because it requires less memory and processing power from the MCU. Advanced algorithms, like support vector machines and artificial neural networks, also require large datasets that pose a challenge for calibration in an artificial environment. The stable response of the ozone sensor was measured at 48 pre-determined temperature, humidity, and ozone levels. It was important to find an equation that satisfied all eight ART devices, with only the coefficients for each device being unique. Best results were obtained by normalizing the ozone sensor response and using an inverse calibration, an approach to regression where the variable intended for prediction is treated as the dependent variable (i.e. ozone) [212].
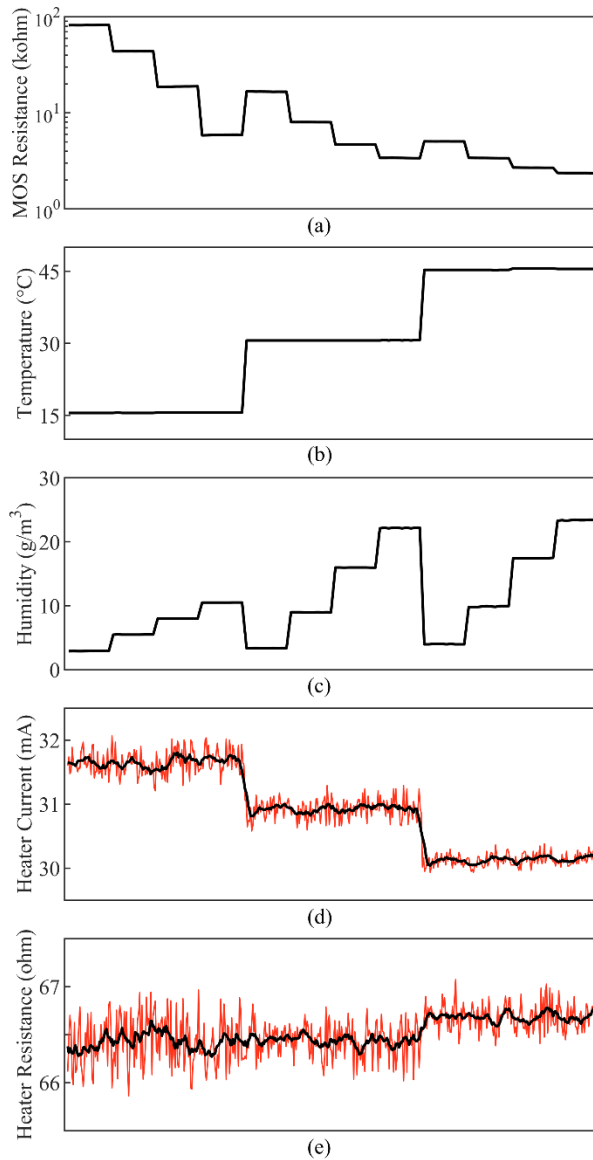
Figure 3.3 Selection of MiCS-2614 ozone sensor steady-state response collected during calibration. Ozone was held constant at 55 μg/m^3. Metal oxide resistance decreases in response to increasing ambient temperature at equivalent absolute humidity levels. Therefore the metal oxide resistance is dependent on ambient temperature and the feedback mechanism is ineffective. An analysis of the output of the heating circuit shows it is properly maintaining the heating element resistance at 66.5 ohms. The circuit is behaving as it was designed to. It is possible that the thermally inefficient insulator separating the heating element and metal oxide is preventing the two from existing in thermal equilibrium and preventing the feedback system from being effective. (a) Metal oxide resistance. (b) Ambient temperature. (c) Absolute humidity. (d) Electrical current through heating element. Red line noisy due to limited ADC resolution. Black line is 10 point moving average. (e) Heating element resistance. Red line noisy due to limited ADC resolution. Black line is 10 point moving average.

Not only does ozone need to be associated with the sensor response, but influence from temperature and humidity must be separated out. The Pearson's correlations (Table 3.1) calculated from calibration data show that temperature and humidity have good correlation with metal oxide resistance, -0.502 and -0.449 respectively, compared with ozone, 0.378. These environmental parameters cannot be ignored. One way to reduce this dependency is to express ozone concentration in terms of $S=R/R_0$, rather than resistance R, where R_0 is the resistance of the sensor in the same environment (i.e. same temperature and humidity) at 0 ppb ozone [131, 213, 214].

TABLE 3.1
PEARSON'S CORRELATION: CALIBRATION DATA

	MOS Resistance (kΩ)	Ozone ($\mu g/m^3$)	Temperature (°C)	Absolute Humidity (g/m^3)
MOS Resistance (kΩ)	1	0.378	-0.502	-0.449
Ozone ($\mu g/m^3$)	0.378	1	-0.011	-0.001
Temperature (°C)	-0.502	-0.011	1	0.434
Absolute Humidity (g/m^3)	-0.449	-0.001	0.434	1

It is well known that MOS sensors have a nonlinear response (root power law in simple case) [130, 215]. I found that expressing the ozone concentration in terms of the

logarithm of *S* vastly improved regression fitting (logarithms approximate roots across a limited range), and the expression takes the form of equation 3.1,

$$[O_3] = B_0 + B_1 Log(S) + B_2 Log(S) \cdot T + B_3 Log(S) \cdot T^2 + B_4 Log(S) \cdot H_{Abs}^2 \tag{3.1}$$

where $[O_3]$ is the ozone concentration in $\mu g/m^3$, *T* is temperature in Celsius, H_{Abs} is absolute humidity in g/m^3, and B_0, B_1, B_2, B_3 and B_4 for all eight ART devices are given in Appendix S2. It is worth noting that ARTs 1, 3, and 6 have poorer regression fitting than the other five devices. Furthermore, no regression model that was tested gave superior fits to these three devices compared with the other five, possibly a consequence of tolerance issues at the manufacturing level.

R_0, the MOS sensor resistance at zero ozone, depends on ambient temperature and humidity. It is necessary for calculation of *S*, which is a term in equation 3.1. This makes it necessary to estimate R_0 for each ozone measurement while the device is operating. Therefore a second regression equation, equation 3.2, was formed with the 12 calibration points (out of 48) pertaining to 0 ppb ozone at different temperatures and humidities, and the results can be fitted with

$$R_0 = C_0 + C_1 T + C_2 H_{RH} \tag{3.2}$$

where H_{RH} is relative humidity in %, *T* is temperature in Celsius, and C_0, C_1 and C_2 for all eight ART devices are listed in Appendix S3.

Lastly, ozone measurements in µg/m³ are converted to ppb since this is a common way to communicate ozone levels. This conversion is easily performed using the ideal gas law. The calculation requires ambient temperature and pressure. Since ART does not have a pressure sensor a default value of one atmosphere is used. For small elevation changes and weather related pressure changes any error introduced by assuming 1 atmosphere is small (eg. 100 ft. gives 0.36% error, 1000 ft. gives 3.56% error). Calibration and testing was all performed in Tempe, AZ so this was not a concern. A future iteration of the device could include a small pressure sensor to improve accuracy. The calibration procedure reported here was performed once with all eight ART devices and was used to make measurements in the following real environments over the course of two months without recalibration.
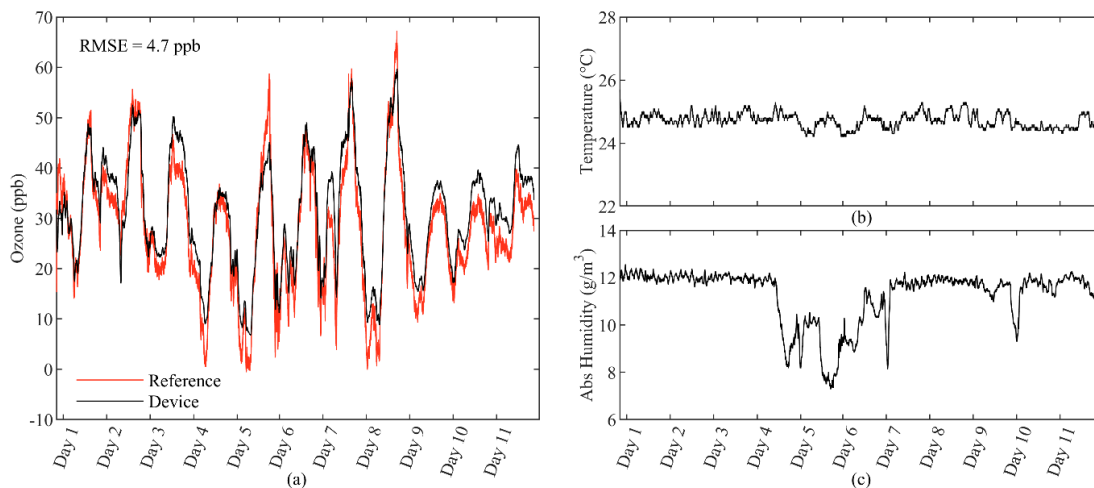

Figure. 3.4 Indoor stationary monitoring with ART # 8 placed inside a laboratory at The Biodesign Institute for 11 days. X-axis ticks represent the start of each day at midnight. (a) Ozone measurement alongside a reference instrument. (b) Temperature. (c) Humidity.

3.5.3 Indoor Stationary Monitoring

ART devices monitored the air inside a laboratory alongside a reference ozone monitor for 11 days during the summer. Ventilation inside the laboratory was high, and as a result a continuous supply of ozone from outdoors was delivered. This environment maintains a constant temperature, while shifts in humidity reflect changing weather conditions outside. Indoor monitoring was a first step in validating the ozone sensor calibration. Figure 3.4 shows measurements made by ART # 8. Appendix S4 contains results from all eight ART devices. Overall ozone accuracy for the devices is good, with an average root-mean-squared error (RMSE) of 5.4 ppb, and standard deviation of RMSE among all eight devices of 0.9 ppb. TVOC plots are omitted because levels were so low, a consequence of high ventilation within the lab. Routine TVOC measurements made with a PID reference were 0.0 ppm (below the detection limit).
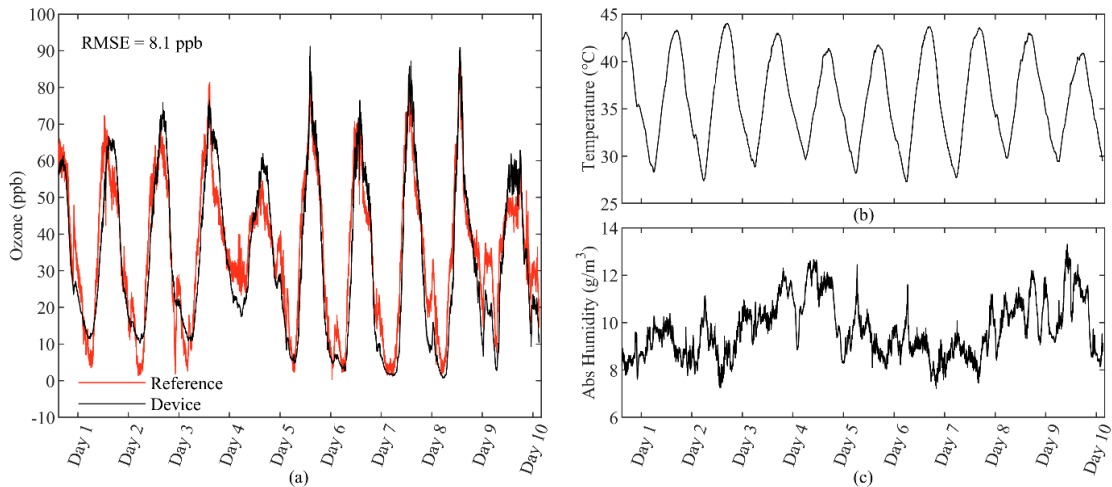

Figure 3.5 Outdoor stationary monitoring with ART # 8 placed behind a researcher's home in Tempe, AZ for 10 days. X-axis ticks represent the start of each day at midnight. (a) Ozone measurement alongside a reference instrument. (b) Temperature. (c) Humidity.

3.5.4 Outdoor Stationary Monitoring

To further validate the devices in a more challenging environment than indoor stationary monitoring, with large swings in temperature, humidity, and ozone each day, the ART devices were placed outdoors behind researcher # 1's home in Tempe, AZ for 10 days during the summer. Measurements were made alongside a reference ozone monitor. Figure 3.5 shows measurements made by ART # 8. Appendix S5 contains results from all eight ART devices. Ozone accuracy decreased compared to the indoor monitoring test, but results are still promising for metal oxide sensors in a real environment. The average RMSE for eight devices is 9.9 ppb, and the standard deviation of RMSE among all devices is 1.3 ppb. TVOC plots are omitted because the reference measurements made outdoors with a PID were 0.0 ppm (below the detection limit).

3.5.5 Alternating Indoor-Outdoor Test

To test the devices' performance for sudden environmental changes they were moved between indoor and outdoor environments at two-hour intervals for 10 hours. The test was performed at researcher # 1's home starting from 10:10 to 20:10. In contrast to the laboratory that had high ventilation, this residential home has an air conditioning system that recirculates air from within. This means less ozone is brought into the house and VOCs have a chance to accumulate. A reference ozone monitor remained stationary outdoors during the entire test. Indoor ozone was assumed to be approximately 0 ppb based on previous measurements made with the reference monitor.
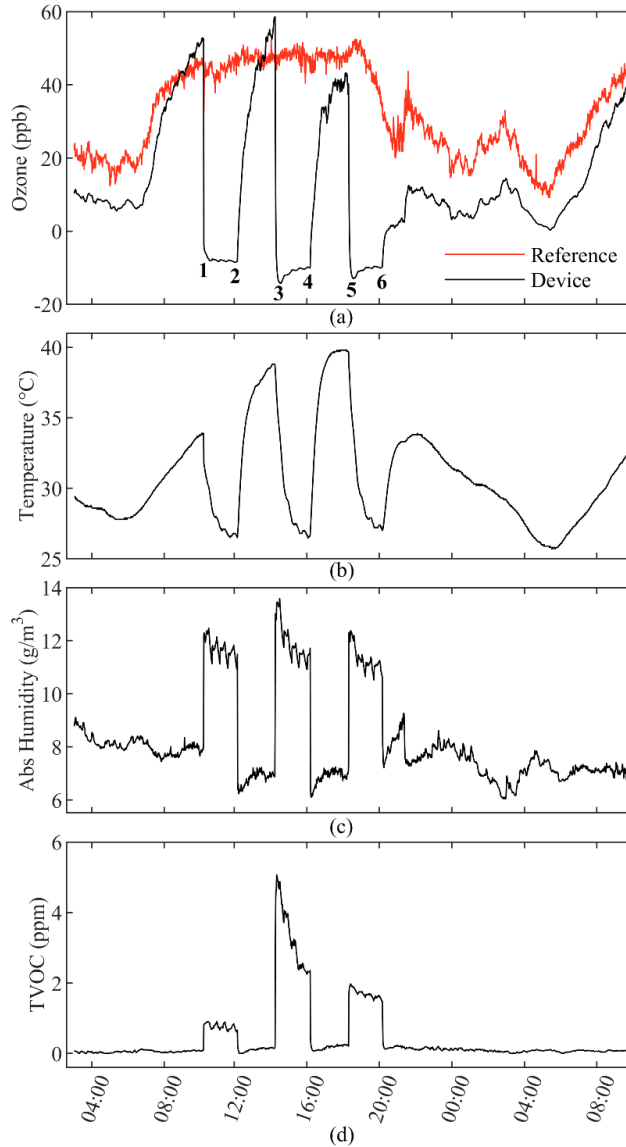
Figure 3.6 Alternating indoor-outdoor test with ART # 8. ART was moved between researcher # 1's backyard and their living room at two hour intervals. (a) Ozone measurement. The test begins with the device outdoors. At 1, 3, and 5 the device was brought indoors and the ozone concentration dropped to below 0 ppb. At 2, 4, and 6 the device was moved outdoors and the ozone concentration increased to the reference instrument value. The reference instrument remained outdoors during the entire test. (b) Temperature dropped each time the device was brought indoors and rose each time the device was moved outside. (c) Absolute humidity increased when the device moved indoors and decreased when moved outdoors. (d) VOCs were approximately 0 ppm outdoors and much higher indoors due to human activities like cooking food.

67

Figure 3.6 shows results from ART # 8. The test began with ART measuring outdoors during the summer in the early hours of the morning. After sunrise, around 06:00, ozone and temperature start to increase. At 10:10 the device was brought indoors for two hours, which led to a drop in ozone and temperature, accompanied by an increase in humidity and VOCs. Periodic ripples in humidity and TVOC measurements made indoors was due to the air conditioning system. At 12:10 the device was moved back outside next to the ozone reference. The ozone sensor response was slow to adjust and required about 30 minutes to get close to the reference monitor reading. At 14:15 the device was moved indoors a second time. At this point the researcher's family had just finished cooking a meal and VOCs were much higher inside the home. During this two-hour period there was a spike in TVOC followed by a steady decrease. At 16:10 the device was moved outdoors next to the ozone reference. Again, the ozone sensor required about 30 minutes for its response to adjust close to the reference value. At 18:15 the device was brought inside a third and final time. Finally the device was taken outside at 20:10 and allowed to measure until the following morning. Appendix S6 contains results from all eight ART devices.

The combination of ozone, TVOC, temperature, and humidity sensors provided complementary information to uniquely describe each environment the device was in and exposure to a potential wearer. The metal oxide sensors used to measure ozone and TVOC were able to adjust to the temperature and humidity swings every time the device changed locations. It is interesting to note that the ozone sensor reported negative values inside the home. It is possible that high VOCs inside the home, which are reducing gases and therefore have the opposite effect on the MOS sensor compared with ozone, may have pushed the measurement into the negatives. The ozone calibration only took into account

68

temperature and humidity, it does not correct for VOCs. It is also important to recognize the ozone sensor response is not immediate when it changes environments. The response is relatively quick when moving from outdoors to indoors (high ozone to low ozone, less than 10 min), but slower when moving from indoors to outdoors (low ozone to high ozone, about 30 min). The exact reason for this asymmetry is unknown, but memory effects from moisture and other gases on MOS sensors have been reported before [216]. A PID was used to verify TVOC. The PID measured 0.0 ppm outdoors, 0.4 ppm indoors before cooking, and 1.1 ppm during cooking with a slow decrease afterwards. The PID measurement is not identical to the Sensirion TVOC sensor because their mechanisms of detection are fundamentally different, but the trends are the same. This test shows ART has potential to provide much more thorough personal exposure data in a study than relying on government monitoring stations, especially with the disparity between indoor and outdoor environments.

3.5.6 24-Hour Wearable Field Test

Researcher # 2 kept the ART devices for 24 hours to monitor their own personal exposure in Tempe, AZ during the summer. Throughout the day they maintained a log and performed scripted activities. Figure 3.7 shows measurements from ART # 8. Appendix S7 contains results from all eight ART devices.
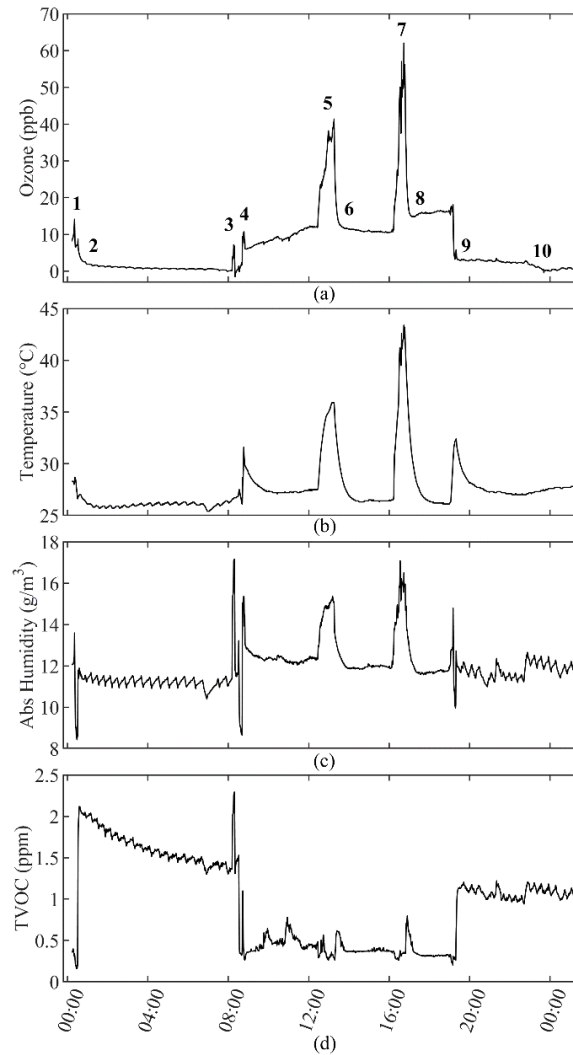
Figure 3.7 24-hour wearable field test with ART # 8. Researcher # 2 wore ART for a full day and performed scripted activities. The four plots are measurements made by ART: (a) Ozone, (b) temperature, (c) absolute humidity, and (d) TVOC. The test began at 1 in the nighttime when the researcher left the lab and drove home. At 2 they entered their home, accompanied by a decrease in ozone and increase in VOCs. In the morning at 3 they took a shower with the device on the bathroom counter. A spike in humidity briefly affected the ozone and TVOC measurements. At 4 they drove back to the laboratory and walked inside. There was an increase in ozone, temperature, and humidity outdoors. VOCs are lower both outdoors and in the lab compared to inside the researcher's home. At 5 they break for lunch and sit outside. Ozone, temperature, and humidity increased outdoors. At 6 they moved to an office adjacent to the lab. Ozone, temperature, and humidity decreased indoors. At 7 they walked around the university campus. Ozone and temperature peaked during this summer afternoon walk. At 8 they returned to the lab. At 9 they leave the building, drive home, and eat dinner. Temperature increased during the walk to the car and inside the hot car. Once inside the home VOCs increased and temperature decreased. At 10 they moved to their bedroom.

This test demonstrates how ART can capture a wearer's activities and exposure. Whenever the researcher is outdoors ozone and temperature are at their highest, especially in the afternoon when solar radiation is most intense. Humidity is highest outdoors, a different weather condition than what was observed during the alternating indoor-outdoor test. Inside the residence VOCs are high and ozone is approximately zero. This is expected in a home that uses an air conditioning system to recirculate air from within, rather than drawing fresh air from outside. The ripples visible in temperature, humidity, and TVOC measurements made inside the home are due to the air conditioning turning on at regular intervals. A PID reference found VOCs inside the home to be 0.3 ppm in the kitchen and living room areas, and 0.2 ppm upstairs in the bedroom, whereas outdoors it measured 0.0 ppm. As explained previously, these PID measurements do not exactly match the Sensirion TVOC sensor because of a difference in sensing principle, but they do match the trend seen outdoors compared with inside the residence.

To take variability of the eight devices into account the peak ozone measurement for each device when outdoors during the daytime at annotations **5** and **7** was recorded, because these are the events where the most exposure to the wearer occurred. At **5** the average peak for eight devices was 33.1 ppb with a standard deviation of 6.8 ppb. At **7** the average peak for eight devices was 55.5 ppb with a standard deviation of 12.1 ppb. ART # 2 has the highest measurement for ozone at 83 ppb putting it well above the other devices, but the rest of its measurements throughout the day were in line with the other ozone sensors. ARTs # 1 & 3 have the most aberration in ozone measurements when changing environments, which may be related to their lower R-squared fits from the regression.

This test shows the ART device is capable of tracking a person's exposure in many changing environments, both indoors and outdoors. A study relying entirely on air quality data from government monitoring stations, which have low spatial and temporal resolution, will not track exposure to this level of detail.

3.6 Discussion

MOS sensors were selected for this work because of their small size and compatibility with semiconductor devices, making them suitable for a compact wearable device. However, the work reveals several areas of improvement needed for the sensors.

One is their intrinsic broadband response and dependency on humidity, compared with sophisticated technologies (e.g., UV absorbance for ozone), making the veracity of their measurements questionable. I also found regulating MOS operating temperature, which is crucial for maintaining sensitivity, was not achieved with the simple feedback mechanism popularized in the literature. There are more advanced control systems to regulate operating temperature, but they require placing temperature sensors within the MOS sensor construction [209-211]. These designs need to be incorporated during the MOS manufacturing process, which is not realistic for most developers relying on COTS parts. There may be other designs capable of preprocessing the air being measured before it reaches the sensors, to eliminate temperature and humidity effects, but these would increase the cost and size of the device, preventing it from succeeding in a wearable format.

The decision was made to compensate for ambient temperature and humidity effects in an exhaustive calibration procedure. This approach was particularly tedious and has its own limitations. For instance, the alternating indoor-outdoor test suggests high

72

VOCs in indoor environments may also be influencing ozone measurements. Other reactive gases found in air pollution, such as nitrogen dioxide, could also affect the sensor. Relying on a calibration procedure to correcting for all types of environmental interference would be too complex. Ozone measurements are also restricted to the feature space of the calibration procedure. Extrapolating outside that space will lead to inaccurate predictions. Expanding the feature space to include a wider range of temperature, humidity, and ozone values would require more calibration points. As the feature space expands and the number of features included increases it is clear that this brute force approach to calibration is not scalable.

MOS sensors have a nonlinear response, which require many data points to determine precise calibration curves. Large datasets are costly and time consuming to obtain. This is especially the case that each sensor must be calibrated individually because of the large manufacturing variability for different sensors [217]. Some groups have tried to work around this problem by collecting large datasets in the natural environment instead of a controlled one for each sensor [218-220]. This approach allows sensors to collect data alongside reference instruments for days, weeks, or even months allowing acquisition of thousands of points easily. However, when the sensor response depends on multiple parameters (eg. temperature and humidity), many of which are collinear in a natural setting, as in the case of ozone detection, it becomes difficult to model precisely. These models are not robust to changes in environment that differ from training sets either (eg. location, weather, seasonal changes). A more intelligent, automated, environmentally controlled calibration system could reduce this difficulty of collecting more data points while

allowing explicit control of the feature space collected on. So far the cost and complexity of this type of calibration system is prohibitive to most researchers.

The indoor-outdoor test and the 24 hour wearable field test both showed the ozone sensor has a delayed response when the environment it is measuring changes quickly (ie. move from indoors to outdoors, or vice versa). When moving from indoors to outdoors with high ozone the response takes as long as 30 minutes. This was also observed during calibration under controlled conditions. The cause for this delay could stem from multiple factors. One is delivery of gas to the sensor surface. ART relies on passive air flow to its sensors, instead of using a pump or fan, to keep the device as small as possible and minimize power consumption. Test results show sensors exhibit a delayed, asymptotic response in both still environments (eg. indoors) and those with constant air flow over the device (eg. calibration chamber, outdoor tests, walking with devices in wearable field test). A more plausible explanation for the delayed response is the surface chemistry taking place on the heated metal oxide, where it takes some finite period of time for the active sites on the surface to equilibrate in the presence of electron withdrawing and electron donating gases. One way to mediate this effect and shorten the response time of a MOS sensor is to increase its operating temperature, but this can have a negative impact on sensitivity, selectivity, stability, and power consumption. Another way is to create a MOS sensor composed of smaller metal oxide crystal granules, but this can also decrease stability and it is not possible when restricted to using COTS sensors [127]. Continuing to improve the response of the ozone sensor is a goal for future iterations.

The EPA has presently concluded that 60 ppb ozone is a threshold for generating lung inflammation in healthy individuals, and those with respiratory illnesses, such as

asthma, may have symptoms at even lower concentrations. With a 10 ppb LOD ART may be useful in making ozone measurements at therapeutically relevant concentrations. Whether or not the data provided by these sensors is useful for linking exposure history with asthma symptoms, even with the slow ozone sensor response under certain conditions, must ultimately be determined in a controlled study by an epidemiologist, where the complicated realities of linking ART data with a patient log book, their medication use, delayed respiratory symptoms, and possibly data from other devices come into play.

A final point that deserves attention, and will be tested in the future, is the stability, or drift, present in MOS sensors used for continuous monitoring. It is well known that MOS sensors suffer from multiple mechanisms of drift including degradation of the measurement electrodes and heating element, structural changes in the metal oxide, and chemical poisoning on the metal oxide surface, all of which typically renders these types of sensors out of calibration on the order of months making recalibration obligatory [133, 184, 221-224]. The ozone and TVOC sensors on ART are no exception. The calibration and testing presented here were all performed within a two month window and no noticeable decrements in performance were observed. It is even possible that pulsing the heater in the ozone sensor could affect the sensor lifespan. The TVOC sensor has built-in algorithms to attempt to correct for electrode fouling and a dynamic baseline correction [198, 199]. Future works includes finding methods for adding a baseline correction algorithm to the ozone sensor and investigating ways to correct for drift by collocating against a reference instrument in the field without necessitating a full, costly recalibration procedure.

3.7 Conclusion

A wrist-worn Asthma Research Tool ("ART") was developed with an aim for identifying and detecting asthma triggers using only COTS components at low cost (under $150). The device can simultaneously track ozone, total volatile organic compounds (TVOC), temperature, humidity, and activity level of the user at one-minute intervals. The data can be either stored locally to a built-in flash memory, or transfer via its Bluetooth module to a centralized database. Comprehensive analytical tests in the lab, and field tests against reference technologies have been performed to examine its capability for both indoor and outdoor chemical exposure monitoring. In a well ventilated indoor laboratory environment the average RMSE between eight ARTs for ozone was approximately 5 ppb. In an outdoor setting with greater swings in ozone concentration, temperature, and humidity the average RMSE between eight ARTs was approximately 10 ppb. The metal oxide sensors show considerable dependence on temperature, humidity, and exposure history, which was a major difficulty in chemical sensing using the sensors. I have developed and examined various calibration and correcting algorithms to compensate for both temperature and humidity interference, and improve the accuracy of the measurements. ART should be able to make therapeutically relevant ozone exposure measurements given its 10 ppb LOD and the 60 ppb threshold found by the EPA to generate lung inflammation in healthy individuals. Whether or not ART can be a useful research tool for studying asthma symptom triggers is still unknown and must be determined by epidemiologists in future studies. At present no commercial device like this exists and perhaps the work here generates interest in chemical tracking devices for health applications. This work shows that an inexpensive and compact wearable device can be

built, and it also reveals additional improvement, particularly in shortening of response time, reducing cross interference from unintended gases present in air, and determining when recalibration is necessary are all important for a device intended for use under real world scenarios.

References

[127] G. Korotcenkov, V. Brinzari, and B. K. Cho, "In2O3- and SnO2-based thin film ozone sensors: Fundamentals," *J. Sensors*, vol. 2016, pp. 1-31, 2016, 10.1155/2016/3816094.

[130] N. Barsan and U. Weimar, "Conduction model of metal oxide gas sensors," *J. Electroceram.*, vol. 7, no. 3, pp. 143-167, 2001, 10.1023/a:1014405811371.

[131] N. Barsan and U. Weimar, "Understanding the fundamental principles of metal oxide based gas sensors; the example of CO sensing with SnO2 sensors in the presence of humidity," *J. Phys. Condens. Matter*, vol. 15, no. 20, pp. 813-839, 2003, 10.1088/0953-8984/15/20/201.

[132] M. Batzill and U. Diebold, "The surface and materials science of tin oxide," *Prog. Surf. Sci.*, vol. 79, no. 2-4, pp. 47-154, 2005, 10.1016/j.progsurf.2005.09.002.

[133] G. Korotcenkov and B. K. Cho, "Instability of metal oxide-based conductometric gas sensors and approaches to stability improvement (short survey)," *Sens. Actuators B Chem.*, vol. 156, no. 2, pp. 527-538, Aug. 2011, 10.1016/j.snb.2011.02.024.

[160] WHO, "Global Health Observatory (GHO) data Urban Population Growth", 2014. [Online] Available: https://www.who.int/gho/urban_health/situation_trends/ urban_population_growth_text/en/, Accessed on: Feb. 11, 2019.

[161] J. M. Baldasano, E. Valera, and P. Jimenez, "Air quality data from large cities," *Sci. Total Environ.*, vol. 307, pp. 141-165, 2003, 10.1016/s0048-9697(02)00537-5.

[162] WHO, "Health risks of air pollution in Europe – HRAPIE project. Recommendations for concentration-response functions for cost-benefit analysis of particulate matter, ozone and nitrogen dioxide." WHO Regional Office for Europe. Copenhagen, Denmark. 2013. [Online] Available: http://www.who.int/iris/handle/10665/153692, Accessed on: Feb. 11, 2019.

[163] WHO, Evolution of WHO air quality guidelines: past, present and future. Copenhagen, Denmark: WHO Regional Office for Europe, 2017. [Online]

Available: http://www.euro.who.int/en/health-topics/environment-and-health/air-quality/publications/2017/evolution-of-who-air-quality-guidelines-past,-present-and-future-2017

[164] S. S. Lim *et al.*, "A comparative risk assessment of burden of disease and injury attributable to 67 risk factors and risk factor clusters in 21 regions, 1990-2010: A systematic analysis for the Global Burden of Disease Study 2010," *Lancet*, vol. 380, pp. 2224-2260, Dec. 2012, 10.1016/s0140-6736(12)61766-8.

[165] B. Brunekreef, S. T. Holgate, "Air pollution and health," *Lancet*, vol. 360, pp. 1233-1242, Oct. 2002, 10.1016/s0140-6736(02)11274-8.

[166] J. Schwartz, "Air pollution and children's health," *Pediatrics*, vol. 113, no. 4, pp. 1037-1043, Apr. 2004, 1073-0397.

[167] M. Guarnieri, J. R. Balmes, "Outdoor air pollution and asthma," *Lancet*, vol. 383, pp. 1581-1592, May 2014, 10.1016/s0140-6736(14)60617-6.

[168] A. Barraza-Villarreal et al., "Air pollution, airway inflammation, and lung function in a cohort study of Mexico City schoolchildren," *Environ. Health Perspect.*, vol. 116, no. 6, pp. 832-838, June 2008, 10.1289/ehp.10926.

[169] K. M. Mortimer, L. M. Neas, D. W. Dockery, S. Redline, and I. B. Tager, "The effect of air pollution on inner-city children with asthma," *Eur. Respir. J.*, vol. 19, pp. 699-705, 2002, 10.1183/09031936.02.00247102.

[170] D. Briggs, "The role of GIS: Coping with space (and time) in air pollution exposure assessment", *J. Toxicol. Environ. Health A*, vol. 68, pp. 1243-1261, 2005, 10.1080/15287390590936094.

[171] C. Monn, "Exposure assessment of air pollutants: a review on spatial heterogeneity and indoor/outdoor/personal exposure to suspended particulate matter, nitrogen dioxide and ozone," *Atmos. Environ.*, vol. 35, pp. 1-32, 2001, 10.1016/S1352-2310(00)00330-7.

[172] P. L. Jenkins, T. J. Phillips, E. J. Mulberg, and S. P. Hui, "Activity patterns of Californians: Use of and proximity to indoor pollutant sources," *Atmos. Environ. Part A*, vol. 26, no. 12, pp. 2141-2148, Aug. 1992, 10.1016/0960-1686(92)90402-7.

[173] N. E. Klepeis, W. C. Nelson, W. R. Ott, J. P. Robinson, A. M. Tsang, P. Switzer, J. V. Behar, S. C. Hern, and W. H. Engelmann, "The national human activity pattern survey (NHAPS): A resource for assessing exposure to environmental pollutants," *J. Expo. Anal. Environ. Epidemiol.*, vol. 11, no. 3, pp. 231-252, 2001, 10.1038/sj.jea.7500165.

[174] EPA, "The inside story: A guide to indoor air quality," U.S. EPA/Office of Air and Radiation. Research Triangle Park, NC, USA. Nov. 27, 2018. [Online] Available: https://www.epa.gov/indoor-air-quality-iaq/inside-story-guide-indoor-air-quality, Accessed on: Feb. 11, 2019.

[175] R. Piedrahita *et al.*, "The next generation of low-cost personal air quality sensors for quantitative exposure monitoring," *Atmos. Meas. Tech.*, vol. 7, no. 10, pp. 3325-3336, 2014, 10.5194/amt-7-3325-2014.

[176] P. J. D. Peterson, A. Aujla, K. H. Grant, A. G. Brundle, M. R. Thompson, J. V. Hey, and R. J. Leigh, "Practical use of metal oxide semiconductor gas sensors for measuring nitrogen dioxide and ozone in urban environments," *Sensors*, vol. 17, no. 7, pp. 1653-677, July 2017, 10.3390/s17071653.

[177] T. Cao, J. E. Thompson, "Personal monitoring of ozone exposure: A fully portable device for under $150 USD cost," *Sens. Actuators B Chem.*, vol. 224, pp. 936-943, Mar. 2016, 10.1016/j.snb.2015.10.090.

[178] J. Dieffenderfer *et al.*, "Low-power wearable systems for continuous monitoring of environment and health for chronic respiratory disease," *J. Biomed. Health Inform.*, vol. 20, no. 5, pp. 1251-1264, Sept. 2016, 10.1109/JBHI.2016.2573286.

[179] J. Dieffenderfer *et al.*, "Wearable wireless sensors for chronic respiratory disease monitoring," in *2015 IEEE 12th Int. Conf. on Wearable and Implant*. BSN, Cambridge, MA, USA, 2015, pp. 1-6.

[180] R. McConnell, K. Berhane, F. Gilliand, S. J. London, T. Islam, W. J. Gauderman, E. Avol, H. G. Margolis, and J. M. Peters, "Asthma in exercising children exposed to ozone: a cohort study," *Lancet*, vol. 359, pp. 386-391, Feb. 2002, 10.1016/s0140-6736(02)07597-9.

[181] J. Schwartz, "Air pollution and hospital admissions for respiratory disease," *Epidemiology*, vol. 7, no. 1, pp. 20-28, Jan. 1996, 1044-3983.

[182] EPA: National Ambient Air Quality Standards for Ozone, Fed. Reg. Vol. 80, No. 206 (final rule Oct. 26, 2015) (to be codified at 40 C.F.R. pts. 50, 51, 52, 53, and 58).

[183] EPA, "Integrated Science Assessment for Ozone and Related Photochemical Oxidants," U.S. EPA/National Center for Environmental Assessment-RTP Division, Office of Research and Development. Research Triangle Park, NC, USA. Feb. 2013. [Online] Available: https://www.epa.gov/isa/integrated-science-assessment-isa-ozone-and-related-photochemical-oxidants, Accessed on: Apr. 4, 2019.

[184] L. Spinelle, M. Gerboles, M. Aleixandre, and F. Bonavitacola, "Evaluation of metal oxide sensors for the monitoring of O3 in ambient air at ppb level," *Chem. Engineer Trans.*, vol. 54, pp. 319-324, 2016, 10.3303/CET1654054.

[185] D. E. Williams *et al.*, "Modelling the response of a tungsten oxide semiconductor as a gas sensor for the measurement of ozone," *Meas. Sci. Technol.*, vol. 13, no. 6, pp. 923-931, 2002, 10.1088/0957-0233/13/6/314.

[186] D. E. Williams, S. R. Aliwell, K. F. E. Pratt, D. J. Caruana, R. L. Jones, R. A. Cox, G. M. Hansford, and J. Halsall, "Development of low-cost ozone and nitrogen dioxide measurement instruments suitable for use in an air quality monitoring network," in *2009 IEEE Sensors*, Christchurch, Cantebury, New Zealand, 2009, pp. 1099-1104.

[187] S. Brienza, A. Galli, G. Anastasi, and P. Bruschi, "A low-cost sensing system for cooperative air quality monitoring in urban areas," *Sensors*, vol. 15, no. 6, pp. 12242-12259, May 2015, 10.3390/s150612242.

[188] SGX Sensortech. Datasheet MiCS-2614 Ozone Sensor. SGX Sensortech. Corcelles-Cormondreche, Switzerland, Ver. 1087 rev. 5.

[189] M. D. Bortoli, S. Kephalopoulos, S. Kirchner, H. Schauenburg, and H. Vissers, "Indoor air quality & its impact on man. European inter-laboratory comparison on VOC emitted from building materials and products," European Commission, European Collaborative Action, Luxembourg, Report no. 21, EUR 18698 EN, 1999.

[190] EPA, "Volatile organic compounds' impact on indoor air quality," U.S. EPA/Office of Air and Radiation. Research Triangle Park, NC, USA. Nov. 6, 2017. [Online] Available: https://www.epa.gov/indoor-air-quality-iaq/volatile-organic-compounds-impact-indoor-air-quality, Accessed on: Feb. 11, 2019.

[191] I. T. Berrios, J. S. Zhang, B. Guo, J. Smith, and Z. Zhang, "Volatile organic compounds (VOCs) emissions from sources in a partitioned office environment and their impact on IAQ," in *Proc. Indoor Air 2005*, Beijing, China, 2005, pp. 2064-2069.

[192] C. P. Weisel, "Assessing Exposure to Air Toxics Relative to Asthma," *Environ. Health Perspect.*, vol. 110, no. 4, pp. 527-537, Aug. 2012, 10.1289/ehp.02110s4527.

[193] U. B. Nurmatov, N. Tagiyeva, S. Semple, G. Devereux, and A. Sheikh, "Volatile organic compounds and risk of asthma and allergy: a systematic review," *Eur. Respir. Rev.*, vol. 24, pp. 92-101, Mar. 2015, 10.1183/09059180.00000714.

[194] European Collaborative Action, "Indoor Air Quality & its Impact on Man, Report No. 19, Total Volatile Organic Compounds (TVOC) in Indoor Air Quality

Investigations," European Commission, Joint Research Centre, Brussels, Belgium, EUR 17676 EN, 1997.

[195] C. Jaen and P. Dalton, "Asthma and odors: The role of risk perception in asthma exacerbation," *J. Psychosom. Res.*, vol. 77, no. 4, pp. 302-308, 2014, 10.1016/j.jpsychores.2014.07.002.

[196] A. C. Romain, P. Andre, and J. Nicolas, "Three years experiment with the same tin oxide sensor arrays for the identification of malodorous sources in the environment," *Sens. Actuators B Chem.*, vol. 84, pp. 271-277, May 2002, 10.1016/S0925-4005(02)00036-9.

[197] S. Herberger and H. Ulmer, "Indoor air quality monitoring improving air quality perception," *Clean-Soil Air Water*, Vol. 40, pp. 578-585, June 2012, 10.1002/clen.201000286.

[198] D. Ruffer, F. Hoehne, and J. Buhler, "New digital metal-oxide (MOx) sensor platform," *Sensors*, vol. 18, no. 4, pp. 1052-1063, Mar. 2018, 10.3390/s18041052.

[199] Sensirion. Datasheet SGPC3 Sensirion Gas Platform. Sensirion. Staefa, Switzerland, Ver. 0.91, Feb. 2018. [Online] Available: http://www.sensirion.com, Accessed on: Feb. 11, 2019.

[200] Asthma and Allergy Foundation of America, "Weather can trigger asthma," 2017. [Online] Available: https://www.aafa.org/weather-triggers-asthma/, Accessed on: Feb. 11, 2019.

[201] D. Hayes, P. B. Collins, M. Khosravi, R. L. Lin, and L. Y. Lee, "Bronchoconstriction triggered by breathing hot humid air in patients with asthma," *Am. J. Respir. Crit. Care Med.*, vol. 185, no. 11, pp. 1190-1196, June 2012, 10.1164/rccm.201201-0088OC.

[202] S. D. Anderson and E. Daviskas, "The mechanism of exercise-induced asthma is…," *J. Allergy Clin. Immunol.*, vol. 106, no. 3, pp. 453-459, 10.1067/mai.2000.109822.

[203] D. Hughes, "Childhood asthma and exercise," *Paediatr. Child Health*, vol. 19, no. 9, pp. 467-468, Nov. 2014, 1205-7088.

[204] C. A. Howe, K. A. Clevenger, R. E. Leslie, and M. A. Ragan, "Comparison of accelerometer-based cut-points for children's physical activity: Counts vs. steps," *Children*, vol. 5, no. 8, pp. 105-115, Aug. 2018, 10.3390/children5080105.

[205] E. Baque, L. Sakzewski, S. G. Trost, R. N. Boyd, and L. Barber, "Validity of accelerometry to measure physical activity intensity in children with an acquired brain injury," *Pediatr. Phys. Ther.*, vol. 29, no. 4, pp. 322-329, 2017, 10.1097/PEP.0000000000000439.

[206] G. Eranna, B. C. Joshi, D. P. Runthala, and R. P. Gupta, "Oxide materials for development of integrated gas sensors – A comprehensive review," *Crit. Rev. Solid State*, vol. 29, no. 3-4, pp. 111-188, Aug. 2010, 10.1080/10408430490888977.

[207] C. Wang, L. Yin, L. Zhang, D. Xiang, and R. Gao, "Metal oxide gas sensors: Sensitivity and influencing factors," *Sensors*, vol. 10, no. 3, pp. 2088-2106, Mar. 2010, 10.3390/s100302088.

[208] M. Benammar and W. C. Maskell, "Temperature control of thick-film printed heaters," *J. Phys. E: Sci. Instrum.*, vol. 22, no. 11, pp. 933-936, 1989, 10.1088/0022-3735/22/11/006.

[209] J. W. Gong, Q. F. Chen, M. R. Lian, N. C. Liu, and C. Daoust, "Temperature feedback control for improving the stability of a semiconductor-metal-oxide (SMO) gas sensor," *IEEE Sens. J.*, vol. 6, no. 1, pp. 139-145, Feb. 2006, 10.1109/jsen.2005.844353.

[210] G. Golan, A. Axelevitch, B. Sigalov, and B. Gorenstein, "Integrated thin film heater-thermocouple systems," *Microelectron. Reliab.*, vol. 43, no. 3, pp. 509-512, 2003, 10.1016/s0026-2714(02)00320-7.

[211] I. Simon, N. Barsan, M. Bauer, and U. Weimar, "Micromachined metal oxide gas sensors: Opportunities to improve sensor performance," *Sens. Actuators B Chem.*, vol. 73, no. 1, pp. 1-26, 2001, 10.1016/S0925-4005(00)00639-0.

[212] P. Parker, G. G. Vining, S. R. Wilson, J. L. Szarka III, and N. G. Johnson, "The prediction properties of classical and inverse regression for the simple linear calibration problem," *J. Qual. Technol.*, vol. 42, no. 4, pp. 332-347, Oct. 2010, 0022-4065.

[213] Z. Nenova and G. Dimchev, "Compensation of the impact of disturbing factors on gas sensor characteristics," *Acta Polytech. Hung.*, vol. 10, no. 3, pp. 97-111, 2013.

[214] R. Huerta, T. Mosqueiro, J. Fonollosa, N. F. Rulkov, and I. Rodriguez-Lujan, "Online decorrelation of humidity and temperature in chemical sensors for continuous monitoring," *Chemometr. Intell. Lab. Syst.*, vol. 157, pp. 169-176, Oct. 2016, 10.1016/j.chemolab.2016.07.004.

[215] N. Barsan and A. Tomescu, "Calibration procedure for SnO2-based gas sensors," *Thin Solid Films*, vol. 259, no. 1, pp. 91-95, Apr. 1995, 10.1016/0040-6090(94)06415-6.

[216] R. Ionescu, A. Vancu, and A. Tomescu, "Time-dependent humidity calibration for drift corrections in electronic noses equipped with SnO2 gas sensors," *Sens. Actuators B Chem.*, vol. 69, no. 3, pp. 283-286, 2000, 10.1016/S0925-4005(00)00508-6.

[217] C. Krutzler, A. Unger, H. Marhold, T. Fricke, T. Conrad, and A. Schutze, "Influence of MOS gas-sensor production tolerances on pattern recognition techniques in electronic noses," *IEEE Trans. Instrum. Meas.*, vol. 61, no. 1, pp. 276-283, Jan. 2012, 10.1109/tim.2011.2161015.

[218] N. Zimmerman, A. A. Presto, S. P. N. Kumar, J. Gu, A. Hauryliuk, E. S. Robinson, A. L. Robinson, and R. Subramanian, "A machine learning calibration model using random forests to improve sensor performance for lower-cost air quality monitoring," *Atmos. Meas. Tech.*, vol. 11, no. 1, pp. 291-313, Jan. 2018, 10.5194/amt-11-291-2018.

[219] L. Spinelle, M. Gerboles, M. G. Villani, M. Aleixandre, and F. Bonavitacola, "Field calibration of a cluster of low-cost commercially available sensor for air quality monitoring. Part B: NO, CO and CO2," *Sens. Actuators B Chem.*, vol. 238, pp. 706-715, Jan. 2017, 10.1016/j.snb.2016.07.036.

[220] A. C. Lewis et al., "Evaluating the performance of low cost chemical sensors for air pollution research," *Faraday Discuss.*, vol. 189, pp. 85-103, 2016, 10.1039/c5fd00201j.

[221] A. C. Romain and J. Nicolas, "Long term stability of metal oxide-based gas sensors for e-nose environmental applications: An overview," *Sens. Actuators B Chem.*, vol. 146, no. 2, pp. 502-506, Apr. 2010, 10.1016/j.snb.2009.12.027.

[222] S. Capone, M. Epifani, L. Francioso, S. Kaciulis, A. Mezzi, P. Siciliano, and A. Taurino, "Influence of electrodes ageing on the properties of the gas sensors based on SnO2," *Sens. Actuators B Chem.*, vol. 115, no. 1, pp. 396-402, May 2006, 10.1016/j.snb.2005.10.001.

[223] H. Esch, G. Huyberechts, R. Mertens, G. Maes, J. Manca, W. D. Ceuninck, and L. D. Schepper, "The stability of Pt heater and temperature sensing elements for silicon integrated tin oxide gas sensors," *Sens. Actuators B Chem.*, vol. 65, no. 1, pp. 190-192, June 2000, 10.1016/S0925-4005(99)00301-9.

[224] A. Tricoli, "Structural stability and performance of noble metal-free SnO2-based gas sensors," *Biosensors (Basel)*, vol. 2, no. 2, pp. 221-233, May 2012, 10.3390/bios2020221.

4   A MICRODROPLET-BASED COLORIMETRIC SENSING PLATFORM ON A CMOS IMAGER CHIP

4.1 Introduction

Over the past decade there has been a staggering increase in attention towards developing low-cost, mobile sensors. Advancements in mobile computing and the ubiquity of smartphones has paved the way for intelligent devices and acquisition of data previously not possible in the so-called Internet-of-Things, or IoT. In the sensor space physical sensors have been extremely successful, finding their way into nearly all of our devices, but chemical sensors still face fundamental challenges that limit their deployment in the real world. Gas sensing in particular has garnered interest for its many practical applications that could benefit from networked or mobile sensors including air quality [225, 151], public safety [226, 227], health screening [228, 229], and food inspection [230, 231], to name a few. Unfortunately, many types of gas sensors are still plagued with technical problems such as power requirements, size limitations, and difficult calibration [215, 232, 233]. A single chip-based sensing platform that solves these complications and also supports the inclusion of multiple sensing elements could be a breakthrough in paving the way to integrating chemical sensors into existing technology (eg. smartphones), innocuous wearable designs, and low-profile networked devices.

Colorimetry has many practical advantages as a sensing technique. Its mechanism of using a chemical reaction to yield a color change gives it the capability to be highly selective, a desirable property for taking measurements in real-world environments [234]. Another key advantage of colorimetry is its optical readout that promises parallel detection of multiple analytes. Despite the promise, traditional colorimetric gas sensors face two

major challenges: One is sensor-to-sensor variation that leads to tedious and costly individual calibrations, limiting their usefulness outside of the laboratory. This stems from the heterogeneous nature of surface reactions where a gas phase analyte must diffuse and react within the solid matrix of an indicator material and substrate [235-237]. The second challenge is traditional imaging systems used with colorimetric arrays require lenses that have finite focal lengths, on the order of centimeters [238-240]. A compact optoelectronic sensor array capable of being integrated into a mobile device would ideally fit into a surface mountable chip with thickness on the order of millimeters.
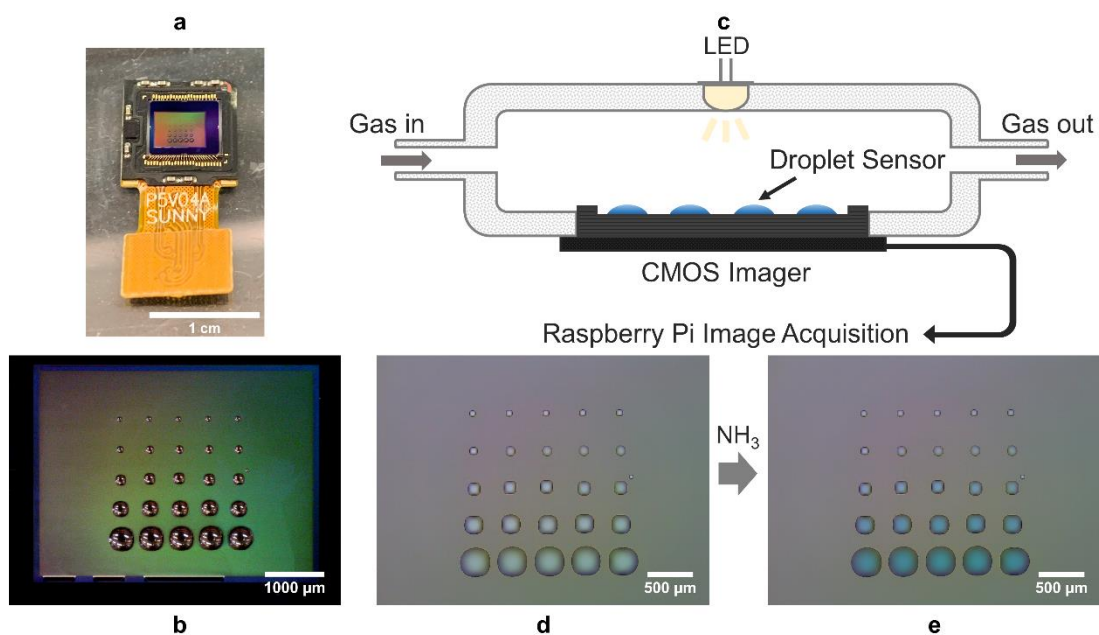

Figure 4.1 (a) Disassembled Raspberry Pi V1 camera module with printed colorimetric sensor array visible on the CMOS imager surface. (b) Optical microscope image of printed colorimetric array on CMOS imager showing droplet sensors of five volumes separated in rows, from top to bottom: 80 pL, 240 pL, 800 pL, 2.4 nL, and 8.0 nL. (c) Experimental test setup for exposing liquid droplet sensors to ammonia gas and recording images with Raspberry Pi. (d) Image acquisition by Raspberry Pi before and (e) after exposure to ammonia gas.

85

Here I propose a microdroplet-based, CMOS imager single-chip solution to address the above challenges. A microdroplet array is printed directly onto the CMOS imager surface (Figure 4.1). The colorimetric microdroplets (CMDs) are composed of a non-volatile solvent that provides a permanent liquid environment; an ideal medium for chemical reactions and optical measurements, being uniform and homogeneous throughout. With the array in contact with the CMOS imager the optoelectronic system is free of additional optical components (eg. lenses), which enables miniaturization while maintaining the ability to take high performance measurements. This technique, known as "contact imaging", has been employed to create lab-on-a-chip microscopy systems and biosensors [241-244], but there are few examples of researchers taking advantage of this compact format to multiplex chemical sensors [245].
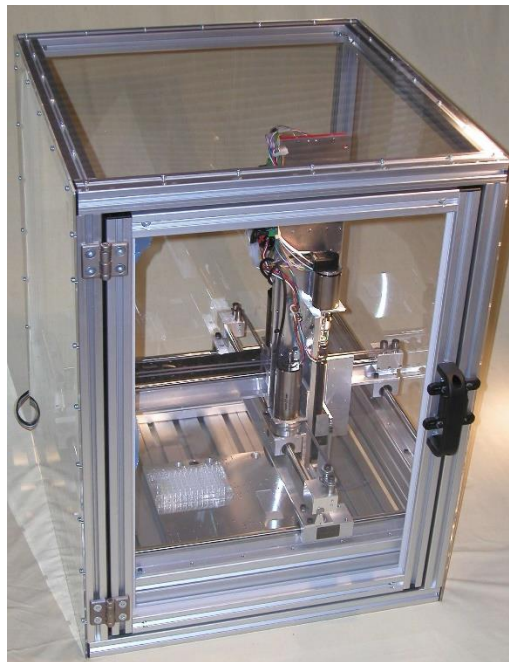

Figure 4.2 PiXY piezoelectric microarrayer for printing sub-nanoliter sensing droplets [249].

Images captured this way have pixel-scale resolution, and with pixels that have dimensions close to 1 micron, this gives near micron resolution across a large field of view [246]. Sensing elements can be dramatically shrunk compared to traditional colorimetric arrays. On a CMOS imager with several million photodiodes an individual sensor can be selectively printed to cover thousands of pixels, leaving room to multiplex many more sensors on the same chip while also having the advantage of averaging the signal of a single sensor over a very large number of photodiodes. The CMOS imager chosen to be a template is from a commercially available Raspberry Pi V1 5 megapixel (MP) camera module (pixel size: 1.4 x 1.4 μm^2) [247], available at the time of authoring this paper for only $7.75 (USD). A highly reproducible PiXY piezoelectric microarrayer [248, 249] capable of delivering sub-nanoliter droplets to the CMOS imager surface without making physical contact with the device was able to generate uniform arrays with minimum sensor-to-sensor variability (Figure 4.2).

This approach is flexible to many types of colorimetric sensing formulations. As an example ammonia gas is detected at low concentrations, down to sub-ppm levels, by complexation of Cu(II) ions in nonvolatile tetraethylene glycol (TEG) (vapor pressure <1 Pa at 20°C) [250]. Although the formation of a coordination complex and concomitant color change of Cu(II) with ammonia is a well-known spot test performed in many introductory chemistry courses [251, 252], this is the first time it has been used to detect and quantify gaseous ammonia. Ammonia was selected because it is relevant in many fields, being an abundant industrial chemical, agriculture fertilizer, air quality indicator, and biomarker for various illnesses [253]. Many of its applications require sensing at low concentrations. For example, NIOSH set the recommended exposure limit (REL) for an 8-

87

hour time-weighted average (TWA) to 25 ppm, while the olfactory threshold lies between 5 and 50 ppm [254]. Outdoor air quality monitoring requires even lower detection limits where concentrations range from low ppb to more than 10 ppm near areas with farming. In the medical field ammonia breath analysis requires measurements, depending on sampling method, from a few ppm to less than 50 ppb [253].

It will be shown that CMDs printed on a single CMOS imager chip can be used to make accurate and reproducible measurements of ammonia at low concentrations, and the mechanism of complexation with Cu(II) may serve as an alternative to the more common pH-sensitive colorimetric indicators [255-258]. The method of printing and homogeneous character of the CMDs yields low variability in sensor responses across multiple chips of less than 10%. That means this type of sensor can be reliably produced to share a single calibration, thus greatly simplifying the steps needed to incorporate a working chemical sensor into mobile technology.

4.2 CMOS Image Sensor Overview

Solid-state image sensors began in the 1960s with MOS fabrication processes [259, 260]. Eventually this was displaced by CMOS fabrication, which gives these types of image sensors (ie. CMOS imagers) their main advantages: full monolithic integration of the image sensor along with processing and control circuits on the same chip in an easy, low-cost manufacturing process [261]. Modern CMOS imagers use silicon substrate active pixel sensors (APS), where each pixel has a built-in amplifier and a light sensitive pinned photodiode (PPD). These typically employ four transistors with each PPD pixel (Figure 4.3). The combination of intrapixel circuitry and pinned photodiode increases sensitivity

88

and reduces noise by enabling techniques like correlated double sampling (CDS). When a photon is absorbed by the photodiode semiconductor material it produces a free electron and hole, which generates a photocurrent. This current builds up as a voltage on a MOS field-effect transistor (MOSFET) proportional to the intensity of light striking the pixel. Voltage is sampled directly at the pixel, digitized on the imager, and cleared for the next image frame. The CMOS imager has completely digital output, and being a voltage driven process makes it very energy efficient [260, 262, 263].
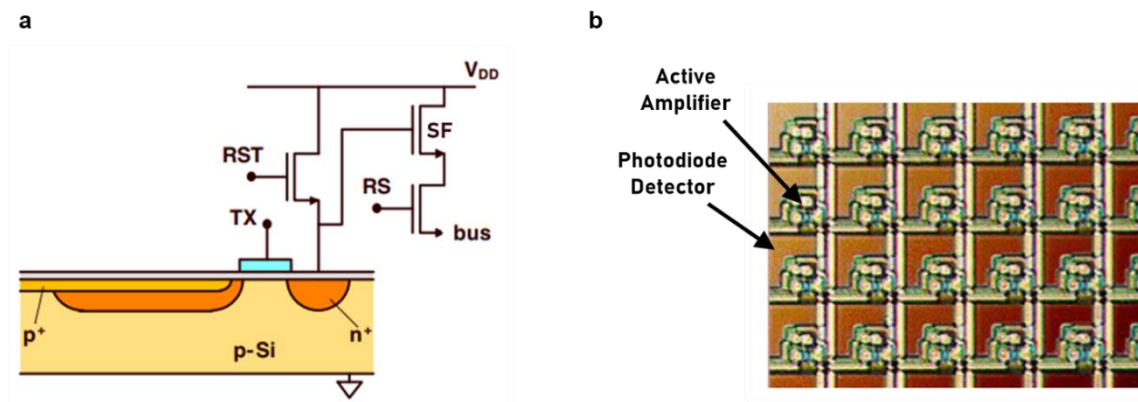

Figure 4.3 (a) PPD APS with four transistors. TX, RST, RS, and SF stand for transfer gate, reset gate, selection gate, and source-follower readout transistor. (b) Array of APS with labels for photodiode material and transistors that make up intrapixel amplifier (microlenses not present) [263].

Color images can be collected when the pixels are coated with pigments in what is known as a Bayer color filter array (Figure 4.4). This makes individual pixels more sensitive to either red, green, or blue light in a repeating pattern. A process known as demosaicing calculates the color of light reaching each pixel based on information from neighboring pixels to create a finished full color image [265]. Microlenses sit on top of each photodiode and pigment layer to help improve light capture (ie. increase sensitivity).

Extensive development has allowed CMOS imagers to surpass other image sensor technology, like the charge coupled device (CCD). As CMOS fabrication processes continue to improve pixels get smaller and imagers are able to incorporate greater numbers of pixels [260].
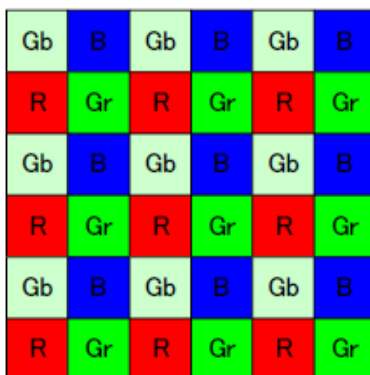

Figure 4.4 A typical Bayer pattern color filter array where green (Gb: green-blue row; Gr: green-red row) coats 50%, red (R) coats 25%, and blue (B) coats 25% of pixels [264].

4.3 Experimental Section

4.3.1 Chemicals

All chemicals were purchased and used without further purification. Tetraethylene glycol (99%) (TEG), cupric nitrate hemipentahydrate (ACS reagent, 98%), and ethanol (ACS reagent, 99.5%) were purchased from Sigma-Aldrich. Tridecafluoro-1,1,2,2-tetrahydrooctyl-1-trichlorosilane (97%) (TCS) was purchased from UCT Specialties, LLC. Ultrapure water (18.2 MΩ·cm) was prepared via an ELGA Purelab Ultra purification system. Ammonia 10 ppm calibration gas, balance nitrogen, was purchased from MESA Specialty Gases & Equipment. Ultra zero grade air was purchased from Matheson.

4.3.2 CMOS Imager Preparation

Each CMD array was printed onto a new CMOS imager that was prepared in the same way. First, a Raspberry Pi V1 camera module was disassembled to reveal its internal OmniVision OV5647 5 MP (2592 x 1944 pixels) CMOS imager (Figure 4.1a). The freshly exposed imager was rinsed under a gentle stream of ultrapure water first, then ethanol, and finally dried under zero air. Next the imager was cleaned under oxygen plasma in a Harrick Plasma PDC-001 plasma cleaner operating at high RF power setting for 5 minutes at 600 mTorr. Then the surface of the CMOS imager was silanized in vapor-phase conditions under house vacuum with 200 µL TCS present in the vacuum chamber. This creates a uniform hydrophobic surface that is best for printing and reproducibility. The silanization process lasted for 30 minutes after which the CMOS imager was rinsed a second time under ethanol and dried with zero air. Finally the CMOS imager was baked in a laboratory oven at 85°C for 30 minutes to cure the silanized surface. All steps were performed immediately consecutive to one another and the prepared CMOS imagers were printed on within 24 hours of completion of this process.

4.3.3 Sensor Array Printing

To make the CMD printing solution 0.465 g cupric nitrate hemipentahydrate was dissolved in 2 mL ultrapure water. This was combined with 2 mL TEG and mixed until a uniform solution was obtained. The CMD arrays were printed with a custom piezoelectric microarray printer (Figure 4.2) capable of delivering 80 pL droplets to the CMOS imager surface without making physical contact with the imager itself to protect the delicate photodiodes. CMDs were produced with sensor volumes of 80 pL, 240 pL, 800 pL, 2.4 nL,

91

and 8.0 nL. Digital optical microscope images captured by a Dino-Lite Edge 3.0 (AM73915MZTL) inspected the finished arrays (Figure 4.1b).

4.3.4 Ammonia Sensor Exposure

Ammonia gas dilutions used in testing were prepared fresh from 10 ppm ammonia gas calibration standard and zero air in 40 L metallized gas sampling bags (Restek). All bags were prepared to 40% RH at a constant laboratory temperature of 23°C using ultrapure water. "Clean air" refers to zero air that has been humidified to 40% RH. To test the CMDs a CMOS imager with finished CMD array was attached to a test fixture machined out of white PTFE block (Figure 4.1c). PTFE was chosen for its inert properties and excellent compatibility with ammonia. A white LED (LEDtronics) embedded in the PTFE block operated at a constant current of 2.5 mA and delivered diffuse white light to the CMOS imager. Gas flow through the test fixture was delivered by PTFE tubing and maintained at 200 sccm.

4.3.5 Image Acquisition and Data Processing

Full resolution 5 MP images were acquired through a Raspberry Pi 4 Model B communicating with the modified CMOS imager (Figure 4.1d-e). Every six seconds the Raspberry Pi recorded a burst of five pictures and averaged them into a single saved image. Using ImageJ software, a region of interest (ROI) was selected within the area of each of the CMDs for making an absorption measurement. Reference ROIs were selected as concentric rings around the perimeter of each CMD with 30 pixel thickness. Absorbance

was calculated as the negative base 10 logarithm of the ratio of the grayscale intensity of the CMD ROI (CMD_g) with the corresponding reference ROI (Ref_g) using equation 4.1.

$$Absorbance = -Log_{10}\left(\frac{CMD_g}{Ref_g}\right) \tag{4.1}$$

The absorbance time series measurement for each CMD was smoothed with a simple moving average filter with window 21 points wide. The smoothed data was numerically differentiated and the slope of the absorbance (AU/min) was correlated with ammonia gas concentration. LOD was calculated with equation 4.2, by measuring the standard deviation of the sensor response in clean air ($SD_{Clean\ Air}$), multiplying by three, and dividing by the sensitivity (S), where the sensitivity is the slope of the best linear fit regression line (AU/min/ppm) [266]. Limit of quantitation (LOQ) was calculated similarly with equation 4.3, by multiplying the standard deviation of the response in clean air by ten and then dividing by the sensitivity. Dynamic range (DR) was calculated with equation 4.4, by taking the ratio of the top concentration of the linear region used in regression ($Conc_{Max}$) by the LOD. ConcMax was determined by finding the concentration range that provides a linear fit with $R^2 > 0.99$.

$$LOD = 3 \cdot \frac{SD_{Clean\ Air}}{S} \tag{4.2}$$

$$LOQ = 10 \cdot \frac{SD_{Clean\ Air}}{S} \tag{4.3}$$

$$DR = \frac{Conc_{Max}}{LOD} \tag{4.4}$$

4.4 Results and Discussion

4.4.1 Ammonia Sensing Mechanism

The interaction of Cu(II) with ammonia to form an intensely blue colored coordination complex is one of the most familiar colorimetric methods among chemists. Just a few drops of ammonia is necessary to indicate the presence of copper in an unknown solution [251]. In the past, this qualitative spot test had been modified into several quantitative methods for the accurate determination of copper, by either visual guides or with the use of a spectrophotometer [267]. Here this concept is used for the first time to quantify trace ammonia gas. The underlying mechanism involves water ligands on the octahedral Cu(II) aqua ion, $[Cu(H_2O)_6]^{2+}$, being successively displaced by stronger ammonia ligands. Cu(II) is a d^9 ion with a single broad absorption band. The aqua ion has weak absorption in the visible region of the spectrum and peaks at approximately 800 nm, giving its solution a faint blue color. Each successive exchange of a water ligand for ammonia increases the magnitude of the ligand field splitting, blueshifting the broad absorption band and increasing its magnitude [268]. The result is the solution turns a deeper darker royal blue, visible in Figure 4.1d-e. While typical colorimetric ammonia sensors use a pH-sensitive indicator embedded in a solid substrate [255-258], this design lets ammonia diffuse directly into liquid CMDs where it can react with Cu(II) in a homogeneous medium. The rate of absorbance change (AU/min) can be correlated with the concentration of ammonia gas present.
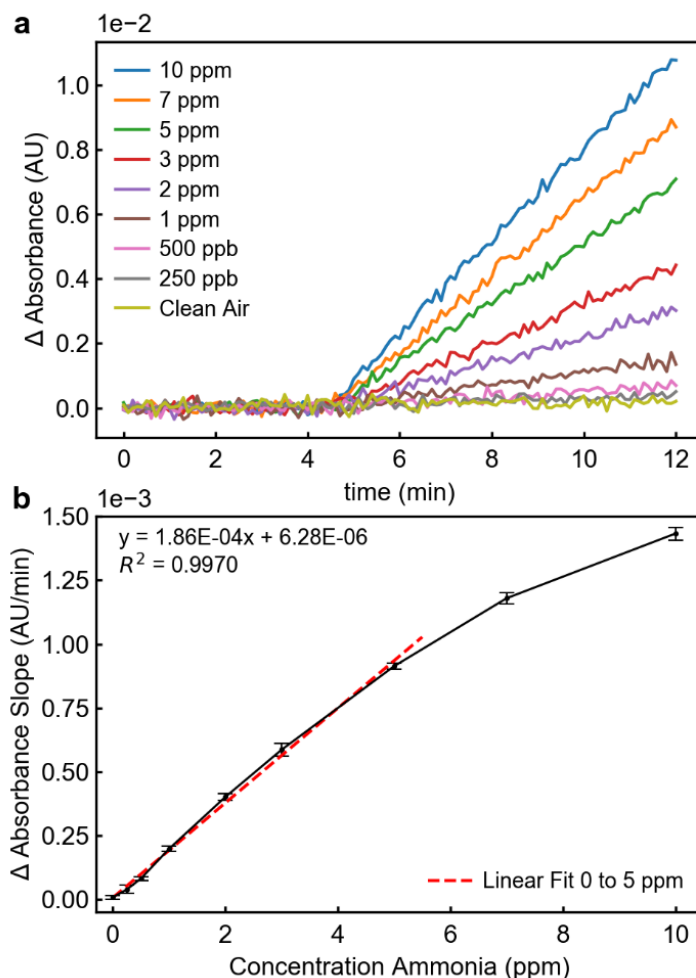
Figure 4.5 (a) Raw absorbance data collected during calibration of a single 2.4 nL CMD. All gas mixtures were prepared to 40% RH at 23°C. (b) Smoothed and numerically derived calibration data forms a response curve. A regression line fits the data within a linear region from 0 to 5 ppm (extended for visual aid). Error bars represent the standard deviation of the calculated slopes.

4.4.2 Calibration of a CMD

To examine the capability of this technique to measure ammonia the CMD arrays were exposed to concentrations of ammonia ranging from 250 ppb to 10 ppm and also clean air, all composed to 40% RH at 23°C. The raw absorbances from a single 2.4 nL CMD are shown in Figure 4.5a. As the concentration of ammonia is increased, the rate of

change in absorption also increases, coinciding with the formation of the blue copper-ammonia complex. The data is smoothed and numerically differentiated, with the slope of the response for each concentration used to form a calibration curve found in Figure 4.5b. Error bars represent the standard deviation of the numerically derived slope spanning five minutes of measurement. The calibration curve has a linear region extending to 5 ppm with good fitting, having an R-squared of 0.9970. The y-intercept with error bars includes zero, which intuitively makes sense for this detection mechanism, there should be no change in absorbance when the unreacted sensor is left in clean air. Beyond 5 ppm the response of the 2.4 nL sensor in Figure 4.5 begins to saturate. It will be shown in the next section that the size of the CMD is responsible for this behavior.

4.4.3 Size Effect

The effect of CMD size was investigated since the mechanism of detection depends on the ability of ammonia to diffuse into the liquid droplets. Figure 4.6 shows calibration curves for five sizes of CMDs ranging from 80 pL to 8.0 nL. The calculated responses are the mean of six replicate sensors, with the error bars representing the standard deviation among those six replicates. Each CMD has a region of linear response that is related to its size. All linear regions are fit by regression lines with $R^2 > 0.99$. As sensor volume increases, dynamic range before saturation in response also increases. The smallest sensor, 80 pL, has the narrowest linear region limited to 500 ppb, but has the greatest sensitivity and lowest LOD, only 27 ppb. On the other end of the spectrum the largest sensor, 8.0 nL, has the widest linear region up to 10 ppm, but it has the lowest sensitivity and greatest LOD of 80 ppb. Table 4.1 provides a summary for the different CMD sizes.
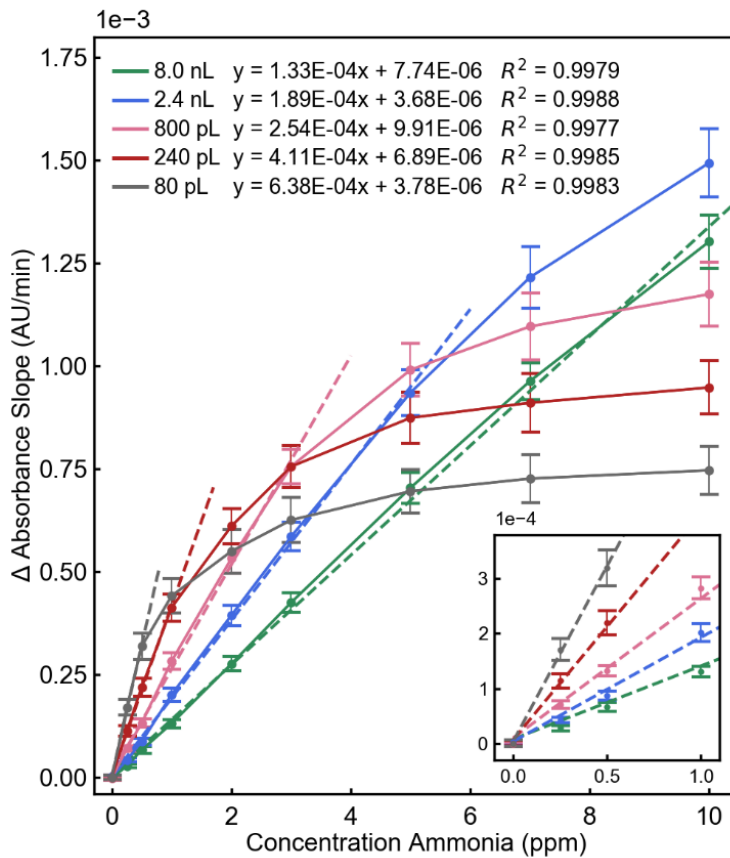
96

Figure 4.6 Response curves from a calibration procedure with five different size CMDs, six replicates of each (n=6). Regression lines fit a linear region in each curve (extended for visual aid) that increases with sensor size. Error bars represent the standard deviations of responses among six replicates. Origin of the plot is magnified in the inset.

Table 4.1 Colorimetric Microdroplet Summary by Size

Printer Droplets	Volume (pL)	Diameter (μm)	Area (pixels)	Noise SD (AU/min)	Sensitivity (AU/min/ppm)	LOD (ppb)	LOQ (ppb)	Dynamic Range
1	80	65	1800	5.74E-06	6.38E-04	27	90	19
3	240	95	3700	5.21E-06	4.11E-04	38	127	26
10	800	140	8300	4.31E-06	2.54E-04	51	170	59
30	2400	200	17500	4.04E-06	1.89E-04	64	213	78
100	8000	300	39000	3.55E-06	1.33E-04	80	267	125

The tradeoff between dynamic range and sensitivity can be visualized in Figure

4.7a. Based on the curvature of this nonlinear relationship, when selecting the optimal

CMD size it may be most advantageous to either maximize dynamic range with a large sensing droplet or maximize sensitivity (low LOD) with a small sensing droplet. CMDs of intermediate sizes seem to have a net reduction in performance. Multiplexing small and large CMDs together in the same array could be used to extend the dynamic range of the instrument while also providing capability for the lowest possible LOD.
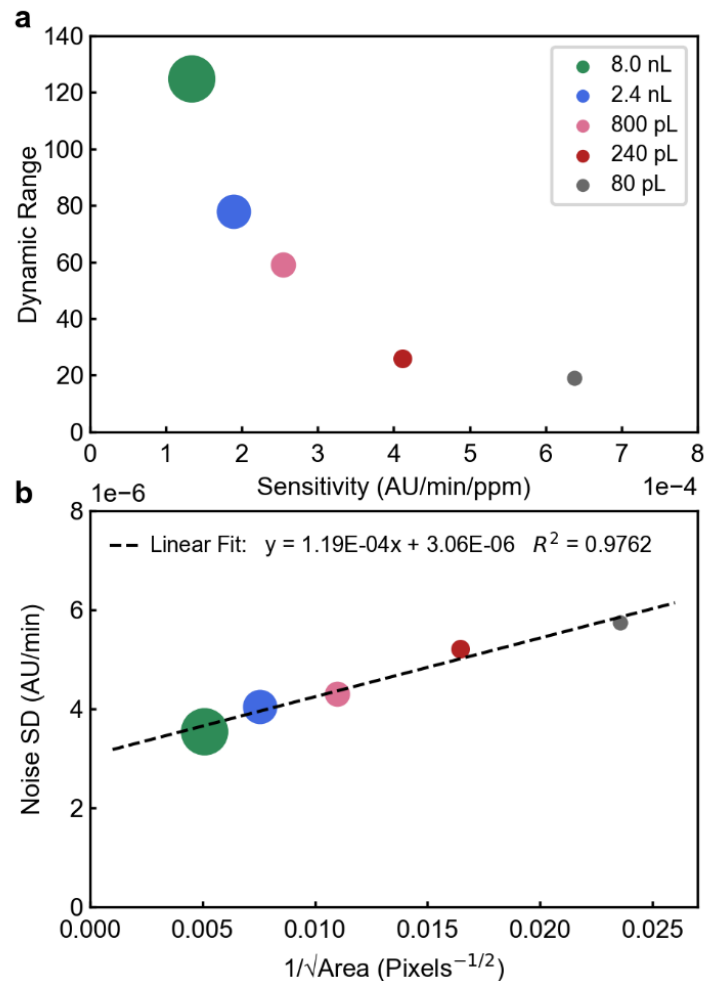

Figure 4.7 (a) Relationship between dynamic range, sensitivity, and sensor size. (b) CMD noise (standard deviation) in clean air decreases with the square root of the area of the CMD. The y-intercept of the regression line is the estimated minimum noise attainable by maximizing sensor size.

Larger volume CMDs cover more pixels on the CMOS imager surface compared with smaller CMDs. Their absorbance is calculated by averaging over more photodiodes (equation 4.1), so they have lower noise compared to the smaller sensors. Spatial averaging decreases noise by $N^{-1/2}$ where N is the number of pixels used in the absorbance calculation. Figure 4.7b illustrates the linear relationship of this type of noise reduction. The finite y-intercept value of 3.06E-6 AU/min estimates the minimum noise attainable by averaging over a large number of pixels. This residual noise can stem from other sources such as the environment, flow rate, and light source, among others. To further reduce noise it would be necessary to average over more image frames (ie. temporally) rather than pixels (ie. spatially). Despite the improvements in noise reduction by increasing the size of the CMD, small CMDs still have better LOD and LOQ. This is because small CMDs have much higher sensitivity from their ability to more efficiently absorb ammonia. The calculations for LOD and LOQ rely on both of these parameters in an opposing manner (equations 4.2 and 4.3). Ultimately, the strong influence of CMD size on sensitivity dominates this relationship and both LOD and LOQ decrease as CMD size decreases.

4.4.4 Reversibility

The formation of a coordination complex between copper and ammonia is reversible, and as a result this ammonia sensing mechanism also displays reversibility. Sensor recovery requires displacing the more strongly coordinating ammonia ligand by a weakly coordinating water ligand. For this reason the rate of change in absorbance for the reverse reaction is slower than it is for the detection of ammonia. Figure 4.8 shows a 2.4 nL CMD exposed to 2 ppm ammonia and then flushed with clean air for three cycles. The

decrease in absorbance during recovery periods appears to be asymptotically approaching the original baseline. Time required to return by 90% is approximately twice the length of time the sensor was exposed to ammonia. Small shifts in the baseline do not inhibit the ability of the sensor to detect ammonia accurately since the calibration is dependent on the slope of the absorbance change (AU/min), not the magnitude of the absorbance itself. This reversible behavior is comparable to other colorimetric ammonia sensors reported in literature using pH-sensitive dyes or the solvatochromic Reichardt's dye [258, 269, 270]. Ammonia sensors relying on chemiresistive interactions using carbon nanotubes or conductive polymers have much slower recovery rates [271-273]. The reversibility of this ammonia sensing mechanism makes the chip-based sensors reusable and helps mitigate the saturation effect so that the sensors are not rendered useless immediately upon exposure to high concentrations of ammonia.
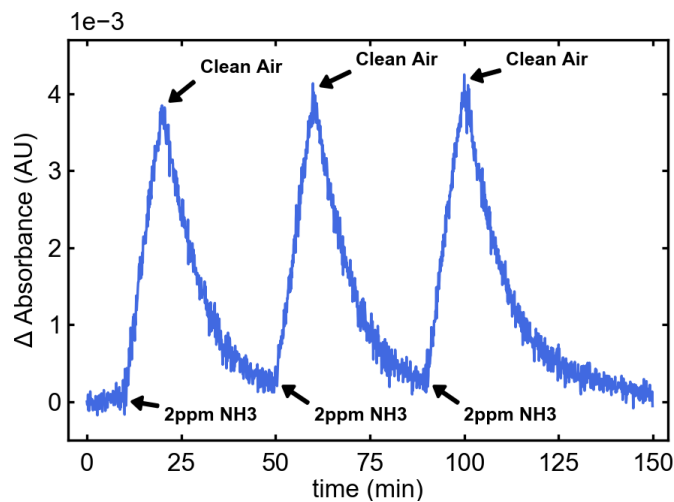

Figure 4.8 Raw absorbance data displaying the reversible behavior of the copper-ammonia colorimetric sensing mechanism. A 2.4 nL CMD is repeatedly exposed to 2 ppm ammonia for 10 minutes, then flushed with clean air for 30 minutes (50 minutes for final cycle).

4.4.5 Selectivity

A primary advantage of colorimetry is the selectivity that can be gained by choosing a chemical reaction that is specific to the analyte of interest. This quality separates it from other common gas sensing techniques, such as MOS, CBS, and ECS. The coordination mechanism of Cu(II) is sensitive to ammonia, but unaffected by many common air pollutants and VOCs. Figure 4.9 shows the responses of the CMD ammonia sensor in clean air, 200 ppb ozone, 200 ppb nitrogen dioxide, 1000 ppm carbon dioxide, 10 ppm toluene, 10 ppm acetone, and 100 ppm ethanol relative to 5 ppm ammonia. The response is less than 1%, and essentially equivalent to the clean air response, for all tests except 10 ppm acetone and 100 ppm ethanol, which respond 1.6% and 3.8%, respectively. The minimal response to typical pollutants at relevant concentrations shows the sensor can operate without the need for chemical scrubbers to remove interferents.
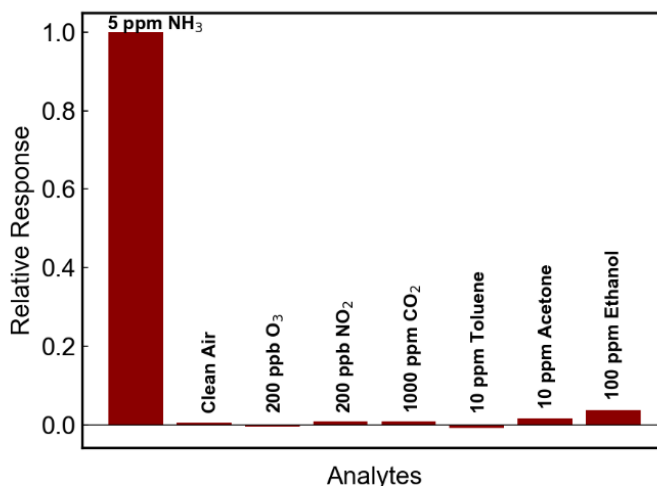

Figure 4.9 Cross-sensitivity with six common air pollutants and VOCs. Responses are relative to 5 ppm ammonia. Clean air is included for comparison.

4.4.6 Sensor Array Variability

The motivation for using permanent liquid CMDs as an alternative to the more common method of depositing a solid indicating material was to produce identical sensing elements that share the closest chemical response possible. Solid indicators suffer from nonuniformities generated during the printing process, like the well-known "coffee ring effect", that lead to greater sensor-to-sensor variation [274, 275]. The heterogeneous nature of gas interaction on the solid sensing matrix can further exacerbate undesirable response characteristics [235-237]. CMDs are a uniform and homogeneous solution throughout, providing an excellent medium for optical measurements and interaction between ammonia and the indicating Cu(II) ions.
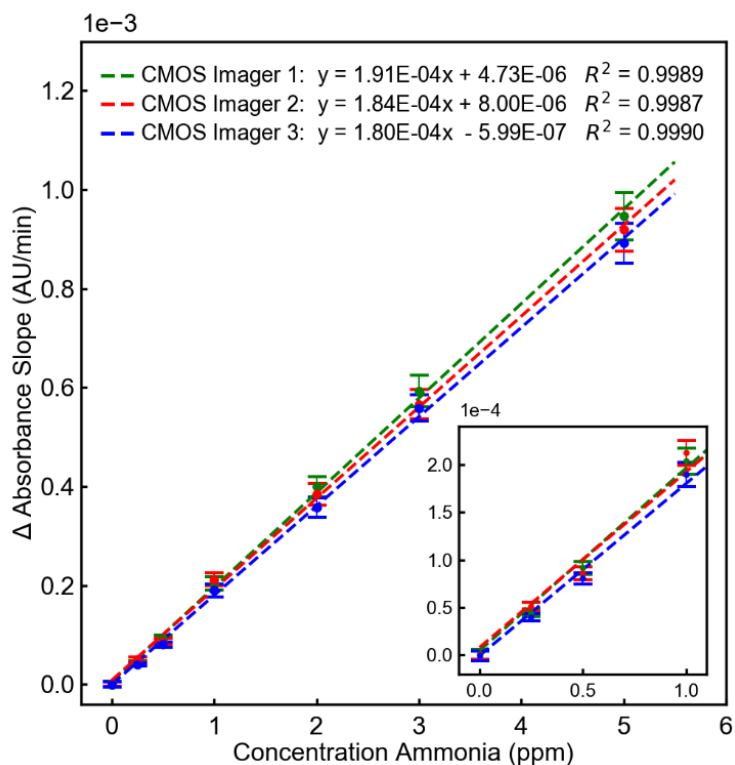

Figure 4.10 Calibration curves for three CMOS imagers, each printed with 30 CMDs (2.4 nL). Error bars represent standard deviations of response among 30 CMDs. Origin of the plot is magnified in the inset.

To test the variance in these sensors three CMOS imagers were prepared in the same way, each with 30 identical 2.4 nL CMDs. The arrays were exposed to a range of ammonia concentrations up to 5 ppm, determined previously to be the upper limit of the linear region for this sensor size. Calibration curves for each CMOS imager can be seen in Figure 4.10. Error bars represent the standard deviation across all 30 CMDs for that particular array. As with previous tests, all regression lines have an $R^2 > 0.99$. The calculated sensitivities of the CMOS imagers are all within 6%, and relative standard deviations of responses for each chip are below 10% (Table 4.2). The small variation in response to ammonia across CMDs on a single chip, and also across multiple chips, means this procedure could be used to produce many sensor arrays in bulk that share a single calibration. Being able to build a calibration into the formulation and printing process so a particular type of sensor only needs to be characterized once and all future sensors share that calibration is critical in reducing the technical and financial burden of calibrating individual sensors in a production setting. It is owed to the homogenous liquid environment making up the CMDs and the color/absorbance change that happens throughout the bulk of the droplet. This is in contrast to popular surface sensitive techniques like MOS and ECS that are extremely sensitive to slight variations in the electrodes from the manufacturing process and environmental contamination, making individual calibration necessary [133, 149, 217, 225, 276].

Table 4.2 Relative Standard Deviations in Responses Across Replicate CMDs

Ammonia (ppm)	0.25	0.50	1.0	2.0	3.0	5.0
CMOS Imager 1	8.5%	7.5%	6.7%	5.1%	5.4%	5.0%
CMOS Imager 2	9.1%	7.7%	6.0%	5.8%	5.2%	4.8%
CMOS Imager 3	9.4%	7.1%	6.5%	5.3%	4.8%	4.6%

The replicate arrays have very similar responses to ammonia, but there is some separation in their calibration curves. To better under-stand this difference the intrinsic sensitivity of each of the three CMOS imagers to light was measured. To do this each imager was exposed to a linear increasing light source by stepping the current of a white LED from 0 to 3 mA in 1 mA increments. The average intensities of each CMOS imager is plotted in Figure 4.11. All three CMOS imagers have nearly identical sensitivities and a linear response to lighting intensity. Therefore, the deviation in calibration curves from Figure 4.10 is not due to differences in the intrinsic sensitivity of the CMOS imagers.
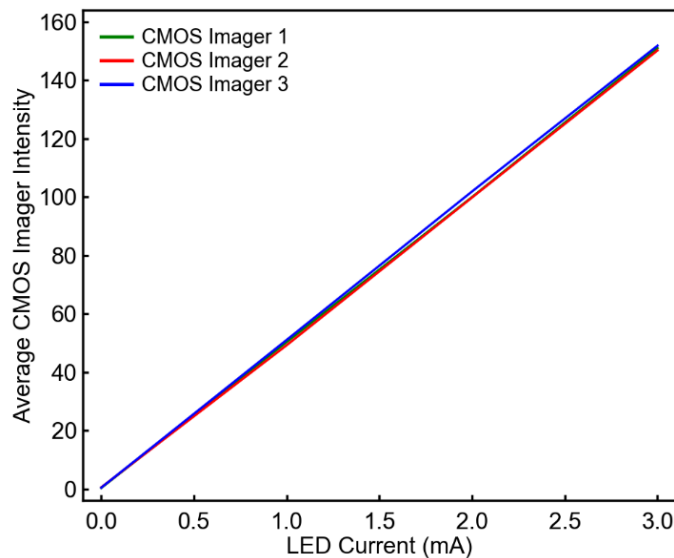

Figure 4.11 The average intensity of CMOS imagers 1-3 measured at 0, 1, 2, and 3 mA LED current. This spanned the relevant range of intensities for the CMOS imagers since experiments were carried out with the LED powered at a constant current of 2.5 mA. The light sensitivity of the three CMOS imagers is linear and essentially identical.

Size differences of the CMDs in the three arrays may also account for variations in their responses. Figure 4.12 shows the three printed CMD arrays from CMOS imagers 1-3. The diameter of each CMD was measured and standard deviations were calculated (Table 4.3). CMOS imager 1, which had the greatest response to ammonia, has smaller diameter droplets than the other two arrays (192 µm average). CMOS imager 3, which had the lowest response to ammonia, has larger diameter droplets than the other two arrays (209 µm average). Variation in droplet diameters in each array was small, approximately 2% relative standard deviation. It is possible the size difference in CMDs is responsible for the shift in response across the three separate chips, albeit small, seeing as it follows the same pattern of CMD size and sensitivity shown earlier. Droplet size variations may arise from inconsistencies in the printing process or slight variation in surface energy and cleanliness of the chips as a result of chip preparation. It should be noted that the chip preparation and microarray printing were performed in a regular laboratory, not a clean room, so all environmental parameters and levels of cleanliness could only be controlled to a reasonable extent. Further improvements on chip-to-chip variability could be made by manufacturing in a designated clean facility with automated procedures to remove human error.
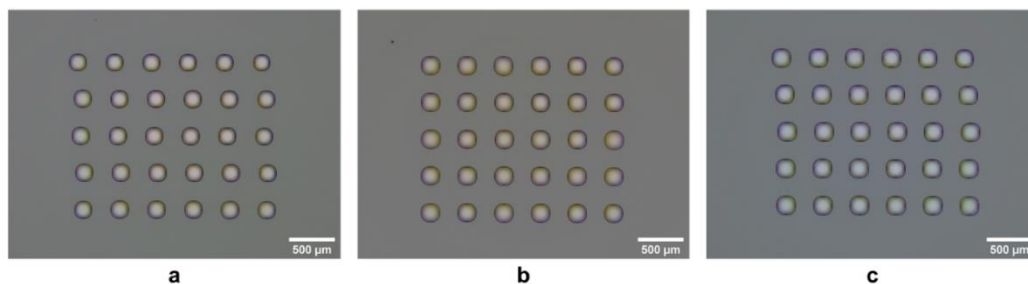

Figure 4.12 2.4 nL CMD arrays printed on (a) CMOS Imager 1, (b) CMOS Imager 2, and (c) CMOS Imager 3.

Table 4.3 Print Size Variability of Replicate CMDs

CMOS Imager	1	2	3
Average Diameter (µm)	192	201	209
Standard Deviation (µm)	3.9	4.2	3.6

The correlation between sensor size and sensitivity may be used to anticipate the calibration curves for CMDs. Data from Table 4.1 can be used to form a power law relationship between sensitivity and diameter with excellent fitting ($R^2 > 0.99$) (Figure 4.13). Testing the derived power law equation with CMD diameters measured from replicate CMOS imagers in Table 4.3 gives predicted sensitivities with less than 5% error from the true experimental values. This suggests that after the size effect for a particular CMD formulation is characterized it could be possible for image processing software to automatically measure CMD size and apply the appropriate calibration curve. An auto-calibration such as this could help ameliorate inconsistencies caused during printing or chip preparation while also improving accuracy and reducing the overhead costs of making these types of corrections manually.
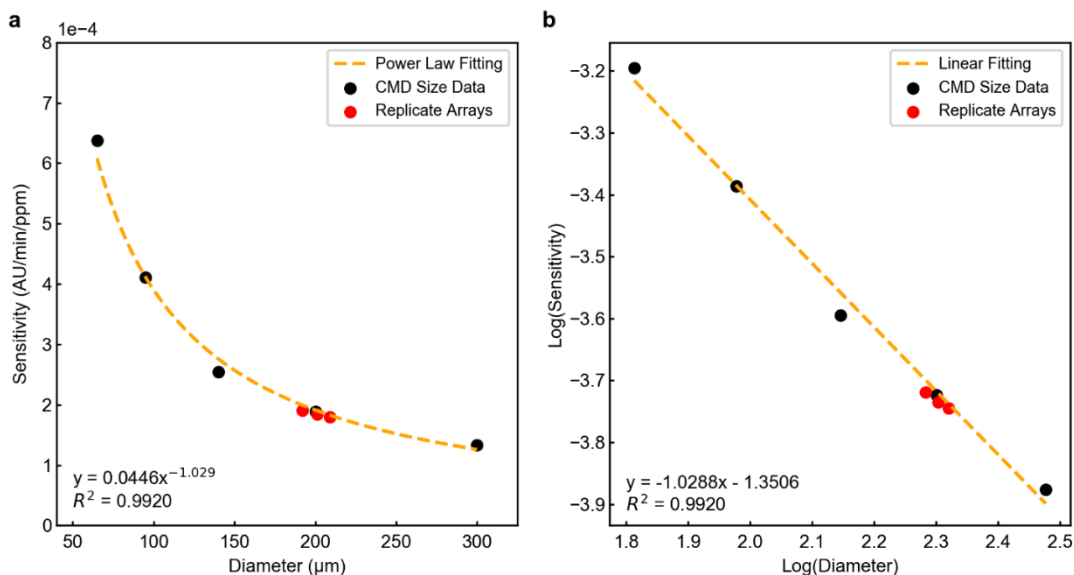
Figure 4.13 (a) The relationship between CMD diameter and sensitivity of the calibration curve can be modeled with a power law using data from Figure 4.6 and Table 4.1 (black dots). Sensitivities calculated during calibration of three independent CMOS imagers from Figure 4.12 and Table 4.3 lie on this line with less than 5% error (red dots). The power law equation can be used to estimate calibration curve sensitivities (slopes) based solely on CMD diameter measured with the camera. (b) Log-log plot of sensitivity and diameter is linear suggesting that a power law may be the appropriate regression method to use in data from part (a). Indeed, the power law did provide best goodness of fit based on R-squared values compared with linear, quadratic, and exponential regressions which were 0.7592, 0.9628, and 0.9094, respectively.

4.5 Conclusion

A low-cost, high-performance optoelectronic gas sensing platform was created by selectively printing CMDs directly onto a CMOS imager surface. The single chip design coupled with the benefits of contact imaging provides a small form factor, approximately 1×1 cm^2 footprint on a PCB and only millimeters thick, making the platform integrable with mobile device technologies. A large field of view combined with excellent resolution facilitates parallel readout by multiplexing many tiny sensing elements at once. Compared with a traditional camera imaging a colorimetric arrays this represents multiple orders of

magnitude reduction in scale. The permanent liquid environment of the CMDs made possible by selecting a suitable nonvolatile solvent, in this case TEG, provides a uniform and homogeneous medium perfect for colorimetric reactions and optical measurements. Evidence for this are the excellent detection limits and low sensor-to-sensor variations between multiple printed arrays. Detection of ammonia by complexation of Cu(II) enabled LODs ranging from 27 ppb to 80 ppb depending on CMD size. The mechanism was shown to be reversible, making the sensors reusable. Interference by common air pollutants was negligible, meaning this technique is selective and could operate without the need for chemical scrubbers. Most importantly, the variation in chemical response of replicate sensors across arrays on three CMOS imagers was less than 10%, meaning a senor formulation could be characterized and share a single calibration. This eliminates the time, expense, and complexity involved in working with sensors that require individual calibration. Moreover, the small size of the CMDs in relation to the area of the CMOS imager allows room for replicate sensors, enabling further improvement in precision of gas measurements by taking the mean response. In addition, the relationship between CMD diameter and sensitivity may be used to predict the calibration curves for arrays printed with different droplet sizes. These characteristics make this new technique of gaseous ammonia detection competitive with existing methods that use pH indicators, solvatochromic dyes, conductive polymers, and chemiresistors. Another advantage of the Cu(II) system is its inherent resistance to typical environmental modes of degradation, like oxidation and hydrolysis, that may attack organic-based indicators. The sensitivity to trace concentrations of ammonia make this type of sensor useful for worker safety (NIOSH REL 8-hour TWA 25 ppm), outdoor ambient air quality monitoring (approx. 50 ppb to 10 ppm),

and breath analysis for health applications (approx. 50 ppb to 5 ppm). With CMOS imagers available for a only couple dollars (USD) and prices continuing to fall I envision this platform could be part of a disposable chip-based sensor system, analogous to the way a microSD card is effortlessly inserted and removed from a mobile device. The added advantage is sensors would never need to be recalibrated, simplifying operation for users. Future work should involve increasing image acquisition framerate and adding real-time onboard processing. This would shorten response time, reduce noise by filtering across more frames, and allow for true real-time chemical monitoring. It would also enable more thorough testing and realization of an algorithm that automatically determines calibration curves by measuring printed droplet diameter. Other work will focus on determining the long-term stability of the system to mechanical and environmental stressors. Currently I am investigating the addition of polymers, gels, and silanes to generate more robust microdroplets. The CMD approach should be generalizable to other colorimetric formulations too. It is important to stress that using other nonvolatile solvents, such as the heavier plasticizers, and different colorimetric indicators should allow tuning of sensing properties for applications of interest beyond just ammonia sensing with Cu(II) and TEG. With time it will be possible to print an array of CMDs on a single CMOS imager chip capable of detecting and quantifying dozens of gases simultaneously.

References

[133] G. Korotcenkov and B. K. Cho, "Instability of Metal Oxide-Based Conductometric Gas Sensors and Approaches to Stability Improvement (Short Survey)," *Sens. Actuators B. Chem.*, vol. 156, pp. 527-538, 2011, 10.1016/j.snb.2011.02.024.

[149] M. Raninec, "Overcoming the Technical Challenges of Electrochemical Gas Sensing," Norwood, MA, USA, Analog Devices, Technical Article, pp. 1-5, 2019.

[151] M. I. Mead, O. A. M. Popoola, G. B. Stewart, P. Landshoff, and M. Calleja, "The Use of Electrochemical Sensors for Monitoring Urban Air Quality in Low-Cost, High-Density Networks," *Atmos. Environ.*, vol. 70, pp. 186-203, 2013, 10.1016/j.atmosenv.2012.11.060.

[215] N. Barsan and A. Tomescu, "Calibration procedure for SnO2-based gas sensors," *Thin Solid Films*, vol. 259, no. 1, pp. 91-95, Apr. 1995, 10.1016/0040-6090(94)06415-6.

[217] C. Krutzler, A. Unger, H. Marhold, T. Fricke, T. Conrad, and A. Schutze, "Influence of MOS gas-sensor production tolerances on pattern recognition techniques in electronic noses," *IEEE Trans. Instrum. Meas.*, vol. 61, no. 1, pp. 276-283, Jan. 2012, 10.1109/tim.2011.2161015.

[225] K. R. Mallires, D. Wang, V. V. Tipparaju, and N. Tao, "Developing a Low-Cost Wearable Personal Exposure Monitor for Studying Respiratory Diseases Using Metal-Oxide Sensors," *IEEE Sens. J.*, vol. 19, pp. 8252-8261, 2019, 10.1109/JSEN.2019.2917435.

[226] K. Schmitt, K. R. Tarantik, C. Pannek, and J. Wollenstein, "Colorimetric Materials for Fire Gas Detection – A Review," *Chemosensors*, vol. 6, pp. 1-15, 2018, 10.3390/chemosensors6020014.

[227] H. Lin and K. S. Suslick, "A Colorimetric Sensor Array for Detection of Triacetone Triperoxide Vapor," *J. Am. Chem. Soc.*, vol. 132, pp. 15519-15521, 2010, 10.1021/ja107419t.

[228] M. K. Nakhleh, H. Amal, R. Jeries, Y. Y. Broza, M. Aboud, A. Gharra, H. Ivgi, S. Khatib, S. Badarneh, L. Har-Shai *et al.*, "Diagnosis and Classification of 17 Diseases from 1404 Subjects via Pattern Analysis of Exhaled Molecules," *ACS Nano*, vol. 11, pp. 112-125, 2017, 10.1021/acsnano.6b04930.

[229] H. Zhao, L. Liu, X. Lin, J. Dai, S. Liu, T. Fei, and T. Zhang, "Proton-Conductive Gas Sensor: A New Way to Realize Highly Selective Ammonia Detection for Analysis of Exhaled Human Breath," *ACS Sens.*, vol. 5, pp. 346-352, 2020, 10.1021/acssensors.9b01763.

[230] Z. Li and K. S. Suslick, "Portable Optoelectronic Nose for Monitoring Meat Freshness," *ACS Sens.*, vol. 1, pp. 1330-1335, 2016, 10.1021/acssensors.6b00492.

[231] T. Konduru, G. C. Rains, and C. Li, "Detecting sour skin infected onions using a customized gas sensor array," *J. Food Eng.*, vol. 160, pp. 19-27, 2015, 10.1016/j.jfoodeng.2015.03.025.

[232] H. Nazemi, A. Joseph, J. Park, and A. Emadi, "Advanced Micro- and Nano-Gas Sensor Technology: A Review," *Sensors*, vol. 19, pp. 1-23, 2019, 10.3390/s19061285.

[233] P. Wei, Z. Ning, S. Ye, L. Sun, F. Yang, K. C. Wong, D. Westerdahl, and P. K. K. Louie, "Impact Analysis of Temperature and Humidity Conditions on Electrochemical Sensor Response in Ambient Air Quality Monitoring," *Sensors*, vol. 18, pp. 1-16, 2018, 10.3390/s18020059.

[234] P. D. Puiu. *Color Sensors and Their Applications. In Optical Nano- and Microsystems for Bioanalytics*. W. Fritzsche, J. Popp, Eds.; Springer Series on Chemical Sensors and Biosensors; Springer-Verlag: Heidelberg, 2012; Vol. 10, pp 4-17.

[235] G. Orellana, M. C. Moreno-Bondi, D. Garcia-Fresnadillo, and M. D. Marazuela. *The Interplay of Indicator, Support and Analyte in Optical Sensor Layers. In Frontiers in Chemical Sensors*. O. S. Wolfbeis, G. Orellana, M. C. Moreno-Bondi, Eds.; Springer Series on Chemical Sensors and Biosensors; Springer-Verlag: Heidelberg, 2005; Vol. 3, pp 189-225.

[236] Z. Li, J. R. Askim, and K. S. Suslick, "The Optoelectronic Nose: Colorimetric and Fluorometric Sensor Arrays," *Chem. Rev.*, vol. 119, pp. 231-292, 2019, 10.1021/acs.chemrev.8b00226.

[237] M. K. LaGasse, J. M. Rankin, J. R. Askim, and K. S. Suslick, "Colorimetric Sensor Arrays: Interplay of Geometry, Substrate and Immobilization," *Sens. Actuators, B*, vol. 197, pp. 116-122, 2014, 10.1016/j.snb.2014.01.102.

[238] X. Qin, R. Wang, F. Tsow, E. Forzani, X. Xian, and N. Tao, "A Colorimetric Chemical Sensing Platform for Real-Time Monitoring of Indoor Formaldehyde," *IEEE Sens. J.*, vol. 15, pp. 1545-1551, 2015, 10.1109/JSEN.2014.2364142.

[239] C. Lin, X. Xian, X. Qin, D. Wang, F. Tsow, E. Forzani, and N. Tao, "High Performance Colorimetric Carbon Monoxide Sensor for Continuous Personal Exposure Monitoring," *ACS Sens.*, vol. 3, pp. 327-333, 2018, 10.1021/acssensors.7b00722.

[240] R. Wang, A. Prabhakar, R. A. Iglesias, X. Xian, X. Shan, F. Tsow, E. S. Forzani, and N. Tao, "A Microfluidic-Colorimetric Sensor for Continuous Monitoring of Reactive Environmental Chemicals," *IEEE Sens. J.*, vol. 12, pp. 1529-1535, 2012, 10.1109/JSEN.2011.2174218.

[241] G. Zheng, "Chip-scale microscopy imaging," *J. Biophotonics*, vol. 5, pp. 639-649, 2012, 10.1002/jbio.201200043.

[242] A. Ozcan and E. McLeod, "Lensless Imaging and Sensing," *Annu. Rev. Biomed. Eng.*, vol. 18, pp. 77-102, 2016, 10.1146/annurev-bioeng-092515-010849.

[243] H. Takehara, K. Miyazawa, T. Noda, K. Sasagawa, T. Tokuda, S. H. Kim, R. Iino, H. Noji, and J. Ohta, "A CMOS image sensor with stacked photodiodes for lensless

observation system of digital enzyme-linked immunosorbent assay," *Jpn. J. Appl. Phys.*, vol. 53, pp. 1-5, 2014, 10.7567/JJAP.53.04EL02.

[244]   R. R. Singh, D. Ho, A. Nilchi, G. Gulak, P. Yau, and R. Genov, "A CMOS/Thin-Film Fluorescence Contact Imaging Microsystem for DNA Analysis," *IEEE Trans. Circuits Syst.*, vol. 57, pp. 1029-1038, 2010, 10.1109/TCSI.2010.2043990.

[245]   D. S. Daivasagaya, L. Yao, K. Y. Yung, M. Hajj-Hassan, M. C. Cheung, V. P. Chodavarapu, and F. V. Bright, "Contact CMOS imaging of gaseous oxygen sensor array," *Sens. Actuators B Chem.*, vol. 157, pp. 408-416, 2011, 10.1016/j.snb.2011.04.074.

[246]   H. Ji, D. Sander, A. Haas, and P. A. Abshire, "Contact Imaging: Simulation and Experiment," *IEEE Trans. Circuits Syst.*, vol. 54, pp. 1698-1710, 2007, 10.1109/TCSI.2007.902409.

[247]   Omnivision, "OV5647 5-Megapixel Product Brief," Santa Clara, CA, USA; Version 1.2 November, 2010.

[248]   P. Wiktor, A. Brunner, P. Kahn *et al.*, "Microreactor Array Device," *Sci. Rep.*, vol. 5, pp. 8736, 2015, 10.1038/srep08736.

[249]   V. J. Nagaraj, S. Eaton, and P. Wiktor, "NanoProbeArrays for the Analysis of Ultra-Low-Volume Protein Samples Using Piezoelectric Liquid Dispensing Technology," *SLAS Technol.*, vol. 16, no. 2, pp. 126-133, 2011, 10.1016/j.jala.2010.07.005.

[250]   Tetraethylene Glycol; MSDS No. 110175; Sigma-Aldrich: St. Louis, MO, Jan 15, 2020.

[251]   M. O. Byrd and C. J. Ohrenberg, "The Use of Ammonia as a Qualitative Test for Determining When Solid Copper Has Completely Precipitated from Aqueous Solutions Containing Copper(II) Ions," *Ga. J. Sci.*, vol. 75, pp. 1-7, 2017.

[252]   A. T. Baker, "The Ligand Field Spectra of Copper(II) Complexes," *J. Chem. Educ.*, vol. 75, pp. 98-99, 1998, 10.1021/ed075p98.

[253]   B. Timmer, W. Olthuis, and A. V. D. Berg, "Ammonia sensors and their applications – a review," *Sens. Actuators B Chem.*, vol. 107, pp. 666-677, 2005, 10.1016/j.snb.2004.11.054.

[254]   D. E. Gardner, D. Krewski, and E. C. Bishop, "Acute Exposure Guideline Levels for Selected Airborne Chemicals, vol. 6," National Academy Press: Washington, DC, 2008; pp 58-114.

[255]   N. Y. Liu, P. Cay-Durgun, T. Lai, M. Sprowls, L. Thomas, M. L. Lind, and E. Forzani, "A Handheld, Colorimetric Optoelectronic Dynamics Analyzer for

Measuring Total Ammonia of Biological Samples," *IEEE J. Transl. Eng. Health Med.*, vol. 6, pp. 1-10, 2018, 10.1109/JTEHM.2018.2840678.

[256] J. H. Bang, S. H. Lim, E. Park, and K. S. Suslick, "Chemically Responsive Nanoporous Pigments: Colorimetric Sensor Arrays and the Identification of Aliphatic Amines," *Langmuir*, vol. 24, pp. 13168-13172, 2008, 10.1021/la802029m.

[257] A. T. Hoang, Y. B. Cho, J. S. Park, Y. Yang, and Y. S. Kim, "Sensitive naked-eye detection of gaseous ammonia based on dye-impregnated nanoporous polyacrylonitrile mats," *Sens. Actuators B Chem.*, vol. 230, pp. 250-259, 2016, 10.1016/j.snb.2016.02.058.

[258] J. Courbat, D. Briand, J. Damon-Lacoste, J. Wollenstein, N. F. D. Rooij, "Evaluation of pH indicator-based colorimetric films for ammonia detection using optical waveguides," *Sens. Actuators B Chem.*, vol. 143, pp. 62-70, 2009, 10.1016/j.snb.2009.08.049.

[259] Y. Adiguzel and H. Kulah, "CMOS Cell Sensors for Point-of-Care Diagnostics," *Sensors*, vol. 12, pp. 10042-10066, 2012, 10.3390/s120810042.

[260] J. Ohta. *Smart CMOS Image Sensors and Applications*. New York, NY, USA. CRC Press, Taylor & Francis Group. 2008. pp. 1-58.

[261] M. El-Desouki, M. J. Deen, Q. Fang, L. Liu, F. Tse, and D. Armstrong, "CMOS Image Sensors for High Speed Applications," *Sensors*, vol. 9, pp. 430-444, 2009, 10.3390/s90100430.

[262] Y. Bulayev, Hamamatsu Corp., "Advances in CMOS Image Sensors Open Doors to Many Applications," 2015. [Online] Available: https://www.photonics.com/Articles/Advances_in_CMOS_Image_Sensors_Open_Doors_to_Many/a57683, Accessed On: Sept. 5, 2020.

[263] A. J. P. Theuwissen, "CMOS Image Sensors: State-of-the-Art," *Solid State Electron.*, vol. 52, pp. 1401-1406, 2008, 10.1016/j.sse.2008.04.012.

[264] Sony, "Sony IMX219PQH5-C Datasheet," rev. 7.0.0, pp. 1-96.

[265] M. Imanbekova, A. S. Perumal, S. Kheireddine, D. V. Nicolau, and S. Wachsmann-Hogiu, "Lensless, Reflection-Based Dark-Field Microscopy (RDFM) on a CMOS Chip," *Biomed. Opt. Express*, vol. 11, pp. 4942-4959, 2020, 10.1364/BOE.394615.

[266] D. A. Skoog and J. J. Leary. *Principles of Instrumental Analysis, Fourth Edition*. Saunders College Publishing: Orlando, FL, USA. 1992. pp 5-8.

[267] J. P. Mehlig, "Colorimetric Determination of Copper with Ammonia A Spectrophotometric Study," *Ind. Eng. Chem. Anal. Ed.*, vol. 13, no. 8, pp. 533-535, 1941, 10.1021/i560096a006.

[268] F. A. Cotton, G. Wilkinson, C. A. Murillo, and M. Bochmann. *Advanced Inorganic Chemistry, Sixth Edition*. John Wiley & Sons, Inc.: New York, NY, USA. 1999. pp 864-869.

[269] S. Wintzheimer, M. Oppmann, M. Dold, C. Pannek, M. L. Bauers-feld, M. Henfling, S. Trupp, B. Schug, and K. Mandel, "Indicator Supraparticles for Smart Gasochromic Sensor Surfaces Reacting Ultrafast and Highly Sensitive," *Part. Part. Syst. Charact.*, vol. 36, pp. 1-7, 2019, 10.1002/ppsc.201900254.

[270] K. Schmitt, K. Tarantik, C. Pannek, G. Sulz, and J. Wollenstein, "Colorimetric gas sensing with enhanced sensitivity," *Procedia Eng.*, vol. 168, pp. 1237-1240, 2016, 10.1016/j.proeng.2016.11.430.

[271] F. Rigoni, S. Tognolini, P. Borghetti, G. Drera, S. Pagliara, A. Goldoni, and L. Sangaletti, "Environmental monitoring of low-ppb ammonia concentrations based on single-wall carbon nanotube chemiresistor gas sensors: detection limits, response dynamics, and moisture effects," *Procedia Eng.*, vol. 87, pp. 716-719, 2014, 10.1016/j.proeng.2014.11.638.

[272] L. A. Panes-Ruiz, M. Shaygan, Y. Fu, Y. Liu, V. Khavrus, S. Oswald, T. Gemming, L. Baraban, V. Bezugly, and G. Cuniberti, "Toward Highly Sensitive and Energy Efficient Ammonia Gas Detection with Modified Single-Walled Carbon Nanotubes at Room Temperature," *ACS Sens.*, vol. 3, pp. 79-86, 2018, 10.1021/acssensors.7b00358.

[273] A. D. Aguilar, E. S. Forzani, L. A. Nagahara, I. Amlani, R. Tsui, and N. J. Tao, "A Breath Ammonia Sensor Based on Conducting Polymer Nanojunctions," *IEEE Sens. J.*, vol. 8, pp. 269-273, 2008, 10.1109/JSEN.2007.913137.

[274] R. D. Deegan, O. Bakajin, T. F. Dupont, G. Huber, S. R. Nagel, and T. A. Witten, "Capillary flow as the cause of ring stains from dried liquid drops," *Nature*, vol. 389, pp. 827-829, 1997, 10.1038/39827.

[275] L. Cui, J. Zhang, X. Zhang, L. Huang, Z. Wang, Y. Li, H. Gao, S. Zhu, T. Wang, and B. Yang, "Suppression of the Coffee Ring Effect by Hydrosoluble Polymer Additives," *ACS Appl. Mater. Interfaces*, vol. 4, pp. 2775-2780, 2012, 10.1021/am300423p.

[276] I. Helm, L. Jalukse, and I. Leito, "Measurement Uncertainty Estimation in Amperometric Sensors: A Tutorial Review," *Sensors*, vol. 10, pp. 4430-4455, 2010, 10.3390/s100504430.

5   PRINTABLE HYDROPHOBIC GAS SENSORS FROM AEROGEL

PARTICLES ON A CMOS IMAGER CHIP

5.1 Introduction

The liquid CMDs presented in the last chapter showed excellent sensing characteristics in terms of their high sensitivity and low sensor-to-sensor variation. Part of this was attributed to the liquid droplets being an ideal medium for chemical reactions as well as optical measurements. The rest was attributed to the controllability of the non-contact piezoelectric printing technique, small size of the sensors, and the sensitivity of the CMOS imager when contact imaging. Another important trait for chemical sensors though, is robustness. A useful sensor must be capable of handling environmental and user-generated disturbances that are expected during typical use. Liquid microdroplets are inherently susceptible to mechanical forces, vibrations, and thermal effects given their loose composition. They can slide or spread across the surface which ruins their good sensing properties. The hydrophilic nature of TEG, an oligomer of polyethylene glycol (PEG), used in the CMDs also makes them sensitive to fluctuations in ambient humidity. This motivated the development of a printable gas sensor formulation that is mechanically stable, exhibits humidity resistance, and still provides high sensitivity and reproducibility.

There has been much attention to the development of different substrates for colorimetric gas sensors over the years and a general consensus has formed as to what traits give the best performance. First and foremost, solid particles and films composed of pure colorimetric indicator do not give the best response to analytes because diffusion of analyte into the bulk is typically very slow [236, 256, 280]. This restricts chemical reactions to the small amount of colorant available on the surface of the particles. It is best for the indicator

115

to be dispersed throughout a plasticizer or polymer, or immobilized across the surface of a solid support [239, 257, 258, 269]. Solid supports with high specific surface areas allow a large amount of indicator to be immobilized while providing a pathway for the gas analyte to diffuse inward easily. This gives high sensitivity and fast response compared with monolithic, low surface area substrates [235, 237, 238, 279, 281, 282]. Hydrophobic substrates are known to limit adsorption of water from the environment and improve sensor stability, resistance to ambient humidity interference, prevent blooming and leaching of colorants, and extend sensor lifetime [236, 256, 277, 278, 280]. These typically come in the form of porous hydrophobic polymer membranes (eg. PVDF, PTFE) and porous organically functionalized silicate-based materials (eg. treated silica gel, ormosils).

One interesting class of materials that have gotten limited attention for colorimetric gas sensors but have ideal properties to be substrates are hydrophobic, silicate-based aerogels. Aerogels are characterized by their high porosity, low density, and large available surface area. Hydrophobic aerogels formed from the condensation of alkyl functionalized alkoxy silanes have tunable pore sizes and surface energies. Their network of siloxane bonds makes them robust, and some can absorb nearly 100 times their own weight in oil with minimal water partition [283]. A mesoporous aerogel could be used to sorb a high concentration of molecular indicating dye, prevent humidity ingress, and provide fast diffusion of gas analyte to the immobilized indicator for an excellent sensor response [284, 285]. Silicate-based aerogels are also transparent with very low refractive index (close to air) giving them good optical properties for absorbance measurement techniques [286].

Figure 5.1 Enova hydrophobic aerogel IC3100 fine particles from Cabot Aerogel with water droplets resting on top illustrating its hydrophobicity.

Specialized colorimetric substrates with hydrophobic qualities, like the treated silicas and ormosils mentioned prior, are generally synthesized by the same researchers that are making the sensors, that is, they are not commercially available [236, 237, 256, 269, 280]. This presents an obstacle in the natural evolution of sensors and sensing devices since only a niche set of researchers want to take on the challenge of developing custom substrates, while most rely on traditional materials that are more easily accessible. Aerogels represent an underutilized alternative that should be as good as, if not better than, ormosils and treated silicas, but historically aerogels have also been difficult to produce and require custom in-house synthesis [283, 286]. This may be why there are not many examples of aerogels being used as gas sensors [286]. Interestingly, over the past few years hydrophobic aerogels have become commercially available and inexpensive (approx. $200/kg USD), being used in composites for thermal insulation, acoustic insulation, and light scattering.

117

They are even available in fine particle form (approx. 0.5-5 µm distribution), which could drastically simplify the steps required for processing and formulating them into chemical sensing inks, dispersions, and slurries (Figure 5.1).
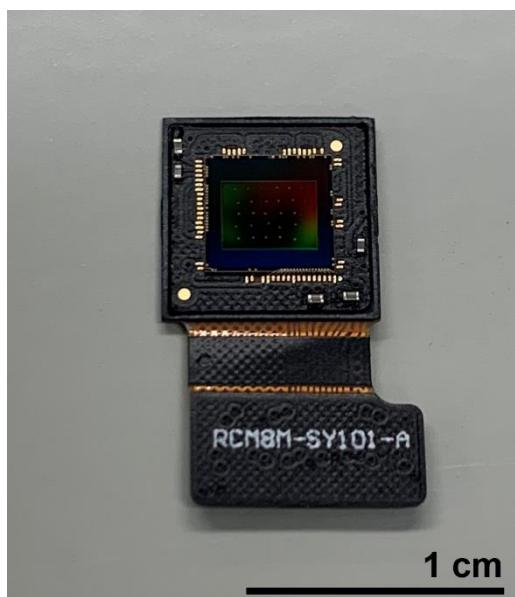

Figure 5.2 Raspberry Pi V2 camera module with internal Sony IMX219 CMOS imager exposed and printed sensor array visible.

This inspired the development of an all-in-one printable sensor ink that contains dispersed colorimetric dye, hydrophobic aerogel particles, solvents, and other additives as necessary to give good printing and sensing qualities. Many colorimetric sensing systems should be compatible with the aerogel particles, but as an example the detection of ammonia was performed with the pH-sensitive molecular dye bromophenol blue (BPB). The aerogel particles imbibe and immobilize the BPB within their pores on a hydrophobic surface that does not adsorb moisture from the atmosphere. An array of ammonia sensors are printed onto the internal CMOS imager of a Raspberry Pi V2 camera module with a

PiXY non-contact piezoelectric microarrayer (Figure 5.2). The challenges of printing solid particles as uniform films are addressed, and the iterative process in developing the best sensor ink formulation by surface treatments and additives to yield uniform sensors is presented. The resulting sensors are characterized in their ability to measure ammonia, and enhancements in sensitivity/reversibility by addition of aerogel particles, as well as humidity resistance, is studied.

5.2 Experimental Section

5.2.1 Chemicals and Materials

All chemicals were purchased and used without further purification. Enova aerogel IC3100 particles were purchased from Cabot Aerogel. Bromophenol blue (ACS reagent, Ph. Eur.) (BPB), polyvinyl chloride (M_w 233k) (PVC), polyethylene oxide (M_w 100k) (PEG100k), polyethylene glycol (M_w 300) (PEG300), polymethyl methacrylate (M_w 350k) (PMMA), ethanol (ACS reagent, 99.5%), isopropanol (ACS reagent, 99.5%) (IPA), tetrahydrofuran (anhydrous, 99.9%, inhibitor-free) (THF), dioctyl phthalate (99.5%) (DOP), and chlorotrimethylsilane (99%) (TMS) were purchased from Sigma-Aldrich. Tridecafluoro-1,1,2,2-tetrahydrooctyl-1-trichlorosilane (97%) (TCS) was purchased from UCT Specialties, LLC. Ultrapure water (18.2 MΩ·cm) was prepared via an ELGA Purelab Ultra purification system. Ammonia 10 ppm and 100 ppm calibration gases, balance nitrogen, were purchased from MESA Specialty Gases & Equipment. Ultra zero grade air was purchased from Matheson.

5.2.2 CMOS Imager & Glass Slide Preparation

Sensors were always printed onto a new CMOS imager that was prepared in the same way. First, a Raspberry Pi V2 camera module was disassembled to reveal its internal Sony IMX219 8 MP (3280 x 2464 pixels; 1.1 x 1.1 μm^2 pixel size) CMOS imager. The freshly exposed imager was rinsed under a gentle stream of ultrapure water first, then ethanol, and finally dried under zero air. Next, the imager was cleaned under oxygen plasma in a Harrick Plasma PDC-001 plasma cleaner operating at high RF power setting for 5 minutes at 600 mTorr. This was the stopping point for a CMOS imager that received plasma cleaning only. Otherwise the imager would go on to be functionalized with either TMS or TCS. To accomplish this the surface of the CMOS imager was silanized in vapor-phase conditions under house vacuum with 200 µL of the respective silane present in the vacuum chamber. This creates a uniform hydrophobic surface (moderate hydrophobicity with TMS, high hydrophobicity with TCS) that is best for printing and reproducibility. The silanization process would last for 30 minutes after which the CMOS imager was rinsed a second time under ethanol and dried with zero air. Finally, the CMOS imager was baked in a laboratory oven at 85°C for 30 minutes to cure the silanized surface. All steps were performed immediately consecutive to one another and the prepared CMOS imagers were printed on within 24 hours of completion of this process. Glass slides (Fisher Scientific) were cleaned and prepared in the same process.

5.2.3 Sensor Array Printing

Initially, different formulations were compared within the constraints of the printer's capabilities to find what additives and surface treatments enhanced a uniform

printed sensor film. Those trial-and-error formulations are described in the results section detailing the iterative process for determining the best aerogel-based ink formulation. After the best formulation and surface treatment was determined it was compared to two other control formulations to understand the effects of the aerogel particles and hydrophobic matrix. The three formulations that were compared are the "Aerogel-based formulation", the "PVC-based formulation", and the "PEG-based formulation". The Aerogel-based ink is 6 mL THF (60% v/v), 4 mL IPA (40% v/v), 200 mg aerogel (2% w/v), 200 mg BPB (2% w/v), 25 mg PVC (0.25% w/v), and 25 µL DOP (0.25% v/v). The PVC-based ink is 6 mL THF (60% v/v), 4 mL IPA (40% v/v), 200 mg BPB (2% w/v), 50 mg PVC (0.5% w/v), and 25 µL DOP (0.25% v/v). The PEG-based ink is 10 mL ultrapure water, 50 mg BPB (0.5% w/v), 50 mg PEG100k (0.5% w/v), and 100 µL PEG300 (1% v/v). Sensor inks were prepared fresh within 24 hours of printing. The sensors were printed with a PiXY piezoelectric microarrayer by delivering 10 nL of sensor ink to the CMOS imager surface without making physical contact with the imager itself to protect the delicate photodiodes. Finally, Aerogel-based sensors were baked for 15 minutes at 85°C to ensure all solvent was removed from the porous matrix. Coating quality was evaluated with pictures captured by the CMOS imager. Glass slides were printed on by micropipetting 2 µL of sensor ink by hand, then baked for 15 minutes at 85°C.

5.2.4 Ammonia Sensor Exposure

Ammonia gas dilutions used in testing were prepared fresh from 10 ppm and 100 ppm ammonia gas calibration standards and zero air in 40 L metallized gas sampling bags (Restek). All bags were prepared to 50% RH at a constant laboratory temperature of 23°C

using ultrapure water. "Clean air" refers to zero air that has been humidified to 50% RH. For the humidity tests clean air and ammonia bags were also prepared to 10% and 90% RH (at 23°C). To test the printed sensors a CMOS imager with finished sensor array was attached to a test fixture machined out of white PTFE block. PTFE was chosen for its inert properties and excellent compatibility with ammonia. A white LED (LEDtronics) embedded in the PTFE block operated at a constant current of 5 mA and delivered diffuse white light to the CMOS imager. Gas flow through the test fixture was delivered by PTFE tubing and maintained at 200 sccm.

5.2.5 Image Acquisition and Data Processing

Full resolution 8 MP images were acquired through a Raspberry Pi 4 Model B communicating with the modified CMOS imager at 1 frame/s (fps). Using ImageJ software, a ROI was automatically selected around the perimeter of each printed sensor for making an absorbance measurement. Reference ROIs were selected as concentric rings around the perimeter of each sensor with 30 pixel thickness. Absorbance was calculated as the negative base 10 logarithm of the ratio of the grayscale intensity of the sensor ROI (CMD_g) with the corresponding reference ROI (Ref_g) using equation 4.1.

$$\text{Absorbance} = -\text{Log}_{10}\left(\frac{CMD_g}{Ref_g}\right) \tag{4.1}$$

Absorbance data was smoothed with a 61 point simple moving average (1 minute window) and numerically differentiated to determine the change in absorbance during exposure to ammonia (AU/s).

5.3 Results and Discussion

5.3.1 Coating Non-Uniformity and Failure Phenomena

The challenge with printing films from suspended particles (ie. nanoparticles, microparticles) and non-volatile solutes is they tend to form non-uniform, cracking, and delaminating films as they dry. Non-uniformity in the distribution of solids as a film dries has been well-studied. The formation of a ring where most of the solids are concentrated at the perimeter of a drying droplet is known as the coffee ring effect and is very common. The mechanism responsible for this phenomena is the pinning of the contact line at the edge of a droplet that ensures evaporating liquid at the perimeter will be replaced with fresh liquid from the bulk. The outward radial flow carries particles with it to the contact line where a ring deposit forms [274]. Multiple ways to mitigate this effect and form uniform coatings have been discovered. One way is to prevent pinning of the contact line at the edge of the droplet by decreasing the surface energy of the surface being printed on, thereby increasing the contact angle of the printed droplets and influencing their evaporation [287]. Another is to generate a Marangoni flow due to surface tension gradients that drives flow inward in opposition to the outward capillary flow. The flows can cancel out to give a uniform coating, or the Marangoni flow can dominate and deposit all of the solids in the center of the droplet [288, 289]. Addition of a co-solvent with different viscosity, surface tension, and boiling point (ie. volatility) from the main solvent produces gradients in the evaporating droplet that can redirect flow [290]. Change in viscosity and surface tension by addition of polymers can also slow outward capillary flow, prevent liquid pinning, and enhance Marangoni flow [275]. Further methods to control the deposition of solids during the drying process are addition of anisotropic particles, surfactants, modulating substrate

temperature, and regulating the composition of the atmosphere above the drying droplet [289, 291, 292].

The other failure mechanisms of drying films: cracking, formation of shear bands, and delamination are also well studied. These dissipate built-up stresses in the film from capillary forces generated by small liquid menisci between particles [293]. Griffith's theory states that a crack will propagate when the reduction in potential energy from crack growth is greater than the increase in surface energy due to the creation of new surfaces. A similar rule can be applied to a peeling film when strain energy stored in the film overcomes the adhesion energy between the film and substrate. Film thickness, particle size, drying rates, and substrate constraints influence these failure mechanisms. Like the coffee ring effect, addition of polymers has been shown to reduce peeling and delamination of drying films, with increasing molecular weight and concentration having more benefit [294]. Subsequent sections will discuss the surface functionalization of the CMOS imager with hydrophobic silanes, the use of a co-solvent, and the addition of dissolved polymers to improve the uniformity and adhesion of printed sensors.

5.3.2 Indicator Selection

The indicator used to detect ammonia in the previous chapter was Cu(II). This ion is only used to complex with ammonia in liquid environments (eg. aqueous), and it is not dispersible in a hydrophobic matrix. Therefore, Cu(II) is not suitable for the hydrophobic gas sensor discussed here. However, many molecular dyes with hydrophobic character have been shown to be sensitive to ammonia. The pH indicators in particular have high molar absorptivity, high contrast color change, and are capable of being dispersed

throughout hydrophobic matrices, like plasticizers (eg. DOP), polymers (eg. PVC), and inorganic substrates (eg. hydrophobic modified silicates) [236, 256, 258]. One of the most important traits when selecting a pH indicator is its pK_a. The pK_a is the pH at which the indicator goes through its color transition. The sensitivity of an ammonia sensor will increase as pKa decreases [258, 279]. The sensitivity and dynamic range can be tuned using this approach. BPB, with a low pKa of 4.1 and easily identifiable yellow to blue color transition, has been used to make ammonia sensors with low detection limits [258, 279, 282]. For this reason BPB has been chosen as the molecular dye for the present development.

5.3.3 Solvent Selection

The solvent needs to fulfill many criteria. It must solubilize the indicator, dissolve potential polymer and plasticizer additives, have good volatility to completely leave the printed sensors, suspend the aerogel particles without damaging them, and remain chemically inert during the entire process. THF was found to be the only solvent that fit all these criteria. BPB has excellent solubility in THF and it does not react chemically. THF being a polar non-protic solvent does not participate in exchanging hydrogen ions with BPB. Its surface tension is 26.4 mN/m (at 20°C), which is below the aerogel manufacturer's limit of 30 mN/m to protect the pore structure from collapsing during drying. It has a low boiling point of 66°C making it easy to remove from the finished sensors by baking at relatively low temperature that does not damage the indicator and other components. It is also compatible with DOP and dissolves PVC which are found to be useful additives.
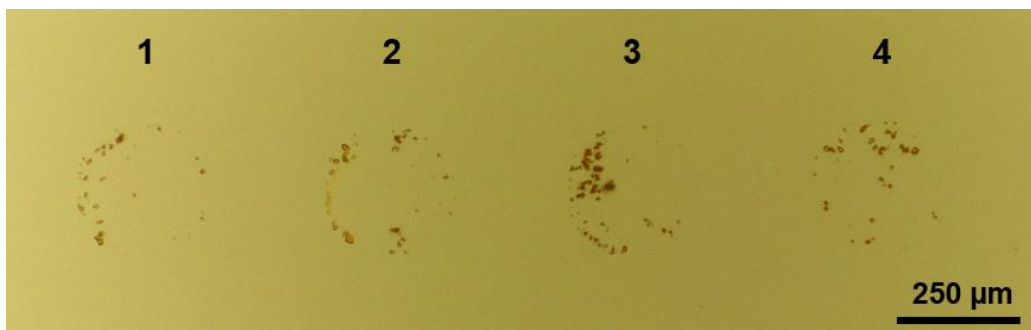
Figure 5.3 Four printed sensors deposited from 10 nL of 2% w/v aerogel particles and 0.5% w/v BPB in THF.

5.3.4 Printing Aerogel Plus Indicator

Initially an attempt was made to print BPB (0.5% w/v) in THF alone to serve as a control. The high volatility of THF caused the 32 µm (inner diameter) printer tip to immediately clog with BPB precipitate. Next, aerogel was added to the formulation (2% w/v). The addition of aerogel particles actually prevented the tip from clogging and facilitated printing. This is evidence that BPB is being absorbed into the matrix of the aerogel so it can no longer precipitate at the printer head as THF evaporates. The printed sensors have very poor uniformity, with dyed particles appearing in a broken ring formation (Figure 5.3). No uniform BPB residue is visible except for the coloring of the dyed aerogel particle aggregates. These initial results prompted investigation of additives and surface treatments to improve uniformity.

5.3.5 Polymer Additives and Surface Treatments

Polymer additives and surface treatments were screened at the same time because they are both known strategies for improving the uniformity of printed films and preventing failure mechanisms. A small amount of polymer can act as a binder and provide cohesion

between particles. This is an obvious potential remedy to the dispersed aerogel particles seen in Figure 5.3. Silanization treatments on the CMOS imager will change its surface energy and therefore affect the contact angle with printed droplets and adhesion of the drying film.
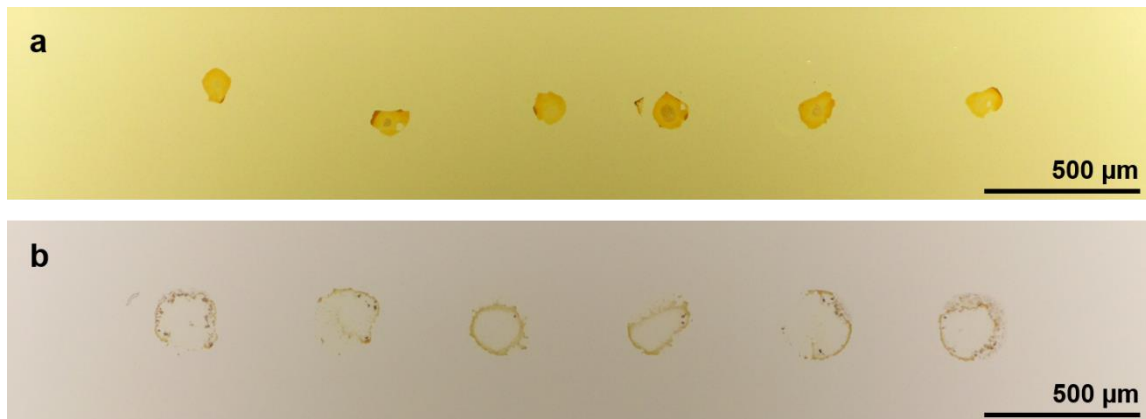
Figure 5.4 Sensor formulation (10 nL printed): 2% w/v aerogel particles, 0.25% w/v PVC, 0.5% w/v BPB, and 0.25% w/v DOP in THF. (a) TCS, fluorinated, very hydrophobic surface treatment gives compact, irregular sensors. (b) TMS, methylated, moderately hydrophobic surface treatment gives coffee ring effected sensors.

The first surface treatment tested was oxygen plasma cleaning without silanization. This gives the CMOS imager high surface energy making it very hydrophilic. It readily wicked the polar THF solvent across the entire imager area during printing. This was not useful so low surface energy, hydrophobic surfaces were investigated instead. Two silanes were compared. TMS coats the surface with trimethyl silyl groups that have moderate hydrophobicity. TCS coats the surface with perfluorinated alkyl silyl groups that have very high hydrophobicity. The revised formulation with polymer additives compared PVC and PMMA. PVC is a very hydrophobic polymer and PMMA has some degree of polarity due to it carboxyl groups. Aerogel did not disperse well in PMMA, possibly a consequence of

the very hydrophobic aerogel and slightly polar PMMA phase segregating. Printing proceeded with the PVC instead. Since PVC is known to be brittle, DOP was added as a hydrophobic, non-volatile (boiling point: 385°C) plasticizer. Combining polymer and plasticizer has been used in the sensor literature to improve mechanical properties, gas permeability, and hydrophobicity of colorimetric sensors [235-237, 258, 282]. Sensors were printed onto TMS and TCS functionalized CMOS imagers with formulation 2% w/v aerogel particles, 0.25% w/v PVC, 0.5% w/v BPB, and 0.25% w/v DOP in THF. Figure 5.4 shows results from these printed sensors. The PVC does act as a binder and provides cohesion so aerogel particles are no longer dispersed around the print site as was visible in Figure 5.3. Silanization has a dramatic effect on the finished films. TCS, which should force a high contact angle with the printed droplets due to its great hydrophobicity, appears to be preventing contact line pinning by allowing the solids to deposit compact in the center of the print sites. In this case the original printed spots were larger and then shrunk down to their final size in Figure 5.4a. Sensors appear cohesive compared to diffuse particles in Figure 5.3, but they are irregular and show signs of cracking. The TMS functionalized surface is not as hydrophobic as TCS, and therefore it is not expected that it will force as high a contact angle with printed droplets. The result is the films show signs of contact line pinning during drying as manifested by the coffee ring effect. They do show cohesion from the PVC though, compared with the particles aggregates in Figure 5.3.

Additional prints on TCS functionalized CMOS imagers would occasionally show multiple sensors with extreme cracking, peeling, and lift-off (Figure 5.5). There appears to be random processes occurring during drying and film formation that are still difficult to

control. Further steps must be taken to improve uniformity by modifying the printing formulation.

Figure 5.5 Sensors that are cracking, peeling, and delaminating from the surface of a CMOS imager treated with TCS (same printing formulation as Figure 5.4).

5.3.6 Binary Solvent System

Adding a co-solvent is a method to influence the drying process and final properties of a film. As mentioned earlier it is a strategy to mitigate non-uniformities like the coffee ring effect. When using a solvent like THF with a low boiling point (66°C) and low viscosity (0.48 cP at 25°C) it can be advantageous to add a solvent with a higher boiling point and higher viscosity. By adding a less volatile solvent the drying process slows down, which can reduce capillary outward flow, and creates gradients in solvent composition along the edge of the droplet that drive inward Marangoni flow. Increase in viscosity will overall slow the movement of particles. The processes combined will help keep the drying droplet homogeneous and give a more uniform film. IPA was chosen because its boiling point (82.5°C) is higher than THF, but still low enough that it is easily removed from the printed sensors without necessitating very high temperatures. Its viscosity is significantly

greater than THF as well (1.96 cP at 25°C). It also has a low surface tension to protect the aerogel pore structure during drying (23.0 mN/m at 20°C).
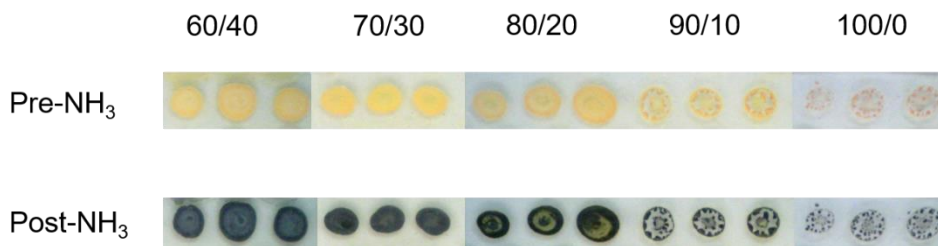
Figure 5.6 Films deposited in triplicates by pipetting 2 µL droplets of sensor formulation onto glass slides functionalized with TMS. Ratios are in THF/IPA by volume. Films shown before and after ammonia exposure.

First, a comparison of films with different THF to IPA ratios was made by pipetting 2 µL of coating solution onto glass slides functionalized with TMS (Figure 5.6). Films deposited from pure THF are cracked and broken into fragments. Films with 10% IPA added have slightly more cohesion, but are cracking and peeling upwards along the edges. At 20% IPA the films are beginning to look uniform, but after ammonia exposure it is obvious there are still non-uniformities in the film. At 30% and 40% IPA the films look completely uniform. Beyond 40% IPA there are issues with PVC solubility, so solutions with greater than 40% IPA are not compared. Based on these results it was decided that 60/40 is the ideal ratio of THF to IPA.

Next, the modified sensor formulation with 40% IPA as a co-solvent was printed onto CMOS imagers treated with either TCS or TMS (Figure 5.7). Sensors printed on TCS treated imager are still very compact, due to prevention of contact line pinning during drying, and now they are much more uniform and do not show signs of cracking. Sensors printed on TMS treated imager are still spread out, due to the higher surface energy and

lower contact angle with printed droplets on this surface, but this time they show a light uniform region of coating with a small compact spot near the center. It seems the binary solvent is doing its job in redirecting particle flow away from the edges, but there are two problems. One is the inward Marangoni flow is dominating and allowing a compact, dark center region to form (should be correctable by tuning THF/IPA ratio). Two is the sensor is very thin and coloration is very faint. To create a good light absorbing sensor over the large area these printed films cover will require much more dissolved solids in the ink formulation. This is more challenging to correct since limitations in the ability of the printer to handle more concentrated inks (ie. too viscous) and deliver larger volumes to the surface without making droplets coalesce prevents this. It was decided that the best Aerogel-based sensor formulation and substrate, which will be tested in subsequent sections, is 2% w/v aerogel particles, 0.25% w/v PVC, 2% w/v BPB, and 0.25% DOP in 60/40 THF/IPA on a TCS treated CMOS imager (Figure 5.7a).
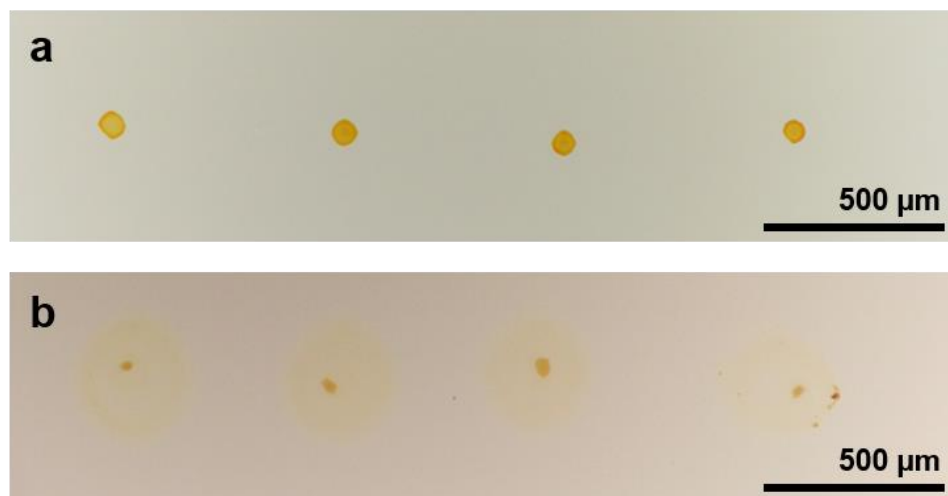
Figure 5.7 Sensor formulation (10 nL printed): 2% w/v aerogel particles, 0.25% w/v PVC, 2% w/v BPB, and 0.25% w/v DOP in 60/40 THF/IPA. (a) TCS treated CMOS Imager has regular compact printed sensors. (b) TMS treated CMOS imager has improvement in uniformity, but sensors are too faint and some solids are concentrating in the center.

5.3.7 Ammonia Detection

To determine the capability of the Aerogel-based formulation to measure ammonia gas the sensors were exposed to a range of concentrations from 250 ppb to 20 ppm, all composed to 50% RH at 23°C. Figure 5.8 shows the resulting calibration curve of six replicate sensors. Linearity across the entire range of concentrations is good, with an R-squared value of 0.9899. The sensitivity is 1.28×10^{-5} AU/s/ppm and the LOD is approximately 60 ppb using three times the standard deviation in clean air. The y-intercept is close to zero which is consistent with observations that there is no change in absorbance in clean air. The high sensitivity and low LOD of this sensor is due to the efficient loading of BPB molecular dye within the aerogel matrix and the high molar absorptivity of the dye. This type of sensor could detect ammonia before a person would be able to smell it (olfactory threshold is 5 to 50 ppm) and would be useful for worker safety where NIOSH has set REL to 25 ppm [254].
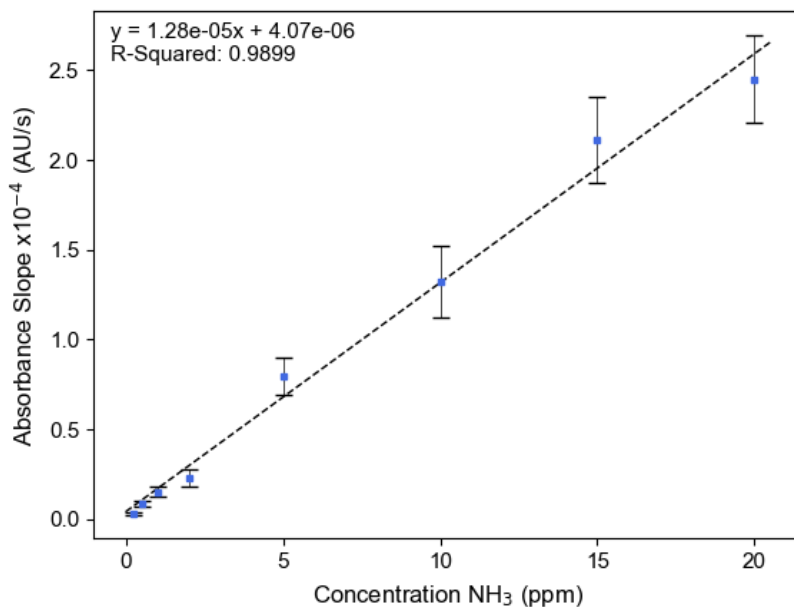
Figure 5.8 Calibration curve for Aerogel-based ammonia sensors (n=6). Error bars are standard deviations. All ammonia concentrations prepared to 50% RH at 23°C.

5.3.8 Reversibility

The mechanism of action of BPB relies on the exchange of a hydrogen ion (proton) between the BPB (weak acid) and ammonia (weak base). This is formally known as a Brønsted-Lowry acid-base interaction. When the BPB loses its proton its absorption of visible light changes and the color shifts from yellow to blue. This type of reaction is fundamentally reversible though. When the conditions change and volatile ammonia escapes the matrix of the sensor the BPB regains its proton and the color returns to its original state. The high surface area of the aerogel particles should enhance transport of ammonia in and out of the printed sensor. To test the effect of the aerogel particles and show the reversibility of the sensor the Aerogel-based formulation was compared with a PVC-based formulation which does not contain aerogel particles (Figure 5.9). The sensors were exposed to cycles of 5 ppm ammonia followed by clean air, all at 50% RH at 23°C, over a period of 30 minutes. Both formulations show sensitivity to ammonia and reversibility. This is expected since even the PVC-based formulation (without aerogel) is a thin film that naturally has gas permeability. However, the Aerogel-based formulation has enhanced sensitivity, about 50% greater than the PVC-based sensor, and also has superior reversibility. This is because the aerogel material provides a high surface area for the colorant to be dispersed throughout and a pathway for ammonia diffusion.
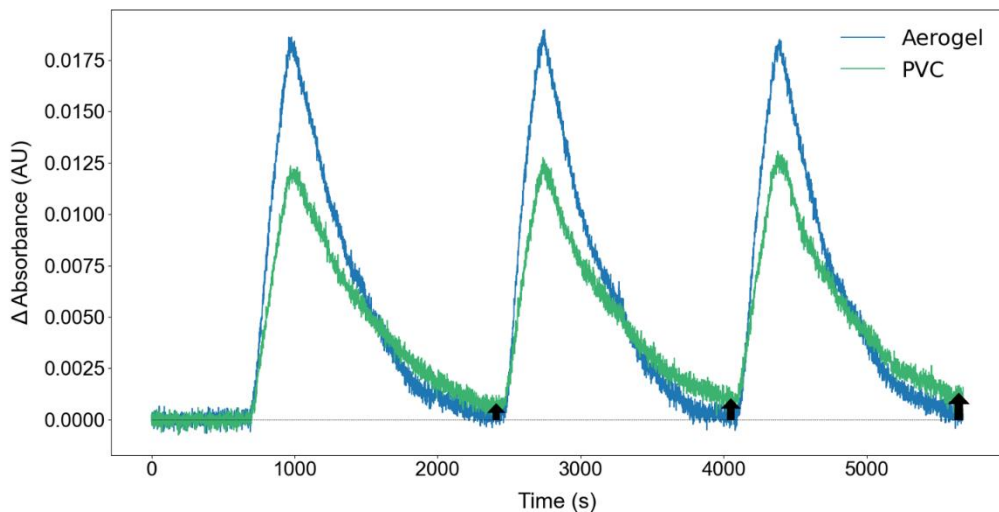
Figure 5.9 Raw absorbance data comparing the sensitivity and reversibility of the Aerogel-based sensor formulation with a PVC-based sensor that does not contain aerogel particles. The sensors were exposed to 5 ppm ammonia for 5 min, then flushed with clean air for 25 minutes in 3 cycles. Aerogel particles enhance sensitivity and reversibility of the sensor. PVC sensor has less reversibility as illustrated by arrows pointing from initial baseline.

5.3.9 Humidity Response

Fluctuations in ambient humidity are a nuisance for nearly all kinds of gas sensors and even professional instruments. While a target gas of interest may be present in only trace concentrations (ppb or ppm), changes in humidity at normal temperatures represent variations in water content in the thousands and even tens of thousands of ppm. Carefully selecting a sensor matrix that is hydrophobic should, in theory, minimize or even eliminate humidity interference. The Aerogel-based sensor formulation was evaluated in its response to humidity in two tests and compared with a hydrophilic PEG-based formulation on an identical CMOS imager.

First, the change in absorbance of the sensor formulations were measured in response to changes in humidity in clean air (no ammonia) relative to a stable baseline at 50% RH (Figure 5.10). The humidities compared were 10% and 90% RH, all at 23°C. The

134

hydrophilic PEG matrix loses and gains a significant amount of water at 10% and 90% RH, respectively. This causes a large change in absorbance because the pH of the system is altered when water is lost or gained. BPB has a pKa of 4.1 and it goes through a complete color transition when its environment passes from a pH of approximately 3.0 to 4.6. Pure water has a pH of 7.0 (pKa 14.0) and is capable of accepting a proton from BPB, thereby forcing its color change from yellow to blue. The large change in water content in the PEG-based sensor alters its color and makes humidity a strong interferent for this formulation. The Aerogel-based formulation, on the other hand, absorbs and desorbs a negligible amount of water when humidity changes. The hydrophobic matrix of the Aerogel-based sensor is preventing unwanted humidity ingress and effectively protects the BPB from reacting with excess moisture.
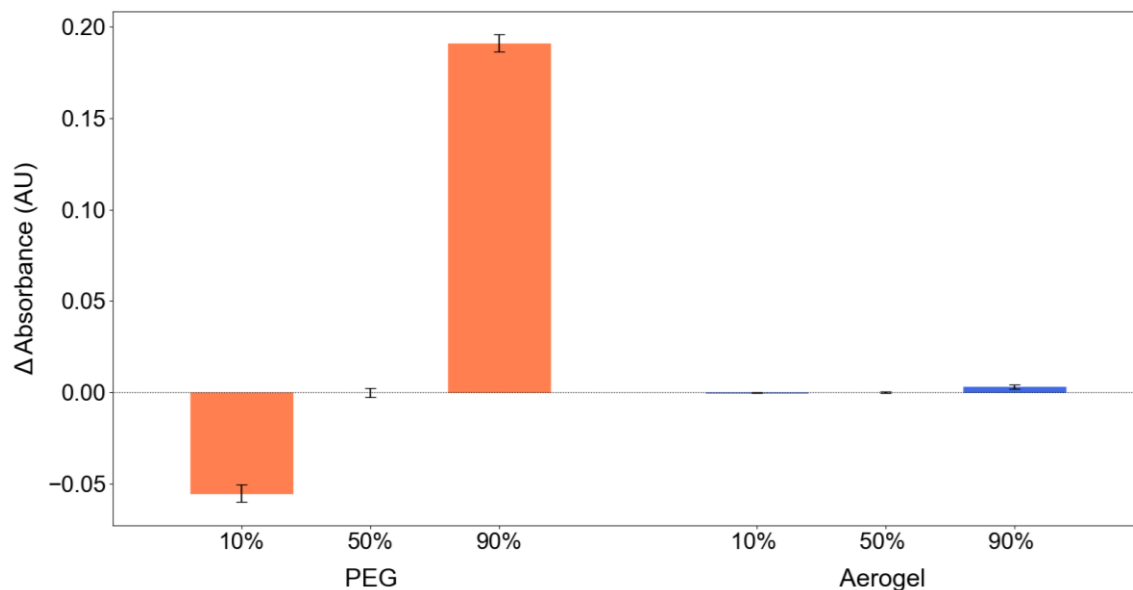
Figure 5.10 Humidity test in clean air comparing change in absorbance at 10% and 90% RH relative to 50% RH (23°C). Hydrophilic PEG-based formulation (n=5) absorbs and desorbs water which influences the color of BPB indicator. Hydrophobic Aerogel-based formulation (n=6) has negligible interference. Error bars are standard deviations.

The second test studied how humidity affected the sensitivity of the sensor formulations to ammonia (Figure 5.11). This is to answer, how does humidity influence the slope of the calibration curve? First examining the hydrophilic PEG-based formulation, at 10% RH the sensitivity of this sensor is very high, even much higher than the Aerogel-based sensor. Even though the PEG-based formulation does not contain aerogel particles to enhance its surface area and porosity, the PEG matrix is hydrophilic and contains water it has absorbed out of the atmosphere, even at only 10% RH. This water provides an environment for fast transport of hydrogen ion, known as "proton hopping", that is responsible for the extremely high mobility of hydrogen ions in protic solvents [295]. This allows ammonia to effectively react with BPB from a distance. Ammonia can accept a proton from a water molecule, which in turn accepts a proton from an adjacent water molecule, and this repeats many times until a hydrogen ion is removed from a BPB molecule a long distance away. It is also enhanced because the PEG-based sensor is only a thin film so the distances necessary are short. If the PEG-based sensor could maintain this sensitivity as humidity increases it would make a very good ammonia sensor, but as can be seen in Figure 5.11 the sensitivity decreases as humidity increases to 50% and again to 90% RH. This is because of a competing process that was illustrated in Figure 5.10. When the RH increases from 10% to 50% the amount of water in the PEG matrix increases. This shifts the pH upwards (as explained in the previous section) and converts some of the BPB from its protonated state to unprotonated state. Now there is less protonated BPB available to react in the presence of ammonia, so the overall sensitivity is diminished. At 90% RH the effect is even more extreme and there is much lower sensitivity to ammonia, even lower than the Aerogel-based formulation at the same humidity. This extreme change

136

in sensitivity of the hydrophilic PEG-based formulation makes it unreliable in real environments that will expectedly have fluctuations in humidity. In contrast, the Aerogel-based formulation shows minimal change in sensitivity in response to humidity. There is about a 20% increase in sensitivity from 10% to 50% RH, and a similar increase from 50% to 90% RH. There is a small increase, and not zero increase, because even a hydrophobic substrate will have some water molecules adsorbed to its surface in a natural environment with ambient humidity. This allows a slight degree of proton hopping to take place across a limited range and enhances sensitivity as humidity increases. The effect is small though, and could potentially even be corrected for, if necessary, by the inclusion of a humidity sensor in a finished device. Figures 5.10 and 5.11 both illustrate how a hydrophobic matrix minimizes humidity interference compared with a hydrophilic one.
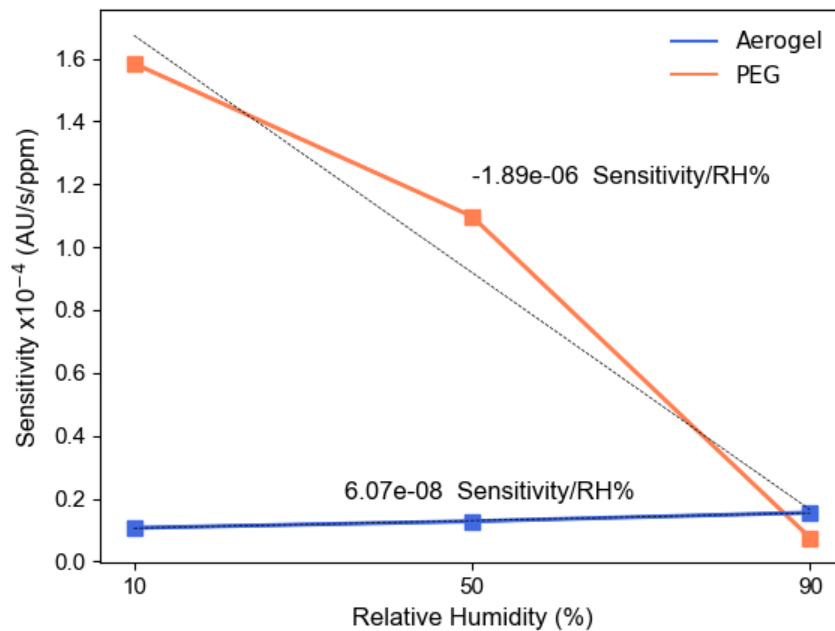
Figure 5.11 Effect of ambient humidity on sensitivity to ammonia for Aerogel-based and PEG-based formulations. All relative humidities at 23°C. Trend lines with annotated slopes show nearly two orders of magnitude difference between formulations.
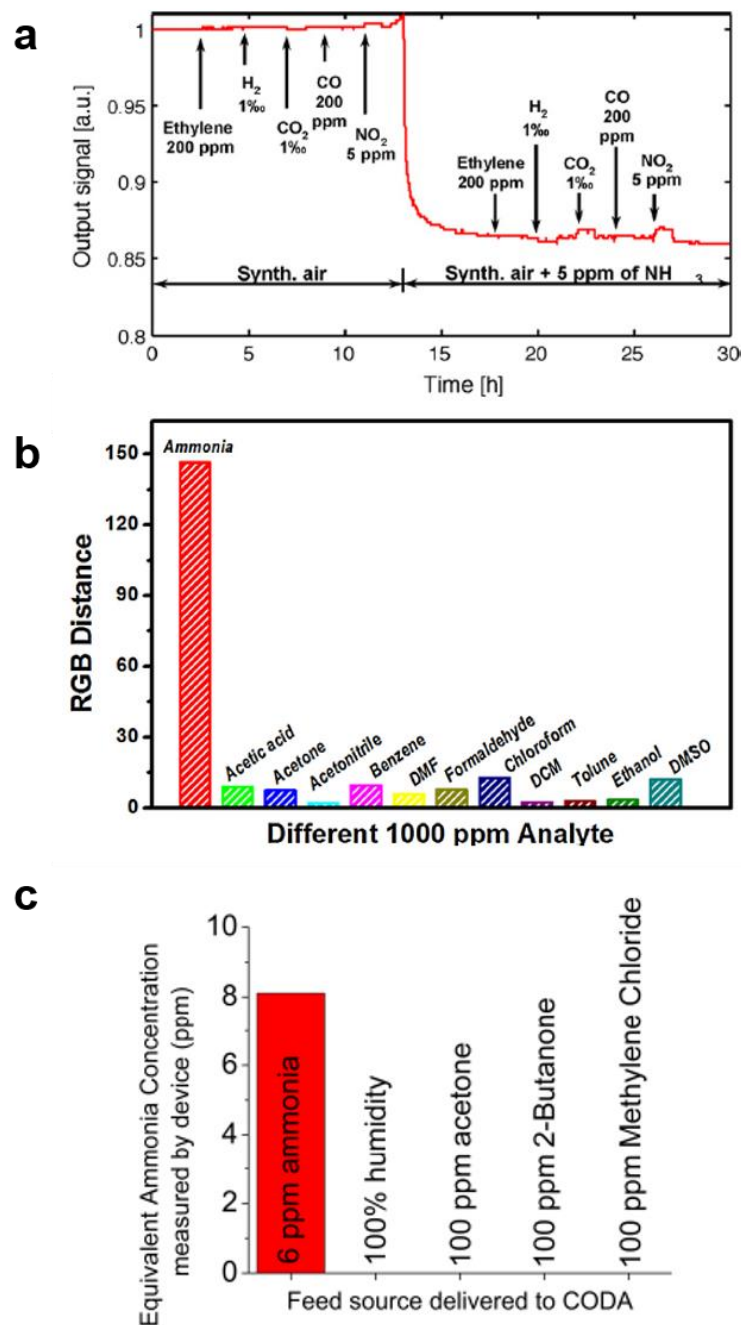
Figure 5.12 Selectivity of pH indicator-based systems for gaseous ammonia: (a) BPB shows negligible interference to 200 ppm ethylene, 1% H_2, 1% CO_2, 200 ppm CO, and 5 ppm NO_2 both in clean air and in the presence of 5 ppm NH_3 [258]. (b) Bromocresol green (pH indicator very similar to BPB) shows negligible interference to 1000 ppm of each of the following VOCs compared to 1000 ppm NH_3: acetic acid, acetone, acetonitrile, benzene, N,N-dimethylformamide (DMF), formaldehyde, chloroform, dichloromethane (DCM), toluene, ethanol, and dimethyl sulfoxide (DMSO) [257]. (c) BPB shows negligible interference to 100% RH clean air (non-condensing), 100 ppm acetone, 100 ppm butanone, and 100 ppm dichloromethane (methylene chloride) compared to 6 ppm NH_3 [255].

5.3.10 Selectivity

The use of BPB and other pH indicators for measurement of gaseous ammonia is well studied and its selectivity has been documented by many researchers. In theory, any gaseous Brønsted acid or base could interfere with its mechanism of detection, but in practice this is uncommon. Ammonia is the most abundant basic/alkaline gas species in the atmosphere [123]. Other volatile organic amines are very rare except in laboratories and chemical facilities that specifically use them, where their presence would be anticipated. In a normal environment they are not expected to be present and interfere with the sensor. Carbon dioxide and nitrogen dioxide are common acids in the atmosphere, but these are Lewis acids and will not interact with BPB directly. They require reaction with water to generate free hydrogen ions, and this is minimized by the hydrophobic matrix of the sensor. Figure 5.12 shows results from three separate research groups examining the interference between common pollutants, VOCs, and moisture with pH indicators. Courbat *et al.* found that BPB has negligible interference from 200 ppm ethylene, 1% H_2, 1% CO_2, 200 ppm CO, and 5 ppm NO_2 both in clean air and in the presence of 5 ppm NH_3 (Figure 5.12a) [258]. Hoang *et al.* tested the pH indicator bromocresol green, which is very similar to BPB, in the presence of several VOCs. They found each VOC at 1000 ppm concentration had minimal interference compared to the signal from 1000 ppm NH_3 (Figure 5.12b) [257]. Liu *et al.* compared the response of 6 ppm NH_3 with 100% humidity, 100 ppm acetone, 100 ppm butanone, and 100 ppm dichloromethane with each having an insignificant response (Figure 5.13c) [255].

5.4 Conclusion

Hydrophobic aerogels appear to be an underutilized sorbent material in colorimetric sensor literature despite their excellent properties for the task: mesoporous structure, high specific surface area, hydrophobic functionalization, transparency, low refractive index, and robust chemically inert silica framework. Although their synthesis may be more complex than what the typical sensor developer wants to tackle, the new commercial availability of inexpensive hydrophobic aerogels eliminates that complication. Of particular interest are the fine particle compositions that can be suspended in solvents to create novel colorimetric inks for printing. This work presented the development of an Aerogel-based printable ink formulation for detecting ammonia that, through addition of additives and surface treatments, was able to yield uniform sensor films with minimal cracking and peeling. The response to ammonia showed good linearity from 250 ppb to 20 ppm with a limit of detection of 60 ppb. The aerogel particles were shown to enhance sensitivity and reversibility compared with a PVC-based formulation that lacked aerogel particles. The hydrophobic matrix of the Aerogel-based sensors gave them excellent humidity resistance compared with a hydrophilic PEG-based formulation. Selectivity for ammonia is anticipated to be good based on extensive data from the research community showing excellent performance of BPB and the related pH indicator bromocresol green in the presence of many common pollutants and VOCs. All of these properties make this sensor a good candidate for ambient air quality monitoring and worker safety, where a low detection limit, reversibility, humidity resistance, and selectivity are key. NIOSH has set the REL for ammonia at 25 ppm for an 8 hour TWA, and outdoor concentrations are expected to be in the sub-ppm range and up to 10 ppm near areas with farming [254]. By

printing sensors on the CMOS imager surface it is possible to take advantage of multiplexing many sensors together. Replicate sensors can be averaged to compute a more reliable response, and other types of colorimetric gas sensor formulations could be added to detect multiple pollutants simultaneously. Future work will focus on the development of additional sensor inks using aerogel particles for detection of pollutants and toxic chemicals besides ammonia.

References

[123] S. N. Behera, M. Sharma, V. P. Aneja, and R. Balasubramanian, "Ammonia in the Atmosphere: A Review on Emission Sources, Atmospheric Chemistry and Deposition on Terrestrial Bodies," *Environ. Sci. Pollut. Res.*, vol. 20, pp. 8092-8131, 2013, 10.1007/s11356-013-2051-9.

[235] G. Orellana, M. C. Moreno-Bondi, D. Garcia-Fresnadillo, and M. D. Marazuela. *The Interplay of Indicator, Support and Analyte in Optical Sensor Layers. In Frontiers in Chemical Sensors*. O. S. Wolfbeis, G. Orellana, M. C. Moreno-Bondi, Eds.; Springer Series on Chemical Sensors and Biosensors; Springer-Verlag: Heidelberg, 2005; Vol. 3, pp 189-225.

[236] Z. Li, J. R. Askim, and K. S. Suslick, "The Optoelectronic Nose: Colorimetric and Fluorometric Sensor Arrays," *Chem. Rev.*, vol. 119, pp. 231-292, 2019, 10.1021/acs.chemrev.8b00226.

[237] M. K. LaGasse, J. M. Rankin, J. R. Askim, and K. S. Suslick, "Colorimetric Sensor Arrays: Interplay of Geometry, Substrate and Immobilization," *Sens. Actuators, B*, vol. 197, pp. 116-122, 2014, 10.1016/j.snb.2014.01.102.

[238] X. Qin, R. Wang, F. Tsow, E. Forzani, X. Xian, and N. Tao, "A Colorimetric Chemical Sensing Platform for Real-Time Monitoring of Indoor Formaldehyde," *IEEE Sens. J.*, vol. 15, pp. 1545-1551, 2015, 10.1109/JSEN.2014.2364142.

[239] C. Lin, X. Xian, X. Qin, D. Wang, F. Tsow, E. Forzani, and N. Tao, "High Performance Colorimetric Carbon Monoxide Sensor for Continuous Personal Exposure Monitoring," *ACS Sens.*, vol. 3, pp. 327-333, 2018, 10.1021/acssensors.7b00722.

[254] D. E. Gardner, D. Krewski, and E. C. Bishop, "Acute Exposure Guideline Levels for Selected Airborne Chemicals, vol. 6," National Academy Press: Washington, DC, 2008; pp 58-114.

[255] N. Y. Liu, P. Cay-Durgun, T. Lai, M. Sprowls, L. Thomas, M. L. Lind, and E. Forzani, "A Handheld, Colorimetric Optoelectronic Dynamics Analyzer for Measuring Total Ammonia of Biological Samples," *IEEE J. Transl. Eng. Health Med.*, vol. 6, pp. 1-10, 2018, 10.1109/JTEHM.2018.2840678.

[256] J. H. Bang, S. H. Lim, E. Park, and K. S. Suslick, "Chemically Responsive Nanoporous Pigments: Colorimetric Sensor Arrays and the Identification of Aliphatic Amines," *Langmuir*, vol. 24, pp. 13168-13172, 2008, 10.1021/la802029m.

[257] A. T. Hoang, Y. B. Cho, J. S. Park, Y. Yang, and Y. S. Kim, "Sensitive naked-eye detection of gaseous ammonia based on dye-impregnated nanoporous polyacrylonitrile mats," *Sens. Actuators B Chem.*, vol. 230, pp. 250-259, 2016, 10.1016/j.snb.2016.02.058.

[258] J. Courbat, D. Briand, J. Damon-Lacoste, J. Wollenstein, N. F. D. Rooij, "Evaluation of pH indicator-based colorimetric films for ammonia detection using optical waveguides," *Sens. Actuators B Chem.*, vol. 143, pp. 62-70, 2009, 10.1016/j.snb.2009.08.049.

[269] S. Wintzheimer, M. Oppmann, M. Dold, C. Pannek, M. L. Bauers-feld, M. Henfling, S. Trupp, B. Schug, and K. Mandel, "Indicator Supraparticles for Smart Gasochromic Sensor Surfaces Reacting Ultrafast and Highly Sensitive," *Part. Part. Syst. Charact.*, vol. 36, pp. 1-7, 2019, 10.1002/ppsc.201900254.

[277] M. C. Janzen, J. B. Ponder, D. P. Bailey, C. K. Ingison, and K. S. Suslick, "Colorimetric Sensor Arrays for Volatile Organic Compounds," *Anal. Chem.*, vol. 78, pp. 3591-3600, 2006, 10.1021/ac052111s.

[278] L. Feng, C. J. Musto, and K. S. Suslick, "A Simple and Highly Sensitive Colorimetric Detection Method for Gaseous Formaldehyde," *J. Am. Chem. Soc.*, vol. 132, pp. 4046-4047, 2009, 10.1021/ja910366p.

[279] A. T. Hoang, Y. B. Cho, and Y. S. Kim, "A Strip of Colorimetric Sensors for Visualizing a Concentration Level of Gaseous Analytes with Basicity," *Sens. Actuator B Chem.*, vol. 251, pp. 1089-1095, 2017, 10.1016/j.snb.2017.06.142.

[280] S. H. Lim, L. Feng, J. W. Kemling, C. J. Musto, and K. S. Suslick, "An Optoelectronic Nose for Detection of Toxic Gases" *Nat. Chem.*, vol. 1, pp. 562-567, 2009, 10.1038/nchem.360.

[281] A. Prabhakar, R. A. Iglesias, R. Wang, F. Tsow, E. S. Forzani, and N. Tao, "Ultrasensitive Detection of Nitrogen Oxides over a Nanoporous Membrane," *Anal. Chem.*, vol. 82, pp. 9938-9940, 2010, 10.1021/ac101908g.

[282] C. Pannek, K. Schmitt, and J. Wollenstein, "Colorimetric Materials for Gas Selective Sensing in Low-Power Applications," *IEEE Transducers 2015, Anchorage, AK, USA*. M3P.037. pp. 1452-1455.

[283] E. Barrios, D. Fox, Y. Y. L. Sip, R. Catarata, and J. E. Calderon, "Nanomaterials in Advanced, High-Performance Aerogel Composites: A Review," *Polymers*, vol. 11, pp. 726-766, 2019, 10.3390/polym11040726.

[284] Z. Mazrouei-Sebdani, A. Khoddami, H. Hadadzadeh, and M. Zarrebini, "Synthesis and Performance Evaluation of the Aerogel-Filled PET Nanofiber Assemblies Prepared by Electro-Spinning," *RSC Adv.*, vol. 5, pp. 12830-12842, 2015, 10.1039/c4ra15297b.

[285] X. You, J. wu, and Y. Chi, "Superhydrophobic Silica Aerogels Encapsulated Fluorescent Perovskite Quantum Dots for Reversible Sensing of SO2 in a 3D-Printed Gas Cell," *Anal. Chem.*, vol. 91, pp. 5058-5066, 2019, 10.1021/acs.analchem.8b05253.

[286] J. E. Amonette and J. Matyas, "Functionalized Silica Aerogels for Gas-Phase Purification, Sensing, and Catalysis: A Review," *Micropor. Mesopor. Mat.*, vol. 250, pp. 100-119, 2017, 10.1016/j.micromeso.2017.04.055.

[287] S. Das, A. Dey, G. Reddy, and D. D. Sarma, "Suppression of the Coffee-Ring Effect and Evaporation-Driven Disorder to Order Transition in Colloidal Droplets," *J. Phys. Chem. Lett.*, vol. 8, pp. 4704-4709, 2017, 10.1021/acs.jpclett.7b01814.

[288] H. Hu and R. G. Larson, "Marangoni Effect Reverses Coffee-Ring Depositions," *J. Phys. Chem. B*, vol. 110, no. 14, pp. 7090-7094, 2006, 10.1021/jp0609232.

[289] D. Mampallil and H. B. Eral, "A Review on Suppression and Utilization of the Coffee-Ring Effect," *Adv. Colloid Interface Sci.*, vol. 252, pp. 38-54, 2018, 10.1016/j.cis.2017.12.008.

[290] X. Yu, R. Xing, Z. Peng, Y. Lin, Z, Du *et al.*, "To Inhibit Coffee Ring Effect in Inkjet Printing of Light-Emitting Polymer Films by Decreasing Capillary Force," *Chinese Chem. Lett.*, vol. 30, pp. 135-138, 2019, 10.1016/j.cclet.2018.09.007.

[291] P. J. Yunker, T. Still, M. A. Lohr, and A. G. Yodh, "Suppression of the Coffee-Ring Effect by Shape-Dependent Capillary Interactions," *Nature*, vol. 476, pp. 308-311, 2011, 10.1038/nature10344.

[292] M. Majumder, C. S. Rendall, J. A. Eukel, J. Y. L. Wang, N. Behabtu *et al.*, "Overcoming the 'Coffee-Stain' Effect by Compositional Marangoni-Flow-

Assisted Drop-Drying," *J. Phys. Chem. B*, vol. 116, pp. 6536-6542, 2012, 10.1021/jp3009628.

[293] A. Osman, L. Goehring, H. Stitt, and N. Shokri, "Controlling the Drying-Induced Peeling of Colloidal Films," *Soft Matter*, July 2020, pp. 1-7, 10.1039/d0sm00252f.

[294] B. Yang, J. S. Sharp, and M. I. Smith, "The Interplay of Crack Hopping, Delamination and Interface Failure in Drying Nanoparticle Films," *Sci. Rep.*, vol. 6, no. 32296, pp. 1-9, 2016, 10.1038/srep32296.

[295] D. W. Oxtoby, H. P. Gillis, and A. Campion, *Principles of Modern Chemistry, Seventh Edition*. Pacific Grove, CA. Brooks/Cole. 2012.

6   CONCLUSION AND FUTURE WORK

Three novel gas sensing solutions for monitoring air pollutants and hazardous chemicals have been presented. The first evaluated COTS components and sensors for use in a wearable personal exposure monitor. The MOS sensors used were compact and sensitive, but they suffered from cross-sensitives, environmental interferences, and a nonlinear response. This makes calibration challenging and interpretation of data in real-world environments difficult. The second project created a new optoelectronic gas sensing platform based on existing COTS technology, the CMOS imager. Tiny CMDs were printed on the surface of the imager and evaluated for the detection of ammonia. Response was linear, with sensitivity and dynamic range dependent on droplet size. The mechanism of detection by complexation with Cu(II) was shown to be non-sensitive to common air pollutants. The advantage of the CMOS imager as a platform is its low cost, small size, compatibility with existing technology, and familiar data output (ie. digital images). Sensors printed directly onto the surface allowed traditional optics (ie. lenses) to be discarded, furthering the extent of miniaturization possible for an optoelectronic sensor array. The approach for printing non-volatile CMDs onto the imager should be generalizable to other colorimetric indicating systems that would allow development of arrays capable of detecting many toxic gases simultaneously. The third project continued development of the lensless CMOS imaging platform with a focus on creating more robust printed sensors. For the first time commercially available hydrophobic aerogel microparticles were evaluated as a novel and inexpensive sorbent material for colorimetric gas sensors in an all-in-one printable ink formulation. The challenges of printing solid films from particles were addressed and steps to improve coating uniformity, and prevent

cracking and delamination, were implemented by modifying the ink formulation and CMOS imager surface properties. High quality sensors printed onto the CMOS imager surface with hydrophobic qualities showed excellent sensitivity, selectivity, humidity response, and reversibility in measuring ammonia when compared with formulations excluding aerogel particles or using hydrophilic media. This approach should also be generalizable to other colorimetric indicating systems which would allow generation of robust printed arrays capable of detecting many different pollutants and hazardous chemicals simultaneously.

The CMOS imager is a versatile platform for low-cost sensing applications. In addition to colorimetric absorbance measurements, it can be used for chemiluminescent and fluorescent techniques, and also particle detection. Future work will focus on integrating multiple sensing modalities that provide a synergistic benefit. One timely application is particle capture, counting, and sizing combined with biological detection for monitoring aerosols in ambient air. In light of the COVID-19 pandemic, which has caused millions of infections globally and many premature deaths, there has been shown to be a need for a fast and easy way to monitor ambient air for suspended virulent particles [296]. The benefit of this would be to limit their spread and provide knowledge to guide action on proper ventilation and elimination of the virus from breathable air, especially in confined spaces and areas with susceptible individuals (eg. hospitals, nursing homes, schools). A summary of the approach for developing this type of device with background information and preliminary results follows.

SARS-CoV-2 transmission occurs primarily by the spread of virulent pathogens given off by an infected host's respiratory system in the form of droplets, aerosols, and

contaminated surfaces where particles settle (ie. fomites) [297-305]. Current methods for collection and analysis of these particles require filters and ex-situ laboratory analysis by reverse transcription polymerase chain reaction (RT-PCR) [299, 301]. A new system could provide real-time, on-site monitoring by collecting suspended particles using impaction plates. Sequential impaction plates allows separation by particle size due to differences in particle inertia [306]. For example, sequential zones could remove large particles (ie. >10 µm) and separate the fine (ie. 0.2 to 2.5 µm) and coarse (ie. 2.5 to 10 µm) fractions of particles for measurement and biological sensing. Figure 6.1 shows a schematic of the impaction principle and a prototype of the SARS-CoV-2 aerosol detection device. Researchers have found SARS-CoV-2 with virulent activity in particles ranging 0.2 to 10 µm, and particles of this size are capable of persisting in the atmosphere without quickly settling and are easily redistributed by the ventilation system within a building [299, 301]. At both impaction stages (ie. fine and coarse) the particles deposit an optical sensors using CMOS imagers that count the particles and detect for SARS-CoV-2 using a fluorescent technique. Collection of particles by impactor plates followed by counting and sizing using a CMOS imager has been done previously, but this will be the first time SARS-CoV-2 is identified optically in real-time from suspended aerosols [307].
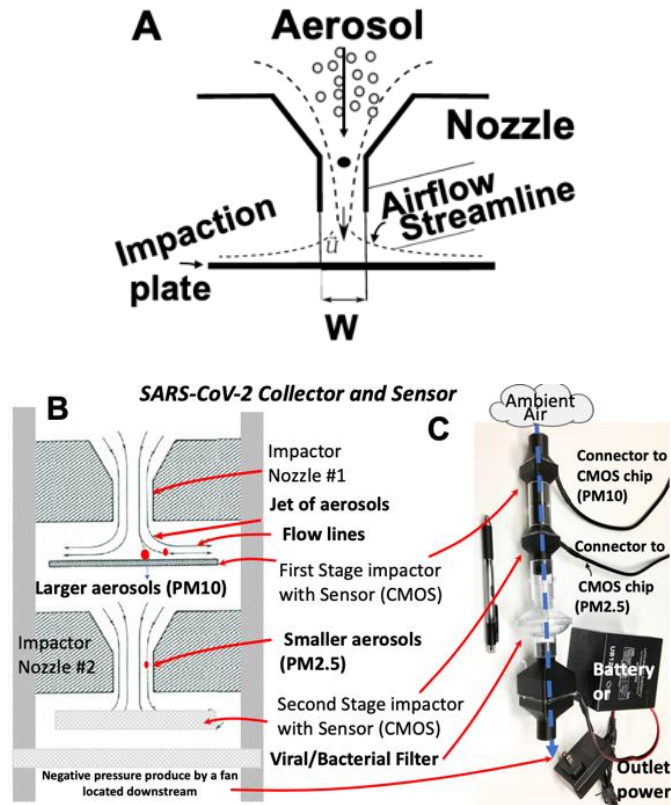
Figure 6.1 A) Impaction Principle. B) Schematic of the SARS-CoV-2 multistage collector. C) 3D printed 2-stage impactor, filter, and fan assembly.

The biological mode of detection relies on sensitivity to the N protein of SARS-CoV-2, which is one of the typical markers used in detecting infection by this virus [308]. The sensor media is composed of non-volatile, amphiphilic (ie. surfactant) ionic liquid and glycerol to prevent evaporation and maintain a liquid environment for biological interactions to take place. The surfactant quality of the chosen ionic liquid breaks apart the virus and releases the N protein, facilitating its detection [309-311]. Detection is made by luminescent CdTe quantum dot (QD)-conjugated aptamer system based on competitive aptamer-antigen interactions utilizing Förster energy resonance transfer (FRET). This approach makes for a more cost effective and robust sensor compared with antibodies conjugated with conventional organic fluorophores. The sensor surface will be

functionalized with SARS-CoV-2 N protein aptamer conjugated with green (525 nm) emitting QD. The analyte-simile antigen (MERS N protein), which is conjugated with red (655 nm) emitting QD, is bound to the N protein aptamer at the functionalized surface. When the red and green QDs are in close proximity (ie. aptamer and MERS N protein are bound) the FRET mechanism quenches the emission of green light under fluorescence and enhances emission of red light [312-314]. In the presence of SARS-CoV-2 (eg. deposited onto the impactor surface of the sensor from aerosols in ambient air) the conjugated MERS N protein is displaced due to its lower affinity towards the aptamer and is replaced by SARS-CoV-2 N protein. This removes the red QD and allows green fluorescent light to be emitted. Figure 6.2 illustrates the displacement and FRET mechanism.
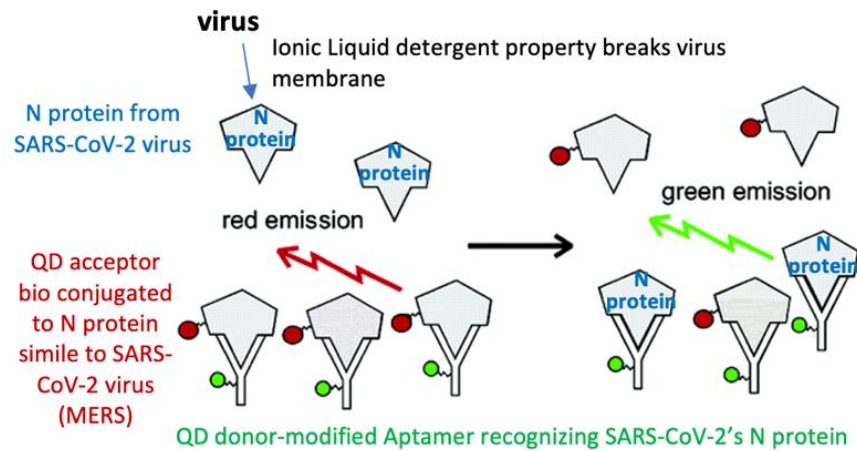
Figure 6.2 Detection principle for SARS-CoV-2 using QD-bioconjugates and FRET.

The large field of view of the CMOS imager leaves room for positive and negative controls around the testing area to guarantee the sensor is functioning properly. This proposed measurement system could be used to trigger an alarm for positive SARS-CoV-2 detection and turn on ventilation and filtration/UV systems until particle numbers drop

below a safe threshold. Preliminary data in the ionic liquid 1-hexadecyl-3-methylimidazolium chloride suggests a detection limit as low as 0.35 pmol (ie. 1.3 nM in 10 µL) is possible, which is in a suitable range for detection of virus proteins in aerosols (Figure 6.3).
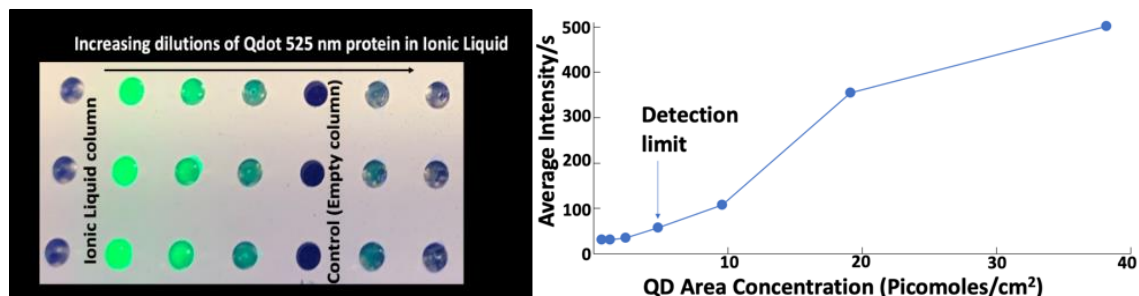
Figure 6.3 Image of 525 nm QD fluorescence in ionic liquid, and corresponding calibration curve of intensity per exposure time vs. QD surface concentration in ionic liquid.

References

[296] WHO, "WHO Coronavirus Disease (COVID-19) Dashboard," World Health Organization 2020.

[297] K. Mizumoto, K. Kagaya, A. Zarebski, and G. Chowell, "Estimating the Asymptomatic Proportion of Coronavirus Disease 2019 (COVID-19) Cases on Board the Diamond Princess Cruise Ship, Yokohama, Japan," *Euro Surveill*, vol. 25, 2020, 10.2807/1560-7917.ES.2020.25.10.2000180.

[298] P. Lines, "Grand Princess Updates", 2020. [Online] Available: https://www.princess.com/news/notices_and_advisories/notices/grand-princess-updates.html Accessed on: September 15, 2020.

[299] J. L. Santarpia, D. N. Rivera, V. Herrera, M. J. Morwitzer, H. Creager *et al.*, "Aerosol and Surface Transmission Potential of SARS-CoV-2," *medRxiv*, 2020, 10.1101/2020.03.23.20039446.

[300] Y. Li, G. M. Leung, J. W. Tang, X. Yang, C. Y. H. Chao *et al.*, "Role of Ventilation in Airborne Transmission of Infectious Agents in the Built Environments – a Multidisciplinary Systematic Review," *Indoor Air*, vol. 17, pp. 2-18, 2007.

[301] Y. Liu, Z. Ning, Y. Chen, M. Guo, Y. L. Liu *et al.*, "Aerodynamic Analysis of SARS-CoV-2 in two Wuhan Hospitals," *Nature*, 2020.

[302] Z. Tufekci, "We Need to Talk About Ventilation. How is it That Six Months Into a Respiratory Pandemic, we are Still Doing so Little to Mitigate Airborne Transmission?," *The Atlantic*, July 30, 2020.

[303] T. Galbadage, B. M. Peterson, R. S. Gunasekera, "Does COVID-19 Spread Through Droplets Alone?," *Front Public Health*, April 24, 2020, 10.3389/fpubh.2020.00163.

[304] G. Correia, L. Rodrigues, M. Gameiro da Silva, and T. Goncalves, "Airborne Route and Bad Use of Ventilation Systems as Non-Negligible Factors in SARS-CoV-2 Transmission," *Med Hypotheses*, vol. 141, 2020, 10.1016/j.mehy.2020.109781.

[305] P. Baron, "Generation and Behavior of Airborne Particles," CDC, NIOSH. [Online] Available: https://www.cdc.gov/niosh/topics/aerosols/pdfs/aerosol_101.pdf Accessed on: August 15, 2020.

[306] V. A. Marple and B. A. Olson, "Sampling and Measurement Using Inertial, Gravitational, Centrifugal, and Thermal Techniques," in *Aerosol Measurement: Principles, Techniques, and Applications*. Wiley Online Library: Hoboken, NJ, USA, 2011:129.

[307] Z. Du, F. Tsow, D. Wang, and N. Tao, "A Miniaturized Particulate Matter Sensing Platform Based on CMOS Imager and Real-Time Image Processing," *IEEE Sens. J.*, vol. 18, pp. 7421-7428, 2018.

[308] I. A. Ysrafil, "Severe Acute Respiratory Syndrome Coronavirus 2 (SARS-CoV-2): An Overview of Viral Structure and Host Response," *Diabetes Metab. Syndr.*, vol. 14, pp. 407-412, 2020.

[309] P. D. Galgano and O. A. El Seoud, "Surface Active Ionic Liquids: Study of Micellar Properties of 1-(1-alkyl)-3-methylimidazolium chlorides and comparison with structurally related surfactants," *J. Colloid Interface Sci.*, vol. 361, pp. 186-194, 2011.

[310] S. Mondal, A. Banerjee, and B. Das, "Spectroscopic and Interfacial Investigation on the Interaction of Hemoglobin with Conventional and Ionic Liquid Surfactants," *J. Mol. Liq.*, vol. 301, 2020.

[311] K. S. Egorova, E. G. Gordeev, and V. P. Ananikov, "Biological Activity of Ionic Liquids and Their Application in Pharmaceutics and Medicine," *Chem. Rev.*, vol. 117, pp. 7132-7189, 2017.

[312]   K. Matsubara and H. Katayama, "Development of a Portable Detection for Enteric Viruses from Ambient Air and its Application to a Wastewater Treatment Plant," *Pathogens*, vol. 8, 2019.

[313]   J. Shen, Y. Zhou, F. Fu, H. Xu, J. Lv *et al.*, "Immunochromatographic Assay for Quantitative and Sensitive Detection of Hepatitis B Virus Surface Antigen Using Highly Luminescent Quantum Dot-Beads," *Talanta*, vol. 142, pp. 145-149, 2015.

[314]   J. Saha, A. R. Datta, D. Dey, D. Bhattacharjee, and A. Hussain, "Role of Quantum Dot in Designing FRET Based Sensors," *Materials Today Proceedings*, vol. 5, pp. 2306-2313, 2018.

REFERENCES

[1]   I. Manisalidis, E. Stavropoulou, A. Stavropoulos, and E. Bezirtzoglou, "Environmental and Health Impacts of Air Pollution: A Review," *Public Health Front.*, vol. 8, no. 14, pp. 1-13, 2020, 10.3389/fpubh.2020.00014.

[2]   R. D. Brook, B. Franklin, W. Cascio, Y. Hong, G. Howard *et al.*, "Air Pollution and Cardiovascular Disease," AHA Scientific Statement, pp. 2655-2671, 2004, 10.1161/01.CIR.0000128587.30041.C8.

[3]   HEI Panel on the Health Effects of Traffic-Related Air Pollution, "Traffic-Related Air Pollution: A Critical Review of the Literature on Emissions, Exposure, and Health Effects," Health Effects Institute Special Report 17, 2010, Health Effects Institute, Boston, MA, USA.

[4]   WHO, "Burden of Disease from the Joint Effects of Household and Ambient Air Pollution for 2016," Public Health, Social and Environmental Determinants of Health Department, World Health Organization, Geneva, Switzerland. 2018.

[5]   WHO, "Air Pollution", 2020. [Online] Available: http://www.who.int/airpollution/en/, Accessed on: June 4, 2020.

[6]   C. J. L. Murray *et al.*, "Global, Regional, and National Comparative Risk Assessment of 79 Behavioural, Environmental and Occupational, and Metabolic Risks or Clusters of Risks, 1990-2015: a Systematic Analysis for the Global Burden of Disease Study 2015," *Lancet*, vol. 388, pp. 1659-1724, 2016.

[7]   OECD, "The economic consequences of outdoor air pollution," The Organisation for Economic Co-operation and Development, Paris, France. 2016.

[8]   WHO, "WHO Global Ambient Air Quality Database," 2018. [Online] Available: https://www.who.int/airpollution/data/cities/en/, Accessed on: June 2, 2020.

[9]   UNFCC, "What is the Kyoto Protocol?," 1997. [Online] Available: https://unfccc.int/kyoto_protocol, Accessed on: October 6, 2019.

[10]   UNFCC, "Copenhagen Climate Change Conference," 2009. [Online] Available: https://unfccc.int/process-and-meetings/conferences/past-conferences/copenhagen-climate-change-conference-december-2009/copenhagenclimate-change-conference-december-2009, Accessed on: October 6, 2019.

[11]   UNFCC, "Durban Climate Change Conference," 2011. [Online] Available: https://unfccc.int/process-and-meetings/conferences/past-conferences/copenhagen-climate-change-conference-december-2009/copenhagenclimate-change-conference-december-2009, Accessed on: October 6, 2019.

[12]   UNFCC, "The Paris Agreement," 2016. [Online] Available: https://unfccc.int/process-and-meetings/the-paris-agreement/the-paris-agreement, Accessed on: June 4, 2020.

[13]   CAAC, "State Council Air Pollution Prevention and Control Action Plan," Clean Air Alliance of China, Beijing, China. 2013.

[14]   A. Miranda, C. Silveira, J. Ferreira, A. Monteiro, D. Lopes, H. Relvas *et al.*, "Current Air Quality Plans in Europe Designed to Support Air Quality Management Policies," *Atmos. Pollut. Res.*, vol. 6, pp. 434-443, 2015, 10.5094/APR.2015.048.

[15]   EPA, "Overview of the Clean Air Act and Air Pollution," 2020. [Online] Available: https://www.epa.gov/clean-air-act-overview, Accessed On: June 4, 2020.

[16]   B. Nemery, P. H. M. Hoet, A. Nemmar, "The Meuse Valley Fog of 1930: an Air Pollution Disaster," *Lancet*, vol. 357, pp. 704-708, 2001.

[17]   W. P. D. Logan, "Mortality in the London Fog Incident, 1952," *Lancet*, Feb. 14, 1953, pp. 336-338.

[18]   USA, "Air Pollution Control Act 1955," Public Law 159, Chapter 360, July 14, 1955, pp. 322-323.

[19]   UK, "Clean Air Act 1956," Chapter 52, July 5, 1956.

[20]   USA, "Clean Air Act 1970," Public Law 91-604, Dec. 31, 1970, pp. 1676-1713.

[21]   EPA, "Evolution of the Clean Air Act," 2017. [Online] Available: https://www.epa.gov/clean-air-act-overview/evolution-clean-air-act, Accessed On: June 4, 2020.

[22]   C. A. Pope III, "Epidemiology of Fine Particulate Air Pollution and Human Health: Biologic Mechanisms and Who's at Risk?," *Environ. Health Perspect.*, vol. 108, no. 4, pp. 713-723, 2000.

[23]   R. D. Brook, J. R. Brook, and S. Rajagopalan, "Air Pollution: The 'Heart' of the Problem," *Curr. Hypertens. Rep.*, vol. 5, pp. 32-39, 2003.

[24]   EPA, "Air Pollution: Current and Future Challenges," 2019. [Online] Available: https://www.epa.gov/clean-air-act-overview/air-pollution-current-and-future-challenges, Accessed On: June 3, 2020.

[25]   X. Q. Jiang, X. D. Mei, and D. Feng, "Air Pollution and Chronic Airway Diseases: What Should People Know and Do?," *J. Thorac. Dis.*, vol. 8, no. 1, pp. E31-E40, 2016, 10.3978/j.issn.2072-1439.2015.11.50.

[26] F. J. Kelly, "Oxidative Stress: Its Role in Air Pollution and Adverse Health Effects," *Occup. Environ. Med.*, vol. 60, pp. 612-616, 2003, 10.1136/oem.60.8.612.

[27] A. J. Ghio, C. Kim, and R. B. Devlin, "Concentrated Ambient Air Particles Induce Mild Pulmonary Inflammation in Healthy Human Volunteers," *Am. J. Respir. Crit. Care Med.*, vol. 162, pp. 981-988, 2000.

[28] R. M. Aris, D. Christian, P. Q. Hearne *et al.*, "Ozone-Induced Airway Inflammation in Human Subjects as Determined by Airway Lavage and Biopsy," *Am. Rev. Respir. Dis.*, vol. 148, pp. 1363-1372, 1993, 10.1164/ajrccm/148.5.1363.

[29] J. J. Godleski, R. W. Clarke, B. A. Coull *et al.*, "Composition of Inhaled Urban Air Particles Determines Acute Pulmonary Responses," *Ann. Occup. Hyg.*, vol. 46, no. 1, pp. 419-424, 2002, 10.1093/annhyg/mef706.

[30] D. L. Costa and K. L. Dreher, "Bioavailable Transition Metals in Particulate Matter Mediate Cardiopulmonary Injury in Healthy and Compromised Animal Models," *Environ. Health Perspect.*, vol. 105, no. 5, pp. 1053-1060, 1997.

[31] J. D. Brain, N. C. Long, S. F. Wolfthal *et al.*, "Pulmonary Toxicity in Hamsters of Smoke Particles from Kuwaiti Oil Fires," *Environ. Health Perspect.*, vol. 106, pp. 141-146, 1998.

[32] X. Y. Li, P. S. Gilmour, K. Donaldson *et al.*, "Free Radical Activity and Pro-Inflammatory Effects of Particulate Air Pollution (PM10) in vivo and in vitro," *Thorax*, vol. 51, pp. 1216-1222, 1996, 10.1136/thx.51.12.1216.

[33] T. Kennedy, A. J. Ghio, W. Reed *et al.*, "Copper-Dependent Inflammation and Nuclear Factor-KappaB Activation by Particulate Air Pollution," *Am. J. Respir. Cell Mol. Biol.*, vol. 19, pp. 366-378, 1998.

[34] N. Kunzli, R. Kaiser, S. Medina, M. Studnicka, O. Chanel, P. Filliger *et al.*, "Public-Health Impact of Outdoor and Traffic-Related Air Pollution: a European Assessment," *Lancet*, vol. 356, pp. 795-801, 2000.

[35] K. R. Pride, J. L. Peel, B. F. Robinson, A. Busacker, J. Grandpre *et al.*, "Association of Short-Term Exposure to Ground-Level Ozone and Respiratory Outpatient Clinic Visits in a Rural Location – Sublette County, Wyoming, 2008-2011," *Environ. Res.*, vol. 137, pp. 1-7, 2015, 10.1016/j.envres.2014.10.033.

[36] M. Ji, D. S. Cohan, and M. L. Bell, "Meta-Analysis of the Association Between Short-Term Exposure to Ambient Ozone and Respiratory Hospital Admissions," *Environ. Res. Lett.*, vol. 6, pp. 1-11, 2011, 10.1088/1748-9326/6/2/024006.

[37] M. Medina-Ramon, A. Zanobetti, and J. Schwartz, "The Effect of Ozone and PM10 on Hospital Admissions for Pneumonia and Chronic Obstructive Pulmonary

Disease: A National Multicity Study," *Am. J. Epidemiol.*, vol. 163, no. 6, pp. 579-588, 2006, 10.1093/aje/kwj078.

[38]   C. Paulu and A. E. Smith, "Tracking Associations Between Ambient Ozone and Asthma-Related Emergency Department Visits Using Case-Crossover Analysis," *J. Public Health Manag. Pract.*, vol. 14, no. 6, pp. 581-591, 2008.

[39]   S. Yamazaki, M. Shima, M. Ando, and H. Nitta, "Modifying Effect of Age on the Association between Ambient Ozone and Nighttime Primary Care Visits Due to Asthma Attack," *J. Epidemiol.*, vol. 19, no. 3, pp. 143-151, 2009, 10.2188/jea.JE20081025.

[40]   Q. Yang, Y. Chen, Y. Shi, R. T. Burnett, K. M. McGrail *et al.*, "Association Between Ozone and Respiratory Admissions Among Children and the Elderly in Vancouver, Canada," *Inhal. Toxicol.*, vol. 15, pp. 1297-1308, 2003, 10.1080/08958370390241768.

[41]   K. K. Lee, M. R. Miller, and A. S. V. Shah, "Air Pollution and Stroke," *J. Stroke*, vol. 20, no. 1, pp. 2-11, 2018, 10.5853/jos.2017.02894.

[42]   C. A. Pope III, R. T. Burnett, M. J. Thun, E. E. Calle, D. Krewski *et al.*, "Lung Cancer, Cardiopulmonary Mortality, and Long-Term Exposure to Fine Particulate Air Pollution," *JAMA*, vol. 287, no. 9, pp. 1132-1141, 2002.

[43]   EPA, "Criteria Air Pollutants," 2018. [Online] Available: https://www.epa.gov/criteria-air-pollutants, Accessed On: June 3, 2020.

[44]   J. H. Seinfeld and S. N. Pandis, *Atmospheric Chemistry and Physics: From Air Pollution to Climate Change*. New York, NY, USA: John Wiley & Sons, 1998, pp. 1-1326.

[45]   EPA, "Initial List of Hazardous Air Pollutants with Modifications," 2020. [Online] Available: https://www.epa.gov/haps/initial-list-hazardous-air-pollutants-modifications, Accessed On: June 4, 2020.

[46]   EPA, "Introduction to Indoor Air Quality," 2020. [Online] Available: https://www.epa.gov/indoor-air-quality-iaq/introduction-indoor-air-quality, Accessed On: June 3, 2020.

[47]   A. P. Jones, "Indoor Air Quality and Health," *Atmos. Environ.*, vol. 33, pp. 4535-4564, 1999.

[48]   T. Tanaka-Kagawa, S. Uchiyama, E. Matsushima, A. Sasaki, H. Kobayashi *et al.*, "Survey of Volatile Organic Compounds Found in Indoor and Outdoor Air Samples from Japan," *Bull. Natl. Inst. Health Sci.*, vol. 123, pp. 27-31, 2005.

[49] EPA, *America's Children and the Environment, Third Edition*. Research Triangle Park, NC, USA: U.S. EPA, 2013, pp. 1-390.

[50] European Collaborative Action, "Urban Air, Indoor Environment, and Human Exposure, Environment and Quality of Life, Report No. 22, Risk Assessment In Relation to Indoor Air Quality," European Commission, Joint Research Centre, Brussels, Belgium, EUR 19529 EN, 2000.

[51] EPA, "Technical Overview of Volatile Organic Compounds," 2017. [Online] Available: https://www.epa.gov/indoor-air-quality-iaq/technical-overview-volatile-organic-compounds, Accessed On: June 4, 2020.

[52] WHO, *WHO Guidelines for Indoor Air Quality, Selected Pollutants*. Copenhagen, Denmark: WHO Regional Office for Europe, 2010, pp. 1-454.

[53] USA, "OSH Act of 1970," Public Law 91-596, Dec. 29, 1970.

[54] Construction Safety Council, *Health Hazards in Construction*. Hillside, IL, USA: Construction Safety Council, 2012, pp. 1-247.

[55] OSHA, "Chemical Hazards and Toxic Substances," 2020. [Online] Available: https://www.osha.gov/SLTC/hazardoustoxicsubstances/, Accessed On: June 4, 2020.

[56] CDC, "Chemicals: Managing Chemical Safety in the Workplace," 2017. [Online] Available: https://www.cdc.gov/niosh/chemicals/default.html, Accessed On: June 4, 2020.

[57] R. Andrews and P. F. O'Connor, *NIOSH Manual of Analytical Methods (NMAM), Fifth Edition*. Washington D.C., USA: CDC, NIOSH, 2020.

[58] OSHA, "Sampling and Analysis," 2020. [Online] Available: https://www.osha.gov/SLTC/samplinganalysis/index.html, Accessed On: June 4, 2020.

[59] OSHA, "OSHA Technical Manual," 2020. [Online] Available: https://www.osha.gov/dts/osta/otm/, Accessed On: June 4, 2020.

[60] EU, "The Protection of the Health and Safety of Workers from the Risks Related to Chemical Agents at Work," Council Directive 98/24/EC, April 7, 1998, pp. 1-22.

[61] EU, "Establishing Indicative Limit Values by Implementing Council Directive 80/1107/EEC on the Protection of Workers From the Risks Related to Exposure to Chemical, Physical and Biological Agents at Work," Commission Directive 91/322/EEC, May 29, 1991, pp. 1-3.

[62]   WHO, "WHO Global Ambient Air Quality Database," 2018. [Online] Available: https://www.who.int/airpollution/data/cities/en/, Accessed On: June 2, 2020.

[63]   M. Eeftens, R. Beelen, K. de Hoogh, T. Bellander, G. Cesaroni *et al.*, "Development of Land Use Regression Models for PM2.5, PM2.5 Absorbance, PM10, and PMCoarse in 20 European Study Areas; Results of the ESCAPE Project," *Environ. Sci. Technol.*, vol. 46, pp. 11195-11205, 2012, 10.1021/es301948k.

[64]   J. D. Marshall, E. Nethery, and M. Brauer, "Within-Urban Variability in Ambient Air Pollution: Comparison of Estimation Methods," *Atmos. Environ.*, vol. 42, pp. 1359-1369, 2008, 10.1016/j.atmosenv.2007.08.012.

[65]   M. Gao, J. Cao, and E. Seto, "A Distributed Network of Low-Cost Continuous Reading Sensors to Measure Spatiotemporal Variations of PM2.5 in Xi'an, China," *Environ. Pollut.*, vol. 199, pp. 56-65, 2015, 10.1016/j.envpol.2015.01.013.

[66]   M. Masiol, S. Squizzato, D. Chalupa, D. Q. Rich, and P. K. Hopke, "Spatial-Temporal Variations of Summertime Ozone Concentrations Across a Metropolitan Area Using a Network of Low-Cost Monitors to Develop 24 Hourly Land-Use Regression Models," *Sci. Total Environ.*, vol. 654, pp. 1167-1178, 2019, 10.1016/j.scitotenv.2018.11.111.

[67]   R. N. Colvile, E. J. Hutchinson, J. S. Mindell, and R. F. Warren, "The Transport Sector as a Source of Air Pollution," *Atmos. Environ.*, vol. 35, pp. 1537-1565, 2001.

[68]   M. Gerboles, D. Buzica, L. Amantini, and F. Lagler, "Laboratory and Field Comparison of Measurements Obtained Using the Available Diffusive Samplers for Ozone and Nitrogen Dioxide in Ambient Air," *J. Environ. Monit.*, vol. 8, pp. 112-119, 2006, 10.1039/B511271K.

[69]   W. F. Cheung, T. H. Lin, and Y. C. Lin, "A Real-Time Construction Safety Monitoring System for Hazardous Gas Integrating Wireless Sensor Network and Building Information Modeling Technologies," *Sensors (Basel)*, vol. 18, pp. 1-24, 2018, 10.3390/s18020436.

[70]   M. Loh, D. Sarigiannis, A. Gotti, S. Karakitsios, A. Pronk *et al.*, "How Sensors Might Help Define the External Exposome," *Int. J. Environ. Res. Public Health*, vol. 14, pp. 1-14, 2017, 10.3390/ijerph14040434.

[71]   W. Y. Yi, K. M. Lo, T. Mak, K. S. Leung, Y. Leung, and M. L. Meng, "A Survey of Wireless Sensor Network Based Air Pollution Monitoring Systems," *Sensors (Basel)*, vol. 15, pp. 31392-31427, 2015, 10.3390/s151229859.

[72]   L. Morawska, P. K. Thai, X. Liu, A. Asumadu-Sakyi, G. Ayoko *et al.*, "Applications of Low-Cost Sensing Technologies for Air Quality Monitoring and

Exposure Assessment: How Far Have They Gone?," *Environ. Int.*, vol. 116, pp. 286-299, 2018, 10.1016/j.envint.2018.04.018.

[73]   S. Steinle, S. Reis, and C. E. Sabel, "Quantifying Human Exposure to Air Pollution – Moving from Static Monitoring to Spatio-Temporally Resolved Personal Exposure Assessment," *Sci. Total Environ.*, vol. 443, pp. 184-193, 2013, 10.1016/j.scitotenv.2012.10.098.

[74]   R. Baron and J. Saffell, "Amperometric Gas Sensors as a Low Cost Emerging Technology Platform for Air Quality Monitoring Applications: A Review," *ACS Sens.*, vol. 2, pp. 1553-1566, 2017, 10.1021/acssensors.7b00620.

[75]   EPA, "Sensor Evaluation Report," U.S. EPA, Office of Research and Development, National Exposure Research Laboratory, EPA/600/R-14/143, 2014.

[76]   EPA, "Research and Development Highlights: Mobile Sensors and Applications for Air Pollutants," U.S. EPA, EPA/600/R-14/051, 2013.

[77]   EPA, "Air Sensor Guidebook," U.S. EPA, Office of Research and Development, National Exposure Research Laboratory, EPA/600/R-14/159, 2014.

[78]   J. A. Anel, "Atmospheric Ozone: Historical Background and State-of-the-Art," *Contemp. Phys.*, vol. 57, no. 3, pp. 417-420, 2016, 10.1080/00107514.2016.1156748.

[79]   R. D. Bojkov, "Surface Ozone During the Second Half of the Nineteenth Century," *J. Appl. Meteorol. Climatol.*, vol. 25, no. 3, pp. 343-352, 1986.

[80]   T. Weidinger, G. Baranka, R. Balazs, and K. Toth, "Comparison of 19th Century and Present Concentrations and Depositions of Ozone in Central Europe," *Acta. Silv. Lign. Hung.*, vol. 7, pp. 23-38, 2011.

[81]   K. C. Clemitshaw, "A Review of Instrumentation and Measurement Techniques for Ground-Based and Airborne Field Studies of Gas-Phase Tropospheric Chemistry," *Crit. Rev. Environ. Sci. Technol.*, vol. 34, pp. 1-108, 2004, 10.1080/10643380490265117.

[82]   EPA, "Sampling Methods for Criteria Pollutants," 2020. [Online] Available: https://aqs.epa.gov/aqsweb/documents/codetables/methods_criteria.html, Accessed On: September 1, 2020.

[83]   EPA, "Air Emission Measurement Center: EMC Promulgated Test Methods," 2020. [Online] Available: https://www.epa.gov/emc/emc-promulgated-test-methods, Accessed On: September 2, 2020.

[84]   EPA, "EPA Scientists Develop and Evaluate Federal Reference & Equivalent Methods for Measuring Key Air Pollutants," 2019. [Online] Available:

https://www.epa.gov/air-research/epa-scientists-develop-and-evaluate-federal-reference-equivalent-methods-measuring-key, Accessed On: September 3, 2020.

[85]   DEFRA, "Air Quality Monitoring Methods," 2020. [Online] Available: https://uk-air.defra.gov.uk/networks/monitoring-methods, Accessed On: August 30, 2020.

[86]   ISO, "International Organization for Standardization Homepage," 2020. [Online] Available: https://www.iso.org/home.html, Accessed On: August 30, 2020.

[87]   EC, "Implementation of Ambient Air Quality Legislation," 2020. [Online] Available: https://ec.europa.eu/environment/air/quality/assessment.htm, Accessed On: August 30, 2020.

[88]   ASTM, "ASTM Homepage," 2020. [Online] Available: https://www.astm.org/, Accessed On: August 30, 2020.

[89]   Australia NSW, "How We Monitor Air Pollution," 2020. [Online] Available: https://www.environment.nsw.gov.au/topics/air/air-quality-basics/sampling-air-pollution, Accessed On: August 30, 2020.

[90]   P. C. Andersen, C. J. Williford, and J. W. Birks, "Miniature Personal Ozone Monitor Based on UV Absorbance," *Anal. Chem.*, vol. 82, no. 19, pp. 7924-7928, 2010, 10.1021/ac1013578.

[91]   D. D. Parrish and F. C. Fehsenfeld, "Methods for Gas-Phase Measurements of Ozone, Ozone Precursors and Aerosol Precursors," *Atmos. Environ.*, vol. 34, pp. 1921-1957, 2000.

[92]   E. J. Williams, S. T. Sandholm, J. D. Bradshaw, J. S. Schendel, A. O. Langford *et al.*, "An Intercomparison of Five Ammonia Measurement Techniques," *J. Geophys. Res.*, vol. 97, no. D11, pp. 11,591-11,611, 1992.

[93]   M. G. Mennen, B. G. Van Elzakker, E. M. Van Putten, J. W. Uiterwijk, T. A. Regts *et al.*, "Evaluation of Automatic Ammonia Monitors for Application in an Air Quality Monitoring Network," *Atmos. Environ.*, vol. 30, no. 19, pp. 3239-3256, 1996.

[94]   Y. I. Yashin and A. Y. Yashin, "Analytical Chromatography. Methods, Instrumentation and Applications," *Russ. Chem. Rev.*, vol. 75, no. 4, pp. 329-340, 2006, 10.1070/RC2006v075n04ABEH003607.

[95]   D. A. Skoog and J. J. Leary, *Principles of Instrumental Analysis, Fourth Edition*. Philadelphia, PA, USA: Saunders College Publishing, 1992, pp. 579-601.

[96]   D. A. Skoog and J. J. Leary, *Principles of Instrumental Analysis, Fourth Edition*. Philadelphia, PA, USA: Saunders College Publishing, 1992, pp. 605-625.

[97] F. L. Dorman, E. B. Overton, J. J. Whiting, J. W. Cochran, and J. Gardea-Torresdey, "Gas Chromatography," *Anal. Chem.*, vol. 80, no. 12, pp. 4487-4497, 2008, 10.1021/ac800714x.

[98] L. N. Williamson and M. G. Bartlett, "Quantitative Gas Chromatography/Time-of-Flight Mass Spectrometry: A Review," *Biomed. Chromatogr.*, vol. 21, pp. 664-669, 2007, 10.1002/bmc.847.

[99] M. Marc, M. Tobiszewski, B. Zabiegala, M. de la Guardia, and J. Namiesnik, "Current Air Quality Analytics and Monitoring: A Review," *Anal. Chim. Acta*, vol. 853, pp. 116-126, 2015, 10.1016/j.aca.2014.10.018.

[100] M. Marc, B. Zabiegala, and J. Namiesnik, "Mobile Systems (Portable, Handheld, Transportable) for Monitoring Air Pollution," *Crit. Rev. Anal. Chem.*, vol. 42, pp. 2-15, 2012, 10.1080/10408347.2011.607079.

[101] J. Dewulf, H. Van Langenhove, and G. Wittmann, "Analysis of Volatile Organic Compounds Using Gas Chromatography," *Trends Anal. Chem.*, vol. 21, pp. 637-646, 2002.

[102] I. Spanik and A. Machynakova, "Recent Applications of Gas Chromatography with High-Resolution Mass Spectrometry," *J. Sep. Sci.*, vol. 41, no. 1, pp. 163-179, 2018, 10.1002/jssc.201701016.

[103] M. R. Jacobs, E. F. Hilder, and R. A. Shellie, "Applications of Resistive Heating in Gas Chromatography: A Review," *Anal. Chim. Acta*, vol. 803, pp. 2-14, 2013, 10.1016/j.aca.2013.04.063.

[104] J. C. Soo, E. G. Lee, R. F. LeBouf, M. L. Kashon, and W. Chisholm, "Evaluation of a Portable Gas Chromatograph with Photoionization Detector Under Variations of VOC Concentration, Temperature, and Relative Humidity," *J. Occup. Environ. Hyg.*, vol. 15, no. 4, pp. 351-360, 2018, 10.1080/15459624.2018.1426860.

[105] H. Tanimoto, H. Mukai, S. Hashimoto, and J. E. Norris, "Intercomparison of Ultraviolet Photometry and Gas-Phase Titration Techniques for Ozone Reference Standards at Ambient Levels," *J. Geophys. Res.*, vol. 111, D16313, pp. 1-11, 2006, 10.1029/2005JD006983.

[106] E. J. Williams, F. C. Fehsenfeld, B. T. Jobson, W. C. Kuster, P. D. Goldan *et al.*, "Comparison of Ultraviolet Absorbance, Chemiluminescence, and DOAS Instruments for Ambient Ozone Monitoring," *Environ. Sci. Technol.*, vol. 40, no. 18, pp. 5755-5762, 2006, 10.1021/es0523542.

[107] 2B Technologies Inc., "Ozone Monitor: Operation Manual, Model 202, Rev. H," Boulder, CO, USA, 2B Technologies Inc., pp. 1-45, 2015.

[108]   2B Technologies Inc., "UV-Absorbing Interferences in Ozone Monitors," Boulder, CO, USA, 2B Technologies Inc., Technical Note No. 40, pp. 1-6, 2015.

[109]   K. L. Wilson and J. W. Birks, "Mechanism and Elimination of a Water Vapor Interference in the Measurement of Ozone by UV Absorbance," *Environ. Sci. Technol.*, vol. 40, no. 20, pp. 6361-6367, 2006, 10.1021/es052590c.

[110]   D. A. Skoog and J. J. Leary, *Principles of Instrumental Analysis, Fourth Edition.* Philadelphia, PA, USA: Saunders College Publishing, 1992, pp. 123-147.

[111]   2B Technologies Inc., "Explanation of Temperature and Pressure Corrections in Ozone Measurements of Mixing Ratios," Boulder, CO, USA, 2B Technologies Inc., Technical Note No. 010, pp. 1-3, 2007.

[112]   RAE Systems Inc., "Comparison of Photoionization Detectors (PIDs) and Flame Ionization Detectors (FIDs)," San Jose, CA, USA, RAE Systems Inc., Application Note AP-226, 01/04/WH, pp. 1-2.

[113]   RAE Systems Inc. The PID Handbook, Theory and Applications of Direct-Reading Photoionization Detectors (PIDs). San Jose, CA, USA. RAE Systems Inc. pp. 1-166, 2013.

[114]   S. Mergemeier, I. Ebner, and F. Scholz, "Basic Experimental Studies on the Operation of Photoionization Detectors," *Fresenius J. Anal. Chem.*, vol. 361, pp. 29-33, 1998.

[115]   Ion Science, "Technical Overview, PID Explained," Stafford, TX, USA, Ion Science, Advanced Gas Sensing Technologies, Application Article 105, pp. 1-2.

[116]   TSI Inc., "Photo-Ionization Detection (PID) Technology," Shoreview, MN, USA, TSI Inc., Application Note TSI-147, Rev. B, pp. 1-3, 2013.

[117]   C. Jia, K. Cao, R. Valaulikar, X. Fu, and A. B. Sorin, "Variability of Total Volatile Organic Compounds (TVOC) in the Indoor Air of Retail Stores," *Int. J. Environ. Res. Public Health*, vol. 16, pp. 4622-4630, 2019, 10.3390/ijerph16234622.

[118]   M. Noguchi, A. Mizukoshi, Y. Yanagisawa, and A. Yamasaki, "Measurements of Volatile Organic Compounds in a Newly Built Daycare Center," *Int. J. Environ. Res. Public Health*, vol. 13, pp. 736-749, 2016, 10.3390/ijerph13070736.

[119]   D. Singh, A. Kumar, B. P. Singh, K. Anandam, M. Singh *et al.*, "Spatial and Temporal Variability of VOCs and its Source Estimation During Rush/Non-Rush Hours in Ambient Air of Delhi, India," *Air Qual. Atmos. Health*, vol. 9, pp. 483-493, 2016, 10.1007/s11869-015-0354-3.

[120]   A. B. Stefaniak, P. N. Breysse, M. P. M. Murray, B. C. Rooney, and J. Schaefer, "An Evaluation of Employee Exposure to Volatile Organic Compounds in Three

Photocopy Centers," *Environ. Res. Sec. A*, vol. 83, pp. 162-173, 2000, 10.1006/enrs.2000.4061.

[121] C. Perrino, D. Ramirez, and I Allegrini, "Monitoring Acidic Air Pollutants Near Rome by Means of Diffusion Lines: Development of a Specific Quality Control Procedure," *Atmos. Environ.*, vol. 35, pp. 331-341, 2001.

[122] M. A. S. Garcia, R. J. Timmis, N. Van Dijk, J. D. Whyatt, I. D. Leith *et al.*, "Directional Passive Ambient Air Monitoring of Ammonia for Fuguitive Source Attribution; A Field Trial with Wind Tunnel Characteristics," *Atmos. Environ.*, vol. 167, pp. 576-585, 2017, 10.1016/j.atmosenv.2017.07.043.

[123] S. N. Behera, M. Sharma, V. P. Aneja, and R. Balasubramanian, "Ammonia in the Atmosphere: A Review on Emission Sources, Atmospheric Chemistry and Deposition on Terrestrial Bodies," *Environ. Sci. Pollut. Res.*, vol. 20, pp. 8092-8131, 2013, 10.1007/s11356-013-2051-9.

[124] NIOSH, *NIOSH Manual of Analytical Methods (NMAM), Fourth Edition*. Washington D.C., USA. Ammonia, Method 6015. 1994.

[125] NIOSH, *NIOSH Manual of Analytical Methods (NMAM), Fourth Edition*. Washington D.C., USA. Ammonia, Method 6016. 1996.

[126] A. Dey, "Semiconductor Metal Oxide Gas Sensors: A Review," *Mat. Sci. Eng. B.*, vol. 229, pp. 206-217, 2018, 10.1016/j.mseb.2017.12.036.

[127] G. Korotcenkov, V. Brinzari, and B. K. Cho, "In2O3- and SnO2-Based Thin Film Ozone Sensors: Fundamentals," *J. Sensors*, vol. 2016, pp. 1-31, 2016, 10.1155/2016/3816094.

[128] Figaro, "Operating Principle: MOS Type," 2018. [Online] Available: https://www.figarosensor.com/technicalinfo/principle/mos-type.html, Accessed On: September 2, 2020.

[129] N. Barsan, M. Schweizer-Berberich, and W. Gopel, "Fundamental and Practical Aspects in the Design of Nanoscaled SnO2 Gas Sensors: A Status Report," *Fresnius J. Anal. Chem.*, vol. 365, pp. 287-304, 1999.

[130] N. Barsan and U. Weimar, "Conduction Model of Metal Oxide Gas Sensors," *J. Electroceramics*, vol. 7, pp. 143-167, 2001.

[131] N. Barsan and U. Weimar, "Understanding the Fundamental Principles of Metal Oxide Based Gas Sensors; The Example of CO Sensing with SnO2 Sensors in the Presence of Humidity," *J. Phys. Condens. Matter*, vol. 15, pp. RR813-RR839, 2003.

[132] M. Batzill and U. Diebold, "The Surface and Materials Science of Tin Oxide," *Prog. Surf. Sci.*, vol. 79, pp. 47-154, 2005.

[133] G. Korotcenkov and B. K. Cho, "Instability of Metal Oxide-Based Conductometric Gas Sensors and Approaches to Stability Improvement (Short Survey)," *Sens. Actuators B. Chem.*, vol. 156, pp. 527-538, 2011, 10.1016/j.snb.2011.02.024.

[134] E. Lackner, J. Krainer, R. Wimmer-Teubenbacher, F. Sosada, C. Gspan *et al.*, "CMOS Integrated Nanocrystalline SnO2 Gas Sensors for CO Detection," *Procedia Eng.*, vol. 168, pp. 297-300, 2016, 10.1016/j.proeng.2016.11.200.

[135] I. Elmi, S. Zampolli, E. Cozzani, F. Mancarella, and G. C. Cardinali, "Development of Ultra-Low-Power Consumption MOX Sensors with ppb-Level VOC Detection Capabilities for Emerging Applications," *Sens. Actuators B. Chem.*, vol. 135, pp. 342-351, 2008, 10.1016/j.snb.2008.09.002.

[136] H. Liu, L. Zhang, K. H. H. Li, and O. K. Tan, "Microhotplates for Metal Oxide Semiconductor Gas Sensor Applications – Towards the CMOS-MEMS Monolithic Approach," *Micromachines*, vol. 9, pp. 557-580, 2018, 10.3390/mi9110557.

[137] J. Chou. Hazardous Gas Monitors: A Practical Guide to Selection, Operation and Applications. New York, NY, USA. McGraw-Hill. 1999. pp. 27-45.

[138] L. Boon-Brett, J. Bousek, and P. Moretto, "Reliability of Commercially Available Hydrogen Sensors for Detection of Hydrogen at Critical Concentrations: Part II – Selected Sensor Test Results," *Int. J. Hydrog. Energy*, vol. 34, pp. 562-571, 2009, 10.1016/j.ijhydene.2008.10.033.

[139] J. Riegel and K. H. Hardtl, "Analysis of Combustible Gases in Air with Calorimetric Gas Sensors Based on Semiconducting BaTiO3 Ceramics," *Sens. Actuators B. Chem.*, vol. B1, pp. 54-57, 1990.

[140] Figaro, "Operating Principle: Catalytic Type," 2018. [Online] Available: https://www.figarosensor.com/technicalinfo/principle/catalytic-type.html, Accessed On: September 2, 2020.

[141] Y. Nemirovsky, S. Stolyarova, T. Blank, S. Bar-Lev, A. Svetlitza *et al.*, "A New Pellistor-Like Gas Sensor Based on Micromachined CMOS Transistor," *IEEE Trans. Electron Devices*, vol. 65, no. 12, pp. 5494-5498, 2018, 10.1109/TED.2018.2878015.

[142] Figaro, "Operating Principle: Electrochemical Type," 2018. [Online] Available: https://www.figarosensor.com/technicalinfo/principle/electrochemical-type.html, Accessed On: September 2, 2020.

[143] R. Baron and J. Saffell, "Amperometric Gas Sensors as a Low Cost Emerging Technology Platform for Air Quality Monitoring Applications: A Review," *ACS Sens.*, vol. 2, pp. 1553-1566, 2017, 10.1021/acssensors.7b00620.

[144] Alphasense, "How Electrochemical Gas Sensors Work," Essex, UK, Alphasense Ltd., Alphasense Application Note AAN 104, Issue 12, pp. 1-4.

[145] M. L. Hitchman, N. J. Cade, T. K. Gibbs, and N. J. M. Hedley, "Study of the Factors Affecting Mass Transport in Electrochemical Gas Sensors," *Analyst*, vol. 122, pp. 1411-1417, 1997.

[146] Alphasense, "Humidity Extremes: Drying Out and Water Absorption," Essex, UK, Alphasense Ltd., Alphasense Application Note AAN 106, Issue 12, pp. 1-7.

[147] Alphasense, "Environmental Changes: Temperature, Pressure, Humidity," Essex, UK, Alphasense Ltd., Alphasense Application Note AAN 110, Issue 12, pp. 1-6.

[148] O. A. M. Popoola, G. B. Stewart, M. I. Mead, and R. L. Jones, "Development of a Baseline-Temperature Correction Methodology for Electrochemical Sensors and its Implications for Long-Term Stability," *Atmos. Environ.*, vol. 147, pp. 330-343, 2016, 10.1016/j.atmosenv.2016.10.024.

[149] M. Raninec, "Overcoming the Technical Challenges of Electrochemical Gas Sensing," Norwood, MA, USA, Analog Devices, Technical Article, pp. 1-5, 2019.

[150] N. Masson, R. Piedrahita, and M. Hannigan, "Quantification Method for Electrolytic Sensors in Long-Term Monitoring of Ambient Air Quality," *Sensors*, vol. 15, pp. 27283-27302, 2015, 10.3390/s151027283.

[151] M. I. Mead, O. A. M. Popoola, G. B. Stewart, P. Landshoff, and M. Calleja, "The Use of Electrochemical Sensors for Monitoring Urban Air Quality in Low-Cost, High-Density Networks," *Atmos. Environ.*, vol. 70, pp. 186-203, 2013, 10.1016/j.atmosenv.2012.11.060.

[152] Drager. Drager-Tubes & CMS-Handbook: Soil, Water, and Air Investigations as well as Technical Gas Analysis, 18th Edition. Lubeck, Germany. Drager Safety AG & Co KGaA. 2015. pp. 1-456.

[153] RAE Systems Inc. *Gas Detection Tubes and Sampling Handbook, Second Edition*. San Jose, CA, USA. RAE Systems Inc. 2013. pp. 1-133.

[154] DHS, "Portable Colorimetric Tubes for Chemical Vapor Detection Market Survey Report," Las Vegas, NV, USA, National Security Technologies, LLC. System Assessment and Validation for Emergency Responders (SAVER), pp. 1-14, 2014.

[155] Honeywell International. *Gas Detection Tubes and Sampling Handbook*. San Jose, CA, USA. Honeywell International. 2014. pp. 1-120.

[156] RAE Systems Inc., "Accuracy Comparisons of RAE Systems Gas Detection Tubes," San Jose, CA, USA, RAE Systems Inc., Technical Note TN-143, 01/05/WH, pp. 1-2.

[157] D. E. Williams, "Low Cost Sensor Networks: How Do We Know the Data Are Reliable?," *ACS Sens.*, vol. 4, pp. 2558-2565, 2019, 10.1021/acssensors.9b01455.

[158] E. G. Snyder, T. H. Watkins, P. A. Solomon, E. D. Thoma, R. W. Williams *et al.*, "The Changing Paradigm of Air Pollution Monitoring," *Environ. Sci. Technol.*, vol. 47, pp. 11369-11377, 2013, 10.1021/es4022602.

[159] S. Reis, E. Seto, A. Northcross, N. W. T. Quinn, M. Convertino *et al.*, "Integrating Modelling and Smart Sensors for Environmental and Human Health," *Environ. Model Softw.*, vol. 74, pp. 238-246, 2015, 10.1016/j.envsoft.2015.06.003.

[160] WHO, "Global Health Observatory (GHO) data Urban Population Growth", 2014. [Online] Available: https://www.who.int/gho/urban_health/situation_trends/urban_population_growth_text/en/, Accessed on: Feb. 11, 2019.

[161] J. M. Baldasano, E. Valera, and P. Jimenez, "Air quality data from large cities," *Sci. Total Environ.*, vol. 307, pp. 141-165, 2003, 10.1016/s0048-9697(02)00537-5.

[162] WHO, "Health risks of air pollution in Europe – HRAPIE project. Recommendations for concentration-response functions for cost-benefit analysis of particulate matter, ozone and nitrogen dioxide." WHO Regional Office for Europe. Copenhagen, Denmark. 2013. [Online] Available: http://www.who.int/iris/handle/10665/153692, Accessed on: Feb. 11, 2019.

[163] WHO, Evolution of WHO air quality guidelines: past, present and future. Copenhagen, Denmark: WHO Regional Office for Europe, 2017. [Online] Available: http://www.euro.who.int/en/health-topics/environment-and-health/air-quality/publications/2017/evolution-of-who-air-quality-guidelines-past,-present-and-future-2017

[164] S. S. Lim *et al.*, "A comparative risk assessment of burden of disease and injury attributable to 67 risk factors and risk factor clusters in 21 regions, 1990-2010: A systematic analysis for the Global Burden of Disease Study 2010," *Lancet*, vol. 380, pp. 2224-2260, Dec. 2012, 10.1016/s0140-6736(12)61766-8.

[165] B. Brunekreef, S. T. Holgate, "Air pollution and health," *Lancet*, vol. 360, pp. 1233-1242, Oct. 2002, 10.1016/s0140-6736(02)11274-8.

[166] J. Schwartz, "Air pollution and children's health," *Pediatrics*, vol. 113, no. 4, pp. 1037-1043, Apr. 2004, 1073-0397.

[167] M. Guarnieri, J. R. Balmes, "Outdoor air pollution and asthma," *Lancet*, vol. 383, pp. 1581-1592, May 2014, 10.1016/s0140-6736(14)60617-6.

[168] A. Barraza-Villarreal et al., "Air pollution, airway inflammation, and lung function in a cohort study of Mexico City schoolchildren," *Environ. Health Perspect.*, vol. 116, no. 6, pp. 832-838, June 2008, 10.1289/ehp.10926.

[169] K. M. Mortimer, L. M. Neas, D. W. Dockery, S. Redline, and I. B. Tager, "The effect of air pollution on inner-city children with asthma," *Eur. Respir. J.*, vol. 19, pp. 699-705, 2002, 10.1183/09031936.02.00247102.

[170] D. Briggs, "The role of GIS: Coping with space (and time) in air pollution exposure assessment", *J. Toxicol. Environ. Health A*, vol. 68, pp. 1243-1261, 2005, 10.1080/15287390590936094.

[171] C. Monn, "Exposure assessment of air pollutants: a review on spatial heterogeneity and indoor/outdoor/personal exposure to suspended particulate matter, nitrogen dioxide and ozone," *Atmos. Environ.*, vol. 35, pp. 1-32, 2001, 10.1016/S1352-2310(00)00330-7.

[172] P. L. Jenkins, T. J. Phillips, E. J. Mulberg, and S. P. Hui, "Activity patterns of Californians: Use of and proximity to indoor pollutant sources," *Atmos. Environ. Part A*, vol. 26, no. 12, pp. 2141-2148, Aug. 1992, 10.1016/0960-1686(92)90402-7.

[173] N. E. Klepeis, W. C. Nelson, W. R. Ott, J. P. Robinson, A. M. Tsang, P. Switzer, J. V. Behar, S. C. Hern, and W. H. Engelmann, "The national human activity pattern survey (NHAPS): A resource for assessing exposure to environmental pollutants," *J. Expo. Anal. Environ. Epidemiol.*, vol. 11, no. 3, pp. 231-252, 2001, 10.1038/sj.jea.7500165.

[174] EPA, "The inside story: A guide to indoor air quality," U.S. EPA/Office of Air and Radiation. Research Triangle Park, NC, USA. Nov. 27, 2018. [Online] Available: https://www.epa.gov/indoor-air-quality-iaq/inside-story-guide-indoor-air-quality, Accessed on: Feb. 11, 2019.

[175] R. Piedrahita *et al.*, "The next generation of low-cost personal air quality sensors for quantitative exposure monitoring," *Atmos. Meas. Tech.*, vol. 7, no. 10, pp. 3325-3336, 2014, 10.5194/amt-7-3325-2014.

[176] P. J. D. Peterson, A. Aujla, K. H. Grant, A. G. Brundle, M. R. Thompson, J. V. Hey, and R. J. Leigh, "Practical use of metal oxide semiconductor gas sensors for measuring nitrogen dioxide and ozone in urban environments," *Sensors*, vol. 17, no. 7, pp. 1653-677, July 2017, 10.3390/s17071653.

[177] T. Cao, J. E. Thompson, "Personal monitoring of ozone exposure: A fully portable device for under $150 USD cost," *Sens. Actuators B Chem.*, vol. 224, pp. 936-943, Mar. 2016, 10.1016/j.snb.2015.10.090.

[178] J. Dieffenderfer *et al.*, "Low-power wearable systems for continuous monitoring of environment and health for chronic respiratory disease," *J. Biomed. Health Inform.*, vol. 20, no. 5, pp. 1251-1264, Sept. 2016, 10.1109/JBHI.2016.2573286.

[179] J. Dieffenderfer *et al.*, "Wearable wireless sensors for chronic respiratory disease monitoring," in *2015 IEEE 12th Int. Conf. on Wearable and Implant*. BSN, Cambridge, MA, USA, 2015, pp. 1-6.

[180] R. McConnell, K. Berhane, F. Gilliand, S. J. London, T. Islam, W. J. Gauderman, E. Avol, H. G. Margolis, and J. M. Peters, "Asthma in exercising children exposed to ozone: a cohort study," *Lancet*, vol. 359, pp. 386-391, Feb. 2002, 10.1016/s0140-6736(02)07597-9.

[181] J. Schwartz, "Air pollution and hospital admissions for respiratory disease," *Epidemiology*, vol. 7, no. 1, pp. 20-28, Jan. 1996, 1044-3983.

[182] EPA: National Ambient Air Quality Standards for Ozone, Fed. Reg. Vol. 80, No. 206 (final rule Oct. 26, 2015) (to be codified at 40 C.F.R. pts. 50, 51, 52, 53, and 58).

[183] EPA, "Integrated Science Assessment for Ozone and Related Photochemical Oxidants," U.S. EPA/National Center for Environmental Assessment-RTP Division, Office of Research and Development. Research Triangle Park, NC, USA. Feb. 2013. [Online] Available: https://www.epa.gov/isa/integrated-science-assessment-isa-ozone-and-related-photochemical-oxidants, Accessed on: Apr. 4, 2019.

[184] L. Spinelle, M. Gerboles, M. Aleixandre, and F. Bonavitacola, "Evaluation of metal oxide sensors for the monitoring of O3 in ambient air at ppb level," *Chem. Engineer Trans.*, vol. 54, pp. 319-324, 2016, 10.3303/CET1654054.

[185] D. E. Williams *et al.*, "Modelling the response of a tungsten oxide semiconductor as a gas sensor for the measurement of ozone," *Meas. Sci. Technol.*, vol. 13, no. 6, pp. 923-931, 2002, 10.1088/0957-0233/13/6/314.

[186] D. E. Williams, S. R. Aliwell, K. F. E. Pratt, D. J. Caruana, R. L. Jones, R. A. Cox, G. M. Hansford, and J. Halsall, "Development of low-cost ozone and nitrogen dioxide measurement instruments suitable for use in an air quality monitoring network," in *2009 IEEE Sensors*, Christchurch, Cantebury, New Zealand, 2009, pp. 1099-1104.

[187] S. Brienza, A. Galli, G. Anastasi, and P. Bruschi, "A low-cost sensing system for cooperative air quality monitoring in urban areas," *Sensors*, vol. 15, no. 6, pp. 12242-12259, May 2015, 10.3390/s150612242.

[188] SGX Sensortech. Datasheet MiCS-2614 Ozone Sensor. SGX Sensortech. Corcelles-Cormondreche, Switzerland, Ver. 1087 rev. 5.

[189] M. D. Bortoli, S. Kephalopoulos, S. Kirchner, H. Schauenburg, and H. Vissers, "Indoor air quality & its impact on man. European inter-laboratory comparison on VOC emitted from building materials and products," European Commission, European Collaborative Action, Luxembourg, Report no. 21, EUR 18698 EN, 1999.

[190] EPA, "Volatile organic compounds' impact on indoor air quality," U.S. EPA/Office of Air and Radiation. Research Triangle Park, NC, USA. Nov. 6, 2017. [Online] Available: https://www.epa.gov/indoor-air-quality-iaq/volatile-organic-compounds-impact-indoor-air-quality, Accessed on: Feb. 11, 2019.

[191] I. T. Berrios, J. S. Zhang, B. Guo, J. Smith, and Z. Zhang, "Volatile organic compounds (VOCs) emissions from sources in a partitioned office environment and their impact on IAQ," in *Proc. Indoor Air 2005*, Beijing, China, 2005, pp. 2064-2069.

[192] C. P. Weisel, "Assessing Exposure to Air Toxics Relative to Asthma," *Environ. Health Perspect.*, vol. 110, no. 4, pp. 527-537, Aug. 2012, 10.1289/ehp.02110s4527.

[193] U. B. Nurmatov, N. Tagiyeva, S. Semple, G. Devereux, and A. Sheikh, "Volatile organic compounds and risk of asthma and allergy: a systematic review," *Eur. Respir. Rev.*, vol. 24, pp. 92-101, Mar. 2015, 10.1183/09059180.00000714.

[194] European Collaborative Action, "Indoor Air Quality & its Impact on Man, Report No. 19, Total Volatile Organic Compounds (TVOC) in Indoor Air Quality Investigations," European Commission, Joint Research Centre, Brussels, Belgium, EUR 17676 EN, 1997.

[195] C. Jaen and P. Dalton, "Asthma and odors: The role of risk perception in asthma exacerbation," *J. Psychosom. Res.*, vol. 77, no. 4, pp. 302-308, 2014, 10.1016/j.jpsychores.2014.07.002.

[196] A. C. Romain, P. Andre, and J. Nicolas, "Three years experiment with the same tin oxide sensor arrays for the identification of malodorous sources in the environment," *Sens. Actuators B Chem.*, vol. 84, pp. 271-277, May 2002, 10.1016/S0925-4005(02)00036-9.

[197] S. Herberger and H. Ulmer, "Indoor air quality monitoring improving air quality perception," *Clean-Soil Air Water*, Vol. 40, pp. 578-585, June 2012, 10.1002/clen.201000286.

[198] D. Ruffer, F. Hoehne, and J. Buhler, "New digital metal-oxide (MOx) sensor platform," *Sensors*, vol. 18, no. 4, pp. 1052-1063, Mar. 2018, 10.3390/s18041052.

[199] Sensirion. Datasheet SGPC3 Sensirion Gas Platform. Sensirion. Staefa, Switzerland, Ver. 0.91, Feb. 2018. [Online] Available: http://www.sensirion.com, Accessed on: Feb. 11, 2019.

[200] Asthma and Allergy Foundation of America, "Weather can trigger asthma," 2017. [Online] Available: https://www.aafa.org/weather-triggers-asthma/, Accessed on: Feb. 11, 2019.

[201] D. Hayes, P. B. Collins, M. Khosravi, R. L. Lin, and L. Y. Lee, "Bronchoconstriction triggered by breathing hot humid air in patients with asthma," *Am. J. Respir. Crit. Care Med.*, vol. 185, no. 11, pp. 1190-1196, June 2012, 10.1164/rccm.201201-0088OC.

[202] S. D. Anderson and E. Daviskas, "The mechanism of exercise-induced asthma is…," *J. Allergy Clin. Immunol.*, vol. 106, no. 3, pp. 453-459, 10.1067/mai.2000.109822.

[203] D. Hughes, "Childhood asthma and exercise," *Paediatr. Child Health*, vol. 19, no. 9, pp. 467-468, Nov. 2014, 1205-7088.

[204] C. A. Howe, K. A. Clevenger, R. E. Leslie, and M. A. Ragan, "Comparison of accelerometer-based cut-points for children's physical activity: Counts vs. steps," *Children*, vol. 5, no. 8, pp. 105-115, Aug. 2018, 10.3390/children5080105.

[205] E. Baque, L. Sakzewski, S. G. Trost, R. N. Boyd, and L. Barber, "Validity of accelerometry to measure physical activity intensity in children with an acquired brain injury," *Pediatr. Phys. Ther.*, vol. 29, no. 4, pp. 322-329, 2017, 10.1097/PEP.0000000000000439.

[206] G. Eranna, B. C. Joshi, D. P. Runthala, and R. P. Gupta, "Oxide materials for development of integrated gas sensors – A comprehensive review," *Crit. Rev. Solid State*, vol. 29, no. 3-4, pp. 111-188, Aug. 2010, 10.1080/10408430490888977.

[207] C. Wang, L. Yin, L. Zhang, D. Xiang, and R. Gao, "Metal oxide gas sensors: Sensitivity and influencing factors," *Sensors*, vol. 10, no. 3, pp. 2088-2106, Mar. 2010, 10.3390/s100302088.

[208] M. Benammar and W. C. Maskell, "Temperature control of thick-film printed heaters," *J. Phys. E: Sci. Instrum.*, vol. 22, no. 11, pp. 933-936, 1989, 10.1088/0022-3735/22/11/006.

[209] J. W. Gong, Q. F. Chen, M. R. Lian, N. C. Liu, and C. Daoust, "Temperature feedback control for improving the stability of a semiconductor-metal-oxide (SMO) gas sensor," *IEEE Sens. J.*, vol. 6, no. 1, pp. 139-145, Feb. 2006, 10.1109/jsen.2005.844353.

[210] G. Golan, A. Axelevitch, B. Sigalov, and B. Gorenstein, "Integrated thin film heater-thermocouple systems," *Microelectron. Reliab.*, vol. 43, no. 3, pp. 509-512, 2003, 10.1016/s0026-2714(02)00320-7.

[211] I. Simon, N. Barsan, M. Bauer, and U. Weimar, "Micromachined metal oxide gas sensors: Opportunities to improve sensor performance," *Sens. Actuators B Chem.*, vol. 73, no. 1, pp. 1-26, 2001, 10.1016/S0925-4005(00)00639-0.

[212] P. Parker, G. G. Vining, S. R. Wilson, J. L. Szarka III, and N. G. Johnson, "The prediction properties of classical and inverse regression for the simple linear calibration problem," *J. Qual. Technol.*, vol. 42, no. 4, pp. 332-347, Oct. 2010, 0022-4065.

[213] Z. Nenova and G. Dimchev, "Compensation of the impact of disturbing factors on gas sensor characteristics," *Acta Polytech. Hung.*, vol. 10, no. 3, pp. 97-111, 2013.

[214] R. Huerta, T. Mosqueiro, J. Fonollosa, N. F. Rulkov, and I. Rodriguez-Lujan, "Online decorrelation of humidity and temperature in chemical sensors for continuous monitoring," *Chemometr. Intell. Lab. Syst.*, vol. 157, pp. 169-176, Oct. 2016, 10.1016/j.chemolab.2016.07.004.

[215] N. Barsan and A. Tomescu, "Calibration procedure for SnO2-based gas sensors," *Thin Solid Films*, vol. 259, no. 1, pp. 91-95, Apr. 1995, 10.1016/0040-6090(94)06415-6.

[216] R. Ionescu, A. Vancu, and A. Tomescu, "Time-dependent humidity calibration for drift corrections in electronic noses equipped with SnO2 gas sensors," *Sens. Actuators B Chem.*, vol. 69, no. 3, pp. 283-286, 2000, 10.1016/S0925-4005(00)00508-6.

[217] C. Krutzler, A. Unger, H. Marhold, T. Fricke, T. Conrad, and A. Schutze, "Influence of MOS gas-sensor production tolerances on pattern recognition techniques in electronic noses," *IEEE Trans. Instrum. Meas.*, vol. 61, no. 1, pp. 276-283, Jan. 2012, 10.1109/tim.2011.2161015.

[218] N. Zimmerman, A. A. Presto, S. P. N. Kumar, J. Gu, A. Hauryliuk, E. S. Robinson, A. L. Robinson, and R. Subramanian, "A machine learning calibration model using random forests to improve sensor performance for lower-cost air quality monitoring," *Atmos. Meas. Tech.*, vol. 11, no. 1, pp. 291-313, Jan. 2018, 10.5194/amt-11-291-2018.

[219] L. Spinelle, M. Gerboles, M. G. Villani, M. Aleixandre, and F. Bonavitacola, "Field calibration of a cluster of low-cost commercially available sensor for air quality monitoring. Part B: NO, CO and CO2," *Sens. Actuators B Chem.*, vol. 238, pp. 706-715, Jan. 2017, 10.1016/j.snb.2016.07.036.

[220] A. C. Lewis et al., "Evaluating the performance of low cost chemical sensors for air pollution research," *Faraday Discuss.*, vol. 189, pp. 85-103, 2016, 10.1039/c5fd00201j.

[221] A. C. Romain and J. Nicolas, "Long term stability of metal oxide-based gas sensors for e-nose environmental applications: An overview," *Sens. Actuators B Chem.*, vol. 146, no. 2, pp. 502-506, Apr. 2010, 10.1016/j.snb.2009.12.027.

[222] S. Capone, M. Epifani, L. Francioso, S. Kaciulis, A. Mezzi, P. Siciliano, and A. Taurino, "Influence of electrodes ageing on the properties of the gas sensors based on SnO2," *Sens. Actuators B Chem.*, vol. 115, no. 1, pp. 396-402, May 2006, 10.1016/j.snb.2005.10.001.

[223] H. Esch, G. Huyberechts, R. Mertens, G. Maes, J. Manca, W. D. Ceuninck, and L. D. Schepper, "The stability of Pt heater and temperature sensing elements for silicon integrated tin oxide gas sensors," *Sens. Actuators B Chem.*, vol. 65, no. 1, pp. 190-192, June 2000, 10.1016/S0925-4005(99)00301-9.

[224] A. Tricoli, "Structural stability and performance of noble metal-free SnO2-based gas sensors," *Biosensors (Basel)*, vol. 2, no. 2, pp. 221-233, May 2012, 10.3390/bios2020221.

[225] K. R. Mallires, D. Wang, V. V. Tipparaju, and N. Tao, "Developing a Low-Cost Wearable Personal Exposure Monitor for Studying Respiratory Diseases Using Metal-Oxide Sensors," *IEEE Sens. J.*, vol. 19, pp. 8252-8261, 2019, 10.1109/JSEN.2019.2917435.

[226] K. Schmitt, K. R. Tarantik, C. Pannek, and J. Wollenstein, "Colorimetric Materials for Fire Gas Detection – A Review," *Chemosensors*, vol. 6, pp. 1-15, 2018, 10.3390/chemosensors6020014.

[227] H. Lin and K. S. Suslick, "A Colorimetric Sensor Array for Detection of Triacetone Triperoxide Vapor," *J. Am. Chem. Soc.*, vol. 132, pp. 15519-15521, 2010, 10.1021/ja107419t.

[228] M. K. Nakhleh, H. Amal, R. Jeries, Y. Y. Broza, M. Aboud, A. Gharra, H. Ivgi, S. Khatib, S. Badarneh, L. Har-Shai *et al.*, "Diagnosis and Classification of 17 Diseases from 1404 Subjects via Pattern Analysis of Exhaled Molecules," *ACS Nano*, vol. 11, pp. 112-125, 2017, 10.1021/acsnano.6b04930.

[229] H. Zhao, L. Liu, X. Lin, J. Dai, S. Liu, T. Fei, and T. Zhang, "Proton-Conductive Gas Sensor: A New Way to Realize Highly Selective Ammonia Detection for Analysis of Exhaled Human Breath," *ACS Sens.*, vol. 5, pp. 346-352, 2020, 10.1021/acssensors.9b01763.

[230] Z. Li and K. S. Suslick, "Portable Optoelectronic Nose for Monitoring Meat Freshness," *ACS Sens.*, vol. 1, pp. 1330-1335, 2016, 10.1021/acssensors.6b00492.

[231] T. Konduru, G. C. Rains, and C. Li, "Detecting sour skin infected onions using a customized gas sensor array," *J. Food Eng.*, vol. 160, pp. 19-27, 2015, 10.1016/j.jfoodeng.2015.03.025.

[232] H. Nazemi, A. Joseph, J. Park, and A. Emadi, "Advanced Micro- and Nano-Gas Sensor Technology: A Review," *Sensors*, vol. 19, pp. 1-23, 2019, 10.3390/s19061285.

[233] P. Wei, Z. Ning, S. Ye, L. Sun, F. Yang, K. C. Wong, D. Westerdahl, and P. K. K. Louie, "Impact Analysis of Temperature and Humidity Conditions on Electrochemical Sensor Response in Ambient Air Quality Monitoring," *Sensors*, vol. 18, pp. 1-16, 2018, 10.3390/s18020059.

[234] P. D. Puiu. *Color Sensors and Their Applications. In Optical Nano- and Microsystems for Bioanalytics*. W. Fritzsche, J. Popp, Eds.; Springer Series on Chemical Sensors and Biosensors; Springer-Verlag: Heidelberg, 2012; Vol. 10, pp 4-17.

[235] G. Orellana, M. C. Moreno-Bondi, D. Garcia-Fresnadillo, and M. D. Marazuela. *The Interplay of Indicator, Support and Analyte in Optical Sensor Layers. In Frontiers in Chemical Sensors*. O. S. Wolfbeis, G. Orellana, M. C. Moreno-Bondi, Eds.; Springer Series on Chemical Sensors and Biosensors; Springer-Verlag: Heidelberg, 2005; Vol. 3, pp 189-225.

[236] Z. Li, J. R. Askim, and K. S. Suslick, "The Optoelectronic Nose: Colorimetric and Fluorometric Sensor Arrays," *Chem. Rev.*, vol. 119, pp. 231-292, 2019, 10.1021/acs.chemrev.8b00226.

[237] M. K. LaGasse, J. M. Rankin, J. R. Askim, and K. S. Suslick, "Colorimetric Sensor Arrays: Interplay of Geometry, Substrate and Immobilization," *Sens. Actuators, B*, vol. 197, pp. 116-122, 2014, 10.1016/j.snb.2014.01.102.

[238] X. Qin, R. Wang, F. Tsow, E. Forzani, X. Xian, and N. Tao, "A Colorimetric Chemical Sensing Platform for Real-Time Monitoring of Indoor Formaldehyde," *IEEE Sens. J.*, vol. 15, pp. 1545-1551, 2015, 10.1109/JSEN.2014.2364142.

[239] C. Lin, X. Xian, X. Qin, D. Wang, F. Tsow, E. Forzani, and N. Tao, "High Performance Colorimetric Carbon Monoxide Sensor for Continuous Personal Exposure Monitoring," *ACS Sens.*, vol. 3, pp. 327-333, 2018, 10.1021/acssensors.7b00722.

[240] R. Wang, A. Prabhakar, R. A. Iglesias, X. Xian, X. Shan, F. Tsow, E. S. Forzani, and N. Tao, "A Microfluidic-Colorimetric Sensor for Continuous Monitoring of Reactive Environmental Chemicals," *IEEE Sens. J.*, vol. 12, pp. 1529-1535, 2012, 10.1109/JSEN.2011.2174218.

[241] G. Zheng, "Chip-scale microscopy imaging," *J. Biophotonics*, vol. 5, pp. 639-649, 2012, 10.1002/jbio.201200043.

[242] A. Ozcan and E. McLeod, "Lensless Imaging and Sensing," *Annu. Rev. Biomed. Eng.*, vol. 18, pp. 77-102, 2016, 10.1146/annurev-bioeng-092515-010849.

[243] H. Takehara, K. Miyazawa, T. Noda, K. Sasagawa, T. Tokuda, S. H. Kim, R. Iino, H. Noji, and J. Ohta, "A CMOS image sensor with stacked photodiodes for lensless observation system of digital enzyme-linked immunosorbent assay," *Jpn. J. Appl. Phys.*, vol. 53, pp. 1-5, 2014, 10.7567/JJAP.53.04EL02.

[244] R. R. Singh, D. Ho, A. Nilchi, G. Gulak, P. Yau, and R. Genov, "A CMOS/Thin-Film Fluorescence Contact Imaging Microsystem for DNA Analysis," *IEEE Trans. Circuits Syst.*, vol. 57, pp. 1029-1038, 2010, 10.1109/TCSI.2010.2043990.

[245] D. S. Daivasagaya, L. Yao, K. Y. Yung, M. Hajj-Hassan, M. C. Cheung, V. P. Chodavarapu, and F. V. Bright, "Contact CMOS imaging of gaseous oxygen sensor array," *Sens. Actuators B Chem.*, vol. 157, pp. 408-416, 2011, 10.1016/j.snb.2011.04.074.

[246] H. Ji, D. Sander, A. Haas, and P. A. Abshire, "Contact Imaging: Simulation and Experiment," *IEEE Trans. Circuits Syst.*, vol. 54, pp. 1698-1710, 2007, 10.1109/TCSI.2007.902409.

[247] Omnivision, "OV5647 5-Megapixel Product Brief," Santa Clara, CA, USA; Version 1.2 November, 2010.

[248] P. Wiktor, A. Brunner, P. Kahn *et al.*, "Microreactor Array Device," *Sci. Rep.*, vol. 5, pp. 8736, 2015, 10.1038/srep08736.

[249] V. J. Nagaraj, S. Eaton, and P. Wiktor, "NanoProbeArrays for the Analysis of Ultra-Low-Volume Protein Samples Using Piezoelectric Liquid Dispensing Technology," *SLAS Technol.*, vol. 16, no. 2, pp. 126-133, 2011, 10.1016/j.jala.2010.07.005.

[250] Tetraethylene Glycol; MSDS No. 110175; Sigma-Aldrich: St. Louis, MO, Jan 15, 2020.

[251] M. O. Byrd and C. J. Ohrenberg, "The Use of Ammonia as a Qualitative Test for Determining When Solid Copper Has Completely Precipitated from Aqueous Solutions Containing Copper(II) Ions," *Ga. J. Sci.*, vol. 75, pp. 1-7, 2017.

[252] A. T. Baker, "The Ligand Field Spectra of Copper(II) Complexes," *J. Chem. Educ.*, vol. 75, pp. 98-99, 1998, 10.1021/ed075p98.

[253] B. Timmer, W. Olthuis, and A. V. D. Berg, "Ammonia sensors and their applications – a review," *Sens. Actuators B Chem.*, vol. 107, pp. 666-677, 2005, 10.1016/j.snb.2004.11.054.

[254] D. E. Gardner, D. Krewski, and E. C. Bishop, "Acute Exposure Guideline Levels for Selected Airborne Chemicals, vol. 6," National Academy Press: Washington, DC, 2008; pp 58-114.

[255] N. Y. Liu, P. Cay-Durgun, T. Lai, M. Sprowls, L. Thomas, M. L. Lind, and E. Forzani, "A Handheld, Colorimetric Optoelectronic Dynamics Analyzer for Measuring Total Ammonia of Biological Samples," *IEEE J. Transl. Eng. Health Med.*, vol. 6, pp. 1-10, 2018, 10.1109/JTEHM.2018.2840678.

[256] J. H. Bang, S. H. Lim, E. Park, and K. S. Suslick, "Chemically Responsive Nanoporous Pigments: Colorimetric Sensor Arrays and the Identification of Aliphatic Amines," *Langmuir*, vol. 24, pp. 13168-13172, 2008, 10.1021/la802029m.

[257] A. T. Hoang, Y. B. Cho, J. S. Park, Y. Yang, and Y. S. Kim, "Sensitive naked-eye detection of gaseous ammonia based on dye-impregnated nanoporous polyacrylonitrile mats," *Sens. Actuators B Chem.*, vol. 230, pp. 250-259, 2016, 10.1016/j.snb.2016.02.058.

[258] J. Courbat, D. Briand, J. Damon-Lacoste, J. Wollenstein, N. F. D. Rooij, "Evaluation of pH indicator-based colorimetric films for ammonia detection using optical waveguides," *Sens. Actuators B Chem.*, vol. 143, pp. 62-70, 2009, 10.1016/j.snb.2009.08.049.

[259] Y. Adiguzel and H. Kulah, "CMOS Cell Sensors for Point-of-Care Diagnostics," *Sensors*, vol. 12, pp. 10042-10066, 2012, 10.3390/s120810042.

[260] J. Ohta. *Smart CMOS Image Sensors and Applications*. New York, NY, USA. CRC Press, Taylor & Francis Group. 2008. pp. 1-58.

[261] M. El-Desouki, M. J. Deen, Q. Fang, L. Liu, F. Tse, and D. Armstrong, "CMOS Image Sensors for High Speed Applications," *Sensors*, vol. 9, pp. 430-444, 2009, 10.3390/s90100430.

[262] Y. Bulayev, Hamamatsu Corp., "Advances in CMOS Image Sensors Open Doors to Many Applications," 2015. [Online] Available: https://www.photonics.com/Articles/Advances_ in_CMOS_Image_Sensors_Open_Doors_to_Many/a57683, Accessed On: Sept. 5, 2020.

[263] A. J. P. Theuwissen, "CMOS Image Sensors: State-of-the-Art," *Solid State Electron.*, vol. 52, pp. 1401-1406, 2008, 10.1016/j.sse.2008.04.012.

[264]   Sony, "Sony IMX219PQH5-C Datasheet," rev. 7.0.0, pp. 1-96.

[265]   M. Imanbekova, A. S. Perumal, S. Kheireddine, D. V. Nicolau, and S. Wachsmann-Hogiu, "Lensless, Reflection-Based Dark-Field Microscopy (RDFM) on a CMOS Chip," *Biomed. Opt. Express*, vol. 11, pp. 4942-4959, 2020, 10.1364/BOE.394615.

[266]   D. A. Skoog and J. J. Leary. *Principles of Instrumental Analysis, Fourth Edition*. Saunders College Publishing: Orlando, FL, USA. 1992. pp 5-8.

[267]   J. P. Mehlig, "Colorimetric Determination of Copper with Ammonia A Spectrophotometric Study," *Ind. Eng. Chem. Anal. Ed.*, vol. 13, no. 8, pp. 533-535, 1941, 10.1021/i560096a006.

[268]   F. A. Cotton, G. Wilkinson, C. A. Murillo, and M. Bochmann. *Advanced Inorganic Chemistry, Sixth Edition*. John Wiley & Sons, Inc.: New York, NY, USA. 1999. pp 864-869.

[269]   S. Wintzheimer, M. Oppmann, M. Dold, C. Pannek, M. L. Bauers-feld, M. Henfling, S. Trupp, B. Schug, and K. Mandel, "Indicator Supraparticles for Smart Gasochromic Sensor Surfaces Reacting Ultrafast and Highly Sensitive," *Part. Part. Syst. Charact.*, vol. 36, pp. 1-7, 2019, 10.1002/ppsc.201900254.

[270]   K. Schmitt, K. Tarantik, C. Pannek, G. Sulz, and J. Wollenstein, "Colorimetric gas sensing with enhanced sensitivity," *Procedia Eng.*, vol. 168, pp. 1237-1240, 2016, 10.1016/j.proeng.2016.11.430.

[271]   F. Rigoni, S. Tognolini, P. Borghetti, G. Drera, S. Pagliara, A. Goldoni, and L. Sangaletti, "Environmental monitoring of low-ppb ammonia concentrations based on single-wall carbon nanotube chemiresistor gas sensors: detection limits, response dynamics, and moisture effects," *Procedia Eng.*, vol. 87, pp. 716-719, 2014, 10.1016/j.proeng.2014.11.638.

[272]   L. A. Panes-Ruiz, M. Shaygan, Y. Fu, Y. Liu, V. Khavrus, S. Oswald, T. Gemming, L. Baraban, V. Bezugly, and G. Cuniberti, "Toward Highly Sensitive and Energy Efficient Ammonia Gas Detection with Modified Single-Walled Carbon Nanotubes at Room Temperature," *ACS Sens.*, vol. 3, pp. 79-86, 2018, 10.1021/acssensors.7b00358.

[273]   A. D. Aguilar, E. S. Forzani, L. A. Nagahara, I. Amlani, R. Tsui, and N. J. Tao, "A Breath Ammonia Sensor Based on Conducting Polymer Nanojunctions," *IEEE Sens. J.*, vol. 8, pp. 269-273, 2008, 10.1109/JSEN.2007.913137.

[274]   R. D. Deegan, O. Bakajin, T. F. Dupont, G. Huber, S. R. Nagel, and T. A. Witten, "Capillary flow as the cause of ring stains from dried liquid drops," *Nature*, vol. 389, pp. 827-829, 1997, 10.1038/39827.

[275] L. Cui, J. Zhang, X. Zhang, L. Huang, Z. Wang, Y. Li, H. Gao, S. Zhu, T. Wang, and B. Yang, "Suppression of the Coffee Ring Effect by Hydrosoluble Polymer Additives," *ACS Appl. Mater. Interfaces*, vol. 4, pp. 2775-2780, 2012, 10.1021/am300423p.

[276] I. Helm, L. Jalukse, and I. Leito, "Measurement Uncertainty Estimation in Amperometric Sensors: A Tutorial Review," *Sensors*, vol. 10, pp. 4430-4455, 2010, 10.3390/s100504430.

[277] M. C. Janzen, J. B. Ponder, D. P. Bailey, C. K. Ingison, and K. S. Suslick, "Colorimetric Sensor Arrays for Volatile Organic Compounds," *Anal. Chem.*, vol. 78, pp. 3591-3600, 2006, 10.1021/ac052111s.

[278] L. Feng, C. J. Musto, and K. S. Suslick, "A Simple and Highly Sensitive Colorimetric Detection Method for Gaseous Formaldehyde," *J. Am. Chem. Soc.*, vol. 132, pp. 4046-4047, 2009, 10.1021/ja910366p.

[279] A. T. Hoang, Y. B. Cho, and Y. S. Kim, "A Strip of Colorimetric Sensors for Visualizing a Concentration Level of Gaseous Analytes with Basicity," *Sens. Actuator B Chem.*, vol. 251, pp. 1089-1095, 2017, 10.1016/j.snb.2017.06.142.

[280] S. H. Lim, L. Feng, J. W. Kemling, C. J. Musto, and K. S. Suslick, "An Optoelectronic Nose for Detection of Toxic Gases" *Nat. Chem.*, vol. 1, pp. 562-567, 2009, 10.1038/nchem.360.

[281] A. Prabhakar, R. A. Iglesias, R. Wang, F. Tsow, E. S. Forzani, and N. Tao, "Ultrasensitive Detection of Nitrogen Oxides over a Nanoporous Membrane," *Anal. Chem.*, vol. 82, pp. 9938-9940, 2010, 10.1021/ac101908g.

[282] C. Pannek, K. Schmitt, and J. Wollenstein, "Colorimetric Materials for Gas Selective Sensing in Low-Power Applications," *IEEE Transducers 2015, Anchorage, AK, USA*. M3P.037. pp. 1452-1455.

[283] E. Barrios, D. Fox, Y. Y. L. Sip, R. Catarata, and J. E. Calderon, "Nanomaterials in Advanced, High-Performance Aerogel Composites: A Review," *Polymers*, vol. 11, pp. 726-766, 2019, 10.3390/polym11040726.

[284] Z. Mazrouei-Sebdani, A. Khoddami, H. Hadadzadeh, and M. Zarrebini, "Synthesis and Performance Evaluation of the Aerogel-Filled PET Nanofiber Assemblies Prepared by Electro-Spinning," *RSC Adv.*, vol. 5, pp. 12830-12842, 2015, 10.1039/c4ra15297b.

[285] X. You, J. wu, and Y. Chi, "Superhydrophobic Silica Aerogels Encapsulated Fluorescent Perovskite Quantum Dots for Reversible Sensing of SO2 in a 3D-Printed Gas Cell," *Anal. Chem.*, vol. 91, pp. 5058-5066, 2019, 10.1021/acs.analchem.8b05253.

[286] J. E. Amonette and J. Matyas, "Functionalized Silica Aerogels for Gas-Phase Purification, Sensing, and Catalysis: A Review," *Micropor. Mesopor. Mat.*, vol. 250, pp. 100-119, 2017, 10.1016/j.micromeso.2017.04.055.

[287] S. Das, A. Dey, G. Reddy, and D. D. Sarma, "Suppression of the Coffee-Ring Effect and Evaporation-Driven Disorder to Order Transition in Colloidal Droplets," *J. Phys. Chem. Lett.*, vol. 8, pp. 4704-4709, 2017, 10.1021/acs.jpclett.7b01814.

[288] H. Hu and R. G. Larson, "Marangoni Effect Reverses Coffee-Ring Depositions," *J. Phys. Chem. B*, vol. 110, no. 14, pp. 7090-7094, 2006, 10.1021/jp0609232.

[289] D. Mampallil and H. B. Eral, "A Review on Suppression and Utilization of the Coffee-Ring Effect," *Adv. Colloid Interface Sci.*, vol. 252, pp. 38-54, 2018, 10.1016/j.cis.2017.12.008.

[290] X. Yu, R. Xing, Z. Peng, Y. Lin, Z, Du *et al.*, "To Inhibit Coffee Ring Effect in Inkjet Printing of Light-Emitting Polymer Films by Decreasing Capillary Force," *Chinese Chem. Lett.*, vol. 30, pp. 135-138, 2019, 10.1016/j.cclet.2018.09.007.

[291] P. J. Yunker, T. Still, M. A. Lohr, and A. G. Yodh, "Suppression of the Coffee-Ring Effect by Shape-Dependent Capillary Interactions," *Nature*, vol. 476, pp. 308-311, 2011, 10.1038/nature10344.

[292] M. Majumder, C. S. Rendall, J. A. Eukel, J. Y. L. Wang, N. Behabtu *et al.*, "Overcoming the 'Coffee-Stain' Effect by Compositional Marangoni-Flow-Assisted Drop-Drying," *J. Phys. Chem. B*, vol. 116, pp. 6536-6542, 2012, 10.1021/jp3009628.

[293] A. Osman, L. Goehring, H. Stitt, and N. Shokri, "Controlling the Drying-Induced Peeling of Colloidal Films," *Soft Matter*, July 2020, pp. 1-7, 10.1039/d0sm00252f.

[294] B. Yang, J. S. Sharp, and M. I. Smith, "The Interplay of Crack Hopping, Delamination and Interface Failure in Drying Nanoparticle Films," *Sci. Rep.*, vol. 6, no. 32296, pp. 1-9, 2016, 10.1038/srep32296.

[295] D. W. Oxtoby, H. P. Gillis, and A. Campion, *Principles of Modern Chemistry, Seventh Edition*. Pacific Grove, CA. Brooks/Cole. 2012.

[296] WHO, "WHO Coronavirus Disease (COVID-19) Dashboard," World Health Organization 2020.

[297] K. Mizumoto, K. Kagaya, A. Zarebski, and G. Chowell, "Estimating the Asymptomatic Proportion of Coronavirus Disease 2019 (COVID-19) Cases on Board the Diamond Princess Cruise Ship, Yokohama, Japan," *Euro Surveill*, vol. 25, 2020, 10.2807/1560-7917.ES.2020.25.10.2000180.

[298] P. Lines, "Grand Princess Updates", 2020. [Online] Available: https://www.princess.com/news/notices_and_advisories/notices/grand-princess-updates.html Accessed on: September 15, 2020.

[299] J. L. Santarpia, D. N. Rivera, V. Herrera, M. J. Morwitzer, H. Creager *et al.*, "Aerosol and Surface Transmission Potential of SARS-CoV-2," *medRxiv*, 2020, 10.1101/2020.03.23.20039446.

[300] Y. Li, G. M. Leung, J. W. Tang, X. Yang, C. Y. H. Chao *et al.*, "Role of Ventilation in Airborne Transmission of Infectious Agents in the Built Environments – a Multidisciplinary Systematic Review," *Indoor Air*, vol. 17, pp. 2-18, 2007.

[301] Y. Liu, Z. Ning, Y. Chen, M. Guo, Y. L. Liu *et al.*, "Aerodynamic Analysis of SARS-CoV-2 in two Wuhan Hospitals," *Nature*, 2020.

[302] Z. Tufekci, "We Need to Talk About Ventilation. How is it That Six Months Into a Respiratory Pandemic, we are Still Doing so Little to Mitigate Airborne Transmission?," *The Atlantic*, July 30, 2020.

[303] T. Galbadage, B. M. Peterson, R. S. Gunasekera, "Does COVID-19 Spread Through Droplets Alone?," *Front Public Health*, April 24, 2020, 10.3389/fpubh.2020.00163.

[304] G. Correia, L. Rodrigues, M. Gameiro da Silva, and T. Goncalves, "Airborne Route and Bad Use of Ventilation Systems as Non-Negligible Factors in SARS-CoV-2 Transmission," *Med Hypotheses*, vol. 141, 2020, 10.1016/j.mehy.2020.109781.

[305] P. Baron, "Generation and Behavior of Airborne Particles," CDC, NIOSH. [Online] Available: https://www.cdc.gov/niosh/topics/aerosols/pdfs/aerosol_101.pdf Accessed on: August 15, 2020.

[306] V. A. Marple and B. A. Olson, "Sampling and Measurement Using Inertial, Gravitational, Centrifugal, and Thermal Techniques," in *Aerosol Measurement: Principles, Techniques, and Applications*. Wiley Online Library: Hoboken, NJ, USA, 2011:129.

[307] Z. Du, F. Tsow, D. Wang, and N. Tao, "A Miniaturized Particulate Matter Sensing Platform Based on CMOS Imager and Real-Time Image Processing," *IEEE Sens. J.*, vol. 18, pp. 7421-7428, 2018.

[308] I. A. Ysrafil, "Severe Acute Respiratory Syndrome Coronavirus 2 (SARS-CoV-2): An Overview of Viral Structure and Host Response," *Diabetes Metab. Syndr.*, vol. 14, pp. 407-412, 2020.

[309] P. D. Galgano and O. A. El Seoud, "Surface Active Ionic Liquids: Study of Micellar Properties of 1-(1-alkyl)-3-methylimidazolium chlorides and comparison with

structurally related surfactants," *J. Colloid Interface Sci.*, vol. 361, pp. 186-194, 2011.

[310]   S. Mondal, A. Banerjee, and B. Das, "Spectroscopic and Interfacial Investigation on the Interaction of Hemoglobin with Conventional and Ionic Liquid Surfactants," *J. Mol. Liq.*, vol. 301, 2020.

[311]   K. S. Egorova, E. G. Gordeev, and V. P. Ananikov, "Biological Activity of Ionic Liquids and Their Application in Pharmaceutics and Medicine," *Chem. Rev.*, vol. 117, pp. 7132-7189, 2017.

[312]   K. Matsubara and H. Katayama, "Development of a Portable Detection for Enteric Viruses from Ambient Air and its Application to a Wastewater Treatment Plant," *Pathogens*, vol. 8, 2019.

[313]   J. Shen, Y. Zhou, F. Fu, H. Xu, J. Lv *et al.*, "Immunochromatographic Assay for Quantitative and Sensitive Detection of Hepatitis B Virus Surface Antigen Using Highly Luminescent Quantum Dot-Beads," *Talanta*, vol. 142, pp. 145-149, 2015.

[314]   J. Saha, A. R. Datta, D. Dey, D. Bhattacharjee, and A. Hussain, "Role of Quantum Dot in Designing FRET Based Sensors," *Materials Today Proceedings*, vol. 5, pp. 2306-2313, 2018.

APPENDIX 1

SUPPLEMENTARY MATERIAL

S1. Calibration Design Points

Temperature (°C)	Relative Humidity (%)	Absolute Humidity (g/m³)	Ozone (mole/m³)	Ozone (g/m³)	Ozone (ppbv)
15	20	2.56	0.00E+00	0.00E+00	0.0
15	20	2.56	1.15E-06	5.52E-05	27.2
15	20	2.56	2.30E-06	1.10E-04	54.3
15	20	2.56	3.45E-06	1.65E-04	81.5
15	40	5.13	3.45E-06	1.65E-04	81.5
15	40	5.13	2.30E-06	1.10E-04	54.3
15	40	5.13	1.15E-06	5.52E-05	27.2
15	40	5.13	0.00E+00	0.00E+00	0.0
15	60	7.69	0.00E+00	0.00E+00	0.0
15	60	7.69	1.15E-06	5.52E-05	27.2
15	60	7.69	2.30E-06	1.10E-04	54.3
15	60	7.69	3.45E-06	1.65E-04	81.5
15	80	10.26	3.45E-06	1.65E-04	81.5
15	80	10.26	2.30E-06	1.10E-04	54.3
15	80	10.26	1.15E-06	5.52E-05	27.2
15	80	10.26	0.00E+00	0.00E+00	0.0
30	8.5	2.58	0.00E+00	0.00E+00	0.0
30	8.5	2.58	1.15E-06	5.52E-05	28.6
30	8.5	2.58	2.30E-06	1.10E-04	57.2
30	8.5	2.58	3.45E-06	1.65E-04	85.8
30	26	7.89	3.45E-06	1.65E-04	85.8
30	26	7.89	2.30E-06	1.10E-04	57.2
30	26	7.89	1.15E-06	5.52E-05	28.6
30	26	7.89	0.00E+00	0.00E+00	0.0
30	49.5	15.01	0.00E+00	0.00E+00	0.0
30	49.5	15.01	1.15E-06	5.52E-05	28.6
30	49.5	15.01	2.30E-06	1.10E-04	57.2
30	49.5	15.01	3.45E-06	1.65E-04	85.8
30	70	21.23	3.45E-06	1.65E-04	85.8
30	70	21.23	2.30E-06	1.10E-04	57.2
30	70	21.23	1.15E-06	5.52E-05	28.6
30	70	21.23	0.00E+00	0.00E+00	0.0
45	4	2.61	0.00E+00	0.00E+00	0.0
45	4	2.61	1.15E-06	5.52E-05	30.0
45	4	2.61	2.30E-06	1.10E-04	60.0
45	4	2.61	3.45E-06	1.65E-04	90.0
45	12	7.84	3.45E-06	1.65E-04	90.0
45	12	7.84	2.30E-06	1.10E-04	60.0
45	12	7.84	1.15E-06	5.52E-05	30.0
45	12	7.84	0.00E+00	0.00E+00	0.0
45	23	15.03	0.00E+00	0.00E+00	0.0
45	23	15.03	1.15E-06	5.52E-05	30.0
45	23	15.03	2.30E-06	1.10E-04	60.0
45	23	15.03	3.45E-06	1.65E-04	90.0
45	32.5	21.24	0.00E+00	1.65E-04	90.0
45	32.5	21.24	1.15E-06	1.10E-04	60.0
45	32.5	21.24	2.30E-06	5.52E-05	30.0
45	32.5	21.24	3.45E-06	0.00E+00	0.0

S2. Equation (3.1) regression results for eight ART devices.

Device #	R-Squared	Std Error ($\mu g/m^3$)	B_0	B_1	B_2	B_3	B_4
1	0.749	30.84	22.6255	945.75	-86.337	1.96503	1.76536
2	0.971	11.09	5.4966	890.51	-77.848	1.92141	1.56107
3	0.786	29.97	17.4804	514.37	-40.806	0.95088	0.71163
4	0.956	13.64	3.0790	579.83	-50.333	1.18020	0.86211
5	0.951	14.28	3.1317	600.42	-52.293	1.22242	0.87996
6	0.738	33.12	21.4522	606.86	-51.814	1.16870	0.97653
7	0.948	14.12	3.5973	469.29	-38.334	0.90367	0.59532
8	0.947	14.93	4.8113	441.22	-36.124	0.87163	0.68088

S3. Equation (3.2) regression results for eight ART devices.

Device #	R-Squared	Std Error (kΩ)	C_0	C_1	C_2
1	0.933	1.081	21.443	-0.3346	-0.12870
2	0.958	0.553	14.598	-0.2161	-0.08628
3	0.957	0.577	15.090	-0.2218	-0.08791
4	0.962	0.524	14.545	-0.2189	-0.08214
5	0.961	0.384	10.895	-0.1605	-0.05825
6	0.959	0.507	13.419	-0.2044	-0.07109
7	0.964	0.590	17.016	-0.2532	-0.09903
8	0.967	0.437	13.113	-0.1933	-0.07473

S4. Indoor Stationary Monitoring, ART devices 1-8.

a) Indoor Stationary Monitoring, ART Device # 1
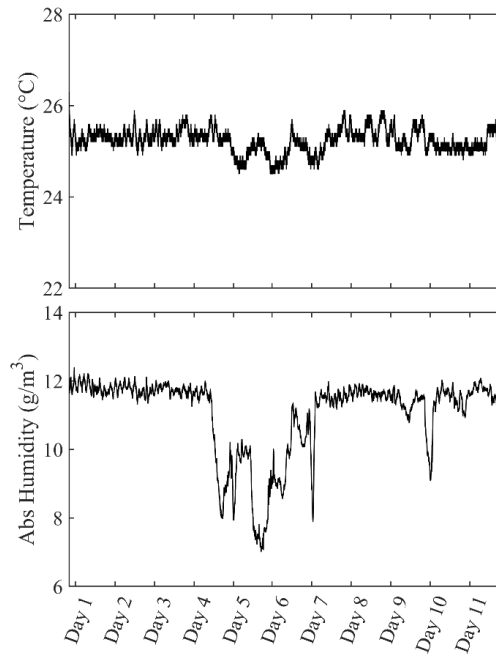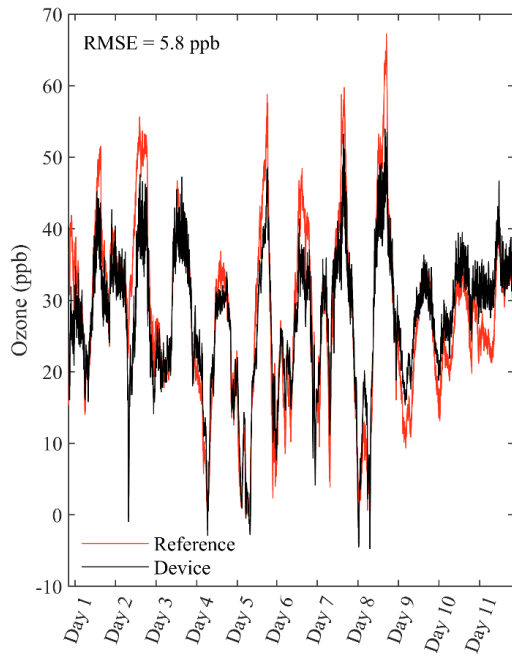
b) Indoor Stationary Monitoring, ART Device # 2
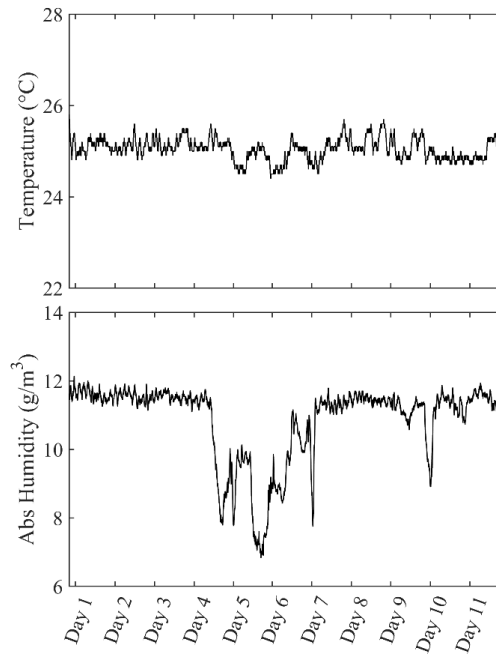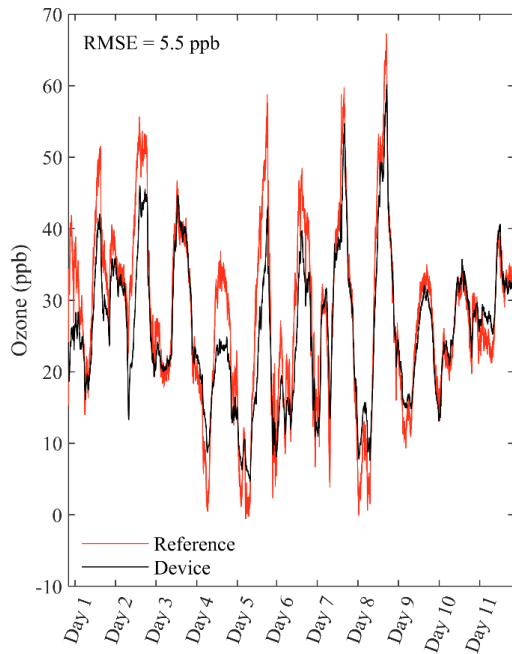
c) Indoor Stationary Monitoring, ART Device # 3
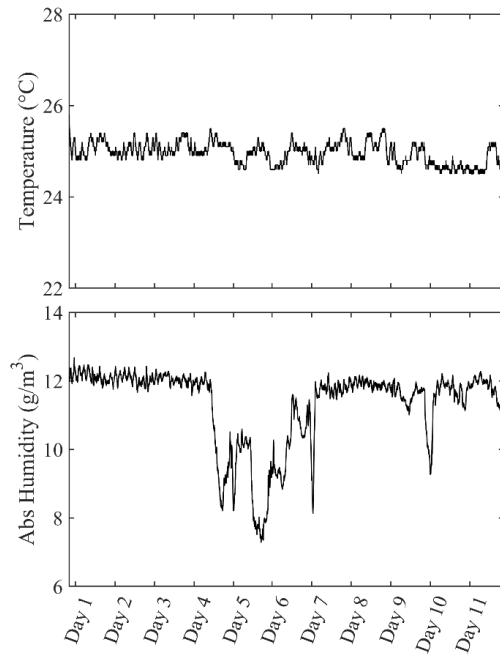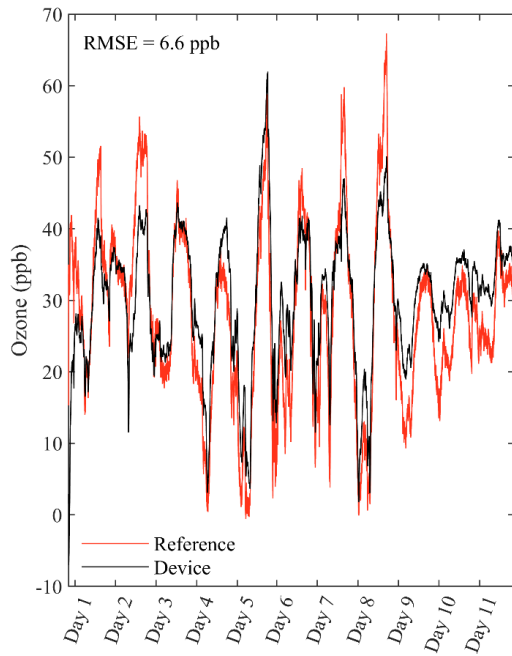
d) Indoor Stationary Monitoring, ART Device # 4
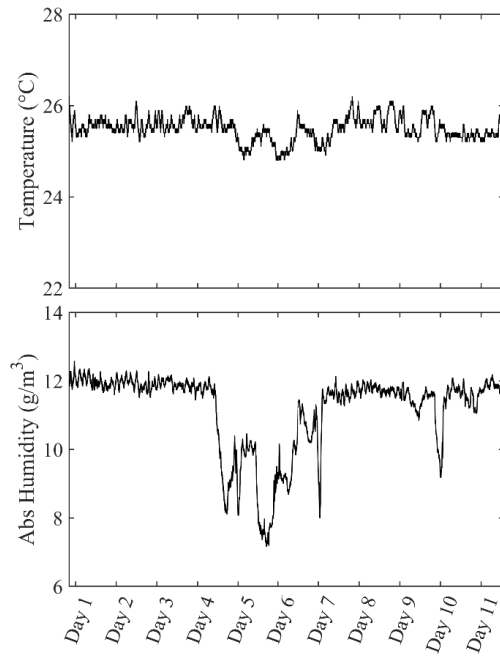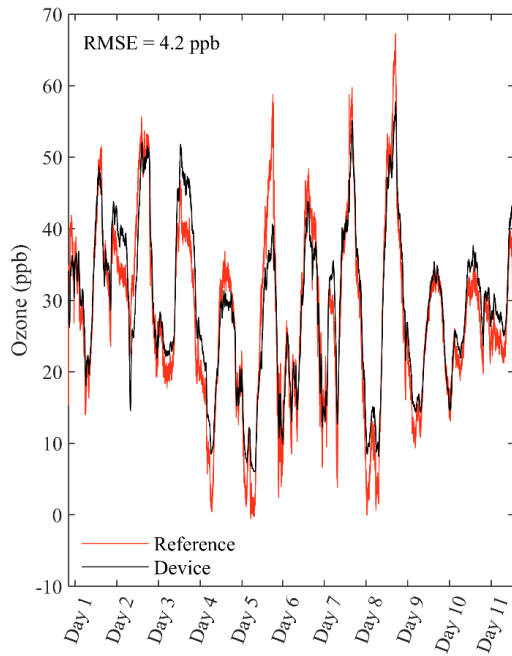
e) Indoor Stationary Monitoring, ART Device # 5
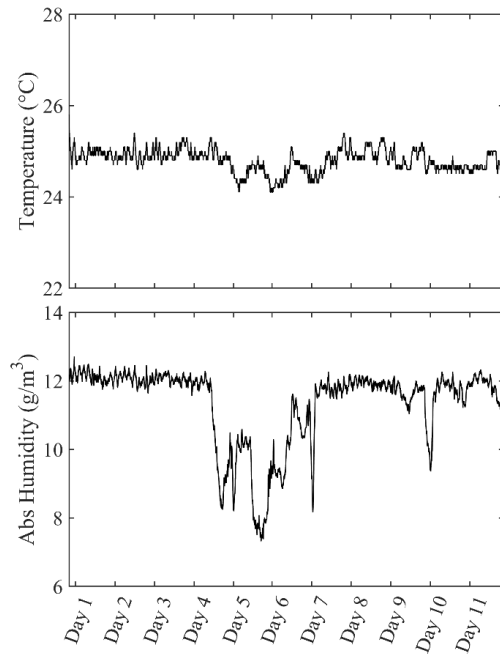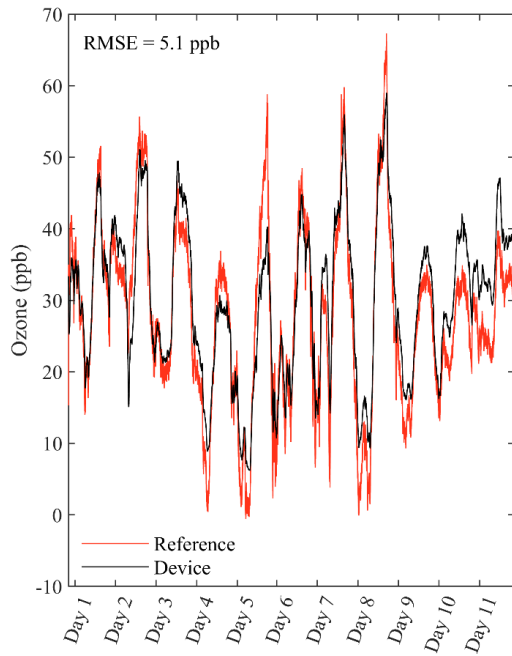
f) Indoor Stationary Monitoring, ART Device # 6

186
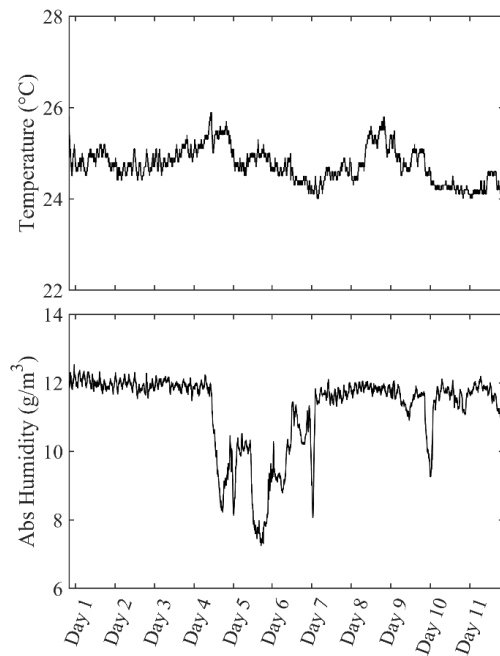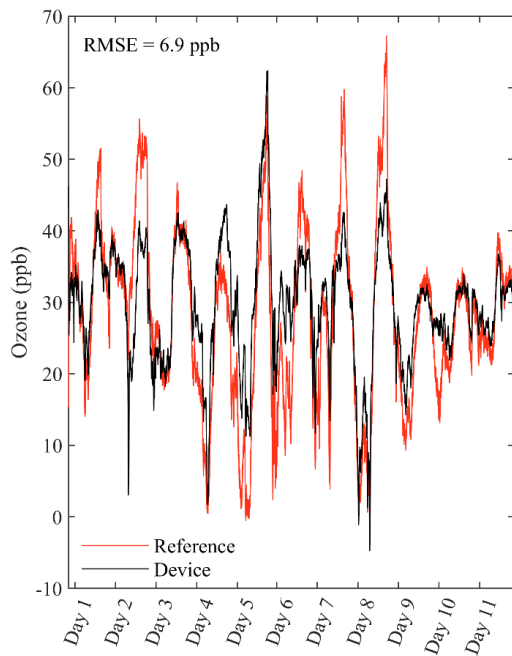
g) Indoor Stationary Monitoring, ART Device # 7
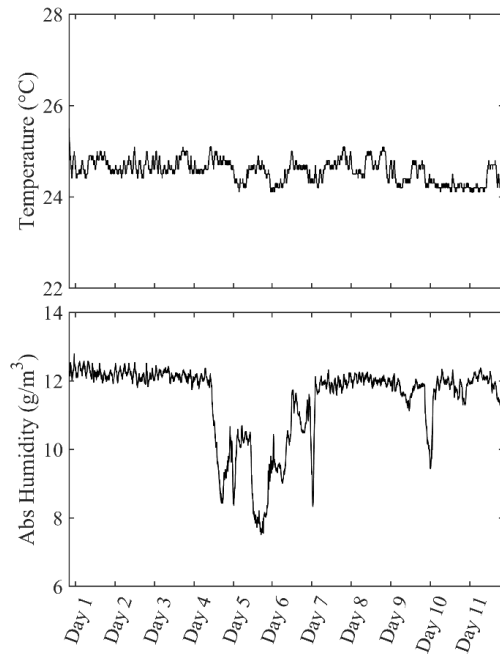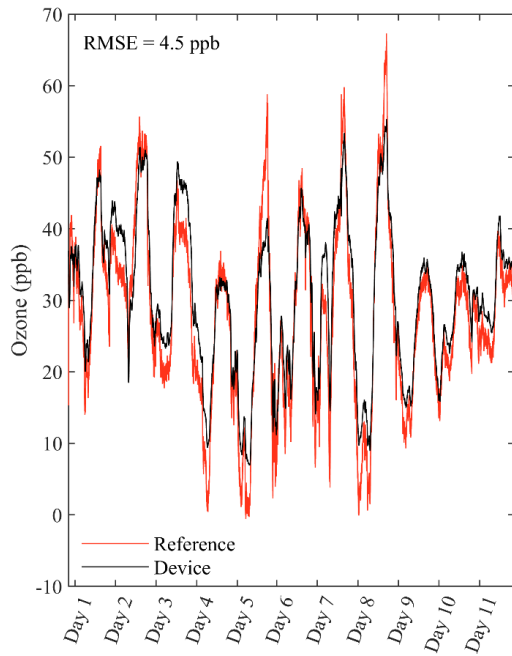
h) Indoor Stationary Monitoring, ART Device # 8

187
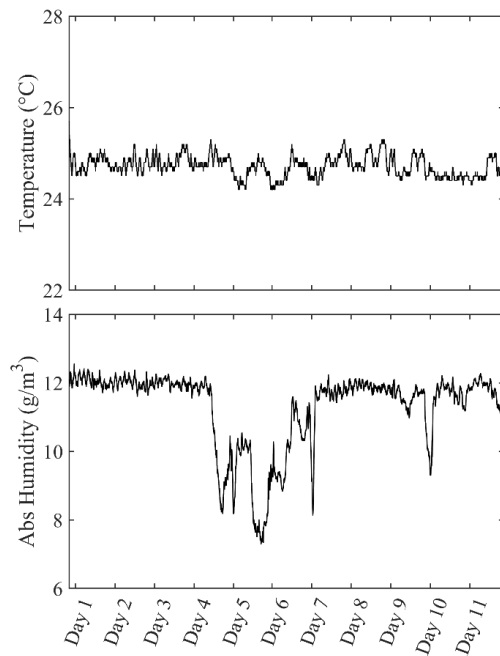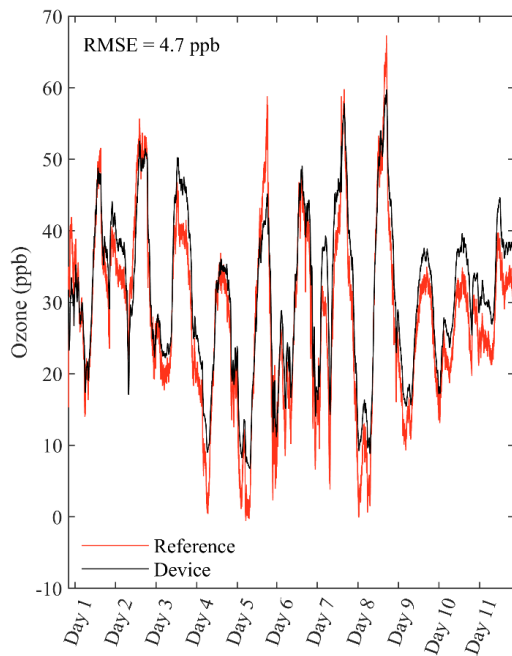
S5. Outdoor Stationary Monitoring, ART devices 1-8.
a) Outdoor Stationary Monitoring, ART Device # 1
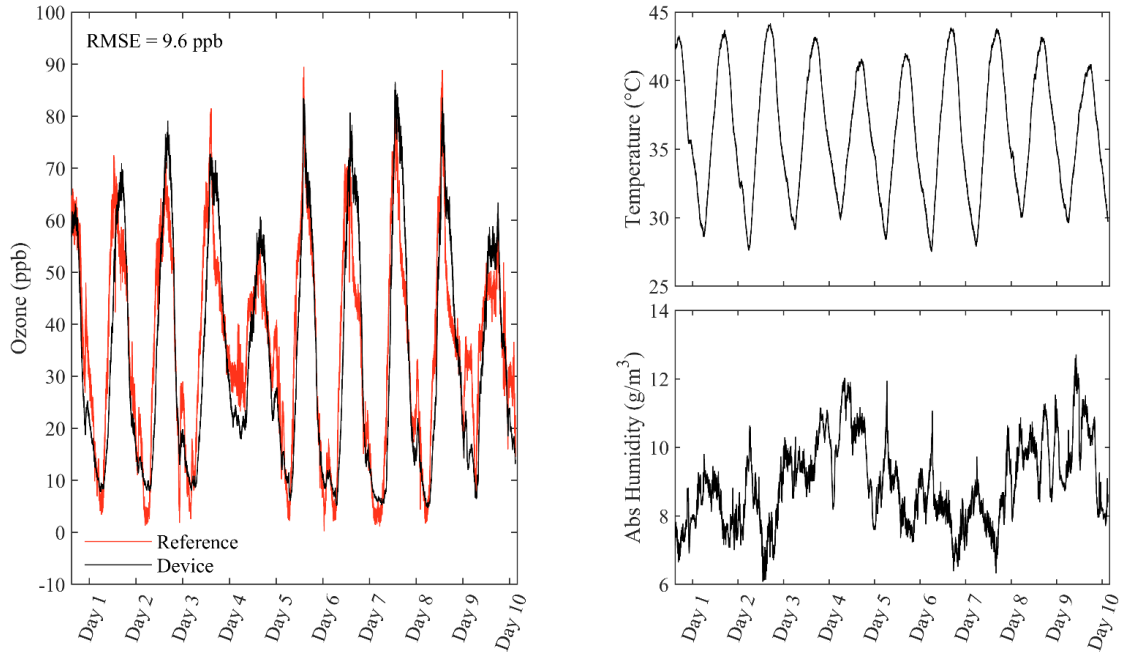
b) Outdoor Stationary Monitoring, ART Device # 2
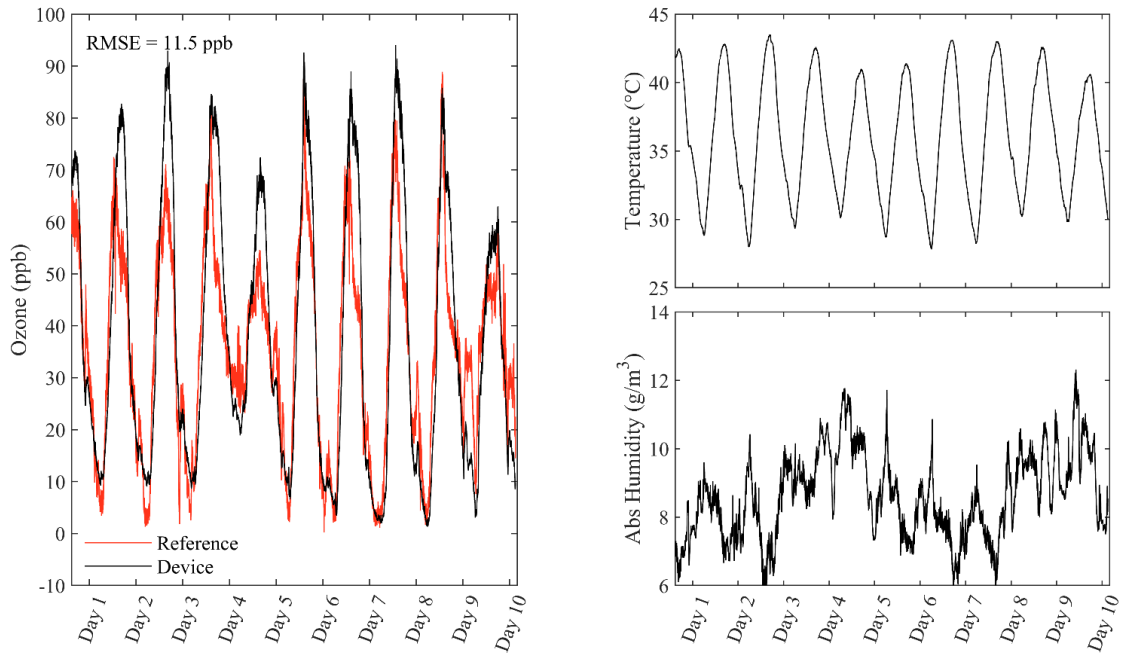
c) Outdoor Stationary Monitoring, ART Device # 3
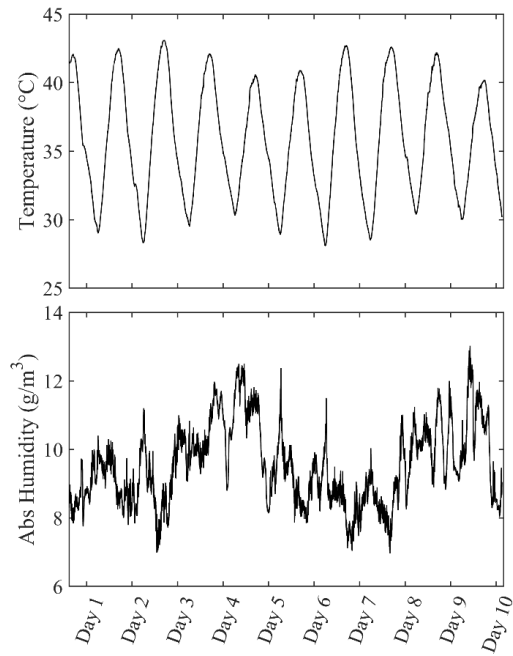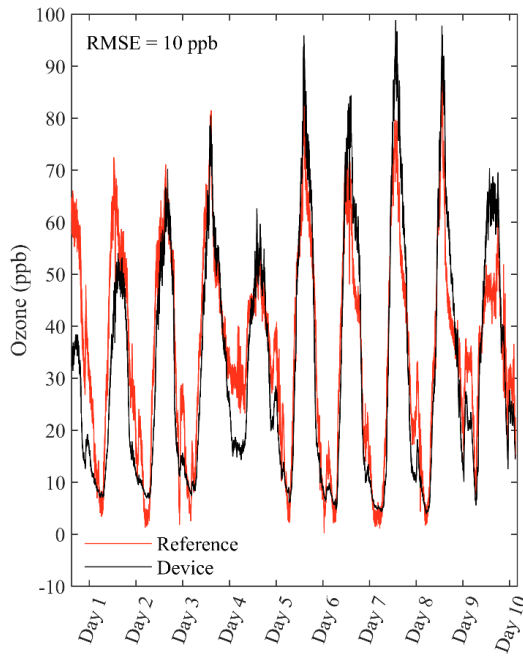
d) Outdoor Stationary Monitoring, ART Device # 4
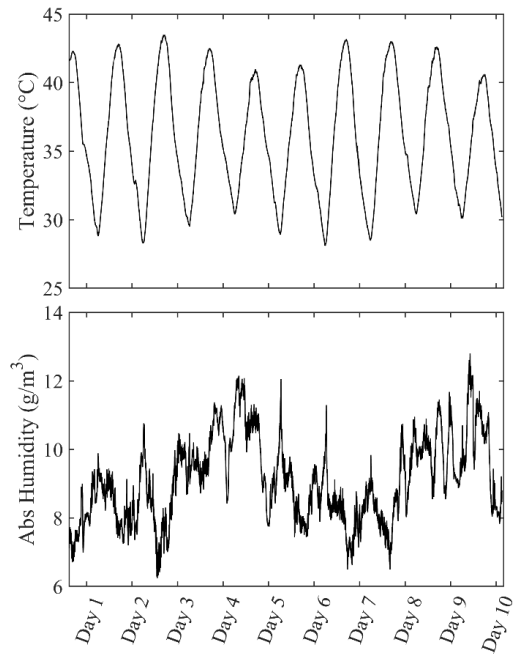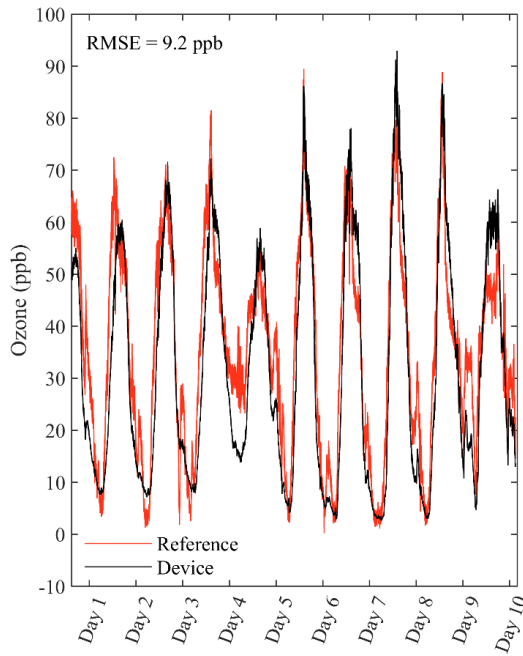
e) Outdoor Stationary Monitoring, ART Device # 5
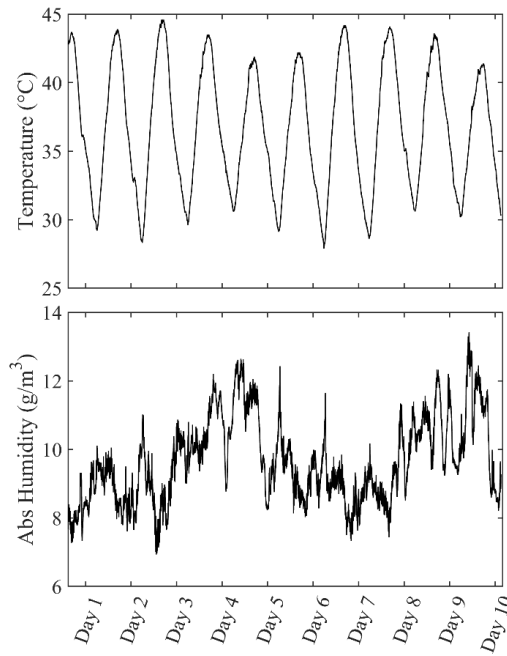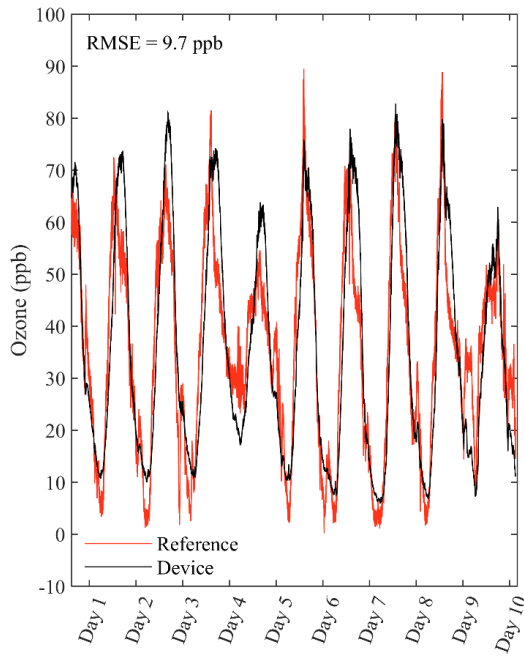
f) Outdoor Stationary Monitoring, ART Device # 6
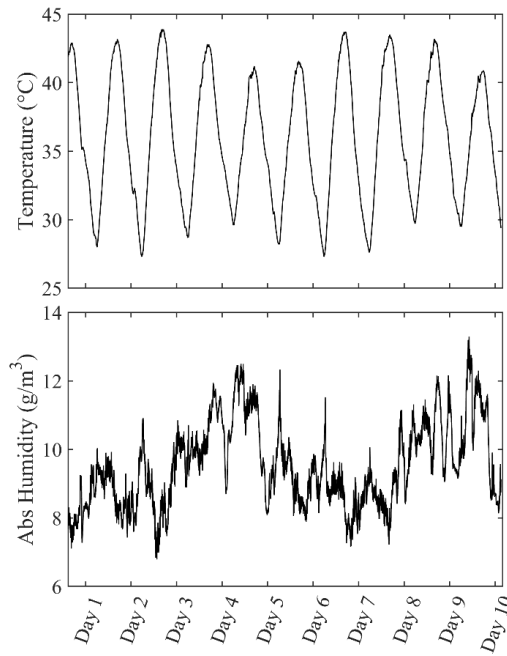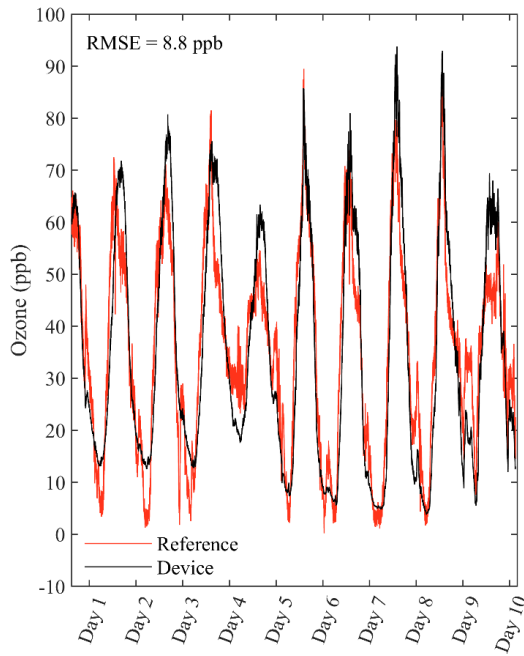
g) Outdoor Stationary Monitoring, ART Device # 7
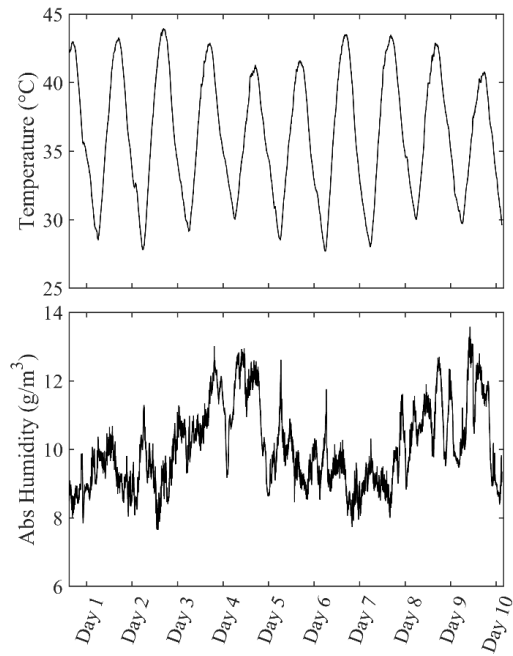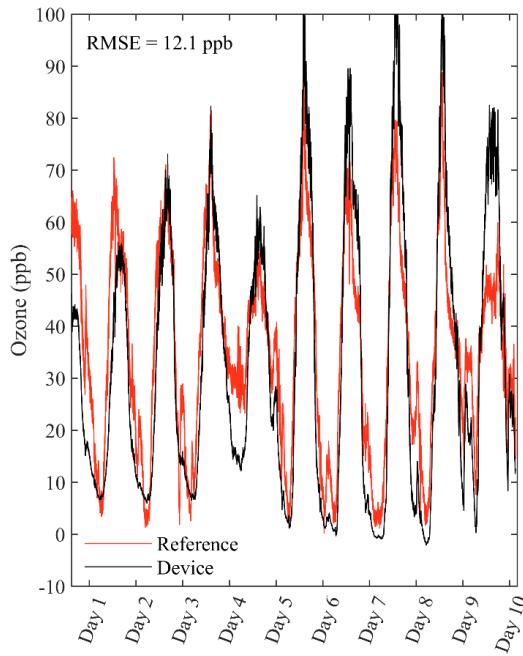
h) Outdoor Stationary Monitoring, ART Device # 8
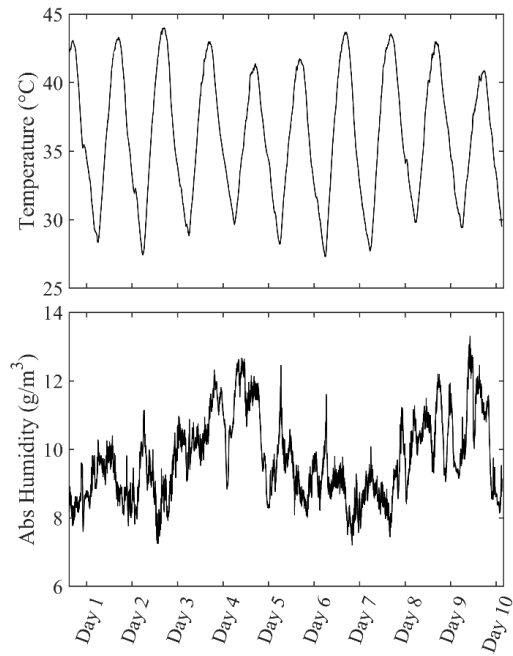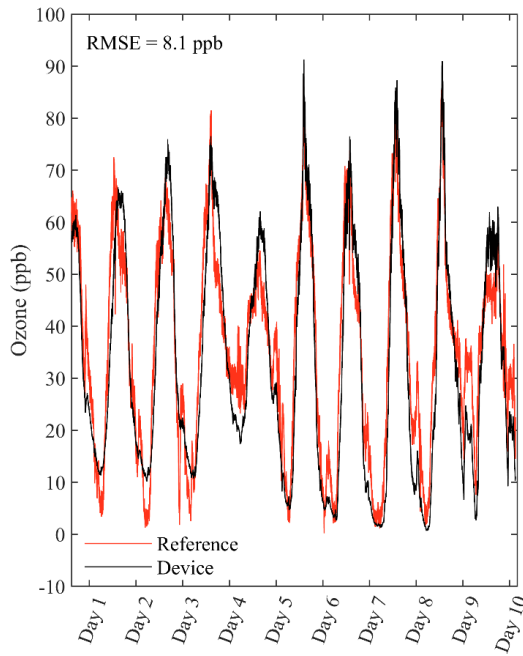
S6. Alternating Indoor-Outdoor Test, ART devices 1-8.

a) Alternating Indoor-Outdoor Test,
    ART Device # 1
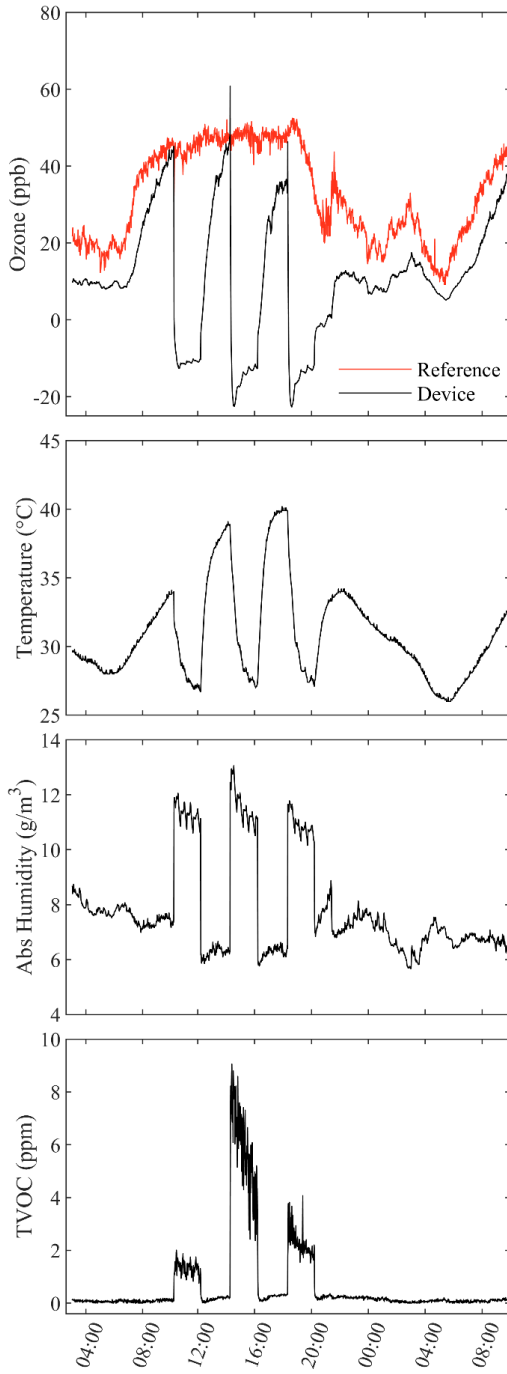
b) Alternating Indoor-Outdoor Test,
    ART Device # 2
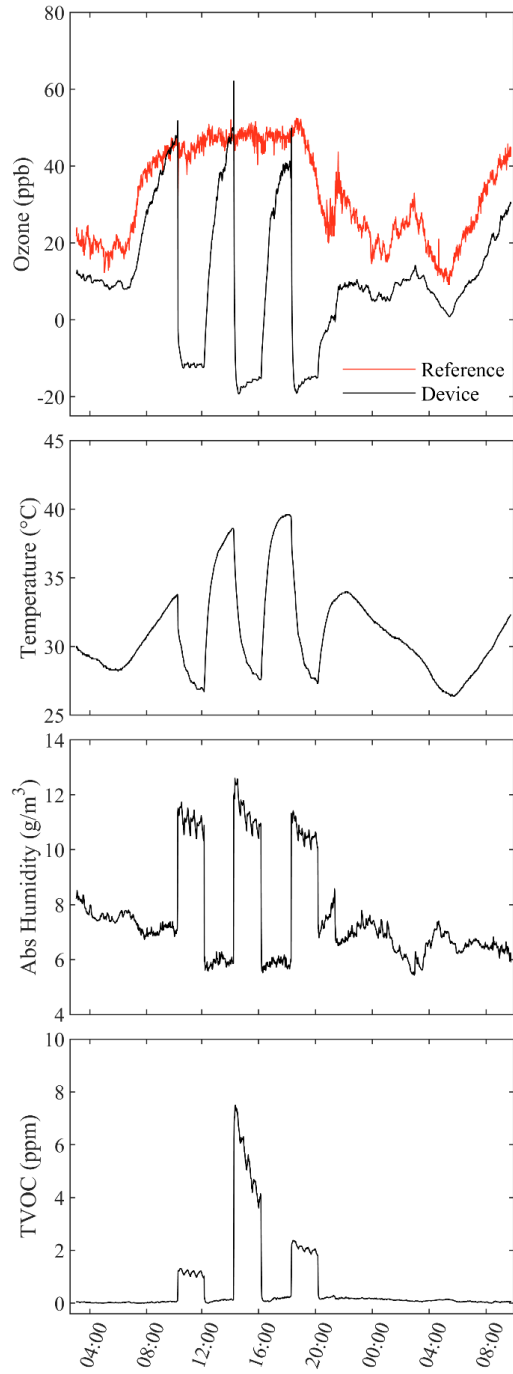
c) Alternating Indoor-Outdoor Test,
   ART Device # 3
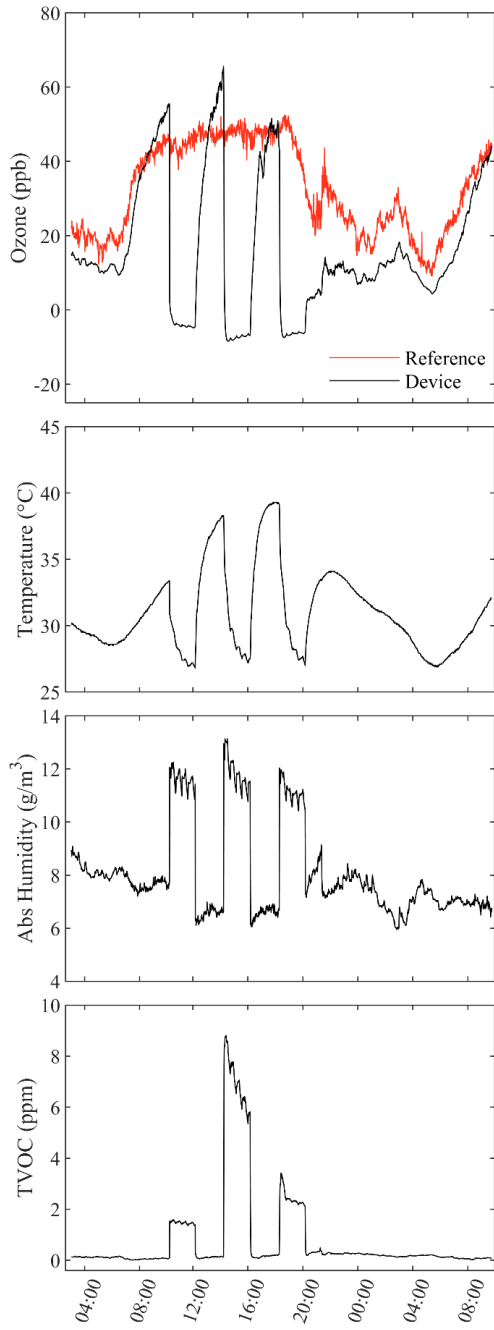
d) Alternating Indoor-Outdoor Test,
   ART Device # 4
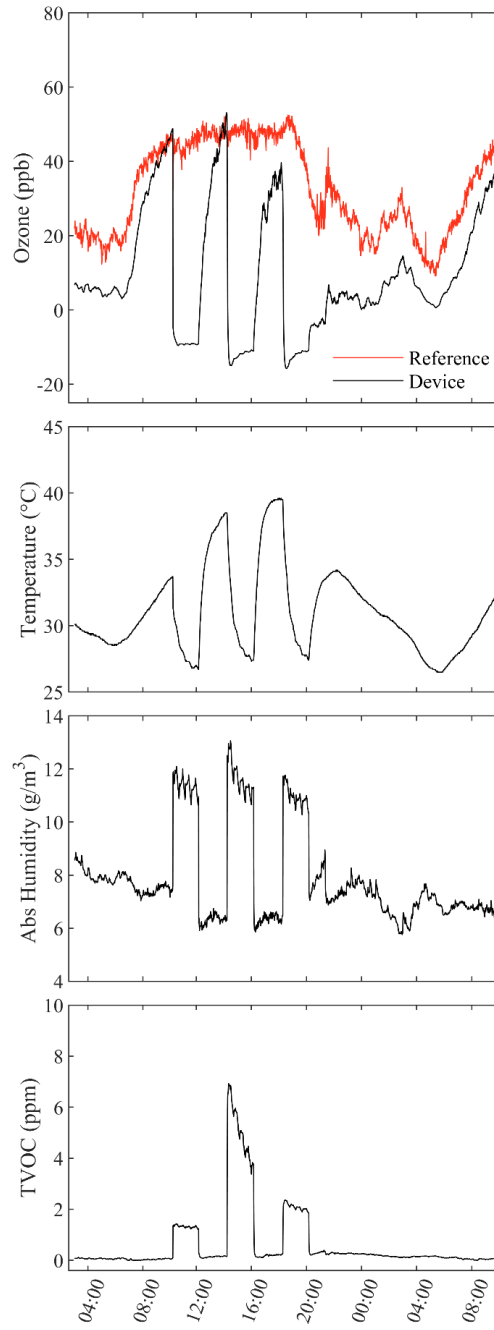
e) Alternating Indoor-Outdoor Test,
   ART Device # 5
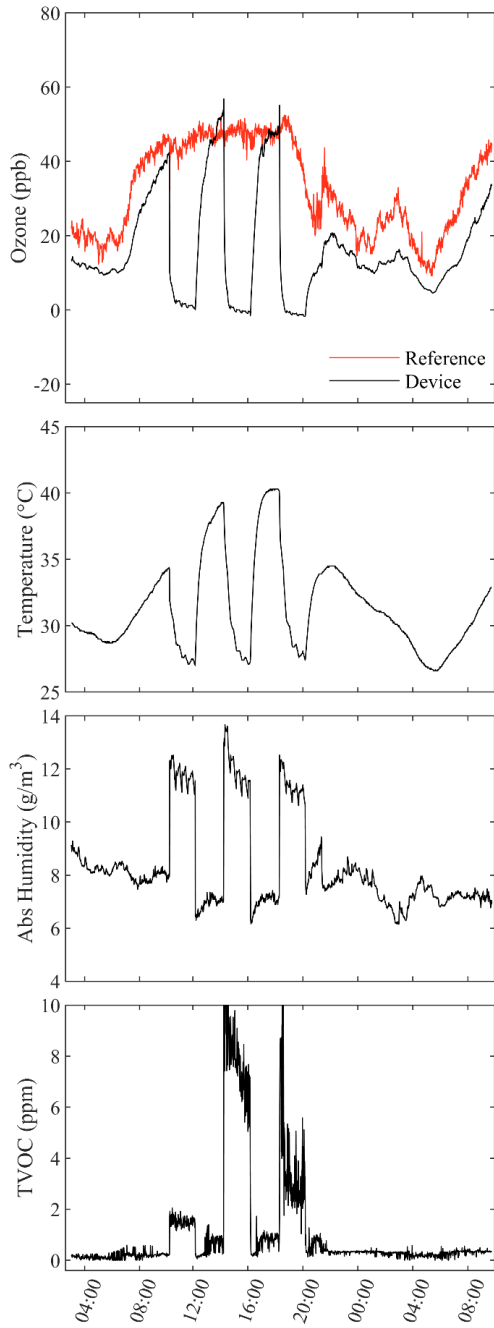
f) Alternating Indoor-Outdoor Test,
   ART Device # 6

194
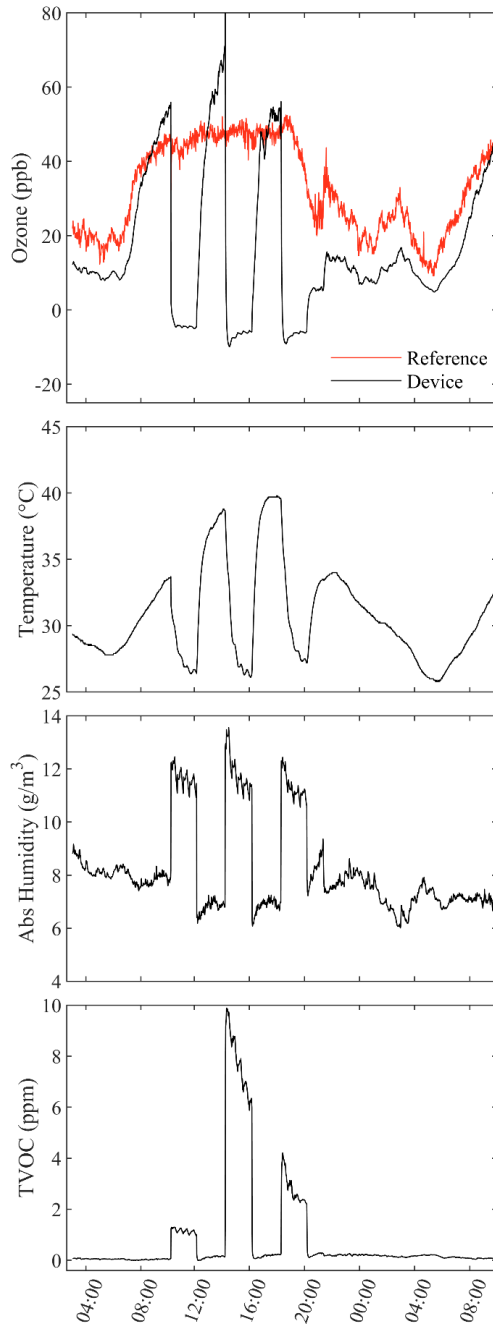
g) Alternating Indoor-Outdoor Test,
ART Device # 7
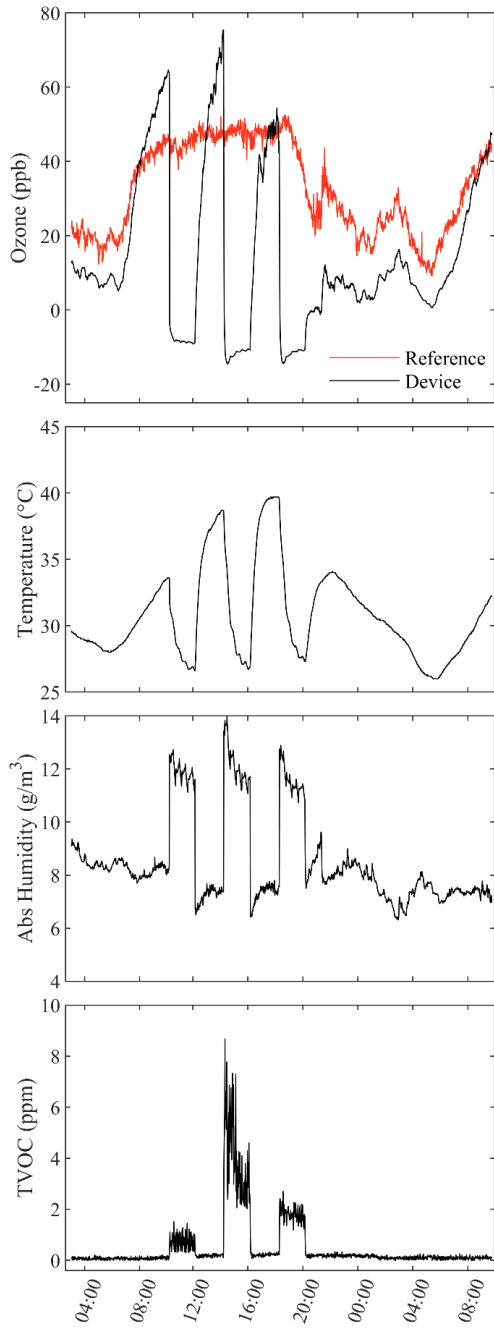
h) Alternating Indoor-Outdoor Test,
ART Device # 8
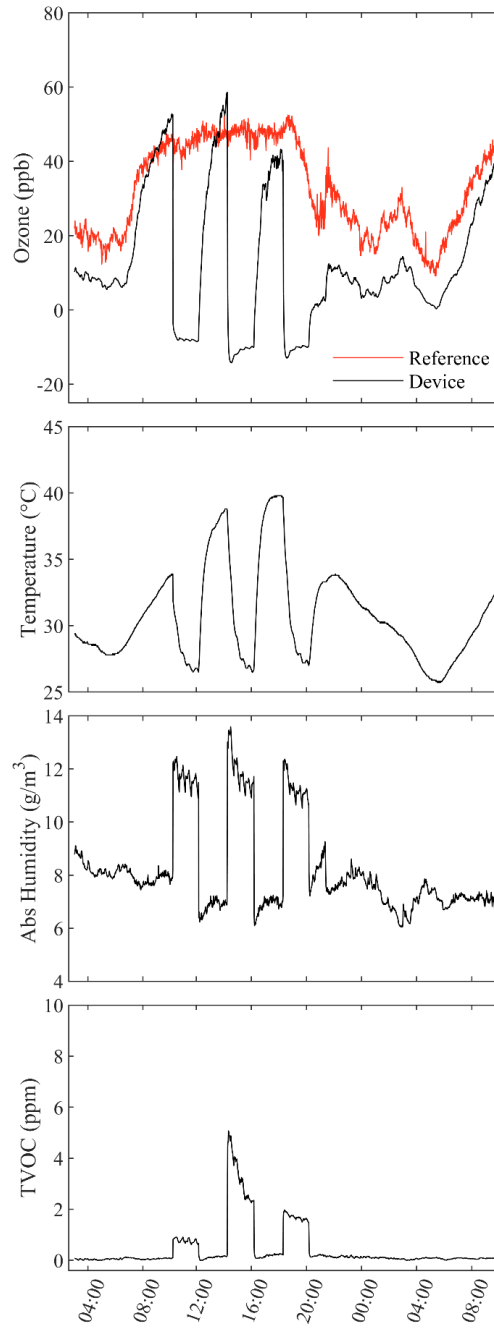
S7. 24-Hour Wearable Field Test, ART devices 1-8.

a) 24-Hour Wearable Field Test,
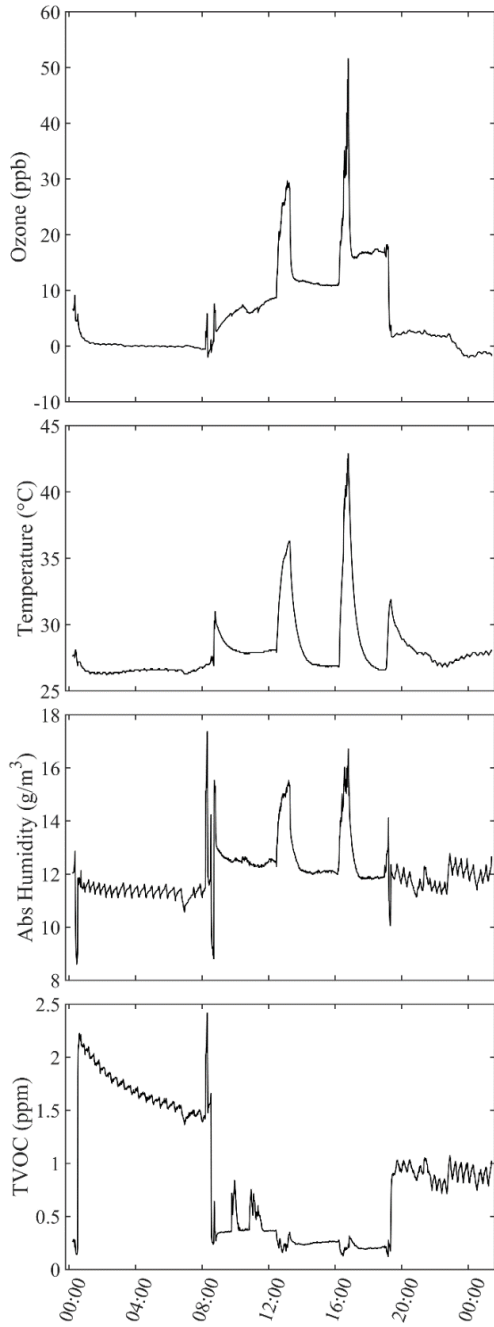ART Device # 1
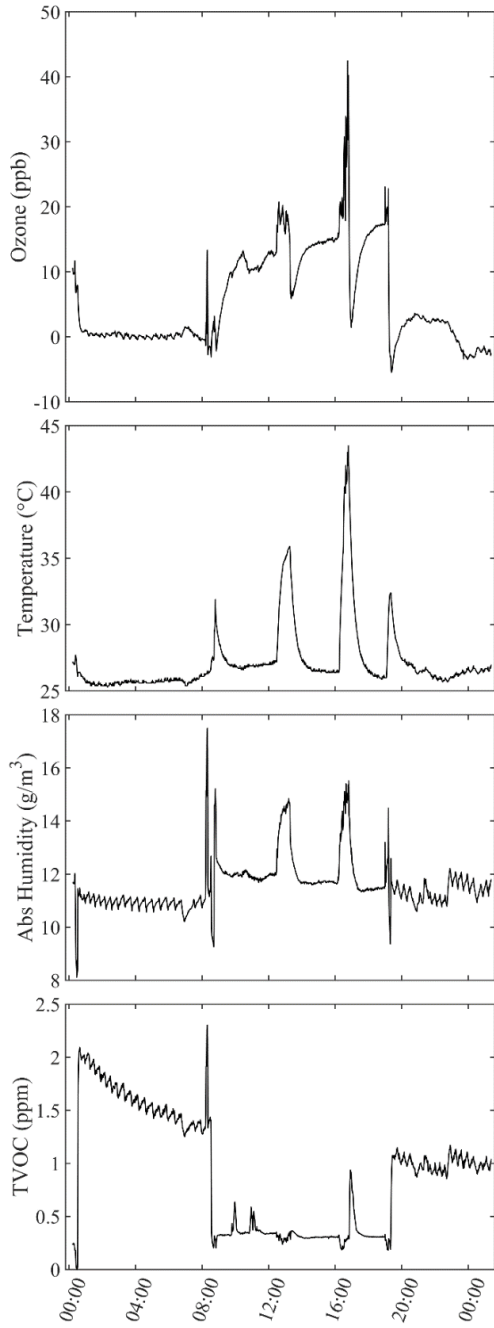
b) 24-Hour Wearable Field Test,
ART Device # 2
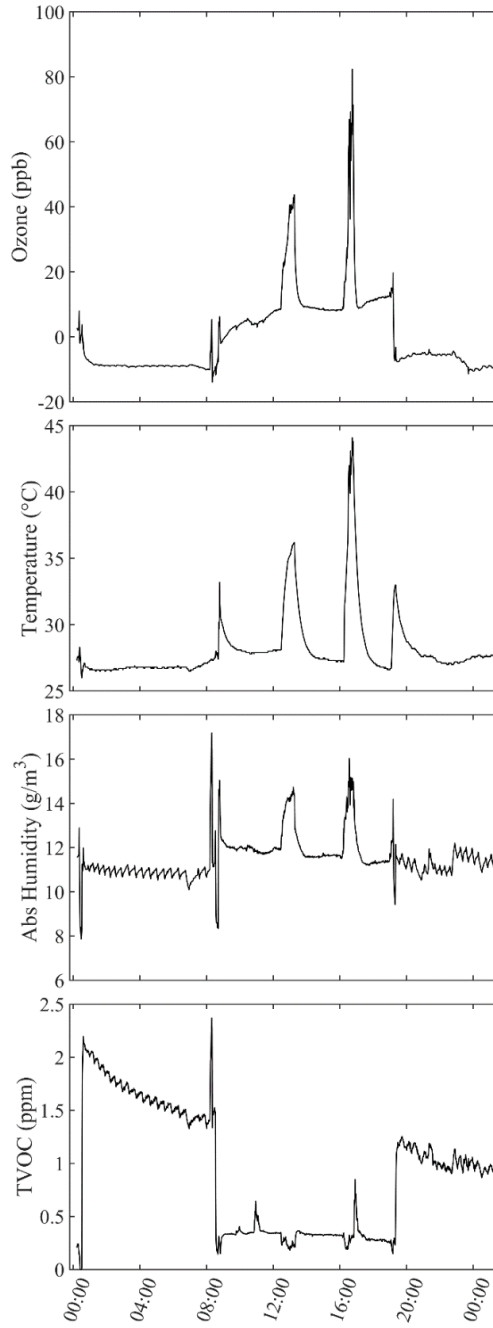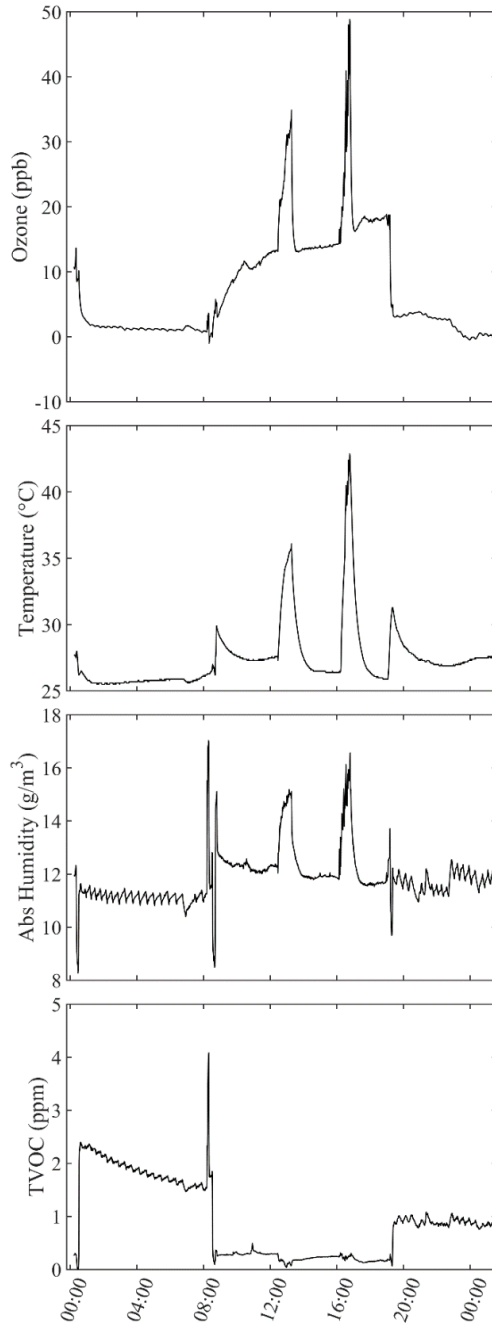
c)   24-Hour Wearable Field Test,
     ART Device # 3
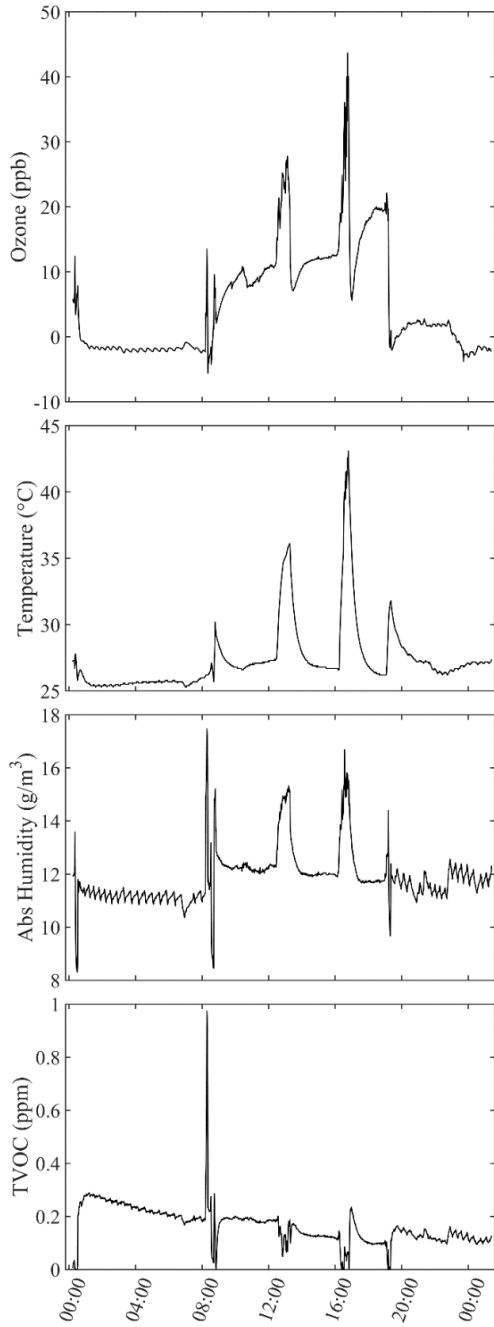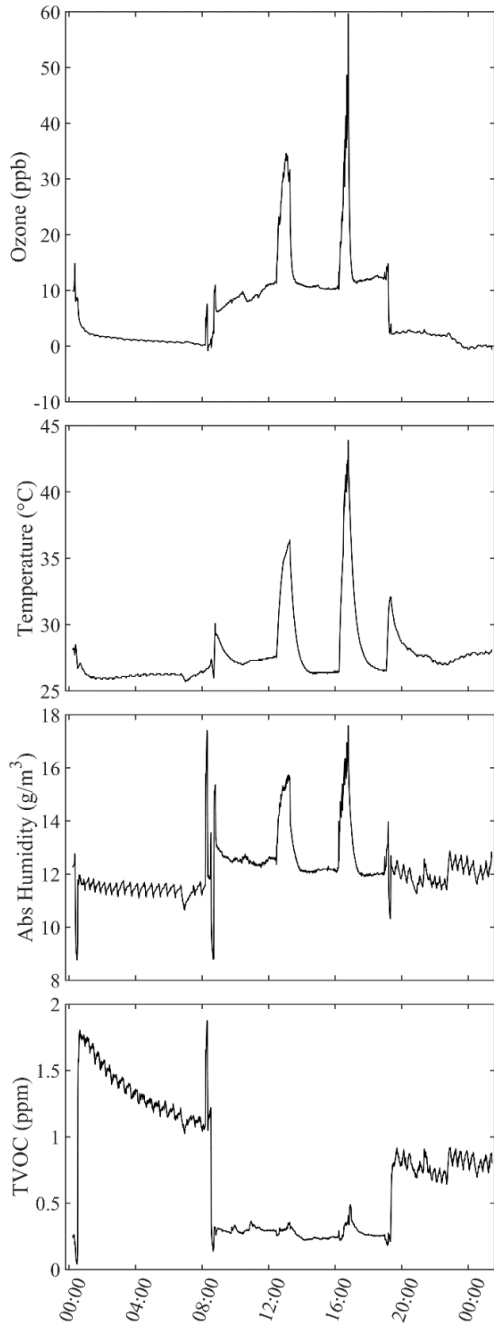
d) 24-Hour Wearable Field Test,
    ART Device # 4
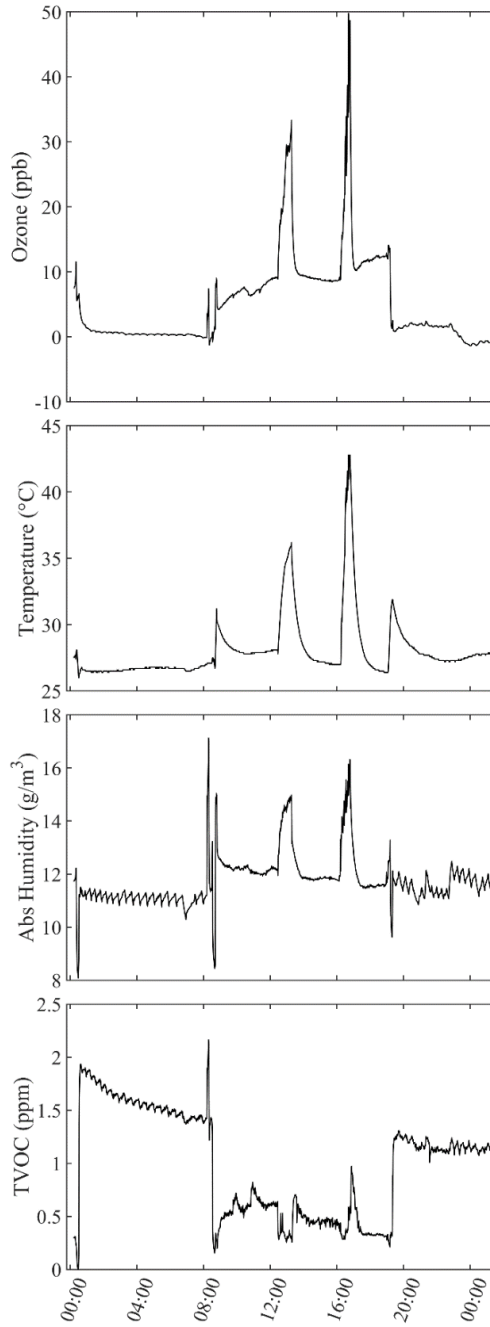
e) 24-Hour Wearable Field Test,
   ART Device # 5

f) 24-Hour Wearable Field Test,
   ART Device # 6

198

g) 24-Hour Wearable Field Test,
ART Device # 7

h) 24-Hour Wearable Field Test,
ART Device # 8